Skull Ecomorphology of Toothed Whales: A three-dimensional geometric morphometric approach

Deborah Vicari

A thesis submitted in partial fulfilment of the requirements of Liverpool John Moores University for the degree of PhD

September 2020

Table of Contents

No portion of the work referred to in the thesis has been submitted in support of an application for another degree or qualification of this or any other university or other institute of learning.

With Love, I dedicate this work to

Mum, Dad and my Brother

Acknowledgements

Years of work are now coming to an end, and there are many people I would like to acknowledge.

I would like to thank my supervisor, Dr. Carlo Meloro who took a risk on me and this project. Thank you for your guidance, patience and expertise. Thank you for lending me your passion and commitment for research and for giving me the opportunity to make all my dreams come true. For that, I can now call you a mentor. I could not have completed this project without you.

Massive thanks to my second supervisor, Professor Richard Brown for being greatly supportive and helpful during my Ph.D. I am very grateful for your time, insights, feedback throughout the length of this Ph.D.

I am grateful to my third supervisor Dr. Richard Sabin and the staff at the NHM of London. Thank you for your help with large specimens, your suggestions and interesting chats about false killer whales and cetaceans in general.

Enormous thanks to my thesis advisors Dr Olivier Lambert, and Professor Giovanni Bianucci for their useful and fundamental feedback that helped to improve this thesis. Special thanks for their encouragement and inspiration in pursuing a Ph.D.

Covid-19 placed us in uncertain, unprecedented and very challenging times. For that, I would like to thank all the LJMU staff for their effort, and for their patience. It must have been very stressful and I would like to thank you all for answering to my dozen emails and organising the online thesis submission.

I wish to thank Dr. Isabelle De Groote and Dr. Alessio Veneziano who provided initial guidance on photogrammetry techniques, and Dr. Ashleigh Wiseman, and Dr. Giada Giacomini for their feedback and friendship.

I am grateful to Roberto Portela Miguez at Natural History Museum (NHM, London, UK), Morten Olsen and Daniel Klingberg Johansson at Natural History Museum of Denmark (NHMD, Copenhagen, Denmark), Paolo Agnelli at "La Specola" Museum of Natural History in Florence (MNHF, Florence, Italy), Christine Lefèvre, Amandine Blin, and Virginie Bouetel at Muséum National d'Histoire naturelle (MNHN, Paris, France), and Andrew Kitchener and Zena Simmons at Natural History Museum of Scotland (NMS, Edinburgh, Scotland), Chiara

Chapter 1: Overview and aims

1.1 Functional morphology

Functional morphology is a branch of biology that seeks to investigate correlation between anatomy, function and adaptation of the organisms (Marshall, 2009). This area of investigation has been particularly useful to investigate variation within vertebrates whose hard endo-skeleton and complex muscular system are key components of their functional adaptations (Thomason, 1997).

The study of vertebrate skull morphology is central to an understanding of the correspondence between functional morphology and ecology (Churchill et al., 2018; Claude, Pritchard, Tong, Paradis, & Auffray, 2004; Cooke & Terhune, 2015; Meloro, 2011; Meloro, Hudson, & Rook, 2015; Meloro, 2007; Meloro, Raia, Piras, Barbera, & O' Higgins, 2008; van Heteren, MacLarnon, Soligo, & Rae, 2014). Indeed, an understanding of how skull shape relates to ecology can help us predict how vertebrates interact with their environment (Marshall, 2009). The field of study that deals with morphological adaptations and their relationship with ecological variables is called ecomorphology (Mourlam and Orliac, 2017; Gillet, Frédérich and Parmentier, 2019; Park *et al.*, 2019; Coombs *et al.*, 2020).

Since the skull is an important component of the vertebrate body, it has received special attention from functional morphology due to its involvement into multiple vital functions of a vertebrate life. These include protection of the central organs of the nervous system (the brain, the eyes), providing attachment for masticatory muscles and holding teeth which are primarly involved in the first step of the digestive process: food ingestion. Hence, variation in skull morphology has been generally interpreted in relation to masticatory/biting adaptations that represent key mammalian adaptive traits (Turnbull, 1970). Multiple investigations have already explored the interaction between mammalian skull morphology and masticatory adaptation as well as diet. However, within different mammalian groups, the skull also shows major diversity that is not always explained merely in terms of chewing adaptations. The cetacean (currently grouped with the hoofed animals in the order Cetartiodactyla) is one such a group.

1.2 Cetacean taxonomy and evolution

Cetaceans currently include about 85 species grouped in 2 major clades (Odontocetes and Mysticetes) and 13 families (**Figure 1.1**). The monophyly of the group is recognised by morphological and molecular features and within this clade we recognised two suborders: the Odontoceti (= toothed whales) and the Mysticeti (= baleen whales) whose split is recorded at 34Mya.

Such long evolutionary history today allows to distinguish clearly Odontocets from Mysticetes based on morphological external and cranial characters. Externally, Odontocetes are characterised by a single blowhole and teeth, while in the Mysticeti teeth have been replaced with baleen hair, and two blowholes are present. Cranial features that characterise the Odontoceti clade are (**Figure 1.2**): the presence of a concave facial area to accommodate the melon, presence of premaxillary foramina and premaxillary sac fossa, posterior expansion of maxilla over the supraorbital region covering the frontal bones, and facial asymmetry. All these features are related to their echolocation abilities (Churchill, Geisler, Beatty, & Goswami, 2018; Martínez-Cáceres, Lambert, & de Muizon, 2017; Marx & Fordyce, 2015; Marx et al., 2016; Uhen, 2004, Coombs et al., 2020; Cranford, Amundin, & Norris, 1996; Geisler, Colbert, & Carew, 2014). In contrast, the skulls of the Mysticeti show toothless maxilla which form most of the arched rostrum. This lack of teeth is associated with the fact that the mysticeti are adapted to various types of filter feeding, with species being classified as skimmers, angulfers and suction filter-feeders. Baleen hair can be used to strain shrimps, zooplankton and krill.

Cetaceans display different sizes ranging from 1.25 m of length and 25 kg for the La Plata dolphin (*Pontoporia blainvillei*) with Mysticeti generally bigger, up to of 33.5 m and 190 tonnes in body size for the blue whale (*Balaenoptera musculus*). Toothed whales are also interesting because they can echolocate, producing and hearing ultrasounds at more than 20 000 Hz, while baleen whales do not retain this sophisticated way of communication, but they have a low-frequency (< 20 Hz) hearing and vocalization (Ketten, 2000).
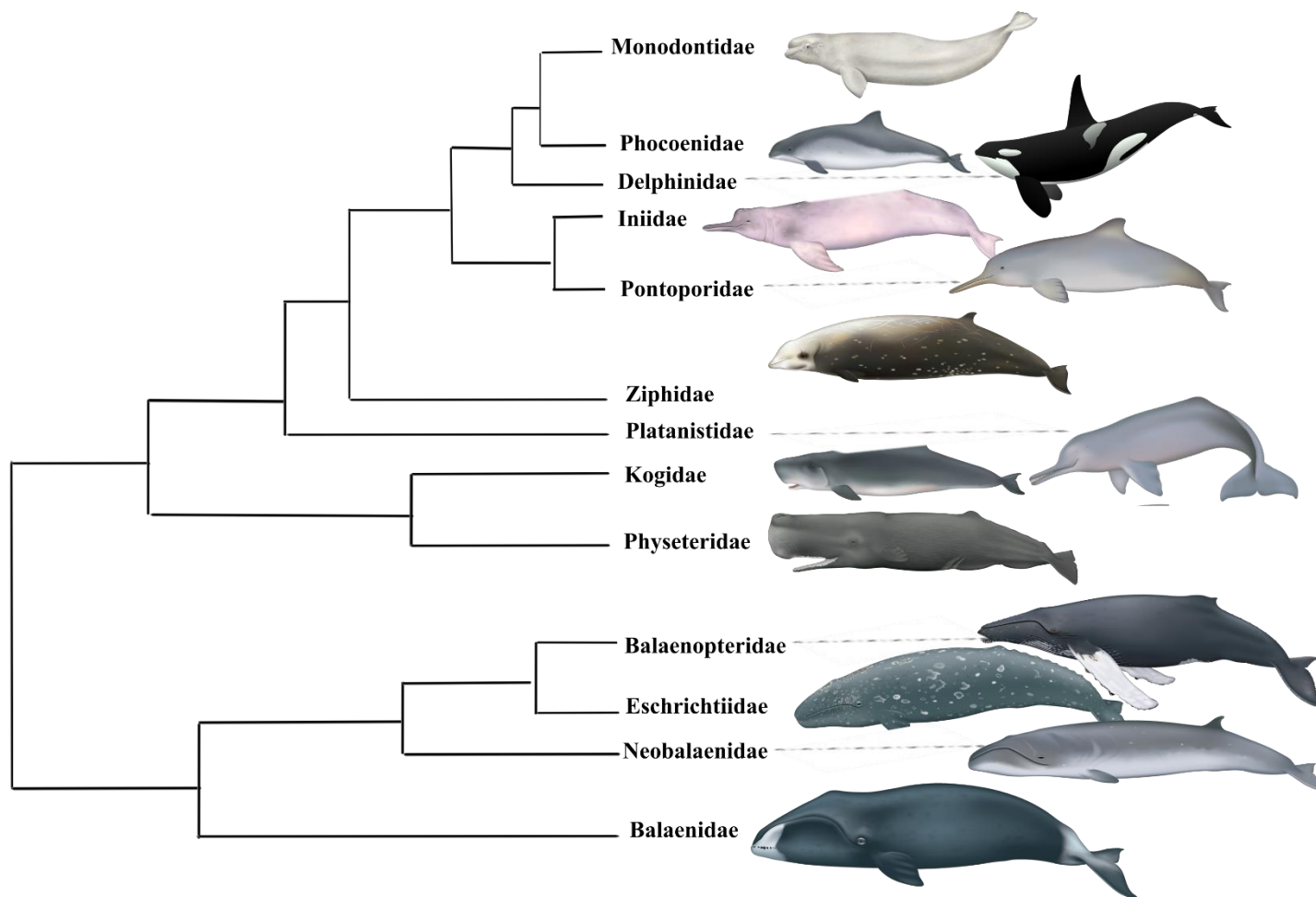
Figure 1.1 Relationship of extant cetaceans based on Gatesy et al. (2012). Artwork by the American Cetacean Society, *Delphinapterus leucas* by NOAA, *Orcinus orca* by Flavia Strani, and *Platanista gangetica* by Uko Gorter.

1.3   Toothed whales: what does drive skull morphological variation?

The term telescoping is often used to describe the general form of the cetacean's skull. This term was coined in 1923 by Miller and refers to the posterior elongation of the rostral elements in relation to the backward shift of the bony nares. As a result, the relative position of the facial bones in the cetacean skull is better described as an overlap of adjacent bones. At some levels, vertical sections of the skull will reveal up to four different overlapping bones (like an ancient telescope folding) (Rommel et al. 2009). The maxilla cover most of the frontals (**Figure 1.2**), odontocetes show polydontia and homodontia, and facial directional asymmetry towards the left in general (Marx et al., 2016).

The skull of odontocetes can be divided into many functional components: brain, feeding apparatus, visual apparatus, auditory apparatus, respiratory apparatus, hearing apparatus and sound production apparatus. These functional components can all be considered as potential drivers of the skull shape variation we observe in living and fossil species. As a result of their opportunistic passages from the land to the water (which did not happen in a gradual and straightforward way), where feeding and diet has had a central role to play in their evolutionary story (Thewissen, 2014).

Toothed Whale Skull Anatomy
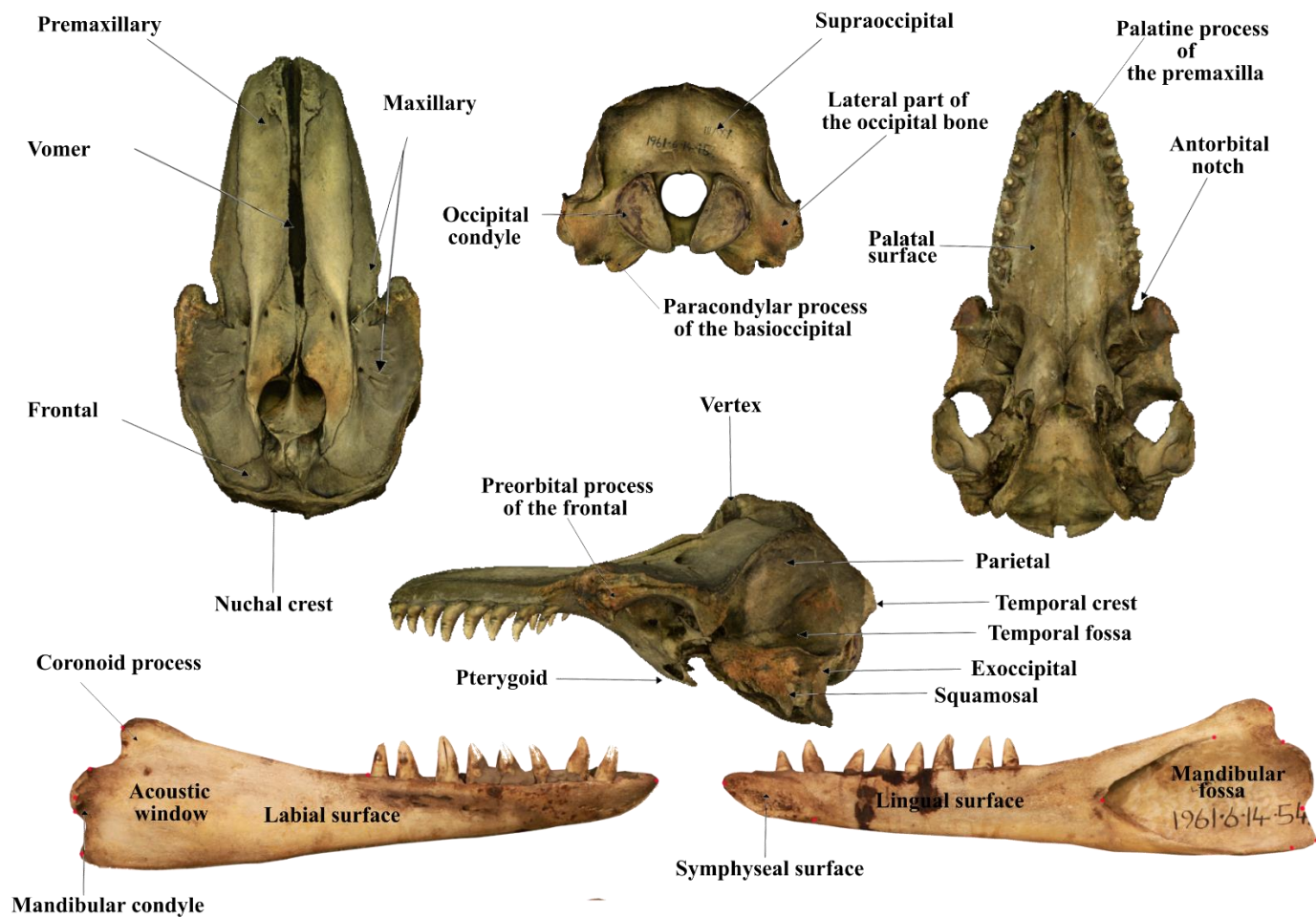
Figure 1.2 Toothed whale skull anatomy of lexicon used throughout the thesis

Diet and skull morphology- Toothed whales have developed the most sophisticated and varied feeding strategies among mammals, likely because of their great ecological diversity and occupation of a large number of habitats, ranging from the tropics to Polar Regions and from large rivers to deep benthopelagic regions. Capture techniques (ram, suction, and lateral snapping) can be related to three feeding strategies that have been characterized for the major groups of odontocetes: ram feeding, raptorial feeding, and suction feeding (Hocking, Marx, Park, Fitzgerald, & Evans, 2017). Several skull features are correlated with feeding strategies and these, in turn, can correlate with main prey type (Werth, 2006a). In fact, odontocetes can also be classified by main prey type, i.e., ichthyophagi (fish feeders), sarcophagi (mammal eaters) and teuthophagi (squid eaters) (Berta & Sumich, 1999). Ichthyophagous taxa generally are longirostrine (McCurry & Pyenson, 2019) having a long rostrum, with a slender mandible and numerous teeth (up to 240) to catch fish (Berta, Sumich, & Kovacs, 1999; Poli & Fabbri, 2012). Mandibular modifications such as shortening of the snout (brevirostrine), a decrease in the tooth count, short and wide tongue (in the sperm whale, situated at the rear of the oral cavity)(Werth, 2004, 2006b), are all morphological features skull-related found together or as subsets in teuthophagous taxa (Marshall, 2009). Sarcophagous taxa have a large rostrum, powerful jaws and a small number of larger and stronger teeth (25 per quadrant) allowing the capture of large prey such as pinnipeds, seabirds, fish and even whales, e.g., *Orcinus orca* (Berta & Sumich, 1999). Nevertheless, some odontocete species, such as *Delphinapterus leucas*, *Globicephala melas*, *Lagenorhynchus obliquidens* and *Tursiops truncatus*, show a mix of suction and raptorial feeding strategies (Barroso, Cranford, & Berta, 2012; Kane & Marshall, 2009; Lewis & Schroeder, 2003; Rossbach & Herzing, 1997) although they exhibit different skull morphologies, making difficult their inclusion in just one feeding category.

Other parts of the skull that are particularly relevant to feeding are the rostrum, the coronoid process (where the temporal muscle attaches; Cozzi et al., 2017), and the temporal fossa (**Figure 1.2**). The temporal fossa (fordefines the origin of the temporal mandibular muscle) that is involved in opening and closing the mouth (hence, prey capturing), the zygomatic process of the squamosal forallows the articulation of the mandible and, the hyoid apparatus and the mandible (Perrin, 1975). As they do not require strength for chewing, the coronoid process is reduced.

The skull has received particular attention in the literature for its importance in the food strategies (aforementioned) as well as for the transmission of sounds from the mandible to the ear (Rommel et al. 2009).

Biosonar mode (Echolocation) and skull size and shape- Odontocetes use echolocation to detect prey underwater. Echolocation is a highly specialized type of acoustic vocal communication in which individuals send information to themselves. As sounds propagate better in water, cetaceans have exploited this property to partly compensate for decreased light transmission and the consequent poor visibility (Berta & Sumich, 1999). Vocal communication involves the production of sounds that can be divided into two types: 1) pulsed-signal sound or clicks, used for both echolocation and communication, and 2) narrow-band sound, such as whistling, which is thought to have only a communicative function. It should be noted that the latter is not emitted by all toothed whales (for example it is absent in *Phocaena phocaena* (Dudzinski, Thomas, & Gregg, 2009), *Neophocaena phocaenoides*, *Phocoenoides dalli*, *Cephalorhynchus commersoni*, *C. hectori* and *Kogia* spp. (Au & Lammers, 2014)). These non-whistling species tend to be smaller than whistling species (Au & Lammers, 2014), and have similar body types (Surlykke, Nachtigall, Fay, & Popper, 2014).

Four biosonar types (Surlykke et al., 2014), with different waveforms and power spectra, are used by odontocetes to echolocate their prey: 1) multi-pulsed (MP) (Møhl, Wahlberg, Madsen, Heerfordt, & Lund, 2003) clicks last 100 µs and they have centroid frequencies of 15 kHz (Møhl et al., 2003), 2) frequency modulated (FM) (Johnson, Madsen, Zimmer, De Soto, & Tyack, 2004, 2006) clicks with frequencies of circa 24 kHz and duration of 350-450 µs (Surlykke et al., 2014), 3) narrow band high frequency (NBHF) (Kyhn et al., 2013, 2009; Kyhn et al., 2010) have narrower bandwidth (11-20 kHz) with peak frequencies at 125-140 kHz (Galatius et al., 2018), and 4) broadband (BB)(Au, 2012) with a broad cover frequency ranges from 10 to 150-170 kHz (Galatius et al., 2018).

The skull alone does not necessarily indicate the outline of the head; in fact, Odontocetes skulls have a concave facial area to accommodate the melon (a fatty tissue that functions as a lens for the propagation of echolocation sounds) which influences greatly the external shape of the head, only defined in part by the underlying bone. The geometric relationship between the bones and soft tissues of the head varies from one species to the other; a striking example is the sperm whale, differing much from other odontocetes in the relationship between cranial profile and head profile (Rommel et al. 2009). The size and shape of the head can also influence the mechanism of propagation and reception of sounds (hearing apparatus). Features such as size and shape of the head/skull can also influence the mechanism of propagation and reception of sounds (hearing apparatus). These capabilities are the result of the evolution of (i) unique high frequency sound generation and propagation organs, such as the melon and the complex

nasal passages, as well as (ii) one or several new paths for the reception of returning sounds, through the posterior portion of the mandible (mandibular foramen) and possibly through the gular region, and from the activity of the auditory areas of central nervous system (Berta & Sumich, 1999). First attempts of evolutionary transformation for improving hearing abilities can be found in *Ambulocetus* and *Dorudon*, that present a small mandibular foramen (this trait allows to chanalize the high frequency sound transmission). Moreover, functional studies on cochlear construction can predict the frequency range of hearing (Ketten and Wartzok, 1990) and differences in echolocation frequencies correspond in changes of periotic shape and different habitats (Gustein et al., 2014).

Studies of sound reception in echolocating toothed whales have mapped acoustically sensitive areas on the dolphin's head and shown that the external auditory canal is six times less sensitive than the mandible (Berta & Sumich, 1999). These results support the hypothesis proposed by Norris in 1964 of a unique sound reception path through the mandible. This hypothesis was based on the finding of fatty acids in the mandibular foramen and the mandibular canal. These low-density lipids act as channels for transporting the high frequency sounds directly to the middle ear, which is enclosed in the tympanic bulla (Berta & Sumich, 1999). Koopman et al. (2006) examined the composition of lipids in the mandibles of six individuals, representing four families of toothed whales (Delphinidae, Phocoenidae, Ziphiidae, Kogidae), and the results showed show that the lipids in the lower jaw have a complex 3D topography, with different odontocete species accumulating different lipid.

Skull asymmetry- Echolocation evolved 34 million years ago, and it is associated with directional asymmetry in the cranium of toothed whales. The ancestor of the Neoceti did not show asymmetry and it is likely that echolocation was not present (Coombs et al., 2020). Asymmetrical rostrum was present in the Archeocetes (Coombs et al., 2020) and it is likely to be related to directional hearing. Rostral asymmetry became nasofacial in odontocetes as results of the evolution of low frequencies in hearing and echolocation (Jensen et al 2017). In fact, echolocation is a highly specialized type of acoustic communication in which individuals send information to themselves, and it is a key feature of toothed whales group. Factors linked with asymmetry seem also to be related to prey size (MacLeod, 2007; MacLeod, 2017), and melon size (Hirose et al., 2015).

Evolutionary events can be reconstructed using fossils, but analysis of the early stages of embryogenesis of modern species can also provide important insights. Studies of *S. attenuata*

have attempted to throw light on the evolution of homodontia from polyodontia (or vice versa) in toothed whales. In the Eocene, the first whale did not show homodontia or polydontia, suggesting that these two features were closely related (Thewissen, 2014). Indeed, the interaction of two proteins seems to regulate these features which are expressed long before the teeth eruption (Thewissen, 2014).

Through the morphology we can attempt to determine principles that allow to determine the function of forms. For that, skulls specimens represent the best way to make inferences on fossil specimens, and to have access to a series of information on whales, which otherwise would not be accessible.

1.4   Thesis structure and aims

The aim of this thesis is to investigate the cranial ecomorphology across Odontocetes clade by testing hypotheses of association between interspecific cranial morphological variation (mainly size and shape traits) and ecological adaptations. Very little previous research has focused on modularity in different species of toothed whales (Guidarelli et al, 2014; del Castillo et al., 2016; Churchill et al., 2019), and those that have, have tended to focus on common species such as *Tursiops truncatus*, *Stenella coeruleoalba*, and *Delphinus delphis*. Moreover, a comprehensive study of the cranial ecomorphology on the whole toothed whale clade is still lacking.

The thesis is structured into four Chapters organised sequentially to cover the methodological approach (Chapter 2), the interspecific variation of odontocetes cranial morphology and its association with ecological adaptation (Chapter 3), the potential for cranial morphology to identify hybrids in two species of Monodontidae (*Delphinapterus leucas* and *Monodon monoceros*) in order to identify the potential of cranial morphology to identify hybrids and their evolutionary adaptation (Chapter 4), and finally the study of intraspecific skull variation in a stranded population of British false killer whale (*Pseudorca crassidens*, Chapter 5). Such a hierarchical taxonomic approach was designed specifically in order to provide a framework for interpreting skull size and shape variation in Odontocetes at all evolutionary scale from macro (=interspecific variation) to micro (one population). Ontogeny was not considered into this thesis because the aim of the proposed methodological framework is to identify its potential applicability to the study and interpretation of paleoecology from fossils, hence adult variation is more relevant due to clear change into feeding functions.

Chapter 2 describes methods, statistical analyses, and protocol used to quantify cranial size and shape variation in three dimensions using three different digitising methods: Microscribe, Photogrammetry and Breuckmann laserscan. Also, this chapter supports Chapter 2 as sources/specimens from two different techniques and datasets used.

In **Chapter 3** I tested the hypothesis that ecological variables correlate with cranial shape and size of Odontocetes at macroevolutionary (= interspecifc) scales with the support of comparative methods. Similar analyses were presented in Churchill et al. (2018) and McCurry et al. (2017) although on a different selection of taxa and using different cranial 3D landmark configuration.

Chapter 4, provides an analysis (by using GMM approach) of the genetically confirmed hybrid between *Delphinapterus leucas* and *Monodon monoceros*, was analysed by using GMM approach confirming the phenotypic dominance of one of his parental species. Sexual dimorphism in size, shape and integration of the skull was also examined within and between the two species.

In **Chapter 5**, a stranded British population of *Pseudorca crassidens* was examined by comparing shape and size skull between sexes. A GMM approach was also used to study the morphological integration between crania and mandibles in separate sexes.

Final remarks chapter summarizes all the previous findings and provides suggestions for future studies.

Chapter three, four, and five are papers in preparation to be submitted to peer-reviewed journals. Chapter two will be apart of the supplementary material of the paper developed from Chapter three.

References

Au, W. W. L. (2012) *The sonar of dolphins*. Springer Science & Business Media.

Au, W. W. L. and Lammers, M. O. (2014) 'Cetacean acoustics', in *Springer Handbook of Acoustics*. Springer, pp. 843–875.

Barroso, C., Cranford, T. W. and Berta, A. (2012) 'Shape analysis of odontocete mandibles: functional and evolutionary implications', *Journal of Morphology*. Wiley Online Library, 273(9), pp. 1021–1030.

Berta, A., Sumich, J. L. and Kovacs, K. M. (1999) 'Cetacean evolution and systematics', *Marine Mammals: Evolutionary Biology. Academic Press, San Diego, CA*, pp. 49–85.

del Castillo, D. L. *et al.* (2016) 'Cranial development and directional asymmetry in Commerson's dolphin, Cephalorhynchus commersonii commersonii: 3D geometric morphometric approach', *Journal of Mammalogy*. Oxford University Press US, 97(5), pp.

1345–1354.

Churchill, M. *et al.* (2018) 'Evolution of cranial telescoping in echolocating whales (Cetacea: Odontoceti)', *Evolution*. Wiley Online Library, 72(5), pp. 1092–1108.

Churchill, M. *et al.* (2019) 'Asymmetry drives modularity of the skull in the common dolphin (*Delphinus delphis*)', *Biological Journal of the Linnean Society*. Oxford University Press UK, 126(2), pp. 225–239.

Claude, J. *et al.* (2004) 'Ecological correlates and evolutionary divergence in the skull of turtles: a geometric morphometric assessment', *Systematic Biology*. Society of Systematic Zoology, 53(6), pp. 933–948.

Cooke, S. B. and Terhune, C. E. (2015) 'Form, function, and geometric morphometrics', *The Anatomical Record*. Wiley Online Library, 298(1), pp. 5–28.

Coombs, E. J. *et al.* (2020) 'Wonky whales: the evolution of cranial asymmetry in cetaceans', *BMC biology*. BioMed Central, 18(1), pp. 1–24.

Cranford, T. W., Amundin, M. and Norris, K. S. (1996) 'Functional morphology and homology in the odontocete nasal complex: implications for sound generation', *Journal of morphology*. Wiley Online Library, 228(3), pp. 223–285.

Dudzinski, K. M., Thomas, J. A. and Gregg, J. D. (2009) 'Communication in marine mammals', in *Encyclopedia of marine mammals*. Elsevier, pp. 260–269.

Galatius, A. *et al.* (2018) 'Raising your voice : evolution of narrow-band high- frequency signals in toothed whales (Odontoceti)', *Biological Journal of the Linnean Society*, pp. 1–12.

Geisler, J. H., Colbert, M. W. and Carew, J. L. (2014) 'A new fossil species supports an early origin for toothed whale echolocation', *Nature*. Nature Publishing Group, 508(7496), pp. 383–386.

Gillet, A., Frédérich, B. and Parmentier, E. (2019) 'Divergent evolutionary morphology of the axial skeleton as a potential key innovation in modern cetaceans', *Proceedings of the Royal Society B*. The Royal Society, 286(1916), p. 20191771.

Guidarelli, G. *et al.* (2014) 'Morphological variation and modularity in the mandible of three Mediterranean dolphin species', *Italian Journal of Zoology*. Taylor & Francis, 81(3), pp. 354–367.

van Heteren, A. H. *et al.* (2014) 'Functional morphology of the cave bear (*Ursus spelaeus*) cranium: a three-dimensional geometric morphometric analysis', *Quaternary International*. Elsevier, 339, pp. 209–216.

Hocking, D. P. *et al.* (2017) 'A behavioural framework for the evolution of feeding in predatory aquatic mammals', *Proceedings of the Royal Society B: Biological Sciences*. The Royal Society, 284(1850), p. 20162750.

Johnson, M. *et al.* (2004) 'Beaked whales echolocate on prey', *Proceedings of the Royal Society of London. Series B: Biological Sciences*. The Royal Society, 271(suppl_6), pp. S383–S386.

Johnson, M. *et al.* (2006) 'Foraging Blainville's beaked whales (*Mesoplodon densirostris*) produce distinct click types matched to different phases of echolocation', *Journal of Experimental Biology*. The Company of Biologists Ltd, 209(24), pp. 5038–5050.

Kane, E. A. and Marshall, C. D. (2009) 'Comparative feeding kinematics and performance of odontocetes: belugas, Pacific white-sided dolphins and long-finned pilot whales', *Journal of Experimental Biology*. The Company of Biologists Ltd, 212(24), pp. 3939–3950.

Ketten, D. R. "Hearing by whales and dolphins." (2000): 43-108.

Kyhn, L. A. *et al.* (2009) 'Feeding at a high pitch: Source parameters of narrow band, high-frequency clicks from echolocating off-shore hourglass dolphins and coastal Hector's dolphins', *The Journal of the Acoustical Society of America*. Acoustical Society of America, 125(3), pp. 1783–1791.

Kyhn, L. A. *et al.* (2010) 'Echolocation in sympatric Peale's dolphins (*Lagenorhynchus australis*) and Commerson's dolphins (*Cephalorhynchus commersonii*) producing narrow-band high-frequency clicks', *Journal of Experimental Biology*. The Company of Biologists Ltd, 213(11), pp. 1940–1949.

Kyhn, L. A. *et al.* (2013) 'Clicking in a killer whale habitat: narrow-band, high-frequency biosonar clicks of harbour porpoise (*Phocoena phocoena*) and Dall's porpoise (*Phocoenoides dalli*)', *PloS one*. Public Library of Science, 8(5).

Lewis, J. S. and Schroeder, W. W. (2003) 'Mud plume feeding, a unique foraging behavior of the bottlenose dolphin in the Florida Keys', *Gulf of Mexico Science*, 21(1), p. 9.

Marshall, C. D. (2009) 'Feeding morphology', in *Encyclopedia of marine mammals*. Elsevier,

pp. 406–414.

Martínez-Cáceres, M., Lambert, O. and de Muizon, C. (2017) 'The anatomy and phylogenetic affinities of *Cynthiacetus peruvianus*, a large Dorudon-like basilosaurid (Cetacea, Mammalia) from the late Eocene of Peru', *Geodiversitas*. BioOne, 39(1), pp. 7–163.

Marx, F. G. and Fordyce, R. E. (2015) 'Baleen boom and bust: a synthesis of mysticete phylogeny, diversity and disparity', *Royal Society Open Science*. The Royal Society Publishing, 2(4), p. 140434.

Marx, F. G., Lambert, O. and Uhen, M. D. (2016) *Cetacean paleobiology*. John Wiley & Sons.

McCurry, M. R. *et al.* (2017) 'The remarkable convergence of skull shape in crocodilians and toothed whales', *Proceedings of the Royal Society B: Biological Sciences*. The Royal Society, 284(1850), p. 20162348.

McCurry, M. R. and Pyenson, N. D. (2019) 'Hyper-longirostry and kinematic disparity in extinct toothed whales', *Paleobiology*. Cambridge University Press New York, USA, 45(1), pp. 21–29.

Meloro, C. (2007) 'Plio-Pleistocene large carnivores from the Italian peninsula: functional morphology and macroecology'. Dottorato di Ricerca in Scienze della Terra, Università degli Studi di Napoli

Meloro, C. *et al.* (2008) 'The shape of the mandibular corpus in large fissiped carnivores: allometry, function and phylogeny', *Zoological Journal of the Linnean Society*. Oxford University Press, 154(4), pp. 832–845.

Meloro, C. (2011) 'Feeding habits of Plio-Pleistocene large carnivores as revealed by the mandibular geometry', *Journal of Vertebrate Paleontology*. Taylor & Francis, 31(2), pp. 428–446.

Meloro, C., Hudson, A. and Rook, L. (2015) 'Feeding habits of extant and fossil canids as determined by their skull geometry', *Journal of Zoology*. Wiley Online Library, 295(3), pp. 178–188.

Møhl, B. *et al.* (2003) 'The monopulsed nature of sperm whale clicks', *The Journal of the Acoustical Society of America*. Acoustical Society of America, 114(2), pp. 1143–1154.

Mourlam, M. J. and Orliac, M. J. (2017) 'Infrasonic and ultrasonic hearing evolved after the

emergence of modern whales', *Current Biology*. Elsevier, 27(12), pp. 1776–1781.

Park, T. *et al.* (2019) 'Convergent evolution in toothed whale cochleae', *BMC evolutionary biology*. Springer, 19(1), p. 195.

Poli, A. and Fabbri, E. (2012) *Fisiologia degli animali marini*. Edises.

Rommel, S. A., Pabst, D. A. and McLellan, W. A. (2009) 'Skull anatomy', in *Encyclopedia of marine mammals*. Second Edi. Elsevier, pp. 1033–1047.

Rossbach, K. A. and Herzing, D. L. (1997) 'Underwater observations of benthic-feeding bottlenose dolphins (*Tursiops truncatus*) near Grand Bahama Island, Bahamas', *Marine Mammal Science*. Wiley Online Library, 13(3), pp. 498–504.

Surlykke, A. *et al.* (2014) *Biosonar*. Springer.

Thewissen, J. G. M. (2014) *The walking whales: from land to water in eight million years*. Univ of California Press.

Thomason, J. (Ed.). (1997). Functional morphology in vertebrate paleontology. Cambridge University Press.

Uhen, M. D. (2004) 'Form, function, and anatomy of *Dorudon atrox* (Mammalia, Cetacea): an archaeocete from the middle to late Eocene of Egypt'. Museum of Paleontology, The University of Michigan.

Werth, A. J. (2004) 'Functional morphology of the sperm whale (*Physeter macrocephalus*) tongue, with reference to suction feeding', *Aquatic Mammals*. European Association for Aquatic Mammals, 30(3), pp. 405–418.

Werth, A. J. (2006a) 'Mandibular and dental variation and the evolution of suction feeding in Odontoceti', *Journal of Mammalogy*. American Society of Mammalogists 810 East 10th Street, PO Box 1897, Lawrence, 87(3), pp. 579–588.

Werth, A. J. (2006b) 'Odontocete suction feeding: experimental analysis of water flow and head shape', *Journal of Morphology*. Wiley Online Library, 267(12), pp. 1415–1428.

2 Chapter 2: A preliminary assessment of the accuracy of 3D models to describe skull morphological variation in toothed whales

Abstract

Scanning technologies for the generation of 3D models comprise a broad range of methods. Odontocete (toothed whale) skulls are large enough to allow comparison of different laser scanning techniques in order to assess their accuracy for subsequent analyses (e.g. landmark based morphometrics). I built 3D models of odontocete skulls for eight different species ranging from small (*Phocoena phocoena*) to medium-large size (*Globicephala* spp). To test the reliability of different scanning methods 3D models were generated for 14 specimens belonging to eight toothed whale species using Photogrammetry and a Breuckmann laser scanner. The models were subjected to subsequent landmarking in order to apply geometric morphometrics, and compare size and shape variation between specimens and techniques. In addition, landmarks were also recorded using Microscribe directly on the skull specimens to allow futher comparison with a traditional landmarking toolkit. Each cranium was landmarked multiple times to allow exploring operator digitising error from different techniques. Shape data obtained from different 3D models and microscribe were highly correlated ($r = 0.97$) and the digitising error was quite negligible explaining less than 1% of variation. Equally, shape variation between individuals was highly congruent across different scanning techniques. Both size and shape variation generated by the different techniques had a much smaller impact than variation between individuals and asymmetry. No difference was equally detectable between shape variance generated by landmark coordinates from different pair of devices. These results suggest that landmark coordinates obtained on the Odontocete skulls from 3D photogrammetry models and microscribe compare quite well with those generated from the Breuckmann laser scanner, a tool used in metrology whose accuracy can achieve good standard for medium size objects (565 mm in lenght).

2.1 Introduction

3D digitization of specimens is nowadays broadly used for scientific research (Fahlke & Hampe, 2015; Katz & Friess, 2014; Mallison & Wings, 2014; Muñoz-Muñoz, Quinto-Sánchez, & González-José, 2016; Santella & Milner, 2017). It allows the archiving, analysis and visualisation of specimens and is consequently proving to be a helpful tool for specimen preservation, education and research (Adams, Strganac, Polcyn, & Jacobs, 2010; Giacomini et al., 2019; www.nhm.ac.uk/discover/blue-whale-skeleton-3d.html). Once digitized, 3D models can be used to create online repositories (DigMorph.org, phenomene10k.org, paleo-org.com, morphosource.org; Copes, Lucas, Thostenson, Hoekstra, & Boyer, 2016) that have provided researchers free access to specimens of interest, reducing research costs (Chang & Alfaro, 2015). The growth of these digitized online sources also encourages the combination of data from different datasets. Unfortunately, this introduces error which requires evaluation (Fruciano et al., 2017; Robinson & Terhune, 2017). Assessments of how to merge datasets obtained under different methods have been investigated (Bryson et al., 2017; Dujardin, Kaba, & Henry, 2010; Evin et al., 2016; Fruciano et al., 2017; Katz & Friess, 2014; Marcy, Fruciano, Phillips, Mardon, & Weisbecker, 2018; Robinson & Terhune, 2017; Sholts, Flores, Walker, & Wärmländer, 2011; Slizewski, Friess, & Semal, 2010; Williams & Richtsmeier, 2003), and 3D models of skulls have already been used in a variety of cetacean studies (Churchill, Miguel, Beatty, Goswami, & Geisler, 2019; Coombs, Clavel, Park, Churchill, & Goswami, 2020; Fahlke & Hampe, 2015), however no study to date has assessed the error generated by different 3D models for the odontocetes (toothed whales). In this study two techniques were employed to generate 3D models of the cetacean skull: Photogrammetry (Ph), and Breuckmann laserscan (Br). Data generated from these 3D models were subsequently compared with those generated from Microscribe (M).

Photogrammetry is the technique of generating 3D models of an object from a collection of digital pictures. Ph uses the principle of *stereoscopic viewing* to allow determination of 3D information points (coordinates) from image sequences ("strip") showing the same object in different orientations (Linder, 2016). By using SIFT (Scale Invariant Feature Transforms) and RANSAC algorithms the photogrammetry software (Agisoft Photoscan is one of the commonest but many more exists: Meshroom, MicMac, 3DF Zephyr, Pix4D) recognises points belonging to the same object in different images and it merges them together in a dense cloud ("block"*)* (Mallison & Wings, 2014). It also reproduces colours (texture) of the object (Falkingham, 2012). Many authors (Evin et al., 2016; Giacomini et al., 2019; Katz & Friess,

2014; Mallison & Wings, 2014; Robinson & Terhune, 2017; Tsuboi et al., 2020; Werth, 1992; Wrobel, Biggs, & Hair, 2019) recommend photogrammetry to generate 3D models of medium size vertebrate skulls as it is very affordable, time effective (60 photographs can be taken in approximately 10 minutes), and requires only a camera and minimal equipment (tripod, remote shutter, SD cards, black velvet, turntable). Fourie et al. (2011) found that photogrammetry may perform better than 3D laserscan and it provides an acceptable and precise alternative when working also with small skull specimens (Giacomini et al., 2019; Katz & Friess, 2014; Muñoz-Muñoz et al., 2016).

Although this method was applied on a range of different mammals, it has never been tested on the cetacean skull. Interestingly, Ph is quite commonly used in the field to estimate body length and size of cetaceans (Christiansen et al., 2019; Webster, Dawson, & Slooten, 2010), and to evaluate the surface area of benthic organisms (Lavy et al., 2015).

Breuckmann laser scanners provide a high-precision semi-automated method of 3D data capture. They describe the object numerically by making an array of coordinate values for all the points that lie on the surface of the object (Bernardini & Rushmeier, 2002). This is a procedure that could also be done manually by measuring how far different points are from a reference point (the origin of a 3D coordinate), and then converting these measurements into *x, y, z* coordinates for each point on the surface (Tocheri, 2009). Coordinates are sent to the computer to create a cloud of points containing geometrical information about the object. The result is a model of the actual object, and not a replica of it. Contrasting Ph, Br is more time consuming (Wrobel et al., 2019) (depending on the size of the object and resolution it may take more than 1 hour to build a 3D model) and is not currently affordable for most researchers (€50,000 is the average cost of a laser scanner; Katz and Friess, 2014). The advantage of generating 3D models of skulls with Ph or Br is that they can be subsequently used to record anatomical points of reference (= landmarks) that mathematically describe their size and shape. These coordinates are currently analysed with geometric morphometrics toolkit. This method is based on the principles of Cartesian geometry and is statistically adequate to describe biological variation (Adams et al., 2004, 2013; Cardini and Loy, 2013).

Unlike Ph and Br, a Microscribe obtains specific located landmarks directly from the object. Landmarks are points of correspondence (with a *x*, *y*, and *z*, coordinates) on specific anatomical features. Distance between each pair of landmarks is equal to a linear measurement. Then, with a high number of landmarks we obtain a high number of measurements on the same specimen.

Differently from Photogrammetry and laserscan a 3D model will not be generated, but using Microscribe it is possible to obtain only the coordinates of the object of interest. This device uses a stylus to provide spatial coordinates data of the object to a computer. It is an accurate tool for determination of 3D coordinates (Bertsatos, Gkaniatsou, Papageorgopoulou, & Chovalopoulou, 2019; Enciso, Shaw, Neumann, & Mah, 2003; Glenzer et al., 2015; Márquez, González-José, & Bigatti, 2011; Owaydhah, Alobaidy, Alraddadi, & Soames, 2017; Stephen, Wegscheider, Nelson, & Dickey, 2015) and time effective compared to Ph and Br. It does not allow the operator to subsequently modify the landmark configuration as it does not provide points covering the entire surface. For this reason, the operator needs to be very careful as object movement will completely obstruct the creation of an accurate 3D model. Hence, it is very important to quantify the error introduced by the operator. Each technique has its pros and cons and their appropriateness is in function of the size and shape of the object.

Here, I investigate the magnitude of random measurement error (ME) introduced by combining different landmark data of toothed whale skulls obtained from three digitizing methods (Ph, Br, M). Most of the 3D studies comparing different methodologies have been conducted on small skulls ranging from 10 mm to 55 mm (Cornette, Baylac, Souter, & Herrel, 2013; Evin, Horáček, & Hulva, 2011; Giacomini et al., 2019; Linder, 2016; Marcy et al., 2018; Muñoz-Muñoz et al., 2016) by using geometric morphometrics (GMM). Here I aim to address the following questions: i) is the ME between devices small relative to the between-specimens variance? ii) How reliable is a 3D dataset which combines data from several devices?

These questions were addressed by comparing 3D morphometric data collected on 10 specimens (cranium range length from 279 mm to 616 mm) belonging to eight toothed whale species: common dolphin (*Delphinus delphis*), Risso's dolphin (*Grampus griseus*), long-finned pilot whale (*Globecephalas melas*), short-finned pilot whale (*Globicephala macrorhynchus*), false killer whale (*Pseudorca crassidens*), white-beaked dolphin (*Lagenorhynchus albirostris*) belonging to Delphinidae, harbour porpoise (*Phocoena phocoena*) belonging to Phocoenidae and beluga (*Delphinapterus leucas*) belonging to Monodontidae. By using the three devices to determine the inter-method error (Fruciano, 2016; Fruciano, 2017; Robinson & Terhune, 2017) ME was assessed quantifying the within- species and within-individual variance and the repeatability index (Fruciano, 2016) to examine the precision of the operator (DV) in digitizing 3D landmarks coordinates obtained with different devices.

2.2 Material and methods

Three subsets of toothed whale specimens were created as larger specimens (i.e. *Globicephala melas*) were not digitised using Microscribe due to limits related to the length of its mechanical arm, and depending on the availability of the specimens digised in the dataset.

Dataset-1 (n= 40 Ph and Br, coordinates replicate 2 times): *Grampus griseus* 1888-291*, Grampus griseus* A3543, *Grampus griseus* A3544, *Globicephala melas* 1983-76, *Globicephala melas* 1927-71, *Globicephala macrorhynchus* 1936-181, *Delphinapterus leucas* 1971-156, *Delphinapterus leucas* 1928-197, *Phocoena phocoena* 1982-155, *Phocoena phocoena* 1982-139.

Dataset-2 (n= 8, M and Ph): *Delphinus delphis* 1973-106, *Pseudorca crassidens* 1961-6-14-13, *Lagenorhynchus albirostris* 1921-15, *Grampus griseus* 1927-25.

Dataset-3 (n= 9, Ph, Br and M): *Grampus griseus* 1888-291*, Grampus griseus* A3543, *Grampus griseus* A3544.

The specimens were housed in the Mammifères et Oiseaux collection at Muséum National d'Histoire Naturelle, Paris (MNHN). Multiple individuals from species of different sizes were selected in order to allow investigation at the intra and interspecific scale.

2.2.1 Breuckmann laserscan -based 3D models

3D models were generated using the Breuckmann 3D surface scanner, StereoSCAN^{3D} (AICON 3D systems, Braunschweig, Germany) model with a camera resolution of 16 megapixels. This instrument has been used for a broad range of projects on musteloids skulls and fore limbs (Dumont et al., 2016; Polly, Lawing, Fabre, & Goswami, 2013). Breuckmann laserscan requires stable lighting and a dark and cool room. Data acquisition was performed using OptoCat software (AICON 3D systems, Braunschweig, Germany) system linked to an automatic rotating table. Individual skulls were scanned in two full rotations (vertically and dorsally to scan the occipital area), each of 12 steps. The 2x12 set of steps were aligned semi-automatically and, as for Ph models (below), exported as .PLY files. The scanner was calibrated before each scanning session.

2.2.2 Photogrammetric -based 3D models

3D Photogrammetry models were reconstructed from a set of photographs taken in three different orientations (ventral, dorsal, and lateral view) obtained by placing the specimen with its vertical axis parallel to the camera to photograph the occipital condyle; **Figure 2.1A**). I used a Canon EOS 1100D camera with a 12 mega-pixel resolution equipped with a standard lens (range of focal lengths: 18-55mm, all photographs were taken at 55mm). Specimens were placed vertically on a rotating table, and photographs were taken at intervals of approximatively 10 degrees. Foam rubber was placed and centrally punctured to mount the specimen vertically on the rotating table. This way, the occipital condyle was held within the rubber assuring the immobility of the specimen. In order to obtain models of considerably high quality, a set of circa 150 photos were taken of each specimen. Pictures were imported into Agisoft Phoscan Professional v. 1.3.4 (Agisoft LLC, 2016, 2018) and processed to mask out the image background or out-of-focus area by drawing an outline around the crania. Then, photos from each chunk/orientation were aligned, and the three dense point clouds that were generated (vertical, dorsal and ventral orientation) were merged together. Unlike Breuckmann, 3D models built using the photogrammetry software Agisoft need to be scaled *a posteriori* generally using linear measurements directly taken on the skull with a meter. Specimens were then scaled in Meshlab 2016.12 software (Cignoni *et al.*, 2008) by using a scale factor obtained from three skull measurements taken directly with a meter.

2.3 Microscribe -based 3D models

The Microscribe 3-dimensional digitizer (Microscribe G2X, Immersion Corp.) has a mechanical arm which supports a stylus and has an accuracy of 0.23 mm (Immersion Corp, 2013). It allows measurements to be captured with Microscribe Utility Software (MUS version 6, Revware Inc.). I digitized 3D coordinates of anatomical homologous landmarks on 10 skulls. Due to the large size of the specimens two landmarking sessions for each specimen were recorded on the crania in order to cover both dorsal and ventral part; these were then merged using DVLR (Dorsal-Ventral-Left-Right fitting, http://www.nycep.org/nmg) software.

2.4 Geometric Morphometric approach

A Three-dimensional landmark- based geometric morphometric approach (Zelditch, Swiderski, & Sheets, 2012) was subsequently employed to test the reliability, reproducibility and accuracy of the 3D data. The selected landmarks placement followed the Booksteins' criteria (Bookstein, 1991; Zelditch et al., 2012). They had to be homologous, repeatable, and needed to represent the general shape of the skull under investigation. To this aim type 1 landmarks were located in the junction of anatomical features while type 2 landmark referred to the maximum and minimum curvature of a structure (Zelditch et al., 2012). In order to analyse shape variation, 26 landmarks (**Figure 2.1**) were digitized from the same observer (DV) on each cranium i) directly on the specimens using Microscribe and ii) using Landmark editor (IDAV: Evolutionary Morphing, 2005) from 3D models made with Ph and Br. Terminology used for skull landmark description followed Mead and Fordyce (2009), and landmarks description can be found in **Table 2.1**.

The 3D landmark coordinates were Procrustes-aligned using Generalised Procrustes Analysis (**Figure 2.2**;GPA; Rohlf & Slice,1990). The Procrustes fit minimizes the sum of squared distances between landmarks from all samples to the (average) mean configuration. This procedure allows to remove all differences in size, location and orientation among the original landmark coordinates by translation, rotation and scaling to unit centroid size[1] (CS). For each specimens log transformed CS was then employed as a proxy for skull size while the coordinates obtained after GPA (Procrustes coordinates) were used as proxy for skull shape. After the Procrustes fit, the Procrustes shape coordinates were used for multivariate analyses.

---

[1] CS = The square root of the sum of the squared distances of the landmarks from the centroid, (Zelditch, Swiderski and Sheets, 2012) of the original landmarks.
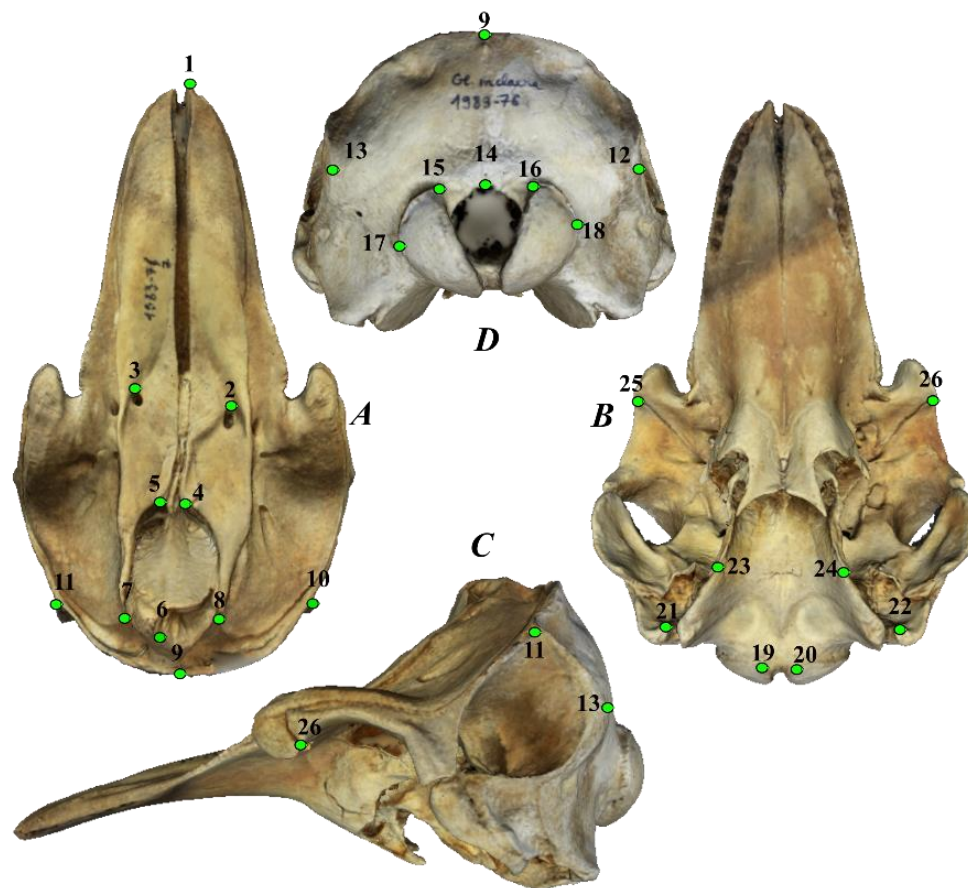
Figure 2.1 Position of 26 landmarks on Photogrammetric-based 3D models of specimen (skull of *Globicephala melas* MNHN 1989-76) in A) dorsal, B) ventral, C) lateral, and D) occipital view. See text for description.

Table 2.1 Description of landmarks taken on odontocete skulls used in GM analysis

Landmarks	Description
1	Anterior tip of the right premaxilla
2- 3	Anteriormost point of the premaxillary foramen
4- 5	Anteromedial point of the external bony nares
6	Anteriormost point of the medial suture between the nasal bones
7- 8	Sutural triple-junction between nasal, frontal and maxilla
9	External occipital protuberance
10- 11	Sutural triple-junction between supraoccipital, frontal and parietal
12- 13	Posterior most point on the temporal crest
14	*Opisthion*; middle point of the dorsal border of the *foramen magnum* on the intercondyloid notch
15- 16	Dorsal tip of the occipital condyle
17- 18	Lateral tip of the occipital condyle
19- 20	Ventral tip of the occipital condyle
21- 22	Medial tip of the paroccipital process; ventral most point of the paraoccipital process
23- 24	Suture of pterygoid and basioccipital at the junction between pharyngeal crest and basioccipital crest
25-26	Anteroventral point of the preorbital process of the frontal
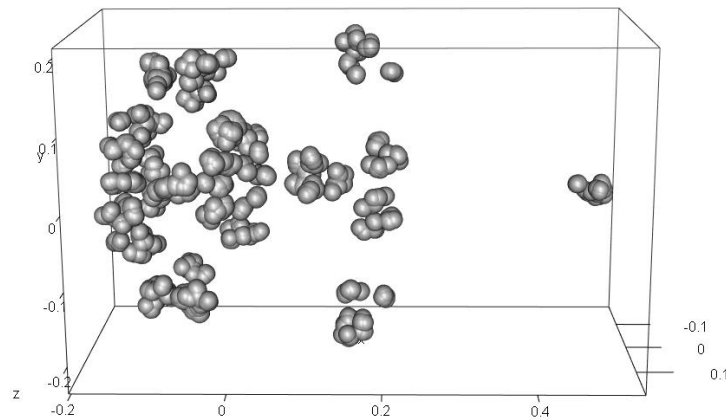
Figure 2.2 Variation in the position of the landmarks on the cranium after GPA

Dataset-1 -Procrustes ANOVA on shape variation including asymmetry

To explore the variance explained by individuals, methods, and replicas ANOVA and Procrustes ANOVA were performed on size and shape variables, respectively using MorphoJ 1.06d (Klingenberg, 2011). Procrustes ANOVA has been adapted to investigate shape variation (Klingenberg, Barluenga, & Meyer, 2002; Klingenberg & McIntyre, 1998), and it is the equivalent of the two-way ANOVA (Palmer & Strobeck, 1986) applied on the multivariate dataset of shape coordinates. Klingenberg (2002) introduced Procrustes ANOVA to test the level of asymmetry in biological obects. For object with symmetric structures, it is assumed that shape coordinates on one side should vary after GPA in the same direction and magnitude as the mirrored side. This is generally true although a small component of shape variation does not follow this expectation, hence it is quantifed as asymmetric variation. The vertebrate skull is generally symmetric although an asymmetric component occurs. This should be generally small and if landmarking is performed multiple times on the same specimens, it is likely that asymmetric variation should be comparable to variation between replicas (Error term in the ANOVA) (Fruciano et al., 2017; Marcy et al., 2018). This is because the variation in the asymmetric component is more greatly impacted by replicates/digitising error as it has smaller effect compared to variation among individuals (Fruciano, 2016; Klingenberg & Gidaszewski, 2010; Leamy & Klingenberg, 2005). Then, the impact of asymmetry and replicates on skull shape data of odontocetes was tested (Marcy et al., 2018) using Dataset-1 only . Subsequent analyses on error were based only on the skull shape symmetric component following the

formula: *3k+2l-4* (Klingenberg et al., 2002). Where *3k* is the free parameters[2] for the number of 3D landmarks used and *l* is the free parameter for the unpaired landmarks. This method uses information from all landmarks to determine the symmetry plane. This computation was carried out automatically in MorphoJ.

Dataset-1-Measurement error: repeatability

Landmark recording was taken twice in four different sessions on 10 individuals (for Br and Ph-Dataset-1) for quantifying the repeatability (Fruciano, 2016), and digitizing ability of the operator (DV). To explore the variance explained by methods (Ph and Br), a Procrustes ANOVA was performed on shape in R, using the function "rep_ability" published in Marcy et al. (2018). This test is based on assessing the same name to each individual belonging to the same specimen specifying which replicate they are (i.e., specimen1 rep1 +specimen1 rep2), so that the replicates are added as an error variable. Then, the percentage of measurement error was calculated by looking at Mean Square (MS) values following the formula below (Fruciano, 2016; Sherratt, 2015):

$$\text{R} = \frac{S^2A = \left(\text{MS}among - \dfrac{\text{MS}within}{2}\right)}{(\text{MS}within + S^2A)}$$

R is the value of repeatability or intraclass correlation coefficient and varies between (0-1), and S^2A is the among-individuals squared variance component. To find S^2A, the MS of the replicas term was subtracted from the individual term and divided by two, that is the number of the replicas. A ratio is then computed by dividing the MS of the replicas terms by the total MS. This computation was also carried out automatically by the "rep_ability" function (Marcy et al., 2018) in R.

---

[2] The free parameter is a mathematical variable that changes depending on the number of landamarks used in the analyses.

Analyses on Dataset-1-2-3

Due to the lack of replicates data for Microscribe, it was not possible to determine the repeatability for Dataset 2 and Dataset 3. ANOVA and Procrustes ANOVA were generally applied to test for differences in CS and shape datasets between methods.

Successively, to examine the pattern of shape variation, a matrix of variance-covariance of individuals shape was created and a PCA on symmetric components of shape was run in R (R Team, 2015). This allows visualization of how the same specimens (from three different methods) were distributed in the morphospace, portrays random (greater spread of device method compare to another) and systematic errors (repeated pattern of one device shifting to another (Marcy et al., 2018), and can reveal misplaced or inaccurate landmarks (Fruciano, 2016; Bastir et al. 2006).

Symmetric component shape matrices obtained from each pair of datasets (Ph-Br, M-Ph, M-Ph-Br) were compared using Mantel's test (Mantel, 1967) in MorphoJ v1.06d (Klingenberg, 2011). This tests the correlation between two matrices, with significance determined by randomization.

Euclidean distances between configurations in PC shape space (Symmetric component) for 3 Datasets were exported from MorphoJ (Klingenberg, 2011) and imported into PAST 2.17 (Hammer, Harper, & Ryan, 2001) to allow similarity of the three methods to be portrayed using the Unweighted Pair Group Method with Arithmetic mean (UPGMA) (Cardini, 2014).

Additionally, morphological disparity (also known as Procrustes variance) was computed for each shape dataset and a permutational procedure, implemented in the package *geomorph*, to test for differences in disparity between Individual/techniques. The pariwise disparity test was applied on the shape coordinates generated from the following pair of datasets: 1) Br-Ph and 2) Ph-M, and 3) M-Ph-Br (Marcy et al., 2018). In this way, the Procrustes variance reflects only variation due to digitization error between methods. This function calculates the Procrustes Variance for both individual and method as the sum of diagonal elements of the covariance matrix divided by the number of observations (Adams et al., 2016; Zelditch et al., 2012). The test performs multiple iterations (default is 999) in order to compare variance distribution for each group of interest. The distribution of iterated variances was showed using

boxplot and the significance of differences between groups tested with Kruskal-Wallis against the null hypothesis of difference between means of Procrustes variance for each dataset.

2.5 Results

PCA on symmetric component for all the datasets

PCA computed on the symmetric component of shape revealed that most of the specimens of the whole sample cluster together regardless of the method (**Figure 2.3**). This result is supported by Procrustes ANOVA (see next section). The fourteen specimens are well-grouped on the plot of PC1 and PC2, which explain respectively 37.8% and 20.2% of variance for the entire dataset. PC3 accounts for 11% and remaining PCs account for 4% or less of the total variation. On PC1 positive scores the harbour porpoise specimens cluster together and are characterised by a relatively short and narrow rostrum and enlarged braincase. Landmarks on the temporal fossa are displaced towards each other, compressing the area and resulting in a higher and longer temporal region. PC1 negatives scores relate with a widening of the rostrum, a more ventral orientation of the foramen magnum, and a wider and shorter temporal area. The post rostral skull is compressed with expansion and a more concave profile of the facial region, which is exhibited by members of the genus *Globicephala*. In specimens GgA3544 and Gm1983-76 the PCA score for just one Breuckmann replica showed higher scores, and in Pp1982-155 it showed lower score on PC1.

PC2 describes changes relative to the width and the height of the skull. On positive scores landmarks on the right and left sides of the occipital condyle and on the opisthion diverge from each other's resulting in a wider foramen magnum. The latter is more ventrally orientated, and the braincase is laterally compressed. On PC2 negative scores the nasal region is narrower and smaller and moved leftwards in *Delphinapterus leucas* specimens resulting in a more marked asymmetry of the skull. On negative PC2 scores *Globicephala* specimens and *Phocoena* exhibit a relatively shrinking of the occipital region but wider area for the temporal fossa and transversely wider zygomatic region.
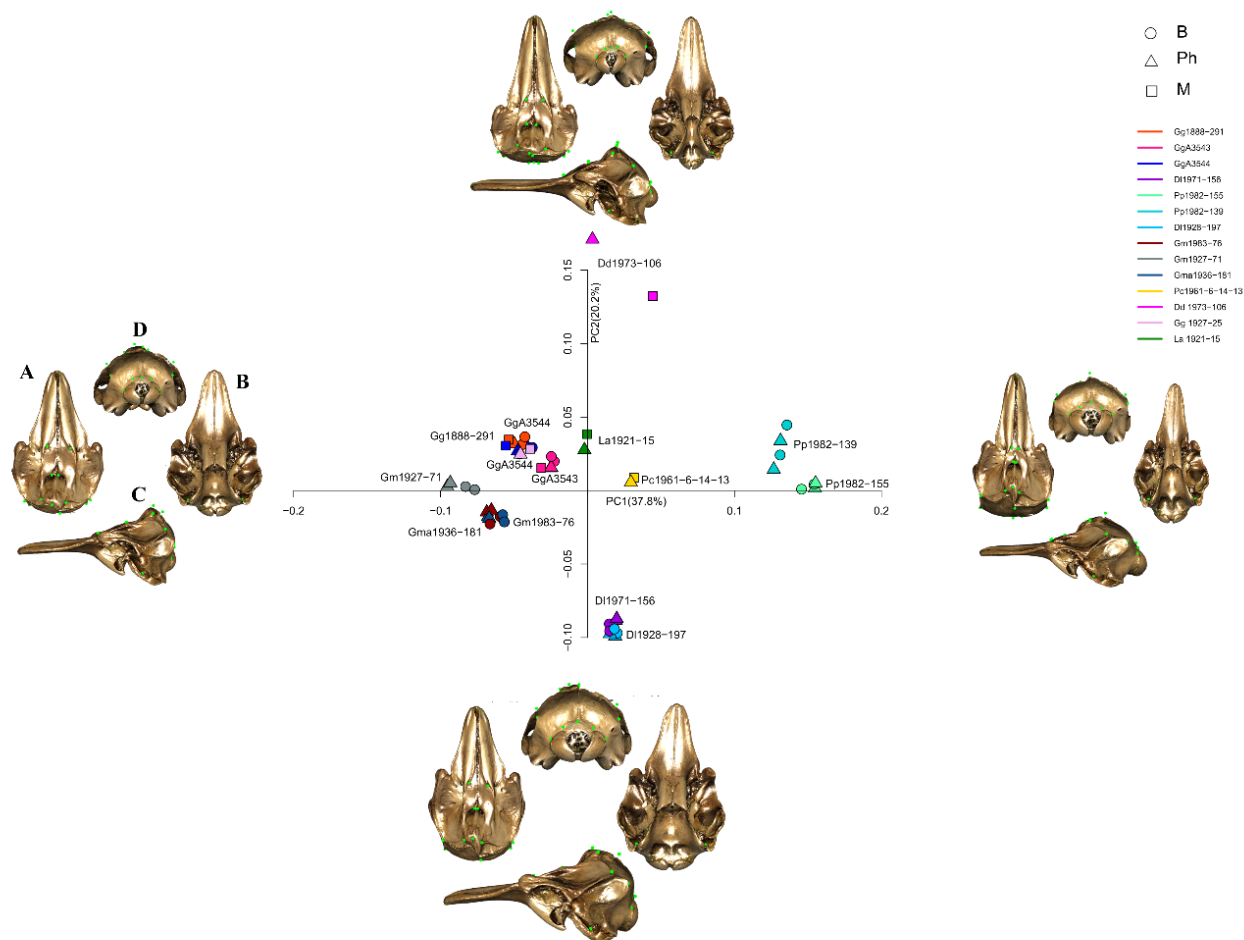
Figure 2.3 PCA: PC1 versus PC2 plot of Symmetric component shape variation. Shape changes are shown by 3D warping Gg1927-25 (NHM) specimen representing shape changes in a) dorsal b) ventral c) lateral and d) occipital view at their respective position on the axes. Each axis reports the total variance explained by that principal component.

Dataset-1

Procrustes ANOVA using asymmetric component

Procrustes ANOVA (**Table 2.2**) showed that shape variation among individuals contributes the most to total variance (**Table 2.2 A**), and the shape variance due to directional asymmetry (Side or DA) accounts for more than residuals or digitization error (Rep). The same analysis applied separately on the methods dataset confirms the presence of a very small or null random landmarking error between two methods (**Table 2.2 B-C**). For both datasets the error term is very small or null, also the individual variation shows similar contributions (Ph-Rsq=0.83; Br-Rsq=0.82).

Table 2.2 Procrustes ANOVA on shape variation on Dataset 1 including asymmetric component. The Rsq of variation explains the contribution of each factor to overall variation.

A) All Specimens_Ph-Br and Rep

	df	SS	MS	Rsq	F	P
Individual	333	0.42644	0.00128	0.81396	16.79	<0.0001
Side	34	0.05075	0.00149	0.09687	19.57	<0.0001
Ind*Side	306	0.02333	7.63E-05	0.04454	4.64	<0.0001
Method	710	0.01166	1.64E-05	0.02226	1.99	<0.0001
Res-Rep	1420	0.01170	8.25E-06	0.02234		
Total		0.52391		1		

B) Only Ph specimens and Rep

	df	SS	MS	Rsq	F	P
Individual	333	0.21974	0.00066	0.83491	15.96	<0.0001
Ind*Side	34	0.02629	0.00077	0.09989	18.71	<0.0001
Method	306	0.01264	4.13E-05	0.04805	6.51	<0.0001
Res-Rep	710	0.00451	6.35E-06	0.01713		
Total		0.26319				

C) Only Br specimens and Rep

	df	SS	MS	Rsq	F	P
Individual	333	0.21344	0.00064	0.82415	14.42	<0.0001
Ind*Side	34	0.02474	0.00072	0.09553	16.38	<0.0001
Method	306	0.01359	4.44E-05	0.05250	4.38	<0.0001
Res-Rep	710	0.00720	1.01E-05	0.02780		
Total		0.25898				

Measurement error: repeatability (R)

To test how different methods can impact repeatability, the repeatability index (R) was computed for the Br and Ph datasets, separately (**Table 2.3**). Procrustes ANOVA showed that most of the shape variance was explained by individuals ($R^2= 0.98$). Repeatability index (R) of shape was slightly higher for the dataset with Ph specimens (Br-R = 0.944; Ph-R = 0.965).

Table 2.3 Procrustes ANOVA on shape variation on Dataset1 including asymmetric component. The R index indicates the repeatability between replicas within each device.

A) Ph

	Df	SS	MS	Rsq	F	Z	Pr(>F)	R
ind	9	0.24431	0.02714	0.98083	56.87142	10.73317	0.001	**0.965**
Res	10	0.00477	0.00047	0.01916				
Total	19	0.24908						

B) Br

	Df	SS	MS	Rsq	F	Z	Pr(>F)	R
ind	9	0.23817	0.02646	0.96926	35.03663	10.12093	0.001	**0.944**
Res	10	0.00755	0.00075	0.03073				
Total	19	0.24572						

A Mantel test between symmetric components of shape obtained from the two methods (Ph and Br) replicates was significant and resulted into a high r value (R=0.97, P < 0.001), which confirmed that matrices are positively associated and the difference between replicates can be considered negligible.

Procrustes ANOVA using symmetric component

Procrustes ANOVA on symmetric component of shape (**Table 2.4A**) confirmed individual shape variation to be the most significant factor when comparing data from different methods (Rsq= 0.96). Difference between scan devices contributes 3.4% of the variance, suggesting minor systematic error.

A similar result by running ANOVA on log transformed CS (**Table 2.4A**). No presence of systematic errors was found, nor differences between methods (P=0.459).

Dataset-2

Procrustes ANOVA on just symmetric component of shape (**Table 2.4B**) supported most of the shape variance due to individual shape variation (Rsq= 0.87). Difference between scan devices accounted for 3.6% of the variance, and this factorwas not significant (P=0.4320).

Same applied to CS (**Table 2.4B**). Differences between methods were not found (P=0.837).

Dataset-3

Procrustes ANOVA on just symmetric component of shape (**Table 2.4 C**) showed again that most of the variance was due to individual shape variation (Rsq= 0.75). Difference between scan devices accounts for 3.4% of the variance and is significant (P=0.041). This suggests some systematic error although it is very small (Rsq=0.1%).

Similar results were obtained by running a Procrustes ANOVA on CS (**Table 2.4C**). Most of the variance was explained by Individuals (Rsq=0.97) and no difference between methods was found (P=0.368).

Table 2.4 Procrustes ANOVA on symmetric shape component and CS within methods for each dataset.

A) Dataset-1

Shape	Df	SS	MS	Rsq	F	Z	Pr(>F)
Ind	9	0.43395	0.04821	0.96171	90.4175	14.3102	**0.001**
Method	1	0.00181	0.00181	0.00402	3.3989	3.0075	**0.001**
Res	29	0.01546	0.00053	0.03427			
CS	**Df**	**SS**	**MS**	**Rsq**	**F**	**Z**	**Pr(>F)**
Ind	9	1051688	116854	0.99832	1952.534	12.8546	**0.001**
Method	1	33	33	0.00003	0.5491	0.2938	0.459
Res	29	1736	60	0.00165			

B) Dataset-2

Shape	Df	SS	MS	Rsq	F	Z	Pr(>F)
Ind	3	0.09941	0.03313	0.87084	9.4154	3.8475	**0.0055**
Method	1	0.00418	0.00418	0.03666	1.1892		0.432
Res	3	0.01055	0.00352	0.09249			
CS	**Df**	**SS**	**MS**	**Rsq**	**F**	**Z**	**Pr(>F)**
Ind	3	157758	52586	0.99894	941.8204	3.0135	**0.018**
Method	1	0	0	0	0.0048		0.837
Res	3	168	56	0.00106			

C) Dataset-3

Shape	Df	SS	MS	Rsq	F	Z	Pr(>F)
Ind	2	0.01465	0.00732	0.75173	17.3863	4.2351	**0.001**
Method	2	0.00315	0.00157	0.1618	3.7421		**0.041**
Res	4	0.00168	0.00042	0.08647			
CS	**Df**	**SS**	**MS**	**Rsq**	**F**	**Z**	**Pr(>F)**
Ind	2	8572.3	4286.1	0.97418	128.0623	2.9644	**0.003**
Method	2	93.4	46.7	0.01061	1.3946	0.368	
Res	4	133.9	33.5	0.01521			

UPGMA based on Euclidean distances of the symmetric component matrix (**Figure 2.4**) showed that the individuals built with different methods cluster together, confirming previous results obtained with PCA and Procrustes ANOVA.

Procrustes variance Dataset1-2-3on all datasets

No difference could be found between devices pairs in Dataset1-2 and 3 for the mean of Procrustes variance (Dataset1= B Proc Var mean = 1.2×10^{-2}, Ph ProcVar mean = 1.2×10^{-2}; Kruskal- Wallis test *P= 0.85*; Dataset2= Kruskal- Wallis test *P=1*; Dataset3=Kruskal- Wallis test *P=0.73;* **Figure 2.5**) which is consistent with previous analyses.
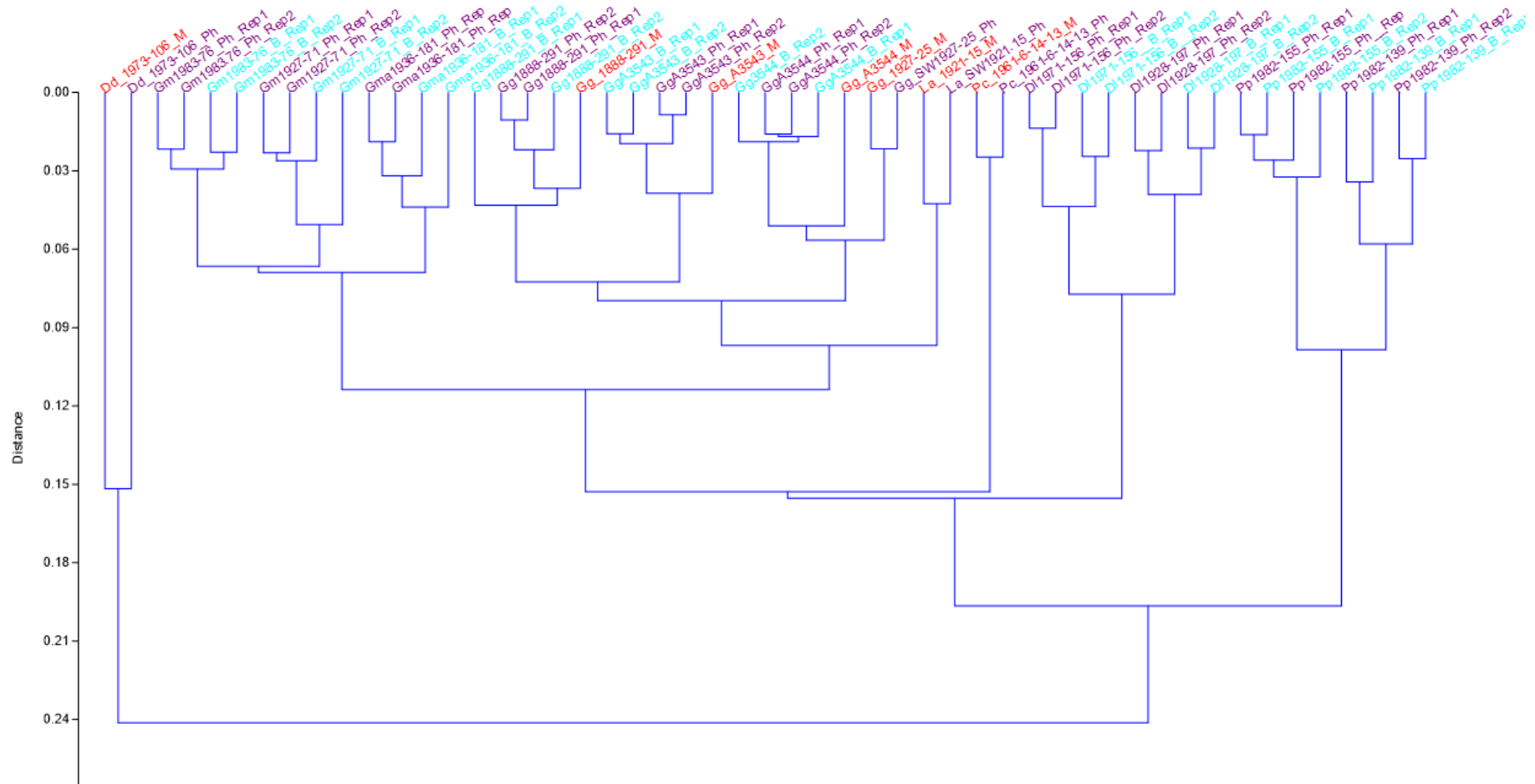
Figure 2.4 Phenogram (UPGMA) illustrating Euclidean distances of Symmetric Component after superimposition. Different models for a single specimen cluster together and it is identified by individual, device (Ph=violet, Br=light blue, M=red) and replicates (Rep1, Rep2).

Dataset-1
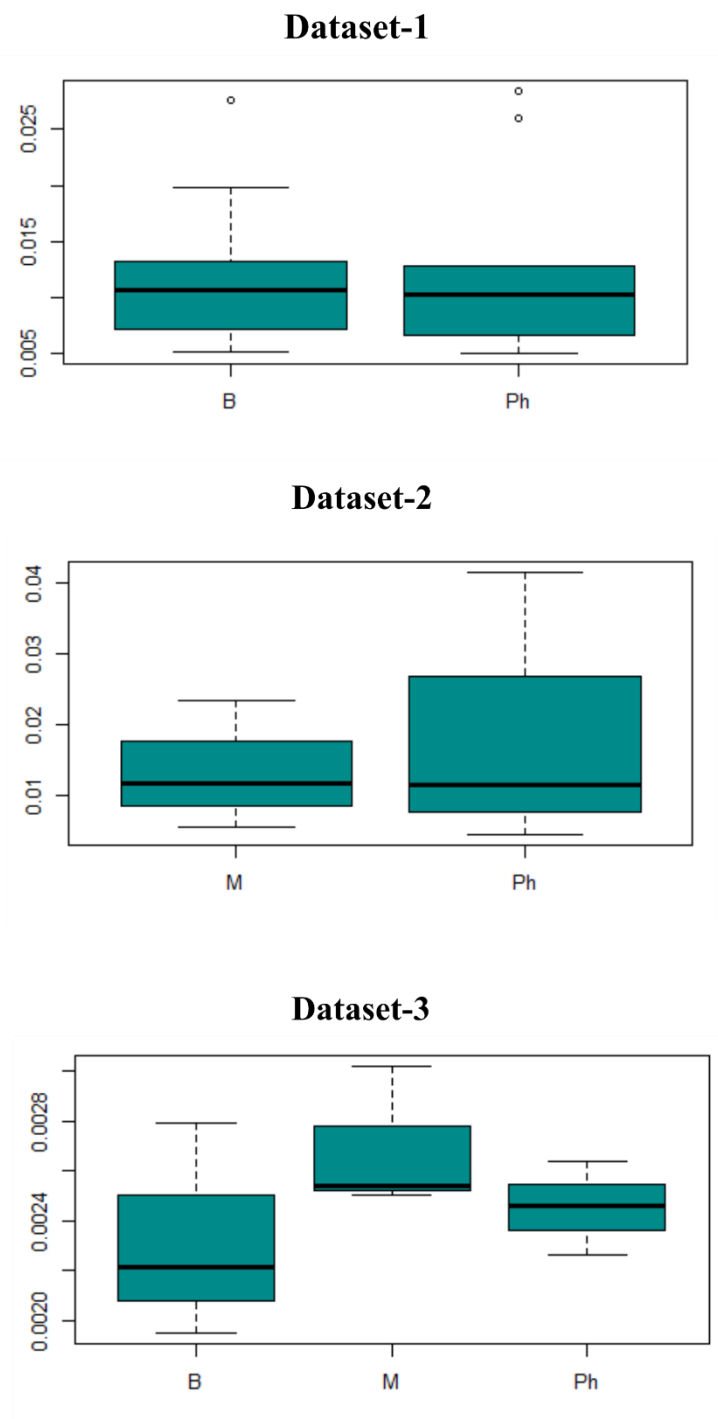
Dataset-2

Dataset-3

Figure 2.5 Morphological Disparity or Procrustes variance on symmetric shape variation of Dataset-1, Dataset-2, and Dataset-3.

2.6   Discussion and Conclusion

Photogrammetry is an increasingly popular technique for the elaboration of 3D models although previous studies (Fruciano et al., 2017; Robinson & Terhune, 2017) recommend caution when merging 3D models generated with photogrammetry with those generated using other devices. For the first time, I tested the accuracy of Photogrammetry (Ph) relative to Breuckmann laserscan (Br) and Microscribe (M) on a diverse sample of toothed whale (odontocete) skulls. The data clearly showed that the amount of error generated by each technique on geometric morphometrics data is minimum and quite comparable to previous approaches (Evin et al., 2016; Katz & Friess, 2014).

ANOVA and Procrustes ANOVA models suggest that on a macroevolutionary scale when merging data from different methods, the biological variation in size and shape obscures the measurement error between methods. Photogrammetric based 3D models showed a slightly higher repeatability in landmarking with a R score of 0.965 compared with the repeatability of 0.944 obtained from models built with Breuckmann laser scan. This result can be due to the presence of texture colour in photogrammetric based models in contrast to the laser scanned 3D models. Indeed, texture can help in detecting sutures and improving landmark placement on the skull surface. Similar coefficients have been found for bats (0.97, 0.99, Giacomini et al., 2019), kangaroo skulls (0.95, Fruciano *et al.*, 2017), and human skulls (0.99, 0.99 Badawi-Fayad & Cabanis, 2007). In accordance with Giacomini et al. (2019), there was no great difference between Ph and Br (Dataset1). PC1 scores differences in GgA3544 and Gm1983-76 were probably due to a random error, and they were also detected when calculating the R score between methods in Dataset1. Despite these small random differences, in the UPGMA tree, methods and individuals clustered together assuring the reproducibility of the shape for the three devices.

In conclusion, Ph is well suited for the reconstruction of toothed whale skulls (Fahlke & Hampe, 2015), and data obtained from Ph can eventually be combined with data from other techniques due to its similar performance in repeatability and accuracy. The landmark configuration used in this study covered only main cranial anatomical features, however if teeth are also of interest Ph can eventually be implemented. As technology advances, resolution is improving for handheld scanners and different techniques (i.e. photo stacking) also appear that can increase the resolution of images for very small objects (Brecko et al., 2014; Santella & Milner, 2017).

References

Adams, D. C., Rohlf, F. J., & Slice, D. E. (2004). Geometric morphometrics: ten years of progress following the 'revolution'. Italian Journal of Zoology, 71(1), 5-16.

Adams, D. C., Rohlf, F. J., & Slice, D. E. (2013). A field comes of age: geometric morphometrics in the 21st century. Hystrix, 24(1), 7.

Adams, D. C. et al. (2016) 'Geomorph: Software for geometric morphometric analyses'. Comprehensive R Archive Network.

Adams, T. L. et al. (2010) 'High resolution three-dimensional laser-scanning of the type specimen of *Eubrontes glenrosensis* Shuler, 1935, from the Comanchean (Lower Cretaceous) of Texas: implications for digital archiving and preservation', *Palaeontologia Electronica*, 13(3), p. 11.

Agisoft LLC (2016) 'Agisoft PhotoScan User Manual', *Professional Edition, Version 0.9.0*. doi: 10.1080/00220671.2013.836468.

Agisoft LLC (2018) 'Agisoft PhotoScan', *Professional Edition, Version 1.2*. doi: 10.1016/j.jss.2015.07.002.

Badawi-Fayad, J. and Cabanis, E. (2007) 'Three-dimensional procrustes analysis of modern human craniofacial form', *The Anatomical Record: Advances in Integrative Anatomy and Evolutionary Biology: Advances in Integrative Anatomy and Evolutionary Biology*. Wiley Online Library, 290(3), pp. 268–276.

Bernardini, F. and Rushmeier, H. (2002) 'The 3D model acquisition pipeline', in *Computer graphics forum*. Wiley Online Library, pp. 149–172.

Bertsatos, A. *et al.* (2019) '" What and how should we share?" An inter-method inter-observer comparison of measurement error with landmark-based craniometric datasets.', *Anthropologischer Anzeiger; Bericht uber die biologisch-anthropologische Literatur*.

Brecko, J. *et al.* (2014) 'Focus stacking: Comparing commercial top-end set-ups with a semi-automatic low budget approach. A possible solution for mass digitization of type specimens', *ZooKeys*. Pensoft Publishers, (464), p. 1.

Bryson, M. *et al.* (2017) 'Characterization of measurement errors using structure-from-motion and photogrammetry to measure marine habitat structural complexity', *Ecology and Evolution*.

Wiley Online Library, 7(15), pp. 5669–5681.

Cardini, A. L., & Loy, A. (2013). On growth and form in the" computer era": from geometric to biological morphometrics. Hystrix, 24: 1-5.

Cardini, A. (2014) 'Missing the third dimension in geometric morphometrics: how to assess if 2D images really are a good proxy for 3D structures?', *Hystrix, the Italian Journal of Mammalogy*, 25(2), pp. 73–81.

Chang, J. and Alfaro, M. E. (2015) 'Crowdsourced geometric morphometrics enable rapid large-scale collection and analysis of phenotypic data', *BioRxiv*. Cold Spring Harbor Laboratory, p. 23382.

Christiansen, F. *et al.* (2019) 'Estimating body mass of free-living whales using aerial photogrammetry and 3D volumetrics', *Methods in Ecology and Evolution*. Wiley Online Library, 10(12), pp. 2034–2044.

Churchill, M. *et al.* (2019) 'Asymmetry drives modularity of the skull in the common dolphin (Delphinus delphis)', *Biological Journal of the Linnean Society*. Oxford University Press UK, 126(2), pp. 225–239.

Cignoni, P. *et al.* (2008) 'MeshLab: an open-source mesh processing tool', *Eurographics Italian Chapter Conference*. doi: 10.2312/LocalChapterEvents/ItalChap/ItalianChapConf2008/129-136.

Cignoni, P., Corsini, M. and Ranzuglia, G. (2008) 'MeshLab: an open-source 3D mesh processing system', *ERCIM News*. doi: 10.2312/LocalChapterEvents/ItalChap/ItalianChapConf2008/129-136.

Coombs, E. J. *et al.* (2020) 'Wonky whales: the evolution of cranial asymmetry in cetaceans', *BMC biology*. BioMed Central, 18(1), pp. 1–24.

Cornette, R. *et al.* (2013) 'Does shape co-variation between the skull and the mandible have functional consequences? A 3D approach for a 3D problem', *Journal of anatomy*. Wiley Online Library, 223(4), pp. 329–336.

Cozzi, B., Huggenberger, S. and Oelschläger, H. A. (2016) *Anatomy of dolphins: insights into body structure and function*. Academic Press.

Dujardin, J.-P. A. L., Kaba, D. and Henry, A. B. (2010) 'The exchangeability of shape', *BMC*

research notes. Springer, 3(1), p. 266.

Dumont, M. *et al.* (2016) 'Do functional demands associated with locomotor habitat, diet, and activity pattern drive skull shape evolution in musteloid carnivorans?', *Biological Journal of the Linnean Society*. Oxford University Press, 117(4), pp. 858–878.

Enciso, R. *et al.* (2003) 'Three-dimensional head anthropometric analysis', in *Medical Imaging 2003: Visualization, Image-Guided Procedures, and Display*. International Society for Optics and Photonics, pp. 590–597.

Evin, A. *et al.* (2016) 'The use of close-range photogrammetry in zooarchaeology: Creating accurate 3D models of wolf crania to study dog domestication', *Journal of Archaeological Science: Reports*. Elsevier, 9, pp. 87–93.

Evin, A., Horáček, I. and Hulva, P. (2011) 'Phenotypic diversification and island evolution of pipistrelle bats (Pipistrellus pipistrellus group) in the Mediterranean region inferred from geometric morphometrics and molecular phylogenetics', *Journal of Biogeography*. Wiley Online Library, 38(11), pp. 2091–2105.

Fahlke, J. M. and Hampe, O. (2015) 'Cranial symmetry in baleen whales (Cetacea, Mysticeti) and the occurrence of cranial asymmetry throughout cetacean evolution', *The Science of Nature*. Springer, 102(9–10), p. 58.

Falkingham, P. L. (2012) 'Acquisition of high resolution three-dimensional models using free, open-source, photogrammetric software', *Palaeontologia electronica*, 15(1), p. 15.

Fruciano, C. (2016) 'Measurement error in geometric morphometrics', *Development genes and evolution*. Springer, 226(3), pp. 139–158.

Fruciano, C. *et al.* (2017) 'Sharing is caring? Measurement error and the issues arising from combining 3D morphometric datasets', *Ecology and evolution*. Wiley Online Library, 7(17), pp. 7034–7046.

Galatius, A. and Goodall, R. N. P. (2016) 'Skull shapes of the Lissodelphininae: radiation, adaptation and asymmetry', *Journal of morphology*. Wiley Online Library, 277(6), pp. 776–785.

Giacomini, G. *et al.* (2019) '3D Photogrammetry of Bat Skulls: Perspectives for Macro-evolutionary Analyses', *Evolutionary Biology*. Springer, 46(3), pp. 249–259.

Glenzer, R. R. *et al.* (2015) 'Comparing morphometric methods in Macaca mulatta crania'. University of Oregon Libraries.

Hammer, Ø., Harper, D. A. and Ryan, D. D. (2001) 'PAST: PALEONTOLOGICAL STATISTICS SOFTWARE PACKAGE FOR EDUCATION AND DATA ANALYSIS', *Palaeontologia Electronica 178kb. T. Harper. Geological Museum*. doi: 10.1016/j.bcp.2008.05.025.

Katz, D. and Friess, M. (2014) '3D from standard digital photography of human crania—a preliminary assessment', *American Journal of Physical Anthropology*. Wiley Online Library, 154(1), pp. 152–158.

Klingenberg, C. P. (2011) 'MorphoJ: An integrated software package for geometric morphometrics', *Molecular Ecology Resources*. doi: 10.1111/j.1755-0998.2010.02924.x.

Klingenberg, C. P., Barluenga, M. and Meyer, A. (2002) 'Shape analysis of symmetric structures: quantifying variation among individuals and asymmetry', *Evolution*. Wiley Online Library, 56(10), pp. 1909–1920.

Klingenberg, C. P. and Gidaszewski, N. A. (2010) 'Testing and quantifying phylogenetic signals and homoplasy in morphometric data', *Systematic biology*. Oxford University Press, 59(3), pp. 245–261.

Klingenberg, C. P. and McIntyre, G. S. (1998) 'Geometric morphometrics of developmental instability: analyzing patterns of fluctuating asymmetry with Procrustes methods', *Evolution*. Wiley Online Library, 52(5), pp. 1363–1375.

Lavy, A. *et al.* (2015) 'A quick, easy and non-intrusive method for underwater volume and surface area evaluation of benthic organisms by 3D computer modelling', *Methods in Ecology and Evolution*. Wiley Online Library, 6(5), pp. 521–531.

Leamy, L. J. and Klingenberg, C. P. (2005) 'The genetics and evolution of fluctuating asymmetry', *Annu. Rev. Ecol. Evol. Syst.* Annual Reviews, 36, pp. 1–21.

Linder, W. (2016) *Introduction. In: Digital Photogrammetry.* Springer, Berlin, Heidelberg. Available at: https://link.springer.com/content/pdf/10.1007/978-3-540-92725-9.pdf.

Mallison, H. and Wings, O. (2014) 'Photogrammetry in paleontology-a practical guide', *Journal of Paleontological Techniques*, 12, pp. 1–31. Available at: http://creativecommons.org/licenses/by-sa/3.0/.www.jpaleontologicaltechniques.org

(Accessed: 22 February 2019).

Mantel, N. (1967) 'The detection of disease clustering and a generalized regression approach', *Cancer research*. AACR, 27(2 Part 1), pp. 209–220.

Marcy, A. E. *et al.* (2018) 'Low resolution scans can provide a sufficiently accurate, cost-and time-effective alternative to high resolution scans for 3D shape analyses', *PeerJ*. PeerJ Inc., 6, p. e5032.

Márquez, F., González-José, R. and Bigatti, G. (2011) 'Combined methods to detect pollution effects on shell shape and structure in Neogastropods', *Ecological Indicators*. Elsevier, 11(2), pp. 248–254.

Muñoz-Muñoz, F., Quinto-Sánchez, M. and González-José, R. (2016) 'Photogrammetry: a useful tool for three-dimensional morphometric analysis of small mammals', *Journal of Zoological Systematics and Evolutionary Research*. Wiley Online Library, 54(4), pp. 318–325.

Owaydhah, W. H. et al. (2017) 'Three-dimensional analysis of the proximal humeral and glenoid geometry using MicroScribe 3D digitizer', *Surgical and Radiologic Anatomy*. Springer, 39(7), pp. 767–772.

P. Cignoni, M. Callieri, M. Corsini, M. Dellepiane, F. Ganovelli, G. R. (2008) 'MeshLab', *MeshLab: an Open-Source Mesh Processing Tool*. doi: 10.1109/TVCG.2012.34.

Palmer, A. R. and Strobeck, C. (1986) 'Fluctuating asymmetry: measurement, analysis, patterns', *Annual review of Ecology and Systematics*. Annual Reviews 4139 El Camino Way, PO Box 10139, Palo Alto, CA 94303-0139, USA, 17(1), pp. 391–421.

Polly, P. D. et al. (2013) 'Phylogenetic principal components analysis and geometric morphometrics', *Hystrix, the Italian Journal of Mammalogy*. Associazione Teriologica Italiana, 24(1), pp. 33–41.

Robinson, C. and Terhune, C. E. (2017) 'Error in geometric morphometric data collection: Combining data from multiple sources', *American journal of physical anthropology*. Wiley Online Library, 164(1), pp. 62–75.

Santella, M. and Milner, A. R. (2017) 'Coupling focus stacking with photogrammetry to illustrate small fossil teeth', *Journal of Paleontological Techniques*, 18, pp. 1–17.

Sherratt, E. (2015) *Tips & Tricks 8: Examining Replicate Error | R-bloggers*. Available

at: https://www.r-bloggers.com/tips-tricks-8-examining-replicate-error/ (Accessed: 19 February 2019).

Sholts, S. B. et al. (2011) 'Comparison of coordinate measurement precision of different landmark types on human crania using a 3D laser scanner and a 3D digitiser: implications for applications of digital morphometrics', *International Journal of Osteoarchaeology*. Wiley Online Library, 21(5), pp. 535–543.

Slizewski, A., Friess, M. and Semal, P. (2010) 'Surface scanning of anthropological specimens: nominal-actual comparison with low cost laser scanner and high end fringe light projection surface scanning systems', *Quartär*, 57, pp. 179–187.

Stephen, A. J. *et al.* (2015) 'Quantifying the precision and accuracy of the MicroScribe G2X three-dimensional digitizer', *Digital Applications in Archaeology and Cultural Heritage*. Elsevier, 2(1), pp. 28–33.

Team, Rs. (2015) 'RStudio: Integrated Development for R', *[Online] RStudio, Inc., Boston, MA URL http://www. rstudio. com*. doi: https://www.nrel.gov/docs/fy16osti/65298.pdf.

Tocheri, M. W. (2009) 'Laser scanning: 3D analysis of biological surfaces', in *Advanced imaging in biology and medicine*. Springer, pp. 85–101.

Tsuboi, M. *et al.* (2020) 'Measuring Complex Morphological Traits with 3D Photogrammetry: A Case Study with Deer Antlers', *Evolutionary Biology*. Springer, pp. 1–12.

Webster, T., Dawson, S. and Slooten, E. (2010) 'A simple laser photogrammetry technique for measuring Hector's dolphins (*Cephalorhynchus hectori*) in the field', *Marine mammal science*. Wiley Online Library, 26(2), pp. 296–308.

Werth, A. J. (1992) 'Anatomy and evolution of odontocete suction feeding: Cambridge, Massachusetts, Harvard University'. Doctoral Thesis.

Williams, F. L. and Richtsmeier, J. T. (2003) 'Comparison of mandibular landmarks from computed tomography and 3D digitizer data', *Clinical Anatomy: The Official Journal of the American Association of Clinical Anatomists and the British Association of Clinical Anatomists*. Wiley Online Library, 16(6), pp. 494–500.

Wrobel, G. D., Biggs, J. A. and Hair, A. L. (2019) 'Digital modeling for bioarchaeologists', *Advances in Archaeological Practice*. Cambridge University Press, 7(1), pp. 47–54.

Zelditch, M. L., Swiderski, D. L. and Sheets, H. D. (2012) *Geometric morphometrics for biologists: a primer*. Academic Press.

3 Chapter 3: Ecomorphology of odontocetes as revealed by 3D geometry of the cranium

Abstract

Extant odontocetes (toothed whales) exhibit differences in feeding strategies, body and brain size, diving adaptations, biosonar mode, and waters they inhabit. Strong selective pressures associated with these factors have likely contributed to the morphological diversification of the odontocete skull. Here, I use a geometric morphometric data of the crania of 60 (out of about 72) extant odontocete species and a well-supported phylogenetic tree to test wether cranial size and shape variation can be associated with ecological adaptations. Odontocete's cranial morphology exhibited a significant phylogenetic signal, which was much stronger in size rather than shape. After accounting for phylogeny, significant associations were detected between cranial size and biosonar mode, body length, brain and body mass, maximum and minimum prey size, and maximum peak frequency. Brain mass was also correlated with cranial shape. When asymmetric and symmetric components of shape were analysed separately, a significant correlation occurred between superficial sea water temperature and both cranial symmetry and asymmetry, and between diving ecology and asymmetry**.** After removing the two landmarks on the front tip of the rostrum (those responsible of the Pinocchio effect), the significant effect of superficial sea temperature, on both symmetric and asymmetric shape components was still detectable, as well as association between diving ecology, brain mass and symmetric shape component. Degree of cranial asymmetry (FA scores) was found to be correlated with body mass and EQ. Cranial shape variation of odontocets was strongly influenced by evolutionary allometry and most of the association with ecological parameters could not be identified after phylogenetic correction. This suggests that ecomorphological feeding adaptations occur within major odontocete families, and functional anatomical patterns across Odontocete clades are canalised by size constraints.

3.1 Introduction

Cetaceans are a of monophyletic group aquatic mammals characterised by a deep functional and taxonomical dichotomy: the division in Odontocetes (= toothed whales) and Mysticetes (= baleen whale). Odontocetes diverged from their sister-group, about 34 Mya (Marx, Lambert, & Uhen, 2016) and this suborder contains 10 extant families, including at least 72 species and 33 genera, with the Delphinidae and Ziphiidae showing the largest number of species (Hooker, 2009). Compared to Mysticetes this group displays wide variation in body size and skull morphology related to feeding ecology (Cozzi et al. , 2016; Werth, 1992; Werth, 2006). Cranial synapomorphies of Odontoceti include the presence of a concave facial area to accommodate the melon, presence of premaxillary foramina and premaxillary sac fossa, posterior expansion of maxilla over the supraorbital region covering the frontal bones, and facial asymmetry, all features that are related to their highly specialized sonar system (Churchill, Geisler, Beatty, & Goswami, 2018; Martínez-Cáceres, Lambert, & de Muizon, 2017; Marx & Fordyce, 2015; Marx et al., 2016; Uhen, 2004, Coombs et al., 2020; Cranford, Amundin, & Norris, 1996; Geisler, Colbert, & Carew, 2014).

Due to such highly specialised system, the odontocetes skull received particular attention in studies of functional morphology (Coombs et al., 2020; Gillet, Frédérich, & Parmentier, 2019; Mourlam & Orliac, 2017; Park, Mennecart, Costeur, Grohé, & Cooper, 2019).

One general evolutionary trend in odontocetes since the Oligocene is the *telescoping* of the skull (Churchill *et al.*, 2018). Winge introduced this term in 1918 and Miller (1923) subsequently formalised it to describe the unique posterior elongation of the rostral elements relative to the backward shift of the bony nares. Such a dramatic anatomical innovation resulted in an overlap of adjacent facial bones, whose shape resembles an antique folding telescope (Miller, 1923; Rommel, Pabst, & McLellan, 2009; Winge, 1918, 1921). This allows the toothed whale skull to be fully adapted for an aquatic lifestyle, in particular increasing the body hydrodynamicity (Fordyce & de Muizon, 2001; Marx et al., 2016).

The skull of odontocetes is also shaped by several sensory, cognitive and feeding functions. The parts of the skull that are more relevant to feeding are the rostrum, the temporal fossa (origin of the temporalis muscle, the main adductor of the jaws in odontocetes), the zygomatic process of the squamosal (point of articulation with the mandible), the teeth, the hyoid apparatus and the mandibles (Perrin, 1975). The latter have received more attention in the

literature for their importance in feeding strategies as well as for the transmission of sounds to the ear (Rommel et al., 2009; Werth, 2006a). In addition, presence of a structure called the melon (a fatty tissue functioning as a lens for the propagation of echolocation sounds) (McKenna *et al.*, 2012) greatly influences the external shape of the head in odontocetes. Indirectly, cranial morphology can provide ecological and trophic information on toothed whales' abilities to exploit surrounding resources (Marshall, 2009).

Previous studies on the odontocetes showed that interspecific differences in mandibular and cranial size are associated with reproductive parameters, peak frequencies, and prey size rather than dietary categories (Barroso et al., 2012; MacLeod et al., 2007; McCurry, Fitzgerald, Evans, Adams, & McHenry, 2017), and a link between size and deep diving abilities has been mentioned in several works (MacLeod et al., 2006; McCurry & Pyenson, 2019). In contrast, across living cetaceans, Slater al. (2010) suggested a relationship between body mass evolution and diet. Nevertheless, a comprehensive cranial ecomorphological analysis of this group within a phylogenetic framework is still lacking.

Geometric morphometrics (GM) (Rohlf and Marcus, 1993) can be a useful tool to study crania shape and size variation across toothed whales. Here, I investigated 60 species of toothed whales covering all the 33 living genera (c.ca 90% of the current species diversity). In order to understand the evolution of odontocete cranial shape and size, multiple abiotic and biotic factors have been considered: diet (MacLeod et al., 2007; McCurry, Evans, et al., 2017; Slater et al., 2010), biosonar mode and maximum and minimum peak frequencies (kHz)(Barroso, Cranford, & Berta, 2012; Galatius et al., 2018; Jensen et al., 2018), diving ecology (Noren & Williams, 2000; Werth, 2006a; Würsig, 2009), prey size (minimum, maximum and average) (MacLeod et al., 2006), superficial water/sea temperature (SST), Encephalization Quozient (EQ) and Brain Mass (Montgomery et al., 2013).

The aim of this chapter is to address the following questions: 1) What is the link between cranial morphological variation and ecological adaptation in extant toothed whales? 2) Does morphological variation exhibit a strong phylogenetic signal? 3) To what extent does such a signal obscure our ability to detect ecomorphological adaptations?

It is expected that cranial shape and size correlate with ecological factors. As ecological factors such as predation have been suggested to be one of the major selective pressures that drove toothed whale body mass and biosonar mode evolution (Galatius et al., 2018), a strong

relationship can be predicted between cranium size and biosonar mode, which should hold even after shared evolutionary history is taken into account.

Indeed, mammalian skull morphologies appear to show a strong phylogenetic signal (Marcus et al. 2000) that might eventually obscure its association with function. Comparative methods (PGLS) were introduced to overcome this issue and to test if a relationship between variables when accounting for their lineage is not independent.

3.2   Material and methods

Specimens eximined- I collected cranial data from 111 individual toothed whales specimens representing 60 species (range between 1-5 individuals per species). Specimens belong to the following museum collections: Natural History Museum of London (NHM), Muséum National d'Histoire Naturelle (MNHN), Natural History Museum of the University of Pisa (MSNUP), La Specola (NHMUF), World Museum (MCM, Liverpool, UK) and the Natural History Museum of Denmark (NHMD). In addition, 3D models were downloaded from the website Phenome 10k (Goswami, 2015) to cover species not available at the visited institutions (see - **Appendix 3.1**-*List of specimens and missing landmarks*).

Sampling: Photogrammetry protocol- Photogrammetry 3D models were reconstructed from a set of photographs taken in three different orientations (ventral, dorsal, and vertical). Canon EOS 1100D 12.2-megapixel resolutions digital single-lens reflex with 18-55mm lens was used attached to a Manfrotto tripod. Specimens were fixed vertically on a rotating table and photographs were taken at intervals of approximatively 10 degrees. A set of ~100-150 photos per specimen were taken. For larger specimens (i.e., *Hyperoodon* spp., *Ziphius cavirostris*, and *Indopacetus pacificus*), the operator (DV) moved the tripod with a mounted camera around the object placed on a pad on the floor, and the "walk-around method" was used (Mallison & Wings, 2014). Millimetres scale measurements (rostrum length and bizygomatic width) were taken for further scaling reference of the virtual models. Images were imported into Agisoft PhotoScan Professional (Agisoft LLC, 2016, 2018) and photos from each chunk/orientation were aligned in order to generate three dense point clouds (ventral, dorsal and vertical orientation) that were subsequently merged together (Agisoft LLC, 2018; Evin et al., 2016; Falkingham, 2012; Katz & Friess, 2014; Linder, 2016; Mallison & Wings, 2014; Heinrich

Mallison, 2018; Muñoz-Muñoz et al., 2016). 3D models with texture were exported as .PLY files and scaled by dividing the scaling factor identified in Meshlab (Cignoni et al., 2008) by the scale measurements (in mm).

Landmarks, size and shape data -A total of 28 landmarks (**Figure 3.1;Table 3.1**) were taken on cranial virtual models using IDAV Landmark software (Wiley et al., 2005). The landmarks were selected to describe broad anatomical cranial regions relavant to the research questions including the rostrum, the temporal region, and the facial concavity. As the shape is defined as all the geometrical characteristics of an object except its size, position and orientation, a Generalized Procrusted Analysis superimposition (GPA; Rholf & Slice, 1993) was applied to extract shape information from samples with multiple landmarks, GPA is an iterative procedure where variation in size is first removed by scaling each configuration so that it has a centroid size (CS) of 1.0; rotation and translation are taken into account by centering and rotating the landmark configuration so to obtain an optimal solution that minimizes the quadratic distances between homologous points (Procrustes method). Due to the well-known pattern of asymmetry in the odontocete cranium (Coombs et al., 2020; McLeod et al. 2007), the Thin Plate Spline (TPS, Gunz et al., 2009) was used to reconstruct the positions of missing landmarks using individuals belonging to the same species and/or genera as reference specimens, to take into account the degree of asymmetry in the given species. Missing landmarks were identified in 34 specimens (**Appendix 3.1**-*List of specimens and missing landmarks*) and in the majority of cases they were concentrated in the pterygoids. In order to detect their impact on subsequent analyses, sensitivity analyses were performed on two separate datasets: one including 28 landmarks and another with a smaller number of landmarks (n =26).

Although photogrammetry models were merged with those generated from Breuckmann laser scanner (phenome10K database, n = 25, see for details), in **Chapter 1,** I demonstrated that the two digitising techniques produce repeatable size and shape data that are appropriate to analyse in macroevolutionary studies. This together with the very small proportion of laser scanned specimens included in this study, ensure that scanning device has no impact on data analyses and interpretation.
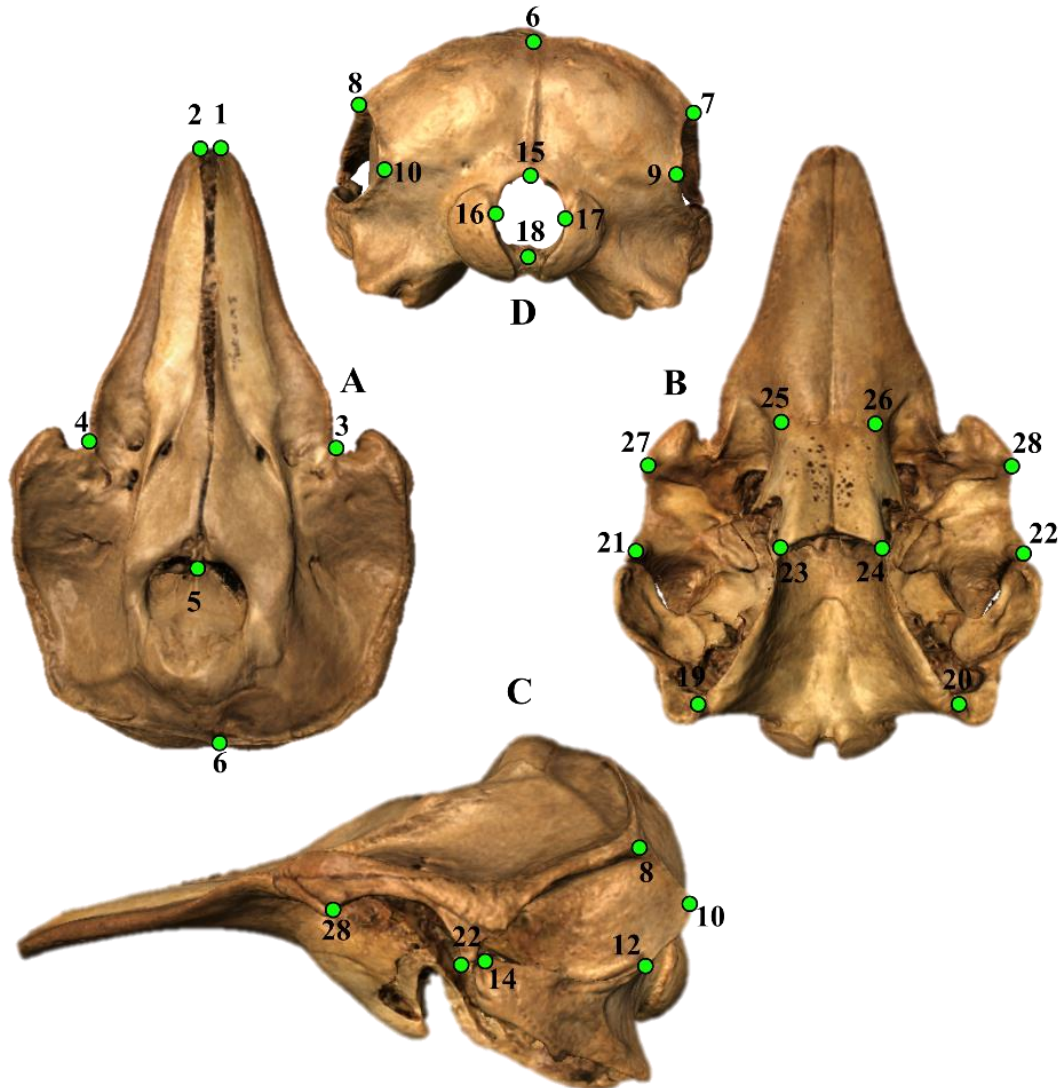
Figure 3.1 Landmark configuration on Photogrammetric-based 3D model cranium of *Grampus griseus* SW1933.14 NHM (London) in A) Dorsal, B) Ventral, C) Lateral, and D) occipital view. See **Table 3.1** for description.

Table 3.1- Description of landmarks taken on odontocetes skull used in our GM analysis

Area	No.	Landmark description
Facial Region area into which the maxilla and premaxilla expand during telescoping; it is bounded posteriorly by the nuchal crest and laterally by the orbitotemporal crest	1-2	Anterior tip of the right and left premaxilla
	3-4	Point between the maxillary flange and the antorbital notch on the right and left lateral portion of the maxilla
	5	*Septum nasi osseum*
	6	Apex of the nuchal crest or lambdoid crest (posteriormost structure) in the midline of the skull/dorsomedial margin of the supraoccipital at the intersection of this margin and the external occipital crest
Planum parietale or temporal fossa where the temporal muscle origins This area is bounded by parietal, squamosal, frontal, and alisphenoid bones	7-8	Junction of nuchal crest, temporal, parietal, occipital and frontal suture on the dorsal border of the temporal fossa
	9-10	Posteriormost point on the temporal crest/on the curve of the parietal
	11-12	Junction of squamosal, exoccipital on the ventral border of temporal fossa/the suture between exoccipital and squamosal
	13-14	Anteriormost point on the squamosal bone *(pars squamosa)* portion of the temporal bone (*squama temporalis*)
Occipital area consists of the interparietal, supraoccipital, and exoccipital ossifications	15	*Opisthion*; middle point of the dorsal border of the *foramen magnum* on the intercondyloid notch
	16-17	Lateralmost margins of the foramen magnum
	18	*Basion*; point located in the middle of the ventral margin of the *foramen magnum* in the incisura intercondyloidae
Paroccipital process lies lateral to the posterior end of the basioccipital crest and the hypoglossal canal	19-20	Medial tip of the paroccipital process/ventralmost point of the paroccipital process
Palatine posterior portion of the hard palate, at the opening of the internal bony nares. It is bounded by the maxilla, frontal, vomer, and pterygoid	23-24	Pterygoid hamulus; posterior margin of the hard palate and the border of the internal bony nares
	25-26	Anteriomost point of the palatine
Pars orbitalis Orbital surface of the frontal region bounded anteriorly by the zygomatic process, posteriorly by the temporal fossa	21-22	Posteroventral point of the supraorbital process of the frontal on the postorbital process
	27-28	Anteroventral point of the preorbital process of the frontal

Measurement error: repeatability on 3D photogrammetric-based models- Landmark recording was taken twice in four different sessions on 111 individuals in order to quantify the measurement error (Fruciano, 2016), repeatability, and digitizing ability of the operator (DV). A Procrustes ANOVA was performed on MorphoJ on the shape component and the percentage of measurement error was calculated by looking at Mean Square (MS) values following the formula below (Fruciano, 2016; Sherratt, 2015):

$$\text{R} = \frac{S^2A = \left(\text{MS}among - \dfrac{\text{MS}within}{2}\right)}{(\text{MS}within + S^2A)}$$

R is the value of repeatability or intraclass correlation coefficient and varies between (0-1), and S^2_A is the among-individuals variance component. To find S^2_A, the MS of the replicas term was subtracted from the individual term and divided by two (the number of replicas). Then, a ratio is computed by dividing the MS of the replicas terms by the total MS. Exploratory procedures can reveal outliers, and misplaced or inaccurate landmarks (Fruciano, 2016; Bastir et al. 2006), and plotOutliers function in "geomorph" was used to this aim. Principal Component Analysis (PCA) scatterplot in R (Team R, 2015), UPGMA (Cardini, 2014) in PAST 2.17 (Hammer et al., 2001) and Mantel test in MorphoJ (Klingenberg, 2011) were performed to allow the identification of individuals affected by the measurement error (**Appendix 3.2 and Appendix 3.3**).

Geometric morphometrics (GM) analyses- The registered shape coordinates and logCS were averaged for each species for subsequent macroevolutionary analyses (Zelditch et al. , 2012a, 2018). GM permits partitioning of the asymmetric and symmetric components of shape variation (Klingenberg et al., 2002). As many species of toothed whales show a high degree of asymmetry in their crania (del Castillo, Viglino, Flores, & Cappozzo, 2017; Fahlke et al., 2011; Galatius & Goodall, 2016; Huggenberger et al., 2017; McLeod, 2002), and the asymmetric component is relevant to answer the introduced research questions, these variables were partitioned using the function bilateral.symmetry in R, while the Fluctuating Asymmetry (FA) scores were exported from MorphoJ (Klingenberg, 2011) and used for further analyses. Analyses were also perfromed on the whole cranial shape data without partitioning it in symmetric and asymmetric components.

In addition, Procrustes-based GM analyses have a limitation known as the "Pinocchio effect" (Viscosi & Cardini, 2011; Zelditch et al., 2012). If the variation of the whole shape is limited to a few landmarks within the configuration, the variation can spread across all the landmarks misleading the real variation at each landmark, and generating an inconsistent estimation of mean shape (Viscosi & Cardini, 2011). As the Pinocchio effect is well known within toothed whale groups (del Castillo, Flores, & Cappozzo, 2014) two landmarks (LM 1-2) on the rostrum were removed and analyses repeated on a configuration of 26 landmarks. A PCA was performed on the whole mean shape and asymmetric component of the Procrustes coordinates to identify pattern of variation in between species at a macroevolutionary scale (describing patterns on the toothed whale tree; above the species level) (Reznick & Ricklefs, 2009).

Nine categorical and continuous variables were identified as ecological descriptors of each species for the following parameters (see **Appendix 3.4**): 1) Superficial Sea water Temperature (SST) can been defined as waters toothed whales inhabits related with sea superficial temperature considering maximum abundance, sightings, and stranding areas (**Appendix 3.4.1**). I divided toothed whales in: Warm, Temperate, Cold, Cold-Temperate, Riverine, and Temperate Mixed riverine, Warm Mixed Riverine. 2) Body mass (weight) and length was calculated as mature adult average measures the mature average adult weight (**Appendix 3.4.2**). 3) Diet was defined following Slater et al. (2010) and comparing his list with the preferable prey eat by each species. From this comparison I obtained three cathegories: Fish, squid, and fish/mammals eaters. 4) Diving ecology considers the species ability to dive in depth. For that, diving range depths have been collected from Dewey et al. (2010) and compared with the diving ecology in Wursig (2009), and species have been divided in: Deep, Semipelagic and Shallow (**Appendix 3.4.5**). 5) Biosonar mode was defined following Surlykke et al. (2014) and Jensen et al. (2018) in Broad band (BB), NBHF, and FM. As the sperm whale (*Physeter macrocephalus)* is not present in the dataset, Multi Pulsed (MP) cathegory is not shown. 6) Frequencies at maximum and minimum energy (dB) of the echolocation sound (kHz) were considered following Jensen et al (2018). 7) Encephalization Quotient (EQ) quantifies the variation in brain mass which is not explained by the allometric component between brain and body mass, and also 8) Brain mass variable were considered following Montogmery et al. (2013). 9) Prey mean, minimum and maximum size were taken from MacLeoad et al. (2017).

The Procrustes ANOVA (function "procD.lm") in geomorph (Adams et al., 2016) was used to test the association between cranial size, whole shape, symmetric and asymmetric shape, and FA scores (indicating the degree of asymmetry) against the ecological descriptors. As

echolocation peak frequencies, prey size, EQ and brain mass were not available for all the species, analyses were run in four datasets with 60, 56, 31 and 26 species.

Comparative methods- Phenotypic data generally contain a phylogenetic signal due to the tendency of species to show variation dependent on their ancestral. For this reason, species data are not statistically independent and they cannot be taken as a single observation. To test if level of species similarity differ with respect to some phenotypic trait, I first quantified phylogenetic signal in cranial data (both size and shape) using K. Secondly, Phylogenetic Generalised Least Square (Rohlf, 2001) approach was implemented using the function "procD.pgls" (Adams & Collyer, 2015). This allowed incorporation of the phylogenetic covariance matrix as an error term in the Procrustes ANOVA models. The phylogeny employed was a molecular one from McGowen et al. (2009). The function "procD.pgls" assume that phenotypic multivariate and univariate traits evolve under Brownian Motion (BM) mode of evolution. This assumption was explored for shape data using disparity throught time plot. This plot is generated by calculating the average disparity (= shape variance) of each subclade defined by the tree nodes at time "*t*" versus the total disparity. "*T*" is the distance from the root of each node in the tree, repeated over all of the tree nodes starting from the root (Harmon et al., 2003). The observed disparity curve is then compared with curves of data simulated under BM. The area differences between the observed curve and the simulated ones is computed using Morphological Disparity Index (MDI) that if is equal or close to zero, supports no departure from Brownian Motion mode of evolution in the trait under investigation (Zelditch, Swiderski and Sheets, 2012a, 2018). This same assumption was tested for univariate continuous and categorical variables using the function "fitContinuous/fitDiscrete" in the package phytools (Revell, 2012).

The complete (mt + nuclear) maximum-likelihood phylogeny from McGowen et al (2009) was employed (**Figure 3.2**) as it covered most of the species in our dataset, except for *Orcaella heinsoni*, *Sousa plumbea* and *S. teuszii*. The function drop.tip allowed to select species present on the skull dataset. The three missing species were added to the topology manually using Mesquite (Maddison & Maddison, 2007) breaking the branch in half and attaching them to the other species in the genus. The time of divergence of the new added taxa from their putatively sister taxa was estimated assuming that would be comparable to their conspecific.

Phylogenetic signal- Phylogenetic signal for single trait values (size) and for shape data (*Kmult*; Adams, 2014) were calculated using the K statistic in different packages in R

(Blomberg et al., 2003). Higher K values represent stronger phylogenetic signal in a trait or charater. A value of K= 1 indicates the trait evolved under Brownian Motion (BM) (Blomberg, Garland & Ives, 2003), while K< (or > 1) means that relatives resemble each other less (or more) than expected by BM (Blomberg et al.2003). To supplement the phylogenetic signal evaluation, the Akaike Information Criterion (AIC) was used to compare two evolutionary models (BM and Ornstein-Uhlenbeck, OU) using the R package Geiger (Harmon, Weir, Brock, Glor, & Challenger, 2007; Harmon et al., 2014) on univariate traits. If the OU is the best fit, this would mean that the entire lineage of odontocetes is under selection for a specific trait (that is directional evolution). Otherwise, if BM is the best fit the evolution of the trait investigated should follow a random walk.

Figure 3.2 Odontocete 3D model crania mapped onto phylogenetic tree of representative genera analysed here (based on McGowen et al., 2009). Colour range from blue to red shows the magnitude of differences in size in each species. Smaller species are in blue while bigger are in red. See **Appendix 3.1** for the list of 3D models, museum specimens, and abbreviations.

Landmark estimation and phylogenetic signal- Measurement error and missing landmarks can influence the phylogenetic signal coefficient. Fruciano et al. (2017) showed that landmarks difficult to recognize and place on the skull can affect the K*mult*, and by removing the one showing highest percentage of measurement error, different K*mult* coefficients can be obtained. Hence, two separate datasets were used to compare K*mult* between them: one contained 28 landmarks and the other 26 after removing landmarks 23 and 24 (these were the commonest missing landmarks in the dataset).

3.3 Results

Measurement error- Matrix correlation between replicas supported a strong positive and significative correlation for both cranial size and shape in the whole dataset of 28 landmarks (r= 0.99; $p < 0.0001$). Repeatability index calculated on the mean square of the replicas was 0.92 (**Table 3.2**), while it was 0.986 with the function "rep_index" (Marcy et al., 2018).

Phylogenetic signal- A significant phylogenetic signal could be identified for both cranial size (K = 0.653, $p < 0.001$) and shape (K*mult* = 0.565, $p < 0.001$). Reducing the landmark configuration from 28 to 26, in order to retain only the more robust configuration, had no effect on K and K*mult* parameter that remained identical and statistically significant.

Table 3.2 Procrustes ANOVA on size [logCS] and shape component. The Rsq of variation explains the contribution of each factor to overall variation. R is the intraclass correlation index.

Toothed Whales Rep ANOVA							
CS ~	**SS**	**MS**	**df**	**Rsq**	**F**	**p**	
Species	2.9E+07	490949.2427	59	0.98184	47.7	<0.0001	
Individual	535181	10291.93861	52	0.01814	2850.3	<0.0001	
Rep	397.191	3.610822	110	1.34E-05			
Total	3E+07						
Shape ~	**SS**	**MS**	**df**	**Rsq**	**F**	**p**	**R**
Species	5.20561	0.0022	2360	0.9449	21.33	<0.0001	0.0013
Individual	0.21513	0.0001	2080	0.03904	15.79	<0.0001	0.0014
Side (DA)	0.02153	0.00058	37	0.0039	88.85	<0.0001	**0.92**
Ind*Side (FA)	0.0269	6.6E-06	4107	0.00488	1.39	<0.0001	
Rep	0.03994	4.7E-06	8470	0.00725			
Total	5.50913						

Overall skull shape: PCA - PC1 and PC2 (**Figure 3.3**) together accounted for 67.5% of the total variance. PC1 describes relative changes in the rostrum proportions from narrow and elongated (as in 'river dolphins', PC1 negative scores) to short and wide (PC1 positive scores, the Kogiidae). The braincase width and length similarly load positively on PC1. For PC1 negative scores, the *foramen magnum,* characterised by 4 landmarks (LM 15,16,17,18), assumes a more circular shape and ventral position. Also, landmarks on the pterygoid hamuli, which delimit the posterior margin of the hard palate and the border of the internal bony nares, shift forward. PC2 axis describes changes in the overall area of the temporal fossa and the concavity of the profile of the facial region. PC2 negative values indicate a reduction in the size of the temporal fossa, where the temporalis muscles, which close the mandible, have their origin. It also shows the dorsal shift of the unpaired landmarks on the nuchal crest. PC2 positive values characterise a shortening of the pterygoids and a forward shift of the nasal area as described by landmark 5, together with the forward shift of the landmarks describing the ventralmost point of the paroccipital process.
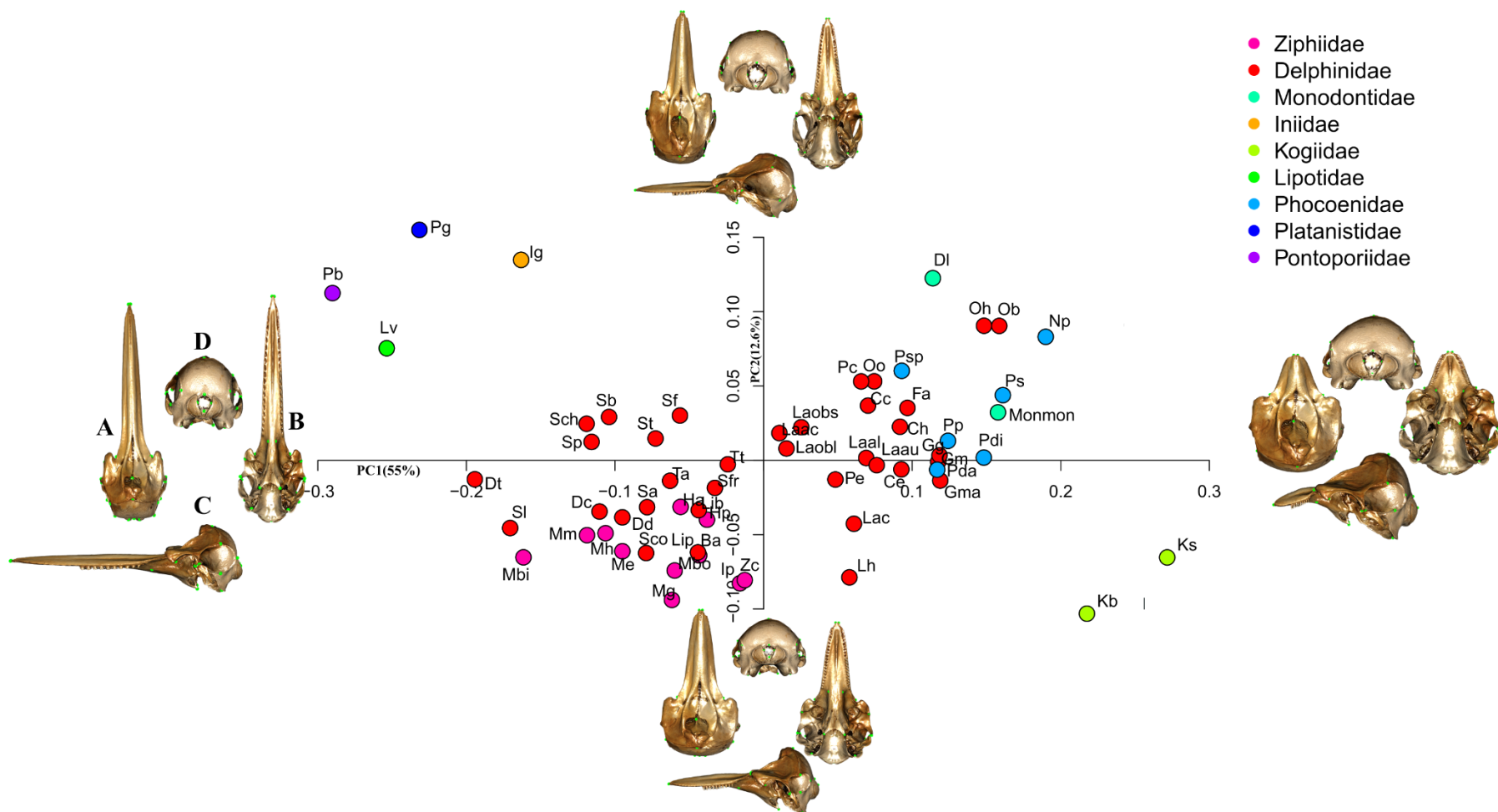
Figure 3.3 Principal component analysis of symmetric odontocetes crania consensus shape for all species (n=60) belonging to 9 families. Species abbreviation in **Appendix 3.1.**

PCA and ecological variables- When the categorical variables were mapped onto the morphospace, the PC2 separates species based on diet, biosonar mode, and diving ecology (**Figure 3.4**), showing a potential pattern of association with cranial shape. The bottom-middle part of the graph is occupied by species who are squid-eaters and deep divers, while on the bottom left specifically shows squid-eaters and deep divers with FM biosonar belonging to the Ziphiidae.
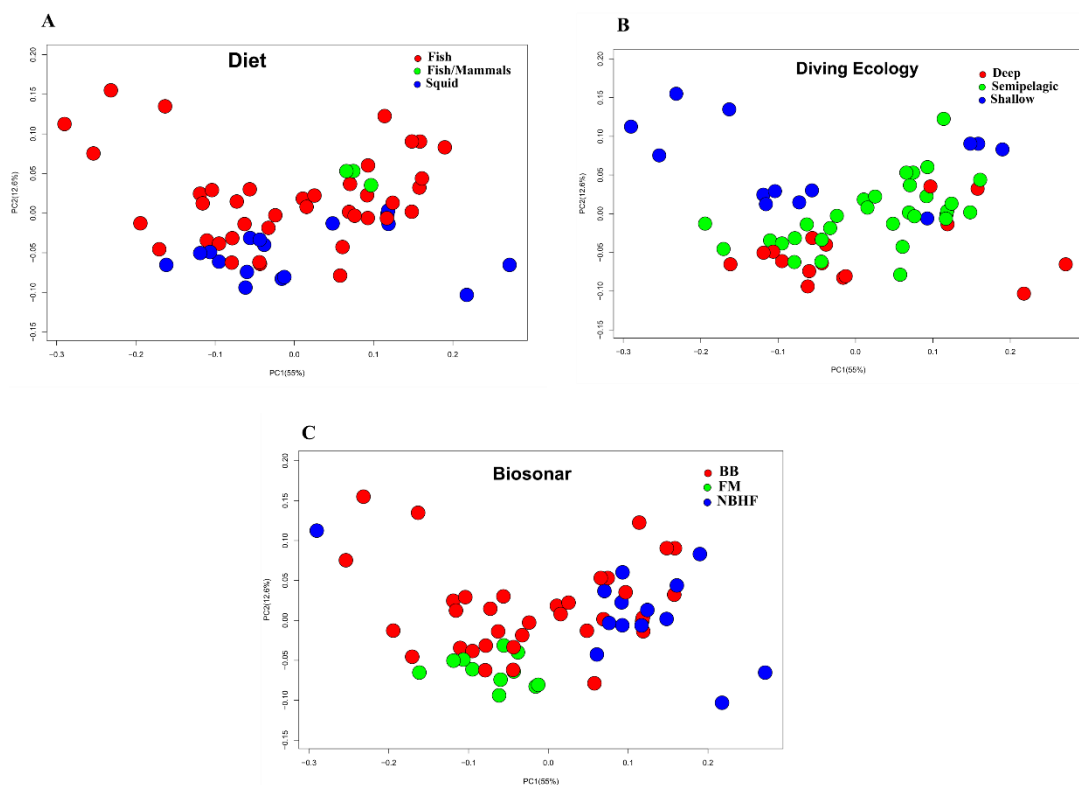
Figure 3.4 PCA and ecological variables: A) diet, B) ecology, and C) biosonar mode.

Ordinary Least Square (OLS) and Phylogenetic Generalized Least Square (PGLS) – The Procrustes ANOVA showed a significant impact of mostly all the ecological variables on both cranial shape and size using the dataset with 28 LM (n=60) (**Table 3.3**). Prey size did not impact cranial shape and size while superficial sea water temperature (SST) had no effect on size. Among all the variables, biosonar and water temperature were the ones explaining most of the variation (Biosonar 21%, SST 25% var.) in cranial shape, while body length (86% var.) and body mass (77% var.) impacted cranial size the most. After phylogenetic correction, only body length, brain and body mass, prey size average and minimum were significantly associated with skull shape (all explained around 5%, while brain mass explained 13% of variation) while size was also impacted by the biosonar mode (10% var.), minimum (9% var.) and maximum (8% var.) peak frequencies, and brain mass (30% var.).

For analyses made with reduced landmark configuration of 26 LM (n=60) (**Table 3.4**), Procrustes ANOVA showed significant associations between most ecological variables and both cranial size (Body mass and Length explained around 80%, while the remaining around 45%) and shape (all of them around 18%). Superficial water temperature was the only variable not associated with cranial size (10% var.; $p = 0.387$). After phylogenetic correction, diving ecology, and superficial water temperature were associated with skull shape (with diving ecology explaining the 8%, and SST 15% of variation), while only body length and mass were correlated with both cranial shape (percentage of variation around 5%) and size (body L explained the 59% and Body Mass the 40% of variation).

In **Supplementary Materials 3.1, Supplementary Materials 3.2**, significances of the above listed variables can be due more to one component (asymmetric or symmetric component) of cranial shape or both of them.

Table 3.3 MANOVA and PGLS analyses performed on toothed whale crania with 28 LM on whole shape in four datasets (60, 56, 31, 26 species), to test covariation between crania size shape and ecological and metric variables. p-values are in bold when significant (p < 0.05).

		Procrustes ANOVA						PGLS					
Whole Shape 28 LM		Shape			Size[CS]			Shape			Size[CS]		
60 species	df	Rsq	F	P	Rsq	F	P	Rsq	F	P	Rsq	F	P
Biosonar	2	0.21016	7.5832	**0.001**	0.57996	39.35	**0.001**	0.03745	1.109	0.321	0.10039	3.1804	**0.049**
Diet	2	0.08937	2.797	**0.017**	0.43384	21.839	**0.001**	0.02114	0.6154	0.825	0.04519	1.3488	0.264
Diving Ecology	2	0.15031	5.0418	**0.001**	0.45936	24.215	**0.001**	0.05561	1.6781	0.089	0.01621	0.4697	0.597
SST	6	0.25498	3.0232	**0.001**	0.05645	0.5284	0.773	0.12115	0.82652	0.209	0.10735	1.0623	0.381
L	1	0.07963	5.0182	**0.003**	0.86023	356.97	**0.001**	0.06507	2.8185	**0.005**	0.55723	72.995	**0.001**
BodyMass	1	0.07127	4.4511	**0.009**	0.77561	200.47	**0.001**	0.05487	3.3671	**0.017**	0.40818	40.004	**0.001**
BM ~ Diet	2				0.43793	22.205	**0.001**				0.12794	4.1814	**0.025**
56 species	df	Rsq	F	P	Rsq	F	P	Rsq	F	P	Rsq	F	P
Preymean	1	0.02537	1.4058	0.187	0.00098	0.0529	0.825	0.05691	3.2584	**0.01**	0.00269	0.1457	0.733
PreyMax	1	0.01159	0.6332	0.597	0.00477	0.259	0.606	0.01301	0.7118	0.612	0.0834	4.9134	**0.031**
PreyMin	1	0.02058	1.1346	0.314	0.00401	0.2175	0.641	0.05709	3.2695	**0.018**	0.09281	5.5247	**0.017**
31 species	df	Rsq	F	P	Rsq	F	P	Rsq	F	P	Rsq	F	P
EQ	1	0.049	1.4929	0.215	0.385	18.156	**0.002**	0.027	0.8008	0.546	0.072	2.2901	0.146
BrainMass	1	0.123	4.0617	**0.018**	0.35	15.594	**0.001**	0.137	4.6107	**0.008**	0.308	12.952	**0.001**
26 species	df	Rsq	F	P	Rsq	F	P	Rsq	F	P	Rsq	F	P
kHzmin	1	0.09897	2.6362	**0.049**	0.36309	13.682	**0.001**	0.04959	1.2523	0.247	0.12578	3.4531	0.081
kHzmax	1	0.12444	3.411	**0.014**	0.66943	48.603	**0.001**	0.04988	1.26	0.261	0.42021	17.394	**0.001**
Biosonar	2	0.28387	4.5586	**0.001**	0.60719	17.776	**0.001**	0.11278	1.4618	0.135	0.17332	2.4111	0.121

Table 3.4 MANOVA and PGLS analyses performed on toothed whale crania with 26 LM on whole shape in four datasets (60, 56, 31, 26 species), to test covariation between crania size shape and ecological and metric variables. p-values are in bold when significant (p < 0.05).

		Procrustes ANOVA						PGLS					
Whole Shape 26 LM		Shape			Size[CS]			Shape			Size[CS]		
60 species	df	Rsq	F	P	Rsq	F	P	Rsq	F	P	Rsq	F	P
Biosonar	2	0.2112	7.6311	**0.001**	0.45302	23.604	**0.001**	0.0296	0.8695	0.602	0.07605	2.3457	0.1
Diet	2	0.14862	4.9749	**0.001**	0.47234	25.512	**0.001**	0.02544	0.744	0.733	0.05274	1.5869	0.208
Diving Ecology	2	0.15031	5.0418	**0.001**	0.45936	24.215	**0.001**	0.0818	2.5389	**0.002**	0.01282	0.3702	0.681
SST	6	0.2515	2.968	**0.001**	0.10623	1.0499	0.387	0.15985	1.6806	**0.007**	0.12124	1.2188	0.299
L	1	0.16393	11.372	**0.001**	0.85573	344.04	**0.001**	0.07223	4.5156	**0.001**	0.59457	85.058	**0.001**
BodyMass	1	0.14408	9.7634	**0.001**	0.8014	234.04	**0.001**	0.04322	2.6201	**0.009**	0.40818	40.003	**0.001**
56 species	df	Rsq	F	P	Rsq	F	P	Rsq	F	P	Rsq	F	P
Preymean	1	0.02793	1.5515	0.138	0.00006	0.0035	0.957	0.08067	4.7386	**0.001**	0.00062	0.0335	0.884
PreyMax	1	0.0318	1.7736	0.083	0.00613	0.3332	0.549	0.07733	4.5259	**0.001**	0.07431	4.3348	**0.038**
PreyMin	1	0.01873	1.0308	0.374	0.00333	0.1803	0.66	0.02058	1.1347	0.312	0.06784	3.9298	0.052
31 species	df	Rsq	F	P	Rsq	F	P	Rsq	F	P	Rsq	F	P
EQ	1	0.10312	3.3344	**0.01**	0.10007	3.2247	**0.081**	0.0436	1.3221	0.226	0.06283	1.9443	0.183
BrainMass	1	0.08736	2.7759	**0.022**	0.72655	77.051	**0.001**	0.06933	2.1602	**0.038**	0.78942	108.72	**0.001**
26 species	df	Rsq	F	P	Rsq	F	P	Rsq	F	P	Rsq	F	P
kHzmin	1	0.08619	2.2637	**0.047**	0.30628	10.596	**0.005**	0.05546	1.4093	0.176	0.10519	2.8212	0.116
kHzmax	1	0.1328	3.6753	**0.003**	0.60485	36.737	**0.001**	0.06497	1.6677	0.096	0.41451	16.991	**0.001**
Biosonar	2	0.20106	2.894	**0.003**	0.5199	12.453	**0.003**	0.10365	1.3299	0.178	0.13689	1.8239	0.204

Asymmetry- For the PCA of asymmetric components of shape, the PC1 summarized 25.8% of the variation (**Figure 3.5**). Along this axis, individuals that are located towards the negative region show higher FA Procrustes score (**Figure 3.6**). The Procrustes ANOVA (**Table 3.2**) showed significant effects of between-individuals variation on shape as well as measurement Side representing the Directional Asymmetry (DA), and interaction between individual and side, representing Fluctuating Asymmetry (FA). Species showed differences in the magnitude of the Fluctuating Asymmetric component (Rsq=0.71891; *p*=0.001) (**Figure 3.6**). Procrustes FA scores, sea surface temperature and biosonar showed a significant correlation with asymmetric shape component (**Table 3.5**), while EQ (explained 22% of the variance) and Body Mass (explained the 12% of the variance) are the only two significant parameters after phylogenetic correction (**Table 3.5**).

Table 3.5 OLS and PGLS analyses performed on toothed whale crania with 28 LM on whole shape in four datasets (60, 56,31, 26 species), to test covariation between the degree of cranial asymmetry and ecological and metric variables. p-values are in bold when significant (p < 0.05).

		OLS FA scores			PGLS FA scores		
Dataset 28 LM							
60 species	df	Rsq	F	P	Rsq	F	P
Biosonar	2	0.109	3.4865	**0.041**	0.01839	0.5339	0.562
Diet	2	0.01959	0.5694	0.554	0.04108	1.221	0.295
DivingEcology	2	0.00007	0.002	0.998	0.08634	2.6932	0.079
SST	6	0.22752	2.6017	**0.04**	0.18971	2.0681	0.091
L	1	0.01369	0.8053	0.365	0.05027	3.0699	0.071
BodyMass	1	0.01822	1.0761	0.297	0.12866	8.5645	**0.01**
56 species	df	Rsq	F	P	Rsq	F	P
Preymean	1	0.00658	0.3576	0.543	0.03524	1.9725	0.184
PreyMax	1	0.00829	0.4515	0.505	0.02571	1.425	0.24
PreyMin	1	0.00475	0.2576	0.629	0.05481	3.1316	0.074
31 species	df	Rsq	F	P	Rsq	F	P
EQ	1	0.04027	1.217	0.27	0.22428	8.3846	**0.006**
BrainMass	1	0.01507	0.4437	0.534	0.03411	1.0242	0.319
26 species	df	Rsq	F	P	Rsq	F	P
kHzmin	1	0.00384	0.0925	0.755	0.00256	0.0617	0.79
kHzmax	1	0.00384	0.0925	0.755	0.00384	0.0925	0.755

Figure 3.5 PCA on asymmetric component of shape for all species (n=60) belonging to 9 families.

Species abbreviation in **Appendix 3.1**
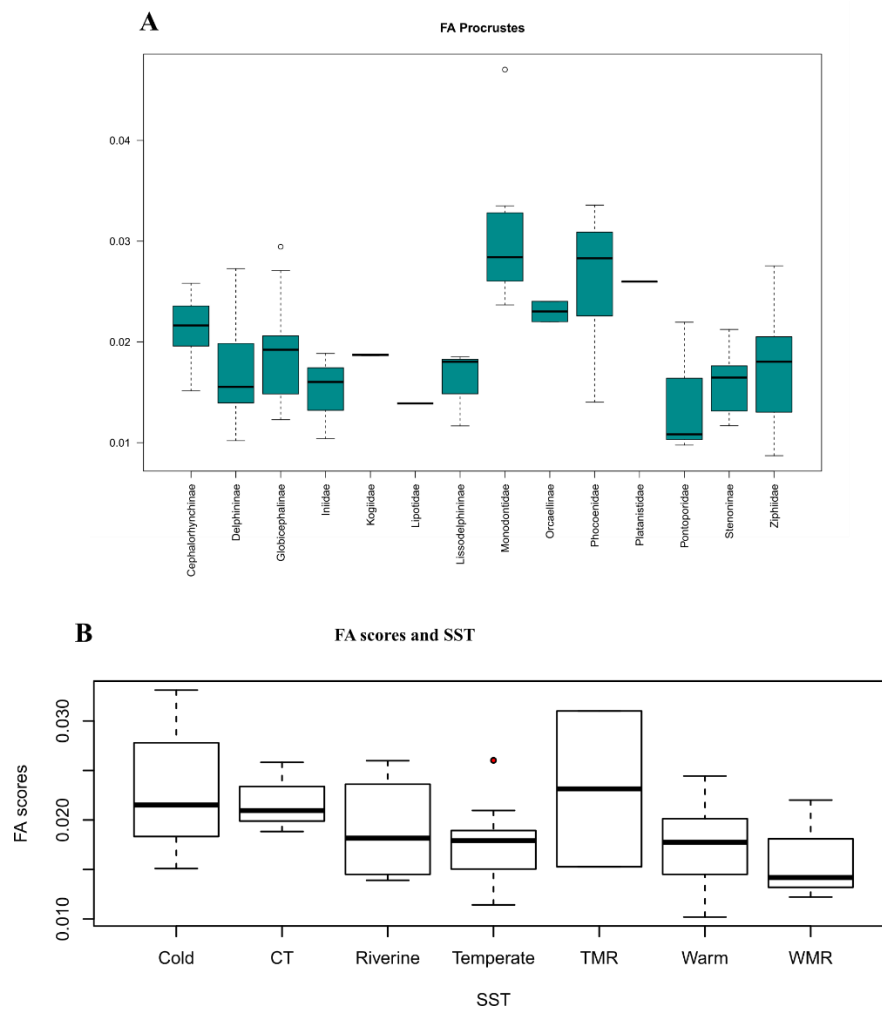
Figure 3.6 Box plot of FA Procrustes scores for A) within subfamilies and B) related to SST to determine whether there is greater variation in FA in one group relative to another.

3.4 Discussion

Cranial morphology and ecological variables- The correlation of cranial anatomical features with ecological and feeding data strongly support the hypothesis that different skull shapes of toothed whales use different feeding strategies, associated with diet, to capture their prey (Werth, 2006a).

PC1, which explains most of the variation in the analysed odontocete cranial shape sample, is associated with the relative elongation of the rostrum along a spectrum from longirostrine (e.g., *Pontoporia*) to brevirostrine (e.g., *Kogia* spp), which is the main feature linked to the diet (Werth, 2006). Longirostrine species (generally ichthyophagous) have a long and slender rostrum that allows for a rapid capture of prey (ram feeding), while brevirostrine species have a broad and short rostrum (McCurry & Pyenson, 2019), usually associated with suction feeding (Werth, 2006a, 2006b). The phenotypes of the extant paraphyletic group of 'river dolphins' (*Platanista*, *Inia*, *Pontporia*, and *Lipotes*) are a good example of how selective pressures such as feeding strategy may cause the ecological convergence in the skull shape with other ichthyophagous forms such as crocodiles (Marshall, 2009; McCurry et al.,2017; Page and Cooper, 2017). It is also interesting to note that marine mammals/fish eaters (*Orcinus orca*, *Pseudorca crassidens* and *Peponocephala electra*) showed a similar robust cranial shape, which is an advantage when catching and killing large prey.

On PC2, the braincase is posteriorly compressed and the facial region has a more concave profile, a character also associated with sound production, directionality of sonar clicks (Galatius & Gol'din, 2011; Galatius & Goodall, 2016), and deeper water/pelagic habitats (Cozzi et al., 2017). Along this axis it is also possible to detect the elevation of the nuchal crest which in ziphiids is mainly due to the presence of a very wide melon (Bianucci, Di Celma, Urbina, & Lambert, 2016). Changes in this area are associated with the development of premaxillary crests, the general elevation of the vertex, increases in the surface area of attachment for facial muscles, which is associated with movement of the melon to focus of echolocation sounds (Cranford et al., 2008; Heyning, 1986). This elevation may also increase the surface insertion of the muscles on the occipital plate. One of these is *m. semispinalis*, which originates from the dorsolateral surface of the skull and progresses in a caudal direction to the middle of the thoracic region (Cozzi et al., 2016). This muscle increases the swimming stability, and is usually associated with pelagic and deep-water ecology (Cozzi et al., 2016).

However, changes in cranial anatomy in ziphiids seems to be more related to echolocation rather than locomotion (Bianucci et al., 2016).

Phylogenetic signal was stronger for size compared to shape. Phylogenetic signal has been detected in the cranial shape of different mammalian groups (Arnaudo, Toledo, Soibelzon, & Bona, 2019; Camargo, Machado, Mendonça, & Vieira, 2019; Cardini & Elton, 2008; Jones & Goswami, 2010) and it has been suggested that complex morphologies (such as the skull) are more likely to reveal a phylogenetic signal rather than simpler structures (Polly, 2001).

In fact, the most basal taxa (such as *Platanista* and *Kogia*) were quite divergent in morphology from all the others and that family groups appears well separated by PC1 vs PC2, a pattern that we commonly see in many mammalian groups (e.g. skulls of primates, carnivores, ungulates). These opposite cranial shapes had a significant influence on the identification of large sources of variation in the analysed cranial morphology dataset. The history of fragments of odontocetes genome (Szöllősi, Tannier, Daubin, & Boussau, 2015) describes that extremely longirostrine species will possibly evolve again in *Lipotes*, *Pontoporia* and *Inia* after giving way to the evolution of deep divers cranial morphology. In extinct odontoceti longirostry feature evolved multiple times, differently if only exant toothed whales are considered. However, data show that all species have adjacent positions to their close relatives (e.g. Globicephalinae, Lissodelphininae) in the morphospace, which is the topology proposed by different studies (Agnarsson & May-Collado, 2008; Galatius & Goodall, 2016; McGowen, Spaulding, & Gatesy, 2009), and cranial features are conserved in Lissodelphininae compared to Delphininae species that occupy a larger range of PC1 scores (Galatius & Goodall, 2016).

Nevertheless, after phylogenetic correction, diet is not significantly associated with cranial shape in the dataset with 60 species. That denotes the importance of considering the orophacial morphology and the shape of the head to test the correlation between diet and clade variation, as in toothed whales the shape of the head differs from the shape of the skull (Marshall, 2009; Werth, 2006a).

Cranial size and biosonar - My results are consistent with previous studies, where size scales positively with diving abilities (Noren & Williams, 2000) and biosonar mode (Galatius et al., 2018; Jensen et al., 2018). Moreover, they support a correlation between maximum peak frequencies and cranial size, even after phylogenetic correction, that is expected based on the well-established pattern of body size constraint on sound production (Jensen et al., 2018). In fact, size and slow clicks rate in Ziphiidae play an important role in foraging performance as

having a large size increases their detection prey range (Jensen et al., 2018). While in mysticetes the body size increased during the Miocene and a correlation with prey abundancy was found, in odontocetes there is a decrease of body size through time (Slater et al., 2010) with a phylogenetic mean body size larger for squid feeders and deep divers. This is consistent with cranial size results. Contrarily to other species, *Orcinus orca* seems to have increased its size for predation instead of feeding and dive abilities (Galatius et al., 2018; Harmon et al., 2014; Slater et al., 2010). Sound production seem to be correlated with body size (Jensen et al., 2018), and a link between size and deep diving abilities has been mentioned in several works (MacLeod et al., 2006; McCurry & Pyenson, 2019). Toothed whales have a wide range of body masses, a characteristic that is correlated with diving abilities (Noren and Williams, 2000). Foraging underwater has an enormous cost due to the challenging 3D environment and whales have evolved ways of minimizing these costs, such as an increased body size. Large body size increases the dive duration through the increase of the amount of oxygen stored in the muscles, and the decrease of the mass specific metabolic rate (Kleiber, 1975). Thereby their ability to perform long dives at depth is improved, and different biosonar types evolved, in order to enhance directional sonar beam for prey echolocation at specific depths (Surlykke et al., 2014), and a convergence of cochlear shape, as adaptation to deep enviroments, has also occurred (Park et al., 2019).

EQ, Brain mass and cranial size and shape- My results show that EQ is only related with the degree of asymmetry while Brain mass correlates with cranial shape and size. In the toothed whale, body size is also related to the encephalization process through encephalization quotient (EQ=brain mass/body mass), which increases in toothed whales compared to baleen whales, related to echolocation abilities (Marino et al., 2008; Marino, McShea, & Uhen, 2004; Montgomery et al., 2013). Having a large brain increases cognitive abilities, facilitating greater information processing (Dudzinski et al., 2009; Marino et al., 2004) social ecology and communication (Montgomery et al., 2013). Small toothed whales, such as species belonging to Delphinidae, with a high EQ (encephalization quotient; *D. delphis* 3.962; Ridgway, Carlin, & van Alstyne, 2018), and bigger brain live in pods. The benefit to living in pods when the body size is so small might be related to reducing predation risk, to increase prey capture, to improve reproduction and to survive in cold temperatures (Acevedo-Gutiérrez, 2009). Also, the encephalization process has been proposed to be related with the invasion of the aquatic environment (Marino et al., 2004; Marx et al., 2016), thermoregulation (Manger, 2006; Marino et al., 2008) and diet (Slater et al., 2010).

Asymmetry- In this study the percentage of variance explained by FA was greater than DA. As the odontocete skulls shows asymmetry (Coombs et al., 2020; Cozzi et al., 2016; Fahlke & Hampe, 2015), these results agreed with expectations based on previous studies (Fahlke, 2015). The FA accounted for 8.8% of total shape variation (**Table 3.2**). Similar results for FA were found when single species were analysed such as *Lagenorhynchus australis* (8.5%), *L. obscurus* (9.5%; del Castillo et al., 2017), *Cephalorhynchus commersoni* (10%; del Castillo et al., 2016), and *Pseudorca crassidens* (10%, **Chapter 5**).

Investigation of degree of asymmetry in cranial shape did not reveal a pattern related to minimum prey size detected and Biosonar mode, after phylogenetic correction. But, a correlation between degree of asymmetry and EQ and body mass was found. However, no relationship between the degree of cranial asymmetry and Biosonar mode has been detected, which is in line with previous studies (Galatius & Goodall, 2016; Galatius et al., 2018), even if skull asymmetry in Odontocetes is strongly related to echolocation (Cranford et al., 2008).

Although potential differences in fluctuating asymmetry scores among species can be detected (**Figure 3.6**), the degree of asymmetry does not seem related to sound production (**Table 3.5**) (Galatius & Goodall, 2016; Hirose, Nakamura, & Kato, 2015), and spectral peaks. This is in contrast with what was predicted by Cranford et al. (1996). However, only peak frequencies for 26 species (out of 60) were available in the literature (Jensen et al., 2018) and a large sample size might change this conclusion. Correlation between asymmetric component of shape and waters they inhabit was found (**Figure 3.6B**) with Temperate Mixed River (TMR) taxa being more asymmetrical. Even though, no correlation was found between level of asymmetry and biosonar mode, there are differences that might not be correlated with the phylogeny (MacLeod et al., 2007; McCurry, Fitzgerald, et al., 2017). Thus, factors linked with asymmetry seem to be associated to melon size (Hirose et al., 2015), and to detect the mininum prey size (MacLeod et al., 2007, 2006; McCurry, Fitzgerald, et al., 2017), and averaged prey size (**Supplementary Materials 3.1**, **Supplementary Materials 3.2**) by using a specific biosonar type.

Several studies (Churchill et al., 2018; Coombs et al., 2020; Cranford et al., 1996; Geisler et al., 2014; MacLeod et al., 2007; Park, Fitzgerald, & Evans, 2016) pointed out that asymmetry of cranial anatomy of toothed whales is driven by adaptations for high frequency sound production. The asymmetric shape and presence of specialized fats in the melon allow direction of energy from biosonar signals into a highly directional sonar beam for prey echolocation and improves sound dispersion in the water (Surlykke et al., 2014). This system of sound

production for echolocation has diversified into different forms resulting in a different degree of cranial asymmetry within toothed whales (Coombs et al., 2020; Fahlke et al., 2011; Huggenberger et al., 2017). Trade-offs between size, frequencies emitted and beam directionality are known (Jensen et al., 2018). The NBHF biosonar mode appears to have evolved four times in small size distinct morphological and ecological groups of toothed whales, i.e., Kogidae, Phocoenidae, Pontoporidae, and Lissodelphininae (Galatius & Goodall, 2016; Galatius et al., 2018; Jensen et al., 2018; Surlykke et al., 2014). Although these lineages show differences in ecology and skull morphology, it seems that the degree of asymmetry is not related to sound production (**Table 3.5**) which is in line with previous studies (Galatius & Goodall, 2016; MacLeod et al., 2007).

Superficial Sea Temperature (SST) and cranial shape and size Prey average, prey maximum size, and SST were correlated with both symmetric and asymmetric component of shape in the dataset with 26 landmarks. Temperature and sea levels fluctuations in glacial and interglacial cycles, cause a habitat variation (Marx et al., 2016). A change in temperature is likely to change abundance, distribution and size of prey, making one cranial shape prevailing instead of another (McCurry & Pyenson, 2019). These oscillations influenced the evolution of longirostrines morphology in toothed whales in the Miocene and the Pliocene (McCurry & Pyenson, 2019), that was linked to the emergence of different ecological feeding niches (McCurry et al., 2017). Moreover, many studies (Natoli et al. 2004, 2006; Escorza-Trevino et al. 2005; Adams and Rosel 2006; Möller et al. 2009; Morin et al. 2010; Charlton-Robb et al. 2011; Amaral et al. 2012a; Andrews et al. 2013; Mendez et al. 2013; Moura et al. 2013) hypothesized the evolution of dolphin morpho ecotypesdue to ecological pressures. *S*ST gradient of the oceans varies as a function of latitude, gradually increasing from Polar Regions towards the equator. This gradient is reflected on the cetaceans world distribution, and body size patterns seem to correlate with temperature in accordance with Bergamann's rule (Bergman, 1847) more evidently in the Southern Hemisphere (Brodie, 1975; Torres-Romero, Morales-Castilla, & Olalla-Tárraga, 2016). Contrarily, in the Northern Hemisphere salinity and (Torres-Romero et al., 2016) productivity (Clementz, Fordyce, Peek, & Fox, 2014; Sergeant & Brodie, 1969; Torres-Romero et al., 2016) seem to be better predictors of body size in cetaceans. In toothed whales evolution, it was also recognised that a global cooling during the early Oligocene and the Plio-Pleistocene promoted cetacean body size decrease instead of increase (Marx et al., 2016). Some parallel on environmental variation and morphological modifications (Grant & Grant, 2002; Hairston et al., 2005; Kinnison & Hendry, 2001; McCurry & Pyenson, 2019; Millien et al.,

2006; Read & Gaskin, 1990) was found, but these species may also be the exception to the Bergmann's rule.

3.5   Conclusion

In spite of the well-established link between body size and diet in cetaceans (Slater et al., 2010), this study found little support for such association in the toothed whales cranium, since cranial size was not related to diet in a dataset of 60 living species. So, it is likely that skull size does not relate to diet because it varies less compared to body mass. Size is related to many aspects of ecomorphological variation, and it correlates with the whole cranial morphology as evidence by the allometric signal detected in this sample. For example, diet and how it shapes the cranium in toothed whales can be strongly related and governed by body size. Other studies (MacLeod et al., 2006, McCurry, Evans, et al., 2017) found a weak correlation between prey size and body size when raptorial and suction feeders where taken as a whole, and when suction feeders were excluded the correlation was stronger. In this study, once the phylogenetic comparative methods were applied, most of these relationships were not significant, and only a correlation between cranial size and biosonar was found together with the expected association between cranial size and body length and body and brain mass. Restricting the sample to the species for which prey size data were available, provides also strong support of association between both cranial size and shape and minimum prey size. This suggests that hunting specialisation plays a key role in cranial morphology of Odontocetes (McCurry, Evans et al. 2017). This applies for average prey mass as well in the case of shape while size correlates positively also with maximum prey size. Larger sizes might be argued to allow production of stronger bite force necessary to catch and hold large prey such as is the case for the killer whale.

References

Acevedo-Gutiérrez, A. (2009) 'Group behavior', in *Encyclopedia of marine mammals*. Elsevier, pp. 511–520.

Adams, D. C. *et al.* (2016) 'Geomorph: Software for geometric morphometric analyses'. Comprehensive R Archive Network.

Adams, D. C. and Collyer, M. L. (2015) 'Permutation tests for phylogenetic comparative analyses of high-dimensional shape data: What you shuffle matters', *Evolution*. Wiley Online Library, 69(3), pp. 823–829.

Agisoft LLC (2016) 'Agisoft PhotoScan User Manual', *Professional Edition, Version 0.9.0*. doi: 10.1080/00220671.2013.836468.

Agisoft LLC (2018) 'Agisoft PhotoScan', *Professional Edition, Version 1.2*. doi: 10.1016/j.jss.2015.07.002.

Agnarsson, I. and May-Collado, L. J. (2008) 'The phylogeny of Cetartiodactyla: the importance of dense taxon sampling, missing data, and the remarkable promise of cytochrome b to provide reliable species-level phylogenies', *Molecular Phylogenetics and Evolution*. Elsevier, 48(3), pp. 964–985.

Arnaudo, M. E. et al. (2019) 'Phylogenetic signal analysis in the basicranium of Ursidae (Carnivora, Mammalia)', *PeerJ*. PeerJ Inc., 7, p. e6597.

Au, W. W. L. (2012) *The sonar of dolphins*. Springer Science & Business Media.

Au, W. W. L. and Lammers, M. O. (2014) 'Cetacean acoustics', in *Springer Handbook of Acoustics*. Springer, pp. 843–875.

Barroso, C., Cranford, T. W. and Berta, A. (2012) 'Shape analysis of odontocete mandibles: functional and evolutionary implications', *Journal of Morphology*. Wiley Online Library, 273(9), pp. 1021–1030.

Berta, A., Sumich, J. L. and Kovacs, K. M. (1999) 'Cetacean evolution and systematics', *Marine Mammals: Evolutionary Biology. Academic Press, San Diego, CA*, pp. 49–85.

Bianucci, G. *et al.* (2016) 'New beaked whales from the late Miocene of Peru and evidence for convergent evolution in stem and crown Ziphiidae (Cetacea, Odontoceti)', *PeerJ*. PeerJ Inc., 4, p. e2479.

Blomberg, S. P., Garland Jr, T. and Ives, A. R. (2003) 'Testing for phylogenetic signal in comparative data: behavioral traits are more labile', *Evolution*. Wiley Online Library, 57(4), pp. 717–745.

Brodie, P. F. (1975) 'Cetacean energetics, an overview of intraspecific size variation', *Ecology*. Wiley Online Library, 56(1), pp. 152–161.

Camargo, N. F. *et al.* (2019) 'Cranial shape predicts arboreal activity of Sigmodontinae rodents', *Journal of Zoology*. Wiley Online Library, 308(2), pp. 128–138.

Cardini, A. and Elton, S. (2008) 'Does the skull carry a phylogenetic signal? Evolution and modularity in the guenons', *Biological Journal of the Linnean Society*. Oxford University Press, 93(4), pp. 813–834.

del Castillo, D. L. *et al.* (2016) 'Cranial development and directional asymmetry in Commerson's dolphin, *Cephalorhynchus commersonii commersonii*: 3D geometric morphometric approach', *Journal of Mammalogy*. Oxford University Press US, 97(5), pp. 1345–1354.

del Castillo, D. L. *et al.* (2017) 'Skull ontogeny and modularity in two species of Lagenorhynchus: Morphological and ecological implications', *Journal of morphology*. Wiley Online Library, 278(2), pp. 203–214.

del Castillo, D. L., Flores, D. A. and Cappozzo, H. L. (2014) 'Ontogenetic development and sexual dimorphism of franciscana dolphin skull: A 3D geometric morphometric approach', *Journal of morphology*. Wiley Online Library, 275(12), pp. 1366–1375.

Churchill, M. *et al.* (2016) 'The origin of high-frequency hearing in whales', *Current Biology*. Elsevier, 26(16), pp. 2144–2149.

Churchill, M. *et al.* (2018) 'Evolution of cranial telescoping in echolocating whales (Cetacea: Odontoceti)', *Evolution*. Wiley Online Library, 72(5), pp. 1092–1108.

Cignoni, P. *et al.* (2008) 'MeshLab: an open-source mesh processing tool', *Eurographics Italian Chapter Conference*. doi: 10.2312/LocalChapterEvents/ItalChap/ItalianChapConf2008/129-136.

Cignoni, P., Corsini, M. and Ranzuglia, G. (2008) 'MeshLab: an open-source 3D mesh processing system', *ERCIM News*. doi: 10.2312/LocalChapterEvents/ItalChap/ItalianChapConf2008/129-136.

Cipriano, F. (2009) 'Atlantic White-Sided Dolphin: *Lagenorhynchus acutus*', in *Encyclopedia of marine mammals*. Elsevier, pp. 56–58.

Claude, J. *et al.* (2004) 'Ecological correlates and evolutionary divergence in the skull of turtles: a geometric morphometric assessment', *Systematic Biology*. Society of Systematic Zoology, 53(6), pp. 933–948.

Clementz, M. T. *et al.* (2014) 'Ancient marine isoscapes and isotopic evidence of bulk-feeding by Oligocene cetaceans', *Palaeogeography, Palaeoclimatology, Palaeoecology*. Elsevier, 400, pp. 28–40.

Cooke, S. B. and Terhune, C. E. (2015) 'Form, function, and geometric morphometrics', *The Anatomical Record*. Wiley Online Library, 298(1), pp. 5–28.

Coombs, E. J. *et al.* (2020) 'Wonky whales: the evolution of cranial asymmetry in cetaceans', *BMC biology*. BioMed Central, 18(1), pp. 1–24.

Costeur, L. *et al.* (2018) 'The bony labyrinth of toothed whales reflects both phylogeny and habitat preferences', *Scientific reports*. Nature Publishing Group, 8(1), pp. 1–6.

Cozzi, B., Huggenberger, S. and Oelschläger, H. A. (2016) *Anatomy of dolphins: insights into body structure and function*. Academic Press.

Cranford, T. W. *et al.* (2008) 'Anatomic geometry of sound transmission and reception in Cuvier's beaked whale (*Ziphius cavirostris*)', *The Anatomical Record: Advances in Integrative Anatomy and Evolutionary Biology: Advances in Integrative Anatomy and Evolutionary Biology*. Wiley Online Library, 291(4), pp. 353–378.

Cranford, T. W., Amundin, M. and Norris, K. S. (1996) 'Functional morphology and homology in the odontocete nasal complex: implications for sound generation', *Journal of morphology*. Wiley Online Library, 228(3), pp. 223–285.

Crespo, E A (2009) 'Franciscana Dolphin', *Pontoporia blainvillei*. Encyclopedia of marine mammals, pp. 463–469.

Crespo, Enrique A (2009) 'South American aquatic mammals', in *Encyclopedia of Marine Mammals*. Elsevier, pp. 1071–1076.

Dewey, T., Shefferly, N. and Havens, A. (2010) 'Animal Diversity Web', *University of Michigan Museum of Zoology*.

Donahue, M. A. and Perryman, W. L. (2009) 'Pygmy Killer Whale: *Feresa attenuata*', in *Encyclopedia of marine mammals*. Elsevier, pp. 938–939.

Dudzinski, K. M., Thomas, J. A. and Gregg, J. D. (2009) 'Communication in marine mammals', in *Encyclopedia of marine mammals*. Elsevier, pp. 260–269.

Escorza-Treviño, S. (2009) 'North Pacific Marine Mammals', in *Encyclopedia of Marine Mammals*. Elsevier, pp. 781–788.

Evin, A. *et al.* (2016) 'The use of close-range photogrammetry in zooarchaeology: Creating accurate 3D models of wolf crania to study dog domestication', *Journal of Archaeological Science: Reports*. Elsevier, 9, pp. 87–93.

Fahlke, J. M. *et al.* (2011) 'Cranial asymmetry in Eocene archaeocete whales and the evolution of directional hearing in water', *Proceedings of the National Academy of Sciences*. National Acad Sciences, 108(35), pp. 14545–14548.

Fahlke, J. M. and Hampe, O. (2015) 'Cranial symmetry in baleen whales (Cetacea, Mysticeti) and the occurrence of cranial asymmetry throughout cetacean evolution', *The Science of Nature*. Springer, 102(9–10), p. 58.

Falkingham, P. L. (2012) 'Acquisition of high resolution three-dimensional models using free, open-source, photogrammetric software', *Palaeontologia electronica*, 15(1), p. 15.

Fordyce, R. E. and de MUIZON, C. (2001) 'Evolutionary history of cetaceans: a review', *Secondary adaptation of tetrapods to life in water*. Verlag Dr. Friedrich Pfeil München, Germany, pp. 169–233.

Fruciano, C. (2016) 'Measurement error in geometric morphometrics', *Development genes and evolution*. Springer, 226(3), pp. 139–158.

Galatius, A. *et al.* (2018) 'Raising your voice : evolution of narrow-band high- frequency signals in toothed whales (Odontoceti)', *Biological Journal of the Linnean Society*, pp. 1–12.

Galatius, A. and Gol'din, P. E. (2011) 'Geographic variation of skeletal ontogeny and skull shape in the harbour porpoise (Phocoena phocoena)', *Canadian Journal of Zoology*. NRC Research Press, 89(9), pp. 869–879.

Galatius, A. and Goodall, R. N. P. (2016) 'Skull shapes of the Lissodelphininae: radiation, adaptation and asymmetry', *Journal of morphology*. Wiley Online Library, 277(6), pp. 776–

785.

Geisler, J. H., Colbert, M. W. and Carew, J. L. (2014) 'A new fossil species supports an early origin for toothed whale echolocation', *Nature*. Nature Publishing Group, 508(7496), pp. 383–386.

Gillet, A., Frédérich, B. and Parmentier, E. (2019) 'Divergent evolutionary morphology of the axial skeleton as a potential key innovation in modern cetaceans', *Proceedings of the Royal Society B*. The Royal Society, 286(1916), p. 20191771.

Goodall, R. N. P. (2009) 'Spectacled porpoise *Phocoena dioptrica*', *Encyclopedia of marine mammals, 2nd ed., WF Perrin, B. Würsig, and JGM Thewissen (eds.). Elsevier, Burlington, Massachusetts*, pp. 1087–1091.

Gowans, S. (2009) 'Bottlenose Whales: Hyperoodon ampullatus and H. planifrons', in *Encyclopedia of marine mammals*. Elsevier, pp. 129–131.

Grant, P. R. and Grant, B. R. (2002) 'Unpredictable evolution in a 30-year study of Darwin's finches', *science*. American Association for the Advancement of Science, 296(5568), pp. 707–711.

Gunz, P. *et al.* (2009) 'Principles for the virtual reconstruction of hominin crania', *Journal of human evolution*. Elsevier, 57(1), pp. 48–62.

Gutstein, C. S. *et al.* (2014) 'High frequency echolocation, ear morphology, and the marine–freshwater transition: A comparative study of extant and extinct toothed whales', *Palaeogeography, Palaeoclimatology, Palaeoecology*. Elsevier, 400, pp. 62–74.

Hairston Jr, N. G. *et al.* (2005) 'Rapid evolution and the convergence of ecological and evolutionary time', *Ecology letters*. Wiley Online Library, 8(10), pp. 1114–1127.

Hammer, Ø., Harper, D. A. and Ryan, D. D. (2001) 'PAST: PALEONTOLOGICAL STATISTICS SOFTWARE PACKAGE FOR EDUCATION AND DATA ANALYSIS', *Palaeontologia Electronica 178kb. T. Harper. Geological Museum*. doi: 10.1016/j.bcp.2008.05.025.

Harmon, L. *et al.* (2014) 'Package "geiger"', *Bioinformatics*. Citeseer, 24, pp. 129–131.

Harmon, L. J., J. A. Schulte, A. Larson, and J. B. Losos. 2003. Tempo and mode of evolutionary radiation in iguanian lizards. Science 301:961–964.

Harmon, L. J. *et al.* (2007) 'GEIGER: investigating evolutionary radiations', *Bioinformatics*. Oxford University Press, 24(1), pp. 129–131.

van Heteren, A. H. *et al.* (2014) 'Functional morphology of the cave bear (*Ursus spelaeus*) cranium: a three-dimensional geometric morphometric analysis', *Quaternary International*. Elsevier, 339, pp. 209–216.

Heyning, J. E. (1986) *Comparative facial anatomy of beaked whales (Ziphiidae) and a systematic revision among the families of extant Odontoceti*. UCLA.

Hirose, A., Nakamura, G. and Kato, H. (2015) 'Some aspects on an asymmetry of nasal bones in toothed whales', *Mammal Study*. BioOne, 40(2), pp. 101–108.

Hocking, D. P. *et al.* (2017) 'A behavioural framework for the evolution of feeding in predatory aquatic mammals', *Proceedings of the Royal Society B: Biological Sciences*. The Royal Society, 284(1850), p. 20162750.

Hooker, S. K. (2009) 'Toothed Whales (Odontoceti)', in *Encyclopedia of Marine Mammals*. Second Edi. Elsevier, pp. 1173–1179.

Huggenberger, S., Leidenberger, S. and Oelschläger, H. H. A. (2017) 'Asymmetry of the nasofacial skull in toothed whales (Odontoceti)', *Journal of Zoology*. Wiley Online Library, 302(1), pp. 15–23.

Jefferson, T. A. (2009) 'Rough-toothed dolphin: *Steno bredanensis*', in *Encyclopedia of marine mammals*. Elsevier, pp. 990–992.

Jensen, F. H. *et al.* (2018) 'Narrow Acoustic Field of View Drives Frequency Scaling in Toothed Whale Biosonar', *Current Biology*. Elsevier, 28(23), pp. 3878–3885.

Johnson, M. *et al.* (2004) 'Beaked whales echolocate on prey', *Proceedings of the Royal Society of London. Series B: Biological Sciences*. The Royal Society, 271(suppl_6), pp. S383–S386.

Johnson, M. *et al.* (2006) 'Foraging Blainville's beaked whales (*Mesoplodon densirostris*) produce distinct click types matched to different phases of echolocation', *Journal of Experimental Biology*. The Company of Biologists Ltd, 209(24), pp. 5038–5050.

Jones, K. E. and Goswami, A. (2010) 'Morphometric analysis of cranial morphology in pinnipeds (Mammalia, Carnivora): convergence, ecology, ontogeny, and dimorphism',

Carnivoran evolution: New views on phylogeny, form anfd function, pp. 342–373.

Kane, E. A. and Marshall, C. D. (2009) 'Comparative feeding kinematics and performance of odontocetes: belugas, Pacific white-sided dolphins and long-finned pilot whales', *Journal of Experimental Biology*. The Company of Biologists Ltd, 212(24), pp. 3939–3950.

Kasuya, T. (2009) 'Giant beaked whales: *Berardius bairdii* and *B. arnuxii*', in *Encyclopedia of marine mammals*. Elsevier, pp. 498–500.

Katz, D. and Friess, M. (2014) '3D from standard digital photography of human crania—a preliminary assessment', *American Journal of Physical Anthropology*. Wiley Online Library, 154(1), pp. 152–158.

Kelkar, N. *et al.* (2018) 'Foraging and feeding ecology of Platanista: an integrative review', *Mammal Review*. Wiley Online Library, 48(3), pp. 194–208.

Kinnison, M. T. and Hendry, A. P. (2001) 'The pace of modern life II: from rates of contemporary microevolution to pattern and process', in *Microevolution rate, pattern, process*. Springer, pp. 145–164.

Kinze, C. C. (2009) 'White-Beaked Dolphin: *Lagenorhynchus albirostris*', in *Encyclopedia of marine mammals*. Elsevier, pp. 1255–1258.

Klingenberg, C. P. (2011) 'MorphoJ: An integrated software package for geometric morphometrics', *Molecular Ecology Resources*. doi: 10.1111/j.1755-0998.2010.02924.x.

Klingenberg, C. P., Barluenga, M. and Meyer, A. (2002) 'Shape analysis of symmetric structures: quantifying variation among individuals and asymmetry', *Evolution*. Wiley Online Library, 56(10), pp. 1909–1920.

Kyhn, L. A. *et al.* (2009) 'Feeding at a high pitch: Source parameters of narrow band, high-frequency clicks from echolocating off-shore hourglass dolphins and coastal Hector's dolphins', *The Journal of the Acoustical Society of America*. Acoustical Society of America, 125(3), pp. 1783–1791.

Kyhn, L. A. *et al.* (2010) 'Echolocation in sympatric Peale's dolphins (*Lagenorhynchus australis*) and Commerson's dolphins (*Cephalorhynchus commersonii*) producing narrow-band high-frequency clicks', *Journal of Experimental Biology*. The Company of Biologists Ltd, 213(11), pp. 1940–1949.

Kyhn, L. A. *et al.* (2013) 'Clicking in a killer whale habitat: narrow-band, high-frequency biosonar clicks of harbour porpoise (*Phocoena phocoena*) and Dall's porpoise (*Phocoenoides dalli*)', *PloS one*. Public Library of Science, 8(5).

Lewis, J. S. and Schroeder, W. W. (2003) 'Mud plume feeding, a unique foraging behavior of the bottlenose dolphin in the Florida Keys', *Gulf of Mexico Science*, 21(1), p. 9.

Li, Y. *et al.* (2010) 'The hearing gene Prestin unites echolocating bats and whales', *Current Biology*. Elsevier, 20(2), pp. R55–R56.

Linder, W. (2016) *Introduction. In: Digital Photogrammetry.* Springer, Berlin, Heidelberg. Available at: https://link.springer.com/content/pdf/10.1007/978-3-540-92725-9.pdf.

Lipsky, J. D. (2009) 'Right whale dolphins', in *Encyclopedia of Marine Mammals*. Elsevier, pp. 958–962.

Louella, M. and Dolar, L. (2009) 'Fraser's dolphin: *Lagenodelphis hosei*', in *Encyclopedia of marine mammals*. Elsevier, pp. 469–471.

MacLeod, C. D. (2002) 'Possible functions of the ultradense bone in the rostrum of Blainville's beaked whale (*Mesoplodon densirostris*)', *Canadian Journal of Zoology*. NRC Research Press, 80(1), pp. 178–184.

MacLeod, C. D. *et al.* (2006) 'Relative prey size consumption in toothed whales: implications for prey selection and level of specialisation', *Marine Ecology Progress Series*, 326, pp. 295–307.

MacLeod, C. D. *et al.* (2007) 'Breaking symmetry: the marine environment, prey size, and the evolution of asymmetry in cetacean skulls', *The Anatomical Record: Advances in Integrative Anatomy and Evolutionary Biology: Advances in Integrative Anatomy and Evolutionary Biology*. Wiley Online Library, 290(6), pp. 539–545.

Maddison, W. P. and Maddison, D. R. (2007) 'Mesquite: a modular system for evolutionary analysis. 2011', *See http://mesquiteproject. org*.

Mallison, H. (2018) *Dinosaurpalaeo; Photogrammetry tutorial 11: How to handle a project in Agisoft Photoscan ; tutorial 12:my workflow for Agisoft Photoscan.* Available at: https://dinosaurpalaeo.wordpress.com/ (Accessed: 22 February 2019).

Mallison, H. and Wings, O. (2014) 'Photogrammetry in paleontology-a practical guide',

Journal of Paleontological Techniques, 12, pp. 1–31. Available at: http://creativecommons.org/licenses/by-sa/3.0/.www.jpaleontologicaltechniques.org (Accessed: 22 February 2019).

Manger, P. R. (2006) 'An examination of cetacean brain structure with a novel hypothesis correlating thermogenesis to the evolution of a big brain', *Biological Reviews*. Cambridge University Press, 81(2), pp. 293–338.

Marcy, A. E. *et al.* (2018) 'Low resolution scans can provide a sufficiently accurate, cost-and time-effective alternative to high resolution scans for 3D shape analyses', *PeerJ*. PeerJ Inc., 6, p. e5032.

Marino, L. *et al.* (2008) 'A claim in search of evidence: reply to Manger's thermogenesis hypothesis of cetacean brain structure', *Biological Reviews*. Wiley Online Library, 83(4), pp. 417–440.

Marino, L., McShea, D. W. and Uhen, M. D. (2004) 'Origin and evolution of large brains in toothed whales', *The Anatomical Record Part A: Discoveries in Molecular, Cellular, and Evolutionary Biology: An Official Publication of the American Association of Anatomists*. Wiley Online Library, 281(2), pp. 1247–1255.

Marshall, C. D. (2009) 'Feeding morphology', in *Encyclopedia of marine mammals*. Elsevier, pp. 406–414.

Martínez-Cáceres, M., Lambert, O. and de Muizon, C. (2017) 'The anatomy and phylogenetic affinities of Cynthiacetus peruvianus, a large Dorudon-like basilosaurid (Cetacea, Mammalia) from the late Eocene of Peru', *Geodiversitas*. BioOne, 39(1), pp. 7–163.

Marx, F. G. and Fordyce, R. E. (2015) 'Baleen boom and bust: a synthesis of mysticete phylogeny, diversity and disparity', *Royal Society Open Science*. The Royal Society Publishing, 2(4), p. 140434.

Marx, F. G., Lambert, O. and Uhen, M. D. (2016) *Cetacean paleobiology*. John Wiley & Sons.

McCurry, M. R., Fitzgerald, E. M. G., *et al.* (2017) 'Skull shape reflects prey size niche in toothed whales', *Biological Journal of the Linnean Society*. Oxford University Press UK, 121(4), pp. 936–946.

McCurry, M. R., Evans, A. R., *et al.* (2017) 'The remarkable convergence of skull shape in crocodilians and toothed whales', *Proceedings of the Royal Society B: Biological Sciences*.

The Royal Society, 284(1850), p. 20162348.

McCurry, M. R. and Pyenson, N. D. (2019) 'Hyper-longirostry and kinematic disparity in extinct toothed whales', *Paleobiology*. Cambridge University Press New York, USA, 45(1), pp. 21–29.

McGowen, M. R., Spaulding, M. and Gatesy, J. (2009) 'Divergence date estimation and a comprehensive molecular tree of extant cetaceans', *Molecular Phylogenetics and Evolution*. Elsevier Inc., 53(3), pp. 891–906. doi: 10.1016/j.ympev.2009.08.018.

McKenna, M. F. *et al.* (2012) 'Morphology of the odontocete melon and its implications for acoustic function', *Marine Mammal Science*. Wiley Online Library, 28(4), pp. 690–713.

Meloro, C. (2007) 'Plio-Pleistocene large carnivores from the Italian peninsula: functional morphology and macroecology'. Dottorato di Ricerca in Scienze della Terra, Università degli Studi di Napoli

Meloro, C. *et al.* (2008) 'The shape of the mandibular corpus in large fissiped carnivores: allometry, function and phylogeny', *Zoological Journal of the Linnean Society*. Oxford University Press, 154(4), pp. 832–845.

Meloro, C. (2011) 'Feeding habits of Plio-Pleistocene large carnivores as revealed by the mandibular geometry', *Journal of Vertebrate Paleontology*. Taylor & Francis, 31(2), pp. 428–446.

Meloro, C., Hudson, A. and Rook, L. (2015) 'Feeding habits of extant and fossil canids as determined by their skull geometry', *Journal of Zoology*. Wiley Online Library, 295(3), pp. 178–188.

Miller, D. L. (2016) *Reproductive biology and phylogeny of cetacea: whales, porpoises and dolphins*. CRC Press.

Miller, G. S. (1923) 'The telescoping of the cetacean skull (with eight plates)', *Smithsonian Miscellaneous Collections*, 76, pp. 1–55.

Millien, V. *et al.* (2006) 'Ecotypic variation in the context of global climate change: revisiting the rules', *Ecology letters*. Wiley Online Library, 9(7), pp. 853–869.

Møhl, B. *et al.* (2003) 'The monopulsed nature of sperm whale clicks', *The Journal of the Acoustical Society of America*. Acoustical Society of America, 114(2), pp. 1143–1154.

Montgomery, S. H. et al. (2013) 'The evolutionary history of cetacean brain and body size', *Evolution*. Wiley Online Library, 67(11), pp. 3339–3353.

Mourlam, M. J. and Orliac, M. J. (2017) 'Infrasonic and ultrasonic hearing evolved after the emergence of modern whales', *Current Biology*. Elsevier, 27(12), pp. 1776–1781.

Muñoz-Muñoz, F., Quinto-Sánchez, M. and González-José, R. (2016) 'Photogrammetry: a useful tool for three-dimensional morphometric analysis of small mammals', *Journal of Zoological Systematics and Evolutionary Research*. Wiley Online Library, 54(4), pp. 318–325.

Natalie, R. and Goodall, P. (2009) 'Hourglass Dolphin: *Lagenorhynchus cruciger*', in *Encyclopedia of Marine Mammals*. Elsevier, pp. 573–576.

Noren, S. R. and Williams, T. M. (2000) 'Body size and skeletal muscle myoglobin of cetaceans: adaptations for maximizing dive duration', *Comparative Biochemistry and Physiology Part A: Molecular & Integrative Physiology*. Elsevier, 126(2), pp. 181–191.

P. Cignoni, M. Callieri, M. Corsini, M. Dellepiane, F. Ganovelli, G. R. (2008) 'MeshLab', *MeshLab: an Open-Source Mesh Processing Tool*. doi: 10.1109/TVCG.2012.34.

Page, C. E. and Cooper, N. (2017) 'Morphological convergence in 'river dolphin'skulls', *PeerJ*. PeerJ Inc., 5, p. e4090.

Park, T. *et al.* (2019) 'Convergent evolution in toothed whale cochleae', *BMC evolutionary biology*. Springer, 19(1), p. 195.

Park, T., Fitzgerald, E. M. G. and Evans, A. R. (2016) 'Ultrasonic hearing and echolocation in the earliest toothed whales', *Biology Letters*. The Royal Society, 12(4), p. 20160060.

Parra, G. J. and Ross, G. J. B. (2009) 'Humpback dolphins: *S. chinensis* and *S. teuszii*', in *Encyclopedia of marine mammals*. Elsevier, pp. 576–582.

Pauly, D. *et al.* (1998) 'Diet composition and trophic levels of marine mammals', *ICES journal of Marine Science*. Oxford University Press, 55(3), pp. 467–481.

Perrin, W. F. (1975) 'Variation of spotted and spinner porpoise (genus *Stenella*) in the eastern Pacific and Hawaii'.

Pitman, R. (2009a) 'Indo-Pacific Beaked Whale: *Indopacetus pacificus*', in *Encyclopedia of marine mammals*. Elsevier, pp. 600–602.

Pitman, R. (2009b) 'Mesoplodont whales:(*Mesoplodon* spp.)', in *Encyclopedia of marine*

mammals. Elsevier, pp. 721–726.

Poli, A. and Fabbri, E. (2012) *Fisiologia degli animali marini*. Edises.

Polly, P. D. (2001) 'On morphological clocks and paleophylogeography: towards a timescale for Sorex hybrid zones', in *Microevolution rate, pattern, process*. Springer, pp. 339–357.

Racicot, R. A. *et al.* (2019) 'Evidence for convergent evolution of ultrasonic hearing in toothed whales (Cetacea: Odontoceti)', *Biology Letters*. The Royal Society, 15(5), p. 20190083.

Racicot, R. A., Darroch, S. A. F. and Kohno, N. (2018) 'Neuroanatomy and inner ear labyrinths of the narwhal, *Monodon monoceros*, and beluga, *Delphinapterus leucas* (Cetacea: Monodontidae)', *Journal of anatomy*. Wiley Online Library, 233(4), pp. 421–439.

Read, A. J. and Gaskin, D. E. (1990) 'Changes in growth and reproduction of harbour porpoises, *Phocoena phocoena*, from the Bay of Fundy', *Canadian Journal of Fisheries and Aquatic Sciences*. NRC Research Press, 47(11), pp. 2158–2163.

Reeves, R. R. and Martin, A. R. (2009) 'River dolphins', in *Encyclopedia of marine mammals*. Elsevier, pp. 976–979.

Reidenberg, J. S. and Laitman, J. T. (2009) 'Cetacean prenatal development', in *Encyclopedia of marine mammals*. Elsevier, pp. 220–230.

Revell, L. J. (2012). phytools: an R package for phylogenetic comparative biology (and other things). Methods in ecology and evolution, 3(2), 217-223.

Reznick, D. N. and Ricklefs, R. E. (2009) 'Darwin's bridge between microevolution and macroevolution', *Nature*. Nature Publishing Group, 457(7231), pp. 837–842.

RG, L. (2009) 'Biogeography', *Encyclopedia of Marine Mammals, 2nd ed. Academic Press, San Diego*, pp. 112–115.

Ridgway, S. H., Carlin, K. P. and Van Alstyne, K. R. (2018) 'Delphinid brain development from neonate to adulthood with comparisons to other cetaceans and artiodactyls', *Marine Mammal Science*. Wiley Online Library, 34(2), pp. 420–439.

Robertson, K. M. and Arnold, P. W. (2009) 'Australian snubfin dolphin: Orcaella heinsohni', in *Encyclopedia of marine mammals*. Elsevier, pp. 62–64.

Rohlf, F. J. (2001) 'Comparative methods for the analysis of continuous variables: geometric interpretations', *Evolution*. Wiley Online Library, 55(11), pp. 2143–2160.

Rommel, S. A., Pabst, D. A. and McLellan, W. A. (2009) 'Skull anatomy', in *Encyclopedia of marine mammals*. Second Edi. Elsevier, pp. 1033–1047.

Rossbach, K. A. and Herzing, D. L. (1997) 'Underwater observations of benthic-feeding bottlenose dolphins (*Tursiops truncatus*) near Grand Bahama Island, Bahamas', *Marine Mammal Science*. Wiley Online Library, 13(3), pp. 498–504.

Sergeant, D. E. and Brodie, P. F. (1969) 'Body size in white whales, *Delphinapterus leucas*', *Journal of the Fisheries Board of Canada*. NRC Research Press, 26(10), pp. 2561–2580.

Sherratt, E. (2015) *Tips & Tricks 8: Examining Replicate Error | R-bloggers*. Available at: https://www.r-bloggers.com/tips-tricks-8-examining-replicate-error/ (Accessed: 19 February 2019).

Shirihai, H. (2006) *Whales, dolphins, and seals: A field guide to the marine mammals of the world*. A. & C. Black.

Slater, G. J. *et al.* (2010) 'Diversity versus disparity and the radiation of modern cetaceans', *Proceedings of the Royal Society B: Biological Sciences*. The Royal Society, 277(1697), pp. 3097–3104.

Surlykke, A. *et al.* (2014) *Biosonar*. Springer.

Szöllősi, G. J. *et al.* (2015) 'The inference of gene trees with species trees', *Systematic biology*. Oxford University Press, 64(1), pp. e42–e62.

Thewissen, J. G. M. (2014) *The walking whales: from land to water in eight million years*. Univ of California Press.

Torres-Romero, E. J., Morales-Castilla, I. and Olalla-Tárraga, M. Á. (2016) 'Bergmann's rule in the oceans? Temperature strongly correlates with global interspecific patterns of body size in marine mammals', *Global Ecology and Biogeography*. Wiley Online Library, 25(10), pp. 1206–1215.

Trites, A. W. and Pauly, D. (1998) 'Estimating mean body masses of marine mammals from maximum body lengths', *Canadian Journal of Zoology*. NRC Research Press, 76(5), pp. 886–896.

Uhen, M. D. (2004) 'Form, function, and anatomy of *Dorudon atrox* (Mammalia, Cetacea): an archaeocete from the middle to late Eocene of Egypt'. Museum of Paleontology, The

University of Michigan.

Viscosi, V. and Cardini, A. (2011) 'Leaf morphology, taxonomy and geometric morphometrics: a simplified protocol for beginners', *PloS one*. Public Library of Science, 6(10), p. e25630.

Van Waerebeek, K. and Würsig, B. (2009) 'Dusky dolphin: *Lagenorhynchus obscurus*', in *Encyclopedia of Marine Mammals*. Elsevier, pp. 335–338.

Wells, R. S. and Scott, M. D. (2009) 'Common bottlenose dolphin: *Tursiops truncatus*', in *Encyclopedia of marine mammals*. Elsevier, pp. 249–255.

Werth, A. J. (1992) 'Anatomy and evolution of odontocete suction feeding: Cambridge, Massachusetts, Harvard University'. Doctoral Thesis.

Werth, A. J. (2004) 'Functional morphology of the sperm whale (*Physeter macrocephalus*) tongue, with reference to suction feeding', *Aquatic Mammals*. European Association for Aquatic Mammals, 30(3), pp. 405–418.

Werth, A. J. (2006a) 'Mandibular and dental variation and the evolution of suction feeding in Odontoceti', *Journal of Mammalogy*. American Society of Mammalogists, 810 East 10th Street, PO Box 1897, Lawrence, 87(3), pp. 579–588.

Werth, A. J. (2006b) 'Odontocete suction feeding: experimental analysis of water flow and head shape', *Journal of Morphology*. Wiley Online Library, 267(12), pp. 1415–1428.

Wiley, D. F. *et al.* (2005) 'Evolutionary morphing', in *Proceedings of the IEEE Visualization Conference*. doi: 10.1109/VIS.2005.30.

Winge, H. (1918) *Udsigt over hvalernes indbyrdes slaegtskab.Videnskabelige Meddelelser fra Dansk Naturhistorisk Forening Kjobenhavn*.

Winge, H. (1921) 'A review of the interrelationships of the Cetacea', *Smithsonian Miscellaneous Collections*, 72(8), pp. 1–97. Available at: https://repository.si.edu/bitstream/handle/10088/23613/SMC_72_Winge_1921_8_1-97.pdf%0Ahttp://books.google.com/books?id=RBYwSQAACAAJ&pgis=1.

Würsig, B. (2009) 'Ecology, overview', in *Encyclopedia of marine mammals*. Elsevier, pp. 361–364.

Zelditch, M. L., Swiderski, D. L. and Sheets, H. D. (2012) *Geometric morphometrics for*

biologists: a primer. Academic Press.

Zelditch, M. L., Swiderski, D. L. and Sheets, H. D. (2013) 'A Practical Companion to Geometric Morphometrics for Biologists: Running analyses in freely-available software', *Free download from https://booksite. elsevier. com/9780123869036/(18 June 2013).*

Supplementary Materials 3.1 MANOVA and PGLS analyses performed on toothed whale crania with 28 LM on symmetric and asymmetric component of shape, to test covariation between crania size shape and ecological and metric variables. p-values are in bold when significant ($p < 0.05$).

		Asymmetric Component 28 LM						Symmetric Component 28 LM					
		procD.lm			procD.pgls			procD.lm			procD.pgls		
60 species	df	Rsq	F	P	Rsq	F	P	Rsq	F	P	Rsq	F	P
Biosonar	2	0.08591	2.6785	**0.002**	0.01595	0.462	0.996	0.15218	5.1157	**0.001**	0.02402	0.7016	0.73
Diet	2	0.05265	1.5838	**0.045**	0.02287	0.667	0.796	0.09116	2.8586	**0.014**	0.02128	0.6196	0.815
DivingEcology	2	0.04364	1.3004	0.146	0.06921	2.1192	**0.016**	0.15163	5.0937	**0.001**	0.05543	1.6725	0.093
SST	6	0.16313	1.7219	**0.007**	0.16572	1.7546	**0.007**	0.25291	2.9904	**0.001**	0.12032	1.2082	0.215
L	1	0.04281	2.594	**0.009**	0.01548	0.9119	0.554	0.08186	5.1713	**0.003**	0.06684	0.06684	**0.005**
BodyMass	1	0.03894	2.3502	**0.018**	0.02781	1.6591	0.086	0.07303	4.5696	**0.008**	0.05566	3.4183	**0.017**
56 species		Rsq	F	P	Rsq	F	P	Rsq	F	P	Rsq	F	P
PreyMean	1	0.02639	1.4634	0.172	0.05081	2.8904	**0.033**	0.02643	1.4657	0.181	0.0604	3.4714	**0.009**
Preymin	1	0.02287	1.2639	0.277	0.05208	2.9669	**0.04**	0.02074	1.1439	0.313	0.05985	3.4376	**0.015**
PreyMax	1	0.01163	0.6355	0.582	0.00881	0.4798	0.791	0.01168	0.638	0.597	0.0143	0.7835	0.554
31 species		Rsq	F	P	Rsq	F	P	Rsq	F	P	Rsq	F	P
EQ	1	0.06648	2.0652	0.031	0.05106	1.5604	0.142	0.0493	1.5039	0.211	0.02666	0.7944	0.549
BrainMass	1	0.06038	1.8634	0.052	0.03709	1.117	0.314	0.12279	4.0595	**0.018**	0.13944	4.699	**0.007**
26 species		Rsq	F	P	Rsq	F	P	Rsq	F	P	Rsq	F	P
kHzmin	1	0.10013	2.6706	**0.048**	0.04793	1.2084	0.266	0.10013	2.6706	**0.048**	0.04793	1.2084	0.266
kHzmax	1	0.1273	3.5007	**0.013**	0.05134	1.2988	0.248	0.1273	3.5007	**0.013**	0.05134	1.2988	0.248
Biosonar	2	0.21828	3.2112	**0.004**	0.09095	1.1506	0.303	0.21828	3.2112	**0.004**	0.09095	1.1506	0.303

Supplementary Materials 3.2 MANOVA and PGLS analyses performed on toothed whale crania with 26 LM on symmetric and asymmetric component of shape, to test covariation between crania size shape and ecological and metric variables. p-values are in bold when significant ($p < 0.05$).

		Asymmetric Component 26 LM						Symmetric Component 26 LM					
		procD.lm			procD.pgls			procD.lm			procD.pgls		
60 species	df	Rsq	F	P	Rsq	F	P	Rsq	F	P	Rsq	F	P
Biosonar	2	0.09302	2.9228	**0.001**	0.01616	0.4682	0.997	0.20048	7.1463	**0.001**	0.02668	0.7812	0.723
Diet	2	0.04775	1.4292	0.094	0.02299	0.6705	0.787	0.15207	5.1113	**0.001**	0.02559	0.7485	0.719
Diving Ecology	2	0.03922	1.1635	0.228	0.05664	1.7113	0.05	0.26826	10.448	**0.001**	0.0827	2.5694	**0.002**
SST	6	0.15872	1.6666	**0.004**	0.14856	1.5412	**0.032**	0.25206	2.9769	**0.001**	0.15945	1.6757	**0.008**
L	1	0.04087	2.4714	**0.012**	0.01444	0.8497	0.613	0.16761	11.679	**0.001**	0.07497	4.7005	**0.001**
BodyMass	1	0.03323	1.9935	**0.037**	0.01584	0.9338	0.504	0.14742	10.029	**0.001**	0.0447	2.7137	**0.008**
56 species		Rsq	F	P	Rsq	F	P	Rsq	F	P	Rsq	F	P
PreyMean	1	0.02721	1.5104	0.131	0.04006	2.2536	**0.011**	0.02952	1.6427	0.117	0.08403	4.954	**0.001**
Preymin	1	0.02235	1.2343	0.221	0.06122	3.5216	**0.001**	0.03288	1.8356	0.078	0.07908	4.6368	**0.001**
PreyMax	1	0.01877	1.0329	0.366	0.01807	0.9937	0.445	0.01894	1.0426	0.366	0.02104	1.1603	0.291
31 species		Rsq	F	P	Rsq	F	P	Rsq	F	P	Rsq	F	P
EQ	1	0.06748	2.0985	**0.026**	0.05442	1.6691	0.126	0.10275	3.3211	**0.011**	0.04337	1.3147	0.233
BrainMass	1	0.05624	1.7281	0.071	0.03065	0.917	0.505	0.08924	2.8416	**0.02**	0.07222	2.2573	**0.034**
26 species		Rsq	F	P	Rsq	F	P	Rsq	F	P	Rsq	F	P
kHzmin	1	0.04315	1.0824	0.345	0.11083	2.9914	**0.007**	0.0888	2.339	**0.038**	0.05374	1.363	0.2
kHzmax	1	0.0578	1.4722	0.137	0.01433	0.3489	0.986	0.13823	3.8496	**0.002**	0.06741	1.7347	0.082
Biosonar	2	0.10847	1.3992	0.126	0.10411	1.3364	0.158	0.20973	3.0519	**0.002**	0.10324	1.324	0.177

Appendix 3.1- List of specimens, missing landmarks, and abbreviations

Genus [33]	Species [60]	Museum [7]	Register Number	Missing Landmarks	Species abbreviation
Berardius	*arnuxii*	NHMD	75.1.8	2	Ba
Cephalorhynchus	*commersonii*	USNM	252568		Cc
Cephalorhynchus	*commersonii*	USNM	550156		
Cephalorhynchus	*commersonii*	USNM	550449		
Cephalorhynchus	*commersonii*	NHM	1992.751		
Cephalorhynchus	*eutropia*	NHM	1881.8.17.1	2 -4 -23-24 -26	Ce
Cephalorhynchus	*heavisidii*	NHM	1948.7.27.1	23-24	Ch
Delphinapterus	*leucas*	MNHN	1928.197	8	Dl
Delphinapterus	*leucas*	MNHN	1971.156		
Delphinapterus	*leucas*	NHM	1933.10.13.1		
Delphinapterus	*leucas*	NHM	1933.10.13.2	22	
Delphinus	*delphis*	NHM	1973.106		Dd
Delphinus	*capensis*	MCM	1981.807		Dc
Delphinus	*c.tropicalis*	NHM	1973.108		Dt
Feresa	*attenuata*	USNM	504916		Fa
Feresa	*attenuata*	USNM	504917	23	
Feresa	*attenuata*	USNM	504918		
Globicephala	*macrorhynchus*	MNHN	1936.181		Gma
Globicephala	*macrorhynchus*	NHM	1912.10.27.1		
Globicephala	*melas*	MNHN	1973.898	13-21-23-24	Gm
Globicephala	*melas*	NHM	1995.382		
Globicephala	*melas*	NHM	1995.383		
Globicephala	*melas*	MNHN	1983.76		
Globicephala	*melas*	MNHN	1927.71		
Grampus	*griseus*	MNHN	A3543	23	Gg
Grampus	*griseus*	MNHN	A3544	21-22-23	
Grampus	*griseus*	NHM	SW1933.14		

Genus [33]	Species [60]	Museum [7]	Register Number	Missing Landmarks	Species abbreviation
Grampus	*griseus*	NHM	SW1927.25		
Grampus	*griseus*	MNHN	1888.291		
Hyperoodon	*ampullatus*	NHM	1978.2559	23	Ha
Hyperoodon	*planifrons*	NHM	1934.7.23.3	2 -23	Hp
Indopacetus	*pacificus*	La Specola	1956.4854	1 -23	Ip
Inia	*geoffrensis*	USNM	239667	23-24	Ig
Inia	*geoffrensis*	USNM	395415		
Inia	*geoffrensis*	USNM	49582		
Kogia	*breviceps*	NHM	SW1980.35		Kb
Kogia	*simus*	NHM	1952.8.28.1		Ks
Lagenodelphis	*hosei*	USNM	571619		Lh
Lagenorhynchus	*acutus*	NHM	SW1936.417	21	Laac
Lagenorhynchus	*cruciger*	NHM	1960.8.24.1	24	Lac
Lagenorhynchus	*albirostris*	NHM	SW1921.15		Laal
Lagenorhynchus	*obliquidens*	NHM	1992.93		Laobl
Lagenorhynchus	*obscurus*	NHM	1846.3.11.8		Laobs
Lagenorhynchus	*australis*	NHM	1944.11.30.1		Laau
Lipotes	*vexillifer*	NHM	1922.6.22.1		Lv
Lissodelphis	*borealis*	USNM	550027		Lib
Lissodelphis	*borealis*	USNM	550188	23-24	
Lissodelphis	*peronii*	MNHN	1944.15		Lip
Mesoplodon	*bowdoini*	MSNUP	269	18	Mbo
Mesoplodon	*bidens*	NHM	SW1932.28	1	Mbi
Mesoplodon	*europaeus*	NHM	1953.10.6.1	23	Me
Mesoplodon	*ginkgondens*	NHM	1957.4.5.1		Mg
Mesoplodon	*hectori*	NHM	1949.8.19.1		Mh
Mesoplodon	*mirus*	NHM	1920.20.1	23	Mm
Mesoplodon	*europaeus*	USNM	504256	24	
Mesoplodon	*europaeus*	USNM	571665		
Mesoplodon	*europaeus*	USNM	593437		

Genus [33]	Species [60]	Museum [7]	Register Number	Missing Landmarks	Species abbreviation
Monodon	*monoceros*	USNM	267959	14-20	Monmon
Monodon	*monoceros*	USNM	267960		
Monodon	*monoceros*	NHM	1937.10.30.2		
Neophocaena	*asiaeorientalis*	USNM	240001	22	Np
Neophocaena	*asiaeorientalis*	USNM	239990		
Neophocaena	*phocaenoides*	NHM	1902.6.10.65		Np
Neophocaena	*asiaeorientalis*	NHM	1966.12.6.1		
Neophocaena	*asiaeorientalis*	NHM	1889.8.6.1	19	
Orcaella	*brevirostris*	NHM	1883.11.20.2		Ob
Orcaella	*heinsohni*	USNM	284430		Oh
Orcinus	*orca*	NHM	1918.10	23-24	Oo
Orcinus	*orca*	NHM	1165b		
Orcinus	*orca*	NHM	1165a		
Orcinus	*orca*	NHM	1965c	24	
Peponocephala	*electra*	USNM	504511	22	Pe
Peponocephala	*electra*	NHM	1980.149	2 -23	
Peponocephala	*electra*	USNM	504510	24	
Phocoena	*phocoena*	MNHN	1982.155	14-23-24	Pp
Phocoena	*phocoena*	MNHN	1982.139	24	
Phocoena	*phocoena*	NHM	1965.1.19.2		
Phocoena	*dioptrica*	NHM	1939.9.30.1	23-24	Pdi
Phocoena	*spinipinnis*	NHM	1900.5.7.29	14-19-20-23-24	Psp
Phocoena	*sinus*	NHM	1969.678		Ps
Phocoenoides	*dalli*	USNM	238083		Pda
Phocoenoides	*dalli*	USNM	276394		
Phocoenoides	*dalli*	NHM	1957.6.4.1		
Platanista	*gangetica*	NHM	1884.3.29.1	23	Pg
Pontoporia	*blainvillei*	NHM	1939.45.2.9	23-24	Pb
Pontoporia	*blainvillei*	NHM	1886.4.10.3	23-24	

Genus [33]	Species [60]	Museum [7]	Register Number	Missing Landmarks	Species abbreviation
Pontoporia	*blainvillei*	USNM	482727		
Pseudorca	*crassidens*	NHM	1961.6.14.1	23-24	Pc
Pseudorca	*crassidens*	NHM	1961.6.14.10	23	
Pseudorca	*crassidens*	NHM	1961.6.14.11		
Pseudorca	*crassidens*	NHM	1961.6.14.12		
Pseudorca	*crassidens*	NHM	1961.6.14.13		
Pseudorca	*crassidens*	NHM	1961.6.14.14	23-24	
Pseudorca	*crassidens*	NHM	1961.6.14.15		
Sotalia	*fluviatilis*	MNHN	1888.793		Sf
Sousa	*chinensis*	NHM	1984.1759	22	Sch
Sousa	*plumbea*	NHM	1937.6.22.1		Sp
Sousa	*plumbea*	NHM	1948.3.13.2		
Sousa	*teuszii*	MNHN	1983.107		St
Stenella	*attenuata*	NHM	1956.11.2.6		Sa
Stenella	*attenuata*	NHM	1957.5.9.7		
Stenella	*euphrosyne (coeruleoalba)*	NHM	1938.2.5.1	13-20-21	Sco
Stenella	*frontalis*	MNHN	A3031		Sfr
Stenella	*microps (longirostris)*	NHM	1920.5.13.2	22-23-24-28	Sl
Steno	*bredanensis*	NHM	345f		Sb
Steno	*bredanensis*	NHM	1851.7.25.4		
Tursiops	*truncatus*	NHM	1984.1757		Tt
Tursiops	*truncatus*	NHM	1984.176		
Tursiops	*aduncus*	NHM	1949.10.27.3		Ta
Tursiops	*aduncus*	NHM	1902.11.25.1	24	
Ziphius	*cavirostris*	NHM	1962.8.7.1		Zc

Appendix 3.2 Principal component analysis of complete sample and replicates (n=222) demonstrating limited inter-specimen measurement error.

Appendix 3.3 UPGMA of replicates (n=222) demonstrating limited inter-specimen error
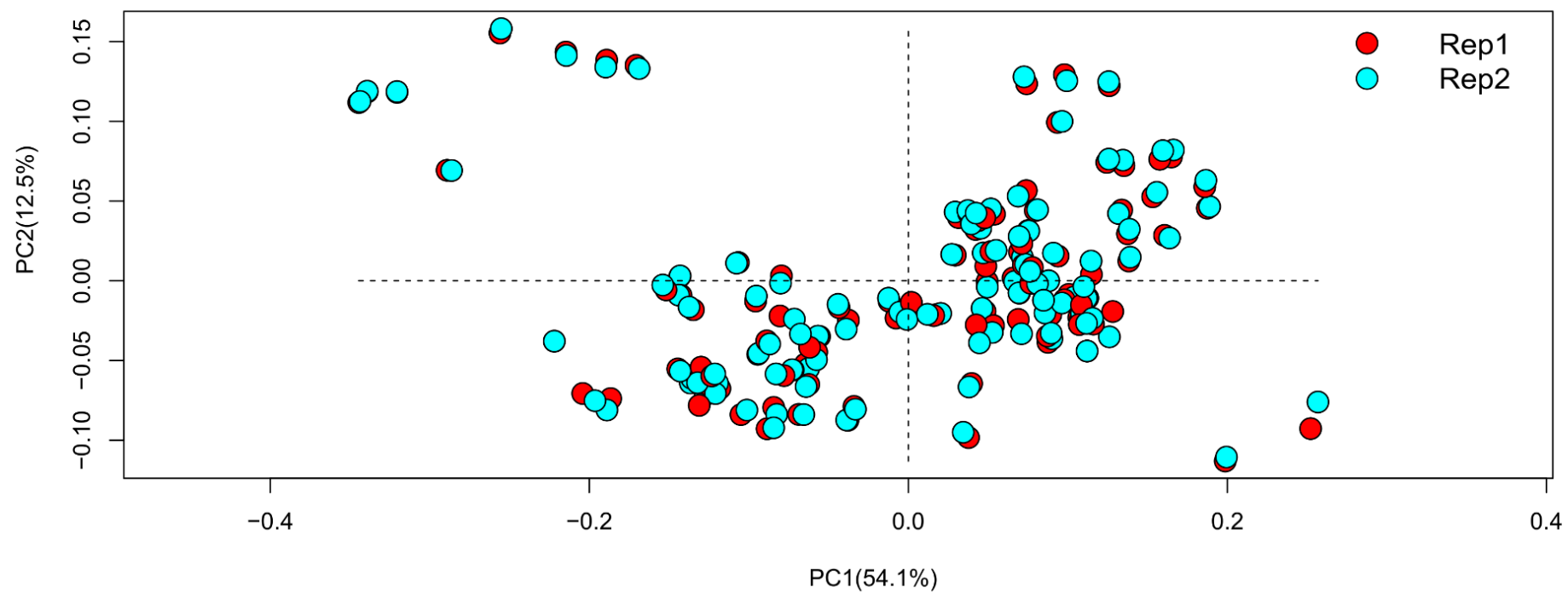
Appendix 3.4- Parameters used for analyses phylogenetically ordered

									Log10(Prey[g])		
Species	SST	Log10(BM[g])	Log10(Length[cm])	Diet	ECOLOGY	Biosonar	KhZmin	KhZmax	Mean	min	Max
REFS	Appendix 3.4.1	Appendix 3.4.2	Appendix 3.4.3	Appendix 3.4.4	Appendix 3.4.5	(Surlykke et al., 2014)	(Jensen et al., 2018)		(MacLeod, 2002), (Kelkar et al., 2018)*		
Dt	Warm	5.066325925	2.342422681	Fish	Semipelagic	BB	NA	NA	NA	NA	NA
Dd	Temperate	5.066325925	2.361727836	Fish	Semipelagic	BB	NA	NA	1.69620897	0.477121	2.369216
Dc	Temperate	5.066325925	2.342422681	Fish	Semipelagic	BB	NA	NA	1.826434765	1.394452	2.190332
Tt	Temperate	5.568201724	2.374748346	Fish	Semipelagic	BB	NA	NA	1.914959865	1.184691	2.477121
Ta	Warm	5.274157849	2.385606274	Fish	Semipelagic	BB	53	141	1.896893486	1	2.361728
Sco	Temperate	5.156851901	2.361727836	Fish	Semipelagic	BB	NA	NA	1.738364776	0.39794	2.672098
Sfr	Warm	5.102090526	2.328379603	Fish	Semipelagic	BB	NA	NA	1.871068513	1.139879	2.369216
Sl	Warm	4.705436047	2.292256071	Fish	Semipelagic	BB	NA	NA	1.610421789	0.462398	2.477121
Lh	Warm	5.301029996	2.431363764	Fish	Semipelagic	BB	NA	NA	1.644023116	0.643453	2.369216
Sa	Warm	5.039414119	2.324282455	Fish	Semipelagic	BB	NA	NA	1.601144723	0.653213	2.477121
St	WMR	4.886208624	2.371067862	Fish	Shallow	BB	NA	NA	2.103803721	1.653213	2.361728
Sch	Temperate	5.26599637	2.387389826	Fish	Shallow	BB	97	117	2.130172889	1.230449	2.672098
Sp	TMR	5.062205809	2.387389826	Fish	Shallow	BB	NA	NA	1.974386071	1.30103	2.39794
Sf	Riverine	4.544068044	2.181843588	Fish	Shallow	BB	NA	NA	1.790016936	1.079181	2.369216
Sb	Warm	5.086359831	2.40654018	Fish	Shallow	BB	NA	NA	1.885560758	0.70757	2.369216
Fa	Warm	5.273001272	2.36361198	Fish/Mammal	Deep	BB	40	100	1.756636108	1.230449	2.146128
Gm	CT	6.006466042	2.709269961	Squid	Semipelagic	BB	33	94	1.834968945	0.477121	2.477121
Gma	Temperate	6.356981401	2.680335513	Squid	Deep	BB	NA	NA	1.911324101	0.653213	2.30103
Pe	Warm	5.337459261	2.409933123	Squid	Semipelagic	BB	NA	NA	1.771320182	1.113943	2.079181
Pc	Temperate	6.161368002	2.704150517	Fish/Mammal	Semipelagic	BB	26	79	1.991637384	1.278754	2.39794
Gg	Temperate	5.698970004	2.563481085	Squid	Semipelagic	BB	42	110	1.658263983	0.39794	2.255273

Ob	WMR	5.070037867	2.439332694	Fish	Shallow	BB	65	125	2.022142745	1.544068	2.477121
Oh	Warm	4.941262909	2.361727836	Fish	Shallow	BB	NA	NA	2.090786928	1.612784	2.672098
Lip	Cold	4.788875116	2.472756449	Fish	Semipelagic	BB	NA	NA	1.890065186	1.30103	2.39794
Lib	Cold	5.06069784	2.330413773	Squid	Semipelagic	BB	NA	NA	1.749285301	1.113943	2.176091
Laobs	Cold	4.77815125	2.285557309	Fish	Semipelagic	BB	30	130	1.81493876	0.69897	2.361728
Laobl	Warm	5.10720997	2.372912003	Fish	Semipelagic	BB	NA	NA	1.904813869	1.30103	2.30103
Lac	CT	4.938269483	2.26245109	Fish	Semipelagic	NBHF	122	131	1.550534087	0.69897	1.977724
Laau	Temperate	5.031408464	2.322219295	Fish	Semipelagic	NBHF	120	133	1.984302232	1.69897	2.30103
Ch	Warm	4.514547753	2.227886705	Fish	Semipelagic	NBHF	118	132	1.934245881	1.230449	2.255273
Ce	CT	4.698970004	2.230448921	Fish	Shallow	NBHF	NA	NA	1.726183661	1.30103	1.97174
Cc	Temperate	4.782	2.164	Fish	Semipelagic	NBHF	119	139	1.902546779	1.819544	1.97174
Laal	Cold	5.431363764	2.484299839	Fish	Semipelagic	BB	NA	NA	1.724070965	0.778151	2.30103
Laac	Temperate	5.311753861	2.385606274	Fish	Semipelagic	BB	NA	NA	1.874771637	1.176091	2.30103
Oo	Temperate	6.8162413	2.898725182	Fish/Mammal	Semipelagic	BB	16	49	2.226176614	1.146128	3.30103
Ps	Cold	4.347330015	2.056904851	Fish	Semipelagic	NBHF	NA	NA	1.51054501	1.474216	1.544068
Psp	Cold	4.877946952	2.222716471	Fish	Semipelagic	NBHF	NA	NA	1.973127854	1.30103	2.190332
Pdi	Cold	4.759667845	2.361727836	Fish	Semipelagic	NBHF	NA	NA	1.476155082	1.176091	1.69897
Pp	Cold	4.812913357	2.269512944	Fish	Semipelagic	NBHF	112	145	1.833579642	0.897627	2.30103
Pda	Cold	5.208172527	2.28780173	Fish	Semipelagic	NBHF	119	143	1.733397909	0.977724	2.033424
Np	TMR	4.544068044	2.149219113	Fish	Shallow	NBHF	118	144	1.981859774	1.176091	2.477121
Dl	Cold	5.977723605	2.580924976	Fish	Semipelagic	BB	10	109	1.878550518	1.30103	2.181844
Monmon	Cold	6	2.630427875	Fish	Deep	BB	55	83	1.99343623	1.511883	2.454845
Ig	Riverine	5.113943352	2.29666519	Fish	Shallow	BB	55	158	2.030734617	1.90309	2.127105
Pb	WMR	4.612783857	2.173186268	Fish	Shallow	NBHF	NA	NA	1.835237473	0.69897	2.39794
Lv	Riverine	5.153814864	2.294466226	Fish	Shallow	BB	NA	NA	NA	NA	NA
Mbo	Temperate	5.523746467	2.650307523	Squid	Deep	FM	NA	NA	NA	NA	NA
Mg	Warm	6.265191769	2.72427587	Squid	Deep	FM	NA	NA	NA	NA	NA
Me	Warm	6.07114529	2.716003344	Squid	Deep	FM	37	37	1.62838893	1.544068	1.69897
Mm	Warm	6.144262774	2.72427587	Squid	Deep	FM	NA	NA	1.825101412	1.60206	1.97174

Mh	Temperate	5.903089987	2.643452676	Squid	Deep	FM	NA	NA	1.698970004	1.69897	1.69897
Mbi	Temperate	5.658011397	2.703291378	Squid	Deep	FM	27	58	1.864288537	1.155336	2.30103
Ip	Warm	6.028977705	2.812913357	Squid	Deep	FM	21	30	1.675778342	1.361728	1.90309
Hp	Cold	6.033021445	2.872156273	Squid	Deep	FM	NA	NA	1.745130581	0.875061	2.477121
Ha	Cold	6.22762965	2.898725182	Squid	Deep	FM	54	54	1.716948853	1.041393	2.30103
Zc	Cold	6.477121255	2.804139432	Squid	Deep	FM	40	40	1.66600042	0.39794	2.255273
Ba	Warm	6.962017116	2.946943271	Fish	Deep	FM	NA	NA	1.740362689	1.740363	1.740363
Pg	Riverine	4.886490725	2.401400541	Fish	Shallow	BB	45	73	1.342422681*	0.69897*	1.69897*
Kb	Cold	5.602059991	2.531478917	Squid	Deep	NBHF	130	130	1.647466462	0.380211	2.322219
Ks	Cold	5.409087369	2.385606274	Squid	Deep	NBHF	NA	NA	1.710040397	0.39794	2.477121

Appendix-3.4.1-SST-superfical sea temperature related with the maximum abundance, sightings, and stranding areas alphabetically ordered.

| Species | Waters they inhabit (Dewey, Shefferly, & Havens, 2010) | | | | | REFS | SST |
	Cold 1	Warm 2	Temperate 3	Mixed 4	River 5		categorical variable
Berardius arnuxii		2				(Kasuya, 2009)	Warm
Cephalorhynchus commersonii			3			(Dewey et al., 2010)	Temperate
Cephalorhynchus eutropia	1		3			(Enrique A Crespo, 2009)	CT
Cephalorhynchus heavisidii		2				(Dewey et al., 2010)	Warm
Delphinapterus leucas			3			(Escorza-Treviño, 2009)	Temperate
Delphinus delphis			3			(Escorza-Treviño, 2009)	Temperate
Delphinus capensis	1					(Escorza-Treviño, 2009)	Cold
Delphinus c. tropicalis		2				(Escorza-Treviño, 2009)	Warm
Feresa attenuata		2				(Escorza-Treviño, 2009)	Warm
Grampus griseus			3			(Escorza-Treviño, 2009)	Temperate
Globicephala melas	1		3			(Escorza-Treviño, 2009)	CT

Globicephala macrorhynchus			3			(Escorza-Treviño, 2009)	Temperate
Hyperoodon ampullatus	1					(Gowans, 2009)	Cold
Hyperoodon planifrons	1					(Gowans, 2009)	Cold
Inia geoffrensis					5	(Escorza-Treviño, 2009)	Riverine
Indopacetus pacificus		2				(Escorza-Treviño, 2009)	Warm
Kogia breviceps	1					(Escorza-Treviño, 2009)	Cold
Kogia simus	1					(Escorza-Treviño, 2009)	Cold
Lagenorhynchus acutus			3			(Cipriano, 2009)	Temperate
Lagenorhynchus albirostris	1					(Kinze, 2009)	Cold
Lagenorhynchus australis			3			(Dewey et al., 2010)	Temperate
Lagenorhynchus cruciger	1		3			(Enrique A Crespo, 2009; Natalie & Goodall, 2009)	CT
Lagenorhynchus obliquidens		2				(Escorza-Treviño, 2009)	Warm
Lagenorhynchus obscurus	1					(Van Waerebeek & Würsig, 2009)	Cold

Lagenodelphis hosei		2				(Escorza-Treviño, 2009)	Warm
Lissodelphis borealis	1					(Escorza-Treviño, 2009)	Cold
Lissodelphis peronii	1					(Dewey et al., 2010)	Cold
Lipotes vexillifer					5	(Escorza-Treviño, 2009)	Riverine
Mesoplodon bidens			3			(Dewey et al., 2010)	Temperate
Mesoplodon bowdoini			3			(Dewey et al., 2010)	Temperate
Mesoplodon europaeus		2				(Pitman, 2009b)	Warm
Mesoplodon ginkgondens		2				(Escorza-Treviño, 2009; Pitman, 2009b)	Warm
Mesoplodon hectori			3			(Dewey et al., 2010)	Temperate
Mesoplodon mirus		2				(Pitman, 2009b)	Warm
Monodon monoceros	1					(Escorza-Treviño, 2009)	Cold
Neophocaena asiaeorientalis			3	4	5	(Escorza-Treviño, 2009)	TMR
Orcaella brevirostris		2		4	5	(Escorza-Treviño, 2009)	WMR
Orcaella heinsohni		2				(Robertson & Arnold, 2009)	Warm

Orcinus orca				3			(Escorza-Treviño, 2009)	Temperate
Pontoporia blainvillei			2		4	5	(E A Crespo, 2009; Reeves & Martin, 2009; RG, 2009)	WMR
Pseudorca crassidens				3			(Escorza-Treviño, 2009)	Temperate
Phocoenoides dalli	1						(Escorza-Treviño, 2009)	Cold
Phocoena dioptrica	1						(Goodall, 2009)	Cold
Peponocephala electra			2				(Escorza-Treviño, 2009)	Warm
Platanista gangetica						5	(Escorza-Treviño, 2009)	Riverine
Phocoena phocoena	1						(Escorza-Treviño, 2009)	Cold
Phocoena sinus	1						(Escorza-Treviño, 2009)	Cold
Phocoena spinipinnis	1						(Dewey et al., 2010)	Cold
Stenella attenuata			2				(Dewey et al., 2010; Escorza-Treviño, 2009)	Warm
Steno bredanensis			2				(Jefferson, 2009)	Warm
Sousa chinensis				3			(Escorza-Treviño, 2009)	Temperate

Stenella coeruleoalba			3			(Escorza-Treviño, 2009)	Temperate
Sotalia fluviatilis					5	(Enrique A Crespo, 2009)	Riverine
Stenella frontalis		2				(Dewey et al., 2010)	Warm
Stenella longirostris		2				(Escorza-Treviño, 2009)	Warm
Sousa plumbea			3	4	5	(Dewey et al., 2010)	TMR
Sousa teuszii		2			5	(Dewey et al., 2010; Parra & Ross, 2009)	WMR
Tursiops truncatus		2				(Escorza-Treviño, 2009)	Warm
Tursiops aduncus			3			(Escorza-Treviño, 2009; Wells & Scott, 2009)	Temperate
Ziphius cavirostris	1					(Escorza-Treviño, 2009)	Cold

Appendix-3.4.2-Body Mass variable created with average weight (between sexes when was possible) from each species alphabetically ordered.

	Mean mass [kg]		Mature adult weight [kg]		
	F	**M**	**Min**	**Max**	
REFS **Species**	(Trites & Pauly, 1998)		(Reidenberg & Laitman, 2009)*		
Berardius arnuxii			644101	9162566	(Shirihai, 2006)
Cephalorhynchus commersonii	29.5	27.3	35*	86*	
Cephalorhynchus eutropia			25	75	(Dewey et al., 2010)
Cephalorhynchus heavisidii	32.7	32.7			
Delphinapterus leucas			400*	1500*	
Delphinus delphis			70	163	
Delphinus capensis			70*	163*	
Delphinus c. tropicalis			70	163	
Feresa attenuata			150*	225*	
Grampus griseus			600*	3950*	
Globicephala melas			280*	1750*	
Globicephala macrorhynchus	211	236		500*	
Hyperoodon ampullatus	1640	1738			
Hyperoodon planifrons	1331	827			
Inia geoffrensis	1210	928		(calf) 228	(Shirihai, 2006)

Indopacetus pacificus			100*	160*	
Kogia breviceps	177	177		400*	
Kogia simus			210*	303*	
Lagenorhynchus acutus	95.4	95.4		200*	
Lagenorhynchus albirostris			180	360	(Kinze, 2009)
Lagenorhynchus australis			100	115	(Shirihai, 2006)
Lagenorhynchus cruciger			40*	80*	
Lagenorhynchus obliquidens			180 (F)	230 (M)	(Cipriano, 2009)
Lagenorhynchus obscurus			125*	160*	
Lagenodelphis hosei	68.3	141		115*	
Lissodelphis borealis	68.3	54.7			
Lissodelphis peronii	462	448			
Lipotes vexillifer	363	305			
Mesoplodon bidens	496	289		1178*	
Mesoplodon bowdoini	430	321	136078	1841585	(Shirihai, 2006)
Mesoplodon europaeus	336	252		800*	
Mesoplodon ginkgondens	473	416		1394*	
Mesoplodon hectori	262	388		1000*	
Mesoplodon mirus	38.1	42.9		35*	
Monodon monoceros			85*	150*	
Neophocaena asiaeorientalis	69.7	105			

Orcaella brevirostris			2600*	10500*	
Orcaella heinsohni			160*	275*	
Orcinus orca	51	64			
Pontoporia blainvillei			40*	90*	
Pseudorca crassidens	24.1	20.4			
Phocoenoides dalli			72	79	
Phocoena dioptrica			123*	200*	
Peponocephala electra			69*	85*	
Platanista gangetica			25*	53*	
Phocoena phocoena			700*	2200*	
Phocoena sinus			73.5	100	(Natalie & Goodall, 2009)
Phocoena spinipinnis			75*	181*	
Stenella attenuata			30*	40*	
Steno bredanensis			85*	284*	
Sousa chinensis	78.8	152			
Stenella euphrosyne (coeruleoalba)	71.9	82			
Sotalia fluviatilis			100*	119*	
Stenella frontalis			131*	156*	
Stenella microps (longirostris)			110*	143*	
Sousa plumbea			26.5*	75*	
Sousa teuszii	87.7	96.3		122*	
Tursiops truncatus			176*	200*	
Tursiops aduncus			90*	650*	
Ziphius cavirostris	886	771		3000*	

Appendix-3.4.3- Length variable created with average length (between sexes when was possible) from each species alphabetically ordered. Lengths have been compared with Shirihai (2006). Sex has been specified when possible.

Species	Length [m]	Length max [m]	REFS
REFS	(Slater et al., 2010)*	(Shirihai, 2006)	
Berardius arnuxii	8.85	9.8 (7.8-9.8)	
Cephalorhynchus commersonii	1.46*	1.74	
Cephalorhynchus eutropia		1.7	
Cephalorhynchus heavisidii	1.69*	1.75	
Delphinapterus leucas	3.81*	5.5	
Delphinus delphis		1.9 -2.5; 2.20 (mean)	
Delphinus capensis	2.30*	2.7	
Delphinus c. tropicalis		2.20 (mean)	
Feresa attenuata	2.31		(Donahue & Perryman, 2009)
Grampus griseus	4.79*		
Globicephala melas	5.12*		
Globicephala macrorhynchus	3.66*		
Hyperoodon ampullatus	7.92*		
Hyperoodon planifrons	7.45*		
Inia geoffrensis	6.5 (F)	6-7	(Pitman, 2009a)
Indopacetus pacificus	1.98		
Kogia breviceps	3.40*		

Kogia simus	2.43*		
Lagenorhynchus acutus	2.7		(Louella & Dolar, 2009)
Lagenorhynchus albirostris	3.05*	3.1	
Lagenorhynchus australis	2.10*	2.2	
Lagenorhynchus cruciger	1.93*	2.2	
Lagenorhynchus obliquidens	2.43*	2.8	
Lagenorhynchus obscurus	1.41 to 2.53		(Dewey et al., 2010)
Lagenodelphis hosei	214.7(M)		(Lipsky, 2009)
Lissodelphis borealis	2.97*		
Lissodelphis peronii	5.05*		
Lipotes vexillifer	4.47*	5	
Mesoplodon bidens	5.2	5.2	(Pitman, 2009b)
Mesoplodon bowdoini	5.3	5.3	(Pitman, 2009b)
Mesoplodon europaeus	4.4	4.4	(Pitman, 2009b)
Mesoplodon ginkgondens	5.3	5.5	(Pitman, 2009b)
Mesoplodon hectori	4.27*	4.7	
Mesoplodon mirus	1.41*		
Monodon monoceros	2.21*	2.75	
Neophocaena asiaeorientalis	2.30		(Robertson & Arnold, 2009)
Orcaella brevirostris	7.92*		
Orcaella heinsohni	2.57*	2.8	

Orcinus orca		2.3	
Pontoporia blainvillei	1.86*	1.9	
Pseudorca crassidens	114		
Phocoenoides dalli	1.67*		
Phocoena dioptrica	1.94*	2.4	
Peponocephala electra	2.52*		
Platanista gangetica	1.37- 1.77(F); 1.21- 1.58 (M); 1.49 (average)	1.8	(E A Crespo, 2009)
Phocoena phocoena	5.06*		
Phocoena sinus	1.83*	1.9	
Phocoena spinipinnis	2.36*	2.5	
Stenella attenuata	1.49*		
Steno bredanensis	2.44*	3	
Sousa chinensis	2.44		
Stenella euphrosyne (coeruleoalba)	2.35*		
Sotalia fluviatilis	2.11*	2.6	
Stenella frontalis	2.30*	2.7	
Stenella microps (longirostris)	2.13*		
Sousa plumbea	1.96*	2.4	
Sousa teuszii	2.55*	2.65	
Tursiops truncatus	2.43	2.6	(Reidenberg & Laitman, 2009)
Tursiops aduncus	2.37*	4.1	
Ziphius cavirostris	6.37*		

Appendix-3.4.4-Diet categorical variable created with the preferable prey from each species alphabetically ordered.

	ADW					Diet
REFS	(Dewey et al., 2010)*(Pauly, Trites, Capuli, & Christensen, 1998)					(Slater et al., 2010)
Species	**Carnivores**	**Piscivores**	**non-insect arthropods**	**Molluscivore**	**Terrestrial & Marine vertebrates**	**Categorical variable**
Berardius arnuxii	X	X		X		Fish
Cephalorhynchus commersonii	X	X	X	X		Fish
Cephalorhynchus eutropia		X	X	X		Fish
Cephalorhynchus heavisidii		X		X		Fish
Delphinapterus leucas		X				Fish*
Delphinus delphis		x				Fish
Delphinus capensis		X				Fish
Delphinus c. tropicalis		x				Fish*
Feresa attenuata	X	x		x	x	Fish/Mammal*
Grampus griseus				X		Squid
Globicephala melas		X		X		Squid

Globicephala macrorhynchus				X		Squid
Hyperoodon ampullatus				X		Squid
Hyperoodon planifrons				X		Squid
Inia geoffrensis		X	X			Fish
Indopacetus pacificus				X		Squid
Kogia breviceps				X		Squid
Kogia simus				X		Squid
Lagenorhynchus acutus		X				Fish
Lagenorhynchus albirostris		X				Fish
Lagenorhynchus australis		X		X		Fish
Lagenorhynchus cruciger		X	X	X		Fish
Lagenorhynchus obliquidens		X				Fish
Lagenorhynchus obscurus		X				Fish
Lagenodelphis hosei		X				Fish
Lissodelphis borealis		X		X		Squid
Lissodelphis peronii		X				Fish
Lipotes vexillifer		X				Fish

Mesoplodon bidens		X		X		Squid
Mesoplodon bowdoini		X		X		Squid
Mesoplodon europaeus		X		X		Squid
Mesoplodon ginkgondens		X		X		Squid
Mesoplodon hectori		X				Squid
Mesoplodon mirus						Squid
Monodon monoceros		X	X	X		Fish
Neophocaena asiaeorientalis		X				Fish
Orcaella brevirostris		X	X	X		Fish
Orcaella heinsohni		X		X		Fish
Orcinus orca		X		X	X	Fish/Mammal*
Pontoporia blainvillei		X				Fish
Pseudorca crassidens		X		X	X	Fish/Mammal*
Phocoenoides dalli		X				Fish
Phocoena dioptrica		X		X		Fish
Peponocephala electra		X		X		Squid

Platanista gangetica		X				Fish
Phocoena phocoena		X				Fish
Phocoena sinus		X				Fish
Phocoena spinipinnis		X				Fish
Stenella attenuata		X		X		Fish
Steno bredanensis		X		X		Fish
Sousa chinensis		X		X		Fish
Stenella euphrosyne (coeruleoalba)		X		X		Fish
Sotalia fluviatilis		X		X		Fish
Stenella frontalis		X				Fish
Stenella microps (longirostris)		X				Fish
Sousa plumbea						Fish
Sousa teuszii		X				Fish
Tursiops truncatus		X				Fish
Tursiops aduncus		X	X	X		Fish
Ziphius cavirostris				X		Squid

Appendix 3.4.5-Diving Ecology-taking into account their ability to dive in depth alphabetically ordered.

REFS	Depth(m) ADW (Dewey et al., 2010)			DIVING ECOLOGY (Würsig, 2009)					
	Range Depth		Average Depth	Shallow waters (<100)	Semipelagic and Coastal (>100-500) and Surface Dwellers			Deep divers >600	Categorical variable
Species	Min	Max			Semipelagic	Coastal	Surface Dwellers		Diving Ecology
Berardius arnuxii		1000						3	Deep
Cephalorhynchus commersonii			200		2				Semipelagic
Cephalorhynchus eutropia	3	20		1					Shallow
Cephalorhynchus heavisidii		180	100		2				Semipelagic
Delphinapterus leucas						2			Semipelagic
Delphinus delphis						2			Semipelagic
Delphinus capensis	0	350			2				Semipelagic
Delphinus c. tropicalis						2			Semipelagic
Feresa attenuata	Pelagic (113)	2862	1218		2			3	Deep
Grampus griseus	400	1200						3	Semipelagic
Globicephala melas	30	1800						3	Semipelagic
Globicephala macrorhynchus		609						3	Deep

Hyperoodon ampullatus	80	1453							3	Deep
Hyperoodon planifrons		> 1000							3	Deep
Inia geoffrensis		surface		1						Shallow
Indopacetus pacificus		1267							3	Deep
Kogia breviceps		deep diver							3	Deep
Kogia simus		300							3	Deep
Lagenorhynchus acutus	40	270			2					Semipelagic
Lagenorhynchus albirostris										Semipelagic
Lagenorhynchus australis		300			2					Semipelagic
Lagenorhynchus cruciger										Semipelagic
Lagenorhynchus obliquidens										Semipelagic
Lagenorhynchus obscurus										Semipelagic
Lagenodelphis hosei	250	500			2				3	Semipelagic
Lissodelphis borealis		200			2					Semipelagic
Lissodelphis peronii		200			2					Semipelagic
Lipotes vexillifer		surface		1						Shallow
Mesoplodon bidens	198	1524							3	Deep

Mesoplodon bowdoini		>1000						3	Deep
Mesoplodon europaeus		pelagico						3	Deep
Mesoplodon ginkgondens								3	Deep
Mesoplodon hectori		5750	3500					3	Deep
Mesoplodon mirus								3	Deep
Monodon monoceros	400	800						3	Deep
Neophocaena asiaeorientalis				1					Shallow
Orcaella brevirostris	2.5	18		1					Shallow
Orcaella heinsohni	0	30		1					Shallow
Orcinus orca	20	300	60				2		Semipelagic
Pontoporia blainvillei	6	35		1					Shallow
Pseudorca crassidens	0	2000	500					3	Semipelagic
Phocoenoides dalli					2				Semipelagic
Phocoena dioptrica									Semipelagic
Peponocephala electra									Semipelagic
Platanista gangetica	0	9	3	1					Shallow

Phocoena phocoena		200				2				Semipelagic
Phocoena sinus										Semipelagic
Phocoena spinipinnis		150				2				Semipelagic
Stenella attenuata							2			Semipelagic
Steno bredanensis	2	>1500-2000		1						Shallow
Sousa chinensis	0	25	20	1						Shallow
Stenella coeruleoalba						2				Semipelagic
Sotalia fluviatilis				1						Shallow
Stenella frontalis						2	3			Semipelagic
Stenella longirostris		400					2			Semipelagic
Sousa plumbea	0	25	20	1						Shallow
Sousa teuszii	20	65		1						Shallow
Tursiops truncatus	2	300				2				Semipelagic
Tursiops aduncus			1			2				Semipelagic
Ziphius cavirostris		>1000							3	Deep

*Pda = "Dall's porpoises are thought to be capable of deep diving because mesopelagic, bathypelagic, and deep-water benthic species are represented in the diet".

References Appendix 3.4

Cipriano, F. (2009). Atlantic White-Sided Dolphin: Lagenorhynchus acutus. In *Encyclopedia of marine mammals* (pp. 56–58). Elsevier.

Crespo, E A. (2009). Franciscana Dolphin. *Pontoporia Blainvillei*, 463–469.

Crespo, Enrique A. (2009). South American aquatic mammals. In *Encyclopedia of Marine Mammals* (pp. 1071–1076). Elsevier.

Dewey, T., Shefferly, N., & Havens, A. (2010). Animal Diversity Web. *University of Michigan Museum of Zoology*.

Donahue, M. A., & Perryman, W. L. (2009). Pygmy Killer Whale: Feresa attenuata. In *Encyclopedia of marine mammals* (pp. 938–939). Elsevier.

Escorza-Treviño, S. (2009). North Pacific Marine Mammals. In *Encyclopedia of Marine Mammals* (pp. 781–788). Elsevier.

Goodall, R. N. P. (2009). Spectacled porpoise Phocoena dioptrica. *Encyclopedia of Marine Mammals, 2nd Ed., WF Perrin, B. Würsig, and JGM Thewissen (Eds.). Elsevier, Burlington, Massachusetts*, 1087–1091.

Gowans, S. (2009). Bottlenose Whales: Hyperoodon ampullatus and H. planifrons. In *Encyclopedia of marine mammals* (pp. 129–131). Elsevier.

Jefferson, T. A. (2009). Rough-toothed dolphin: Steno bredanensis. In *Encyclopedia of marine mammals* (pp. 990–992). Elsevier.

Jensen, F. H., Johnson, M., Ladegaard, M., Wisniewska, D. M., & Madsen, P. T. (2018). Narrow Acoustic Field of View Drives Frequency Scaling in Toothed Whale Biosonar. *Current Biology*, *28*(23), 3878–3885.

Kasuya, T. (2009). Giant beaked whales: Berardius bairdii and B. arnuxii. In *Encyclopedia of marine mammals* (pp. 498–500). Elsevier.

Kelkar, N., Dey, S., Deshpande, K., Choudhary, S. K., Dey, S., & Morisaka, T. (2018). Foraging and feeding ecology of Platanista: an integrative review. *Mammal Review*, *48*(3), 194–208.

Kinze, C. C. (2009). White-Beaked Dolphin: Lagenorhynchus albirostris. In *Encyclopedia of marine mammals* (pp. 1255–1258). Elsevier.

Lipsky, J. D. (2009). Right whale dolphins. In *Encyclopedia of Marine Mammals* (pp. 958–962). Elsevier.

Louella, M., & Dolar, L. (2009). Fraser's dolphin: Lagenodelphis hosei. In *Encyclopedia of marine mammals* (pp. 469–471). Elsevier.

MacLeod, C. D. (2002). Possible functions of the ultradense bone in the rostrum of Blainville's beaked whale (Mesoplodon densirostris). *Canadian Journal of Zoology*, *80*(1), 178–184.

Natalie, R., & Goodall, P. (2009). Hourglass Dolphin: Lagenorhynchus cruciger. In *Encyclopedia of Marine Mammals* (pp. 573–576). Elsevier.

Parra, G. J., & Ross, G. J. B. (2009). Humpback dolphins: S. chinensis and S. teuszii. In *Encyclopedia of marine mammals* (pp. 576–582). Elsevier.

Pauly, D., Trites, A. W., Capuli, E., & Christensen, V. (1998). Diet composition and trophic levels of marine mammals. *ICES Journal of Marine Science*, *55*(3), 467–481.

Pitman, R. (2009a). Indo-Pacific Beaked Whale: Indopacetus pacificus. In *Encyclopedia of marine mammals* (pp. 600–602). Elsevier.

Pitman, R. (2009b). Mesoplodont whales:(Mesoplodon spp.). In *Encyclopedia of marine mammals* (pp. 721–726). Elsevier.

Reeves, R. R., & Martin, A. R. (2009). River dolphins. In *Encyclopedia of marine mammals* (pp. 976–979). Elsevier.

Reidenberg, J. S., & Laitman, J. T. (2009). Cetacean prenatal development. In *Encyclopedia of marine mammals* (pp. 220–230). Elsevier.

RG, L. (2009). Biogeography. *Encyclopedia of Marine Mammals, 2nd Ed. Academic Press, San Diego*, 112–115.

Robertson, K. M., & Arnold, P. W. (2009). Australian snubfin dolphin: Orcaella heinsohni. In *Encyclopedia of marine mammals* (pp. 62–64). Elsevier.

Shirihai, H. (2006). *Whales, dolphins, and seals: A field guide to the marine mammals of the world*. A. & C. Black.

Slater, G. J., Price, S. A., Santini, F., & Alfaro, M. E. (2010). Diversity versus disparity and the radiation of modern cetaceans. *Proceedings of the Royal Society B: Biological Sciences*, *277*(1697), 3097–3104.

Surlykke, A., Nachtigall, P. E., Fay, R. R., & Popper, A. N. (2014). *Biosonar* (Vol. 51). Springer.

Trites, A. W., & Pauly, D. (1998). Estimating mean body masses of marine mammals from maximum body lengths. *Canadian Journal of Zoology*, *76*(5), 886–896.

Van Waerebeek, K., & Würsig, B. (2009). Dusky dolphin: Lagenorhynchus obscurus. In *Encyclopedia of Marine Mammals* (pp. 335–338). Elsevier.

Wells, R. S., & Scott, M. D. (2009). Common bottlenose dolphin: Tursiops truncatus. In *Encyclopedia of marine mammals* (pp. 249–255). Elsevier.

Würsig, B. (2009). Ecology, overview. In *Encyclopedia of marine mammals* (pp. 361–364). Elsevier.

4 Chapter 4: Skull morphological variation in beluga whales (*Delphinapterus leucas*) and narwhals (*Monodon monoceros*) reveals hybrid phenotypes

Abstract

Beluga whales (*Delphinapterus leucas*) and narwhals (*Momodon monoceros*) are peculiar toothed whales belonging to the family Monodontidae. Having both a circumpolar Arctic distribution, their geographic ranges overlap and they are able to produce hybrid offspring. In this study, I employed geometric morphometrics to explore morphological differences among monodontids with a very large sample of 3D models of skulls, including 157 specimens (86 *M. monoceros*, 69 *D. leucas*, one hybrid and one putative hybrid), and 2D left hemi-mandibles, including 85 specimens (64 *M. monoceros*, 20 *D. leucas* and one hybrid). Shape analyses showed clear distinctions in 3D cranial shape between narwhals (characterised by relatively short rostrum and wide neurocranium) and beluga whales (more elongated and narrower cranium). 3D models of crania for hybrid specimens plotted within intermediate regions of the morphological space while the 2D hemi-mandible of the hybrid was indistinguishable from that of the *M. monoceros* group. Cluster analyses supported classification of one hybrid (NHMD MCE-1356) in the beluga phenotype while the putative hybrid specimen (NHMD 1963.44.1.4) was classified as a narwhal. This work demonstrates that although hybrids could be discriminated from narwhals and belugas in the shape of their cranium, they will still retain dominant phenotypic traits of one species or the other due to different cross breeds of male and female.

4.1 Introduction

Monodontidae is a family of Odontoceti (toothed whales) that includes only two extant species: *Monodon monoceros* (Mm, narwhals), *Delphinapterus leucas* (Dl, beluga) which have only recently been adapted to cold waters (Bianucci, Pesci, Collareta, & Tinelli, 2019). These two species have a year-round Artic distribution and their habitats overlap especially during the winter migrations towards Disko Bay in Greenland (**Figure 4.1-** *Map of Greenland and the eastern Canadian Artic*) (Heide- Jørgensen & Reeves, 1993; Wiig, Heide-Jørgensen, Laidre, Garde, & Reeves, 2012). This is a feeding area where monodontids can find the pleuronectid flatfish *Renhardius hippoglossoides*. It also represents a sparse amount of open water with no complete sea-ice coverage and an exchange area for narwhals and beluga whales (Heide-Jørgensen et al., 2010). On the 30th March 1990, researchers found the skull of an hybrid in Disko Bay (Heide-Jørgensen & Reeves, 1993) which showed features from both monodontid species due to a wider and longer rostrum, and a number of horizontal teeth with a dental formula differing from both the beluga and the narwhal (the latter being virtually toothless except for the maxillary tusk). According to an Inuit hunter, the animal was killed in mid-May 1986-87, and it looked like a combination of the two species with a narwhal tail, and beluga pectoral fins with grey colouration (Heide-Jørgensen & Reeves, 1993). The hybrid ancestry of this "narluga" has recently been confirmed by genomic analyses (Skovrind et al., 2019). *D. leucas* and *M. monoceros* are phylogenetically very close (McGowen et al., 2009) and a spring interbreeding between the two does not seem impossible (Heide-Jørgensen et al., 2010; Kelly, Whiteley, & Tallmon, 2010).

In Cetacea, there are 57 described cases of hybridization (natural=27, and captivity=30) (do Nascimento Schaurich, Lopes, & de Oliveira, 2012) across species and genera, involving 22 species, of which 14 are listed as endangered (Bérubé, 2009; Kelly et al., 2010). In fact, natural hybridisation in mysticetes (Árnason, Lammers, Kumar, Nilsson, & Janke, 2018; Bérubé, 2009; Bérubé & Aguilar, 1998) and natural and in captivity hybridisation in odontocetes (Baird, Willis, Guenther, Wilson, & White, 1998; Willis et al., 2004,Yadzi, 2002), were abundantly described (Bérubé, 2009, 2009; do Nascimento Schaurich et al., 2012; Sylvestre & Tasaka, 1985; Zornetzer & Duffield, 2003).

Map of Greenland and the eastern Canadian Arctic
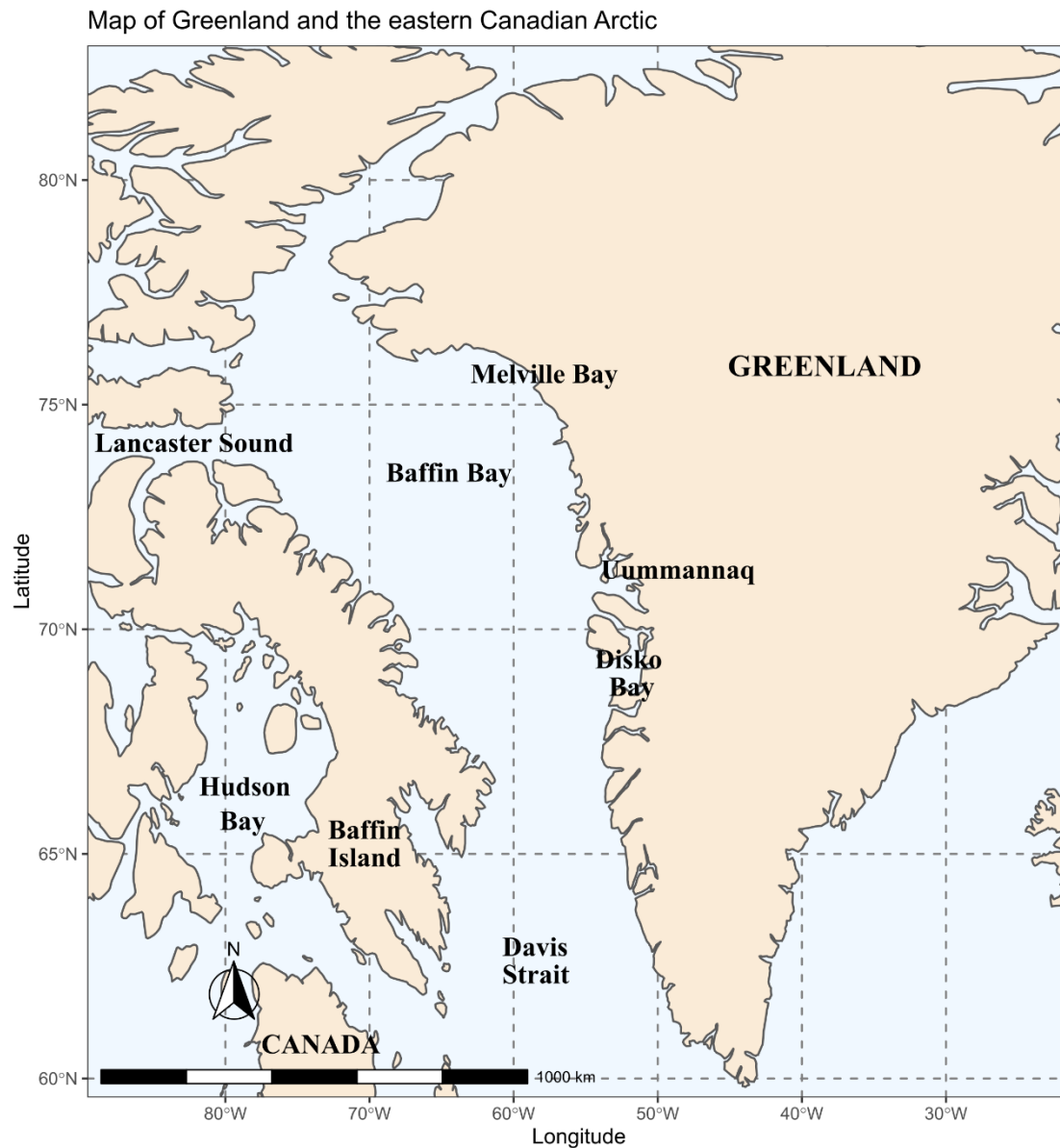
Figure 4.1 Localities related to narwhals (*Monodon monoceros*) and belugas (*Delphinapterus leucas*) distribution in Greenland and the eastern Canadian Arctic (created with "ggplot2" and "fs" packages in R).

Cetaceans are karyologically uniform (chromoson number 2n= 44), with only seven species where 2n=42 (Árnason & Benirschke, 1973; Árnason, Benirschke, Mead, & Nichols, 1978; Benirschke & Kumamoto, 1978; Jarrell, 1979; Kurihara, Tajima, Yamada, Matsuda, & Matsuishi, 2017; Pause, Bonde, McGuire, Zori, & Gray, 2006) which means that they evolve slowly at the molecular scale and have hybridisation cases more often than other mammals (Willis et al., 2004). In addition, large seasonal migrations, synchronous breeding seasons (Kelley, Stewart, Yurkowski, Ryan, & Ferguson, 2015), absence of geographical barriers in

the sea, as in the case of the mysticete clade, and global warming (Miralles, Oremus, Silva, Planes, & Garcia-Vazquez, 2016) can promote the interbreeding. It is unknown how hybridisation will affect the behavioural, feeding and breeding traits. Moreover, in the natural hybridisation it still need to be verified if the hybrid is fertile or with a reduced fertility, despite captive hybrids have been confirmed to be fertile as in the case of *T. truncatus* and *D. capensis* (Zornetzer & Duffield, 2003).

With regard to other marine mammals, 1144 natural and 7 in captivity hybridization events have been described within Pinnipedia (do Nascimento Schaurich et al., 2012) among the Phocidae (true seals) (Kovacs et al., 1997; Savriama et al., 2018) and the Otariidae (eared seals) (Melanie L Lancaster, Bradshaw, Goldsworthy, & Sunnucks, 2007; Melanie L Lancaster, Goldsworthy, & Sunnucks, 2010; Melanie Louise Lancaster, Gemmell, Negro, Goldsworthy, & Sunnucks, 2006), involving 13 species (do Nascimento Schaurich et al., 2012), and they have also been documented in the Ursidae (Doupe, England, Furze, & Paetkau, 2007; Pongracz, Paetkau, Branigan, & Richardson, 2017; Preuß, Gansloßer, Purschke, & Magiera, 2009; Stirling, 2009). Differently from cetaceans, pinnipeds show a higher degree of variation in chromosome number (2n= 32 to 36) (Arnason, 1990), for this reason only three hybridization cases can be found between different genera   (do Nascimento Schaurich et al., 2012).

Within the class of mammals in general, differences in hybrid morphologies, and genetics have been detected in the Rodentia (Patton, 1993; Runck, Matocq, & Cook, 2009; Spiridonova, Chelomina, Tsuda, Yonekawa, & Starikov, 2006), Carnivora (Gaubert, Taylor, Fernandes, Bruford, & Veron, 2005), Primates (Gligor et al., 2009), Artiodactyla (Senn & Pemberton, 2009; Senn, Swanson, Goodman, Barton, & Pemberton, 2010), and Lagomorpha (Thulin, Stone, Tegelström, & Walker, 2006).

Hybrid morphology is generally described as intermediate, displaying similar phenotypic characteristics to both parental species (Doupe et al., 2007; Yadzi, 2002; Zornetzer & Duffield, 2003) even among different vertebrate classes (Grant & Grant, 1996). It can also effect diet habit, and have long-term ecological and evolutionary consequences depending on the mating system, hybrid's frequency, and speciation process (Shurtliff, 2013). Most of the hybrids among marine mammals have been described morphologically (Baird et al., 1998; Brunner, 2002; Heide-Jørgensen & Reeves, 1993; Reyes, 1996; Willis et al., 2004) and only in the recent years molecular techniques have been applied for the identification of their parental species (do Nascimento Schaurich et al., 2012; Lancaster et al., 2007; Melanie Louise Lancaster et al.,

2006; Shurtliff, 2013; Skovrind et al., 2019; Willis et al., 2004). It is important to highlight the fact that all of the above-mentioned non-cetacean mammals hybridisation cases are examples within the same genus, which makes the inter-genus hybridization within cetaceans, and pinnipeds (in minor scale) very peculiar.

Geometric morphometrics demonstrated to be an effective tool to identify hybrid morphologies and their parental species across a range of vertebrates, including the fish Teleostei (Costa, Tibaldi, Pasqualetto, & Loy, 2006; Geiger, Schreiner, Delmastro, & Herder, 2016; Valentin, Sévigny, & Chanut, 2002), the bivalve Unionidae (Beauchamp, Beyett, Scott, & Zanatta, 2020), the mammalian Carnivora (Gaubert et al., 2005), and Primates (Gligor et al., 2009). In this work, I use a geometric morphometrics approach to characterise skull size and shape of one hybrid and one putative hybrid within the Monodontidae family. The hypotheses to be tested are the following: i) the narluga and the putative hybrid show a skull shape morphology that is intermediate between those of their parental species; ii) the putative hybrid crania belong to an anomalous narwhal or beluga, iii) they are testifying that a hybridisation event occurred between the two species (as already demonstrated for one of them; Skovrind et al., 2019), and they express different phenotypes depending on their parental species.

4.2   Material and Methods

Sample size

Data were collected on 157 monodontid crania including 86 *M. monoceros*, 69 *D. leucas*, one hybrid (MCE 1356) and one putative hybrid (NHMD 44.1.4.1963) and 85 disjointed left hemi-mandibles (64 *M. monoceros*, 20 *D. leucas*, one hybrid hemi-left mandible MCE 1356) **(Figure 4.2)** housed at Natural History Museum of Denmark (NHMD), National Museum of Scotland (NMS), and La Specola Museum, Florence (Italy) (**Appendix 4.1-**List of specimens). The hybrid "narluga" specimen MCE 1356 is the one found in Disko Bay in 1990 (Heide--Jørgensen & Reeves, 1993; Skovrind et al., 2019) and the putative hybrid NHMD 44.1.4.1963 included in the analysis has been found by D.V. during data collection at the NHMD. The latest was labelled as *Delphinapterus leucas*, but its cranial shape looked more like a narwhal, with beluga-like teeth. Crania were all adult specimens as the maxillary bones reached caudally the nuchal crest and part of the frontal bone was not visible (Cozzi et al., 2016).

For each cranium I collected 3D landmarks using a Microscribe digitiser directly on the specimens while mandibles were photographed in lateral view at a standard 1-meter distance using a Canon EOS 1100D digital camera (f/8, ISO 100, focal length = 37mm). The disjunct left hemi-mandibles generally belonged to the same individuals for which crania were available (n= 45) however, in order to maximise sample size, hemi-mandibles from specimens with no cranium (n= 40) were additionally included.
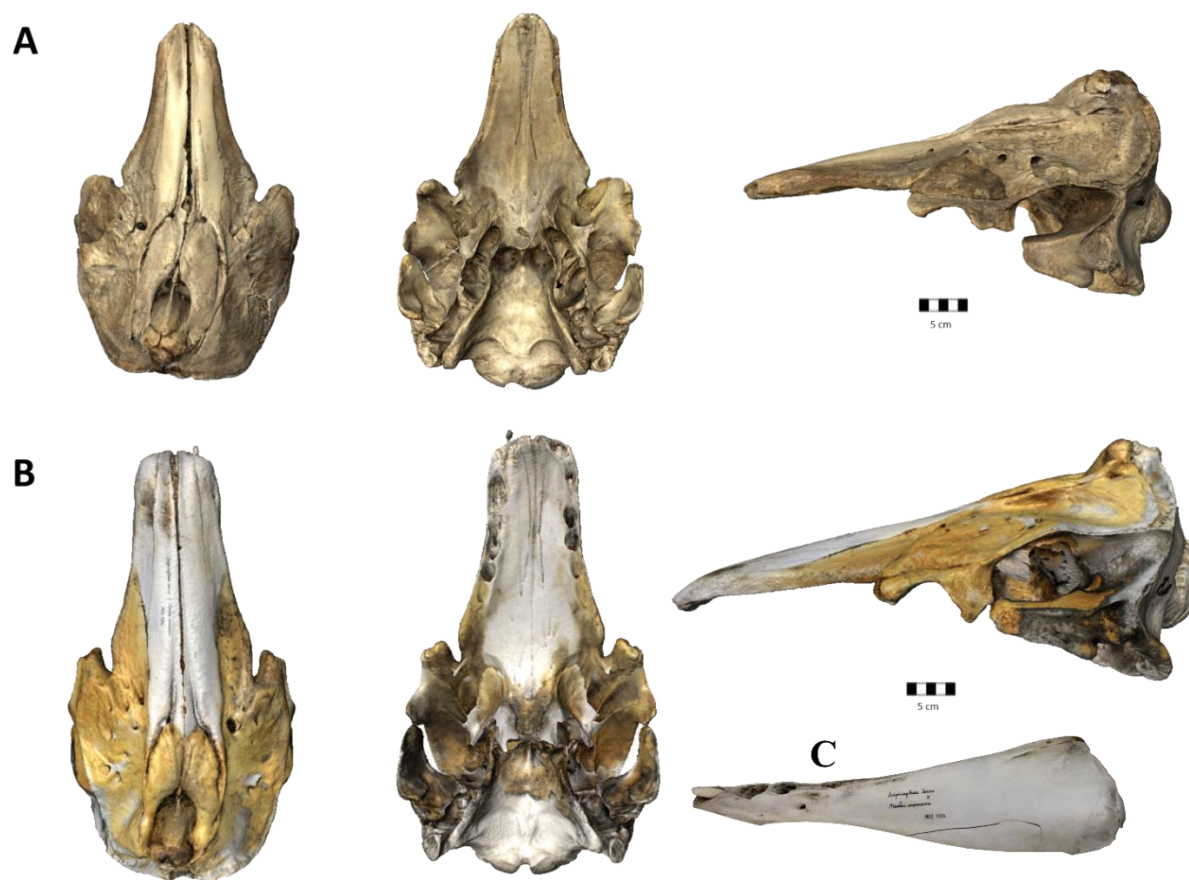
Figure 4.2 3D models of the crania of A) the putative hybrid specimen NHMD 44.1.4.1963 and B) the narluga MCE 1356 (Heide-Jorgensen & Randall, 1993). C) photo of the left hemi-mandible of MCE 1356 in lateral view. Scale bar 5cm.

For the cranium 42 three-dimensional landmarks were collected as representative of both dorsal and ventral part of the skull (**Figure 4.3**; **Table 4.1**). Most of these landmarks were type 2 (landmarks on the maximum or minimum curvature of a structure; Bookstein, 1991) and showed good level of repeatability. Due to the large size of the specimens, two landmarking sessions for each specimen were recorded on the crania in order to cover both dorsal and ventral parts, and these were then merged using DVLR (Dorsal-Ventral-Left-Right fitting, www.nycep.org/nmg) software. Due to missing landmarks occurring in 30 specimens of *D.leucas* and 40 *M.monoceros* specimens (for example the putative hybrid had missing landmarks on the pterygoids while the hybrid cranium was complete) the function *estimate.missing* on geomorph package (Adams & Otárola-Castillo, 2013; Sherratt, 2015) was used within each species group. Missing landmarks on the putative hybrid specimen (labelled as *D. leucas*) were estimated within *M. monoceros* group, as the DNA of this specimen suggested it is a narwhal (Eline D. Lorenzen, pers. comm.).

On the 85 hemi-mandibles, 22 two-dimensional landmarks were recorded using the software TPSDig (Rohlf, 2015). Of the 22 points, 7 were homologous landmarks as described in (Guidarelli, Nicolosi, Fusco, De Francesco, & Loy, 2014) and 16 were semilandmarks (**Figure 4.4**; see **Table 4.1** for landmarks description). A scale bar next to the specimen ensured scaling for each digital image. Subsequently sliders files indicating the semi-landmarks were prepared with TPSUtil, and a Generalized Procrustes Analysis (GPA), with sliding of semilandmarks (Bookstein, 1997) was performed in TpsRelw (Rohlf, 2015). The aligned 2D landmark coordinates were subsequently imported in R (Team & R Development Core Team, 2016) using function developed in the library geomorph for subsequent analyses.
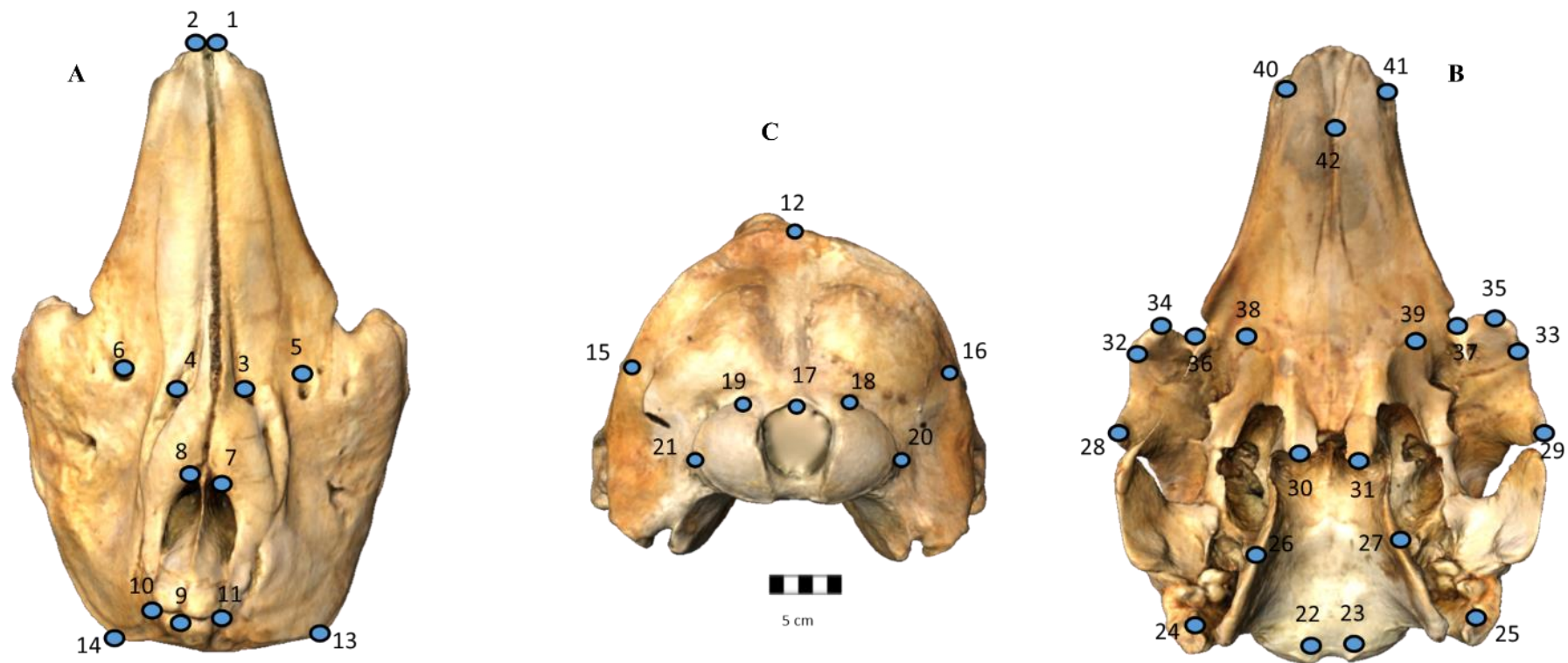
Figure 4.3 Landmark configuration on Photogrammetric-based 3D model specimen for the cranium of *Monodon monoceros* NHM 1937.10.30.2, in A) dorsal, B) ventral, and C) occipital view. See **Table 4.1** for landmark description. Scale bar 5 cm.
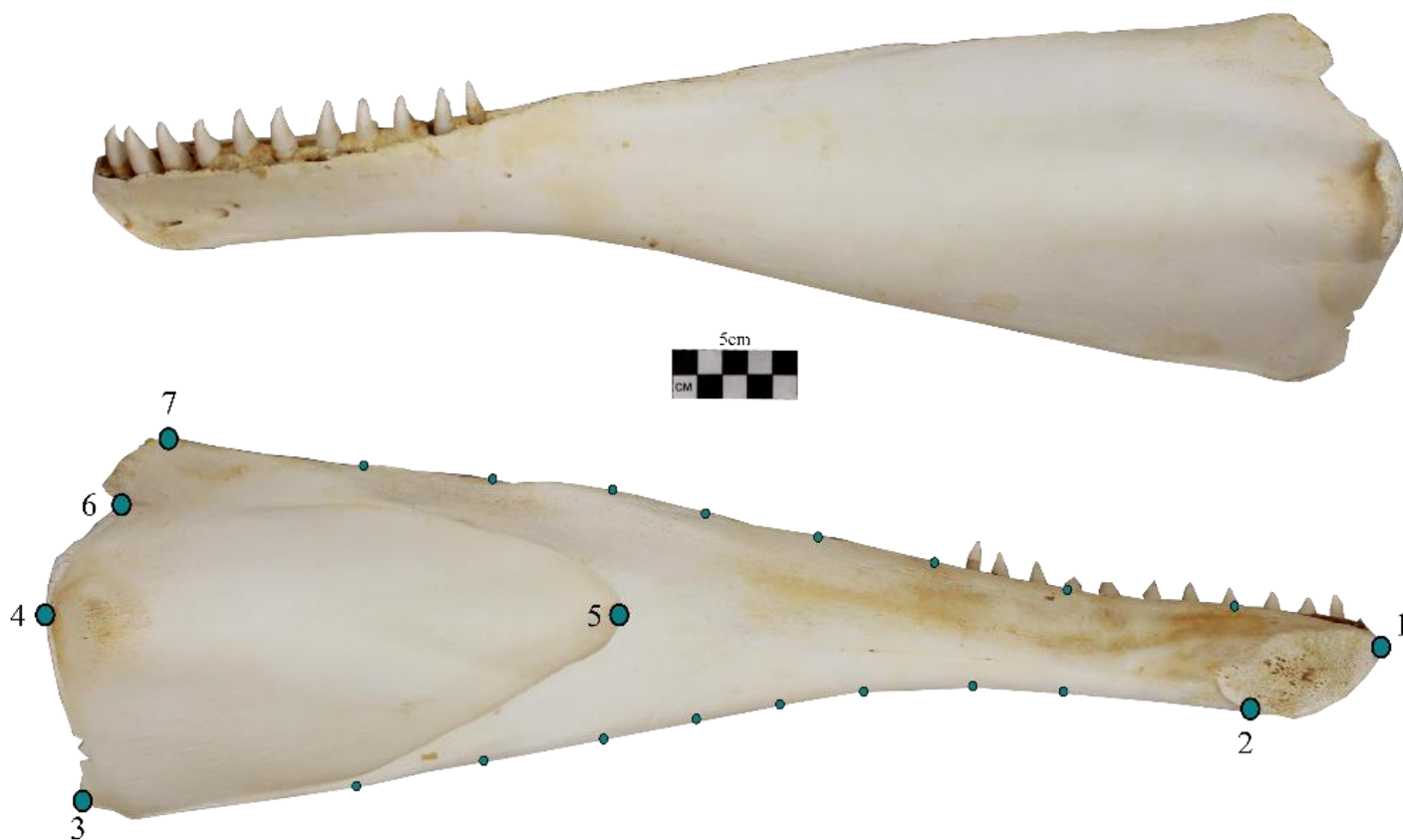
Figure 4.4 The position of the 7 anatomical landmarks, and 16 semilandmarks on a beluga whale mandible (*D. leucas* NHMN 1098) in lateral (above) and medial (below) view. See **Table 4.2** for landmark description. Scale bar is 5 cm.

Table 4.1 Description of landmarks taken on monodontid skulls used in GM analysis

	Homologous landmarks on the cranium
1-2	Tip of the rostrum
3-4	Anteriormost point of the premaxillary foramen
5-6	Anterior dorsal infraorbital foramen
7-8	Anteromedial point of the external bony nares
9	Anteriormost point of the medial suture between the nasal bones
10-11	Sutural triple-junction between nasal, frontal and maxilla
12	External occipital protuberance
13-14	Sutural triple-junction between supraoccipital, frontal and parietal
15-16	Posteriormost point on the temporal crest
17	*Opisthion*; middle point of the dorsal border of the *foramen magnum* on the intercondyloid notch
18-19	Dorsal tip of the occipital condyle
20-21	Lateral tip of the occipital condyle
22-23	Ventral tip of the occipital condyle
24-25	Medial tip of the paraoccipital process; ventralmost point of the paraoccipital process
26-27	Suture of pterygoid and basioccipital at the junction between pharyngeal crest and basioccipital crest
28-29	Posteroventral point of the postorbital process
30-31	Pterygoid *hamulus*; posterior margin of the hard palate and the border of the internal bony nares
32-33	Anteroventral point of the preorbital process of the frontal
34-35	Anterior tip of lacrimal bone
36-37	Antorbital notch
38-39	Anteriomost point of the palatine
40-41	Posteriormost point of the upper alveolar groove
42	Medial junction of vomer and premaxilla

Table 4.2 Description of landmarks taken on monodontid 2D mandibles used in GM analysis

	Homologous landmarks on the lingual view of the mandible
1	*Pogonion*; Tip of the mandible
2	*Gnathion*, the lowest point of the midline of the mandibular symphysis
3	Posterior ventral tip of the angular process
4	Posteriormost point of the condyle
5	Anteriormost point of the internal mandibular foramen
6	Most concave point of the mandibular notch
7	Dorsal tip of the coronoid process

Measurement Error

In order to explore the degree of measurement error introduced by the 3D landmarking with the Microscribe, linear measurements between selected anatomical landmarks were taken with a measuring tape (accuracy of 0.1 mm), and successively compared with inter-landmark distances (Ross & Williams, 2008) taken on dorsal and ventral view, as well as on the not combined and combined landmark configurations with DVLR. These distances were derived from the raw landmark coordinates using the software PAST (Hammer et al., 2001). To test the Microscribe accuracy, 18 landmarks on a 5 cm scale bar were taken right before the beginning of each landmarking session on skulls, and were compared with another Microscribe 2GX. The accuracy of landmarking sessions performed with the Microscribe was equally validated by comparing it with the landmarking sessions generated from virtual 3D models using Photogrammetry and Breuckmann laser scan (**Chapter 2**).

For the mandibles, each specimen was digitised twice with TPSDig and error computed on both size and shape data (see next section) following recommendations from Fruciano (2006) and Cardini (2004).

Geometric Morphometrics

For both crania and mandibles, the raw landmark coordinates were separately subjected to Generalised Procrustes Analysis (GPA) (Rohlf & Slice, 1990) by using "geomorph" package on R (Adams et al., 2016; D. C. Adams & Otárola-Castillo, 2013; Sherratt, 2014, 2015). This technique removes (3D in cranium and 2D in mandibles) the effect of differences in size, position, and orientation from the spatial coordinates (Rohlf & Marcus, 1993; Zelditch et al., 2012). This is an iterative procedure where variation in size is first removed by scaling each configuration so that it has a centroid size (CS = the squared root of the sum of squared distances between each landmark and the centroid) equal to 1.0; rotation and translation are taken into account by centring and rotating the landmark configuration in order to obtain an optimal solution that minimizes the quadratic distances between homologous points (Procrustes method, Bookstein, 1991; Zeldich,2012). After GPA, a new set of coordinates (named Procrustes) are then used as a proxy for shape variables to explore the potential for differences in cranial morphology between the specimens examined.

Due to the lack of replicas in the cranial data, it was not possible to assess the level of asymmetry in the analysed species so the covariance matrix of the whole shape data was not divided into symmetric and asymmetric component. Shape coordinates were subsequently

analysed with Principal Component Analysis (PCA). This technique allows to explore the degree of shape variation between specimens without any a priori hypotheses about species grouping and classification (Zelditch et al., 2012). Cranial shape variation along PCs axes was visualised using warping of 3D models already available via photogrammetry, while mandible shape changes from the mean were described using Thin Plate Spline (TPS) (Bookstein, 1991).

Allometry, that is the impact of size on shape variation (Zelditch et al., 2012) was separately explored on crania and mandibles after using log transformed CS as independent variable, and shape coordinates as dependent. Both PCA and allometry analysis were performed using the R package geomorph (Team, 2015).

Sexual size (SSD) and shape dimorphism within species was evaluated by Procrustes ANOVA (using the function "procD.lm" of "geomorph") on both crania and mandibles datasets. A subset of sexed cranial specimens ($n = 73$; *D. leucas* = 24, ♀ = 11, ♂ = 13; *M. monoceros* = 49, ♀ = 25, ♂ = 24) was used and hybrid and putative hybrid specimens were discarded from these analyses. The angle generated by allometric vectors between sexes per each species were calculated on MorphoJ (Klingenberg, 2011) and tested against the null hypotheses of perpendicularity (if the hypotheses is rejected it means that trajectories are significantly different from 90 degree, implying parallelism).

Classification tests

In order to identify phenotypic similarities of the hybrid and putative hybrid specimens to one species or the other in the selected sample of Monodontidae, multiple statistical approaches were adopted.

The Unweighted Pair Group Method with Arithmetic mean (UPGMA) clustering algorithm was used on Procrustes distances (independently in the cranium and mandible datasets) to detect similarities and clustering of specimens without any a priori hypotheses (Amaral, Coelho, Marugán-Lobón, & Rohlf, 2009; Cardini, 2014) in PAST (Hammer et al., 2001).

Then, Discriminant Function Analysis (DFA) in SPSS (IBM Corp.Released, 2017) was employed to identify specimens correctly ascribed to belugas or narwhals based on the morphological shape variables (Zelditch et al., 2012) Data entry for DFA were represented by Principal Component vector scores. To reduce data dimensionality, we adopted a stepwise method that proved already to be effective with shape variables (Meloro, 2011; Meloro et al., 2015). This method allows through an F-value and P value threshold detected with the

ANOVA, to keep only significant selection of variables that maximises differences between groups. All those variables are, then, added into the DFA equation iteratively in order to detect changes in Wilks lambda values. Wilks lambda varies between 0 and 1 and it measures how well groups are separated with smaller values indicating better discrimination. After variable selection, the Discriminant Function vector scores were employed to identify the percentage of correctly classified cases and predict group membership for the hybrid specimens that were set as unclassified. This was done through an iterative jacknifed process (cross-validation, Kovarovic et al. 2011).

Lastly, a K-mean clustering algorithm was adopted by setting two groups in order to predict, based on shape variables only, the clustering classification into one species or another in PAST (Hammer et al., 2001). In the K-mean clustering analysis, specimens are a priori divided into k-groups so that members of one group are more similar to each other, minimizing the within group variation (MacQueen, 1967). This analysis proceeds in steps that generate a loop: first, defining centroids of the K-mean groups, then associate each specimen with the closest centroid, before a new K centroid is re-calculated. This procedure will end when no more K centroids need recalculation as no more changes will occur. This analysis differs from the DFA as no a priori classification about the specimens is required, and the clusters will be formed considering similarity in morphological variables only.

Partial Least Squares (PLS)- Patterns of covariation between cranium and mandibular shape were explored using a two-block Partial Least Squares (2B-PLS) analysis (Zelditch et al., 2012, 2013) in a dataset of 46 complete skulls (*D. leucas* = 12, *M. monoceros* = 34 and 1 hybrid). For that, 2D mandibular coordinates were transformed into 3D coordinates by adding the z axis scores of 0.0 for each specimen. PLS is useful for studies on integration between two blocks of variables (Klingenberg, 2009; Klingenberg & Marugán-Lobón, 2013; Zelditch et al., 2012). Differently from the PCA, the PLS uses Singular Value Decomposition (SDV) to identify vectors called Singular Axes (SAs; Zelditch et al., 2012), which explain covariance in the same way as PCA explains variance. Unlike the PCs, SAs come in pairs, and each SA score accounts for the covariance between blocks (Klingenberg, 2009; Zelditch et al., 2012). Differences in covariation trajectories between species were tested using angular comparison of the PLS vectors in MorphoJ (Klingenberg, 2011; Klingenberg & Marugán-Lobón, 2013). The angle quantification provides an assessment of the possible interspecific dissimilarities in morphological integration of two species. Like the PCs, SAs can be described by deformations along axes, helping with the interpretation of the results (Zelditch et al., 2012). Statistical

significance was tested with a permutation test against the null hypothesis of no covariation between cranium and mandible (Zelditch et al., 2012).

4.2.1   Results

Crania

Dataset 1

Shape variation- PCA (**Figure 4.5**) computed on the shape data, was based on 42 homologous landmarks (**Figure 4.3**). PC1 and PC2 accounted for 77.3% of the total variance and PC3 described 2.6% only, for this reason its variation was discarded. On PC1 positive scores, crania show lateral compression of the maxilla and premaxillary bones. Compared with PC1 negative values the braincase is broader with a shorter nuchal crest, resulting in a spindle-shaped skull. The area of the occipital condyles described by 7 landmarks (LM 17, 18, 19, 20, 21, 22, 23), assumes a wider shape of the occipital condyles, located higher on the cranium. Landmarks on pterygoid *hamulus*, which delimits the posterior margin of the hard palate, and the border of the internal bony nares, converge towards the sagittal plane. Also, the landmarks on the teeth shift forwards in the narwhal, in relation with the presence of the maxillary tusk that is characteristic of this species.

PC2 axis was the one that better describes the changes in the relative elongation of the rostrum, the temporal area and the concavity of the profile of the facial region. In PC2 negative values the rostrum shows a shrinking and lengthening of the temporal fossa where the temporal muscles attach. It shows the dorsal displacement of the unpair landmark on the nucal crest. PC2 positive values describe a shortening of the pterygoids and forward shift of the nasal area together with the forward shift of the landmarks that cover the ventral most point of the paroccipital process and the beginning of the alveolar groove. The PCA plot shows the two putative hybrids (in violet) occupying the middle part of the morphospace right in between the two species group.
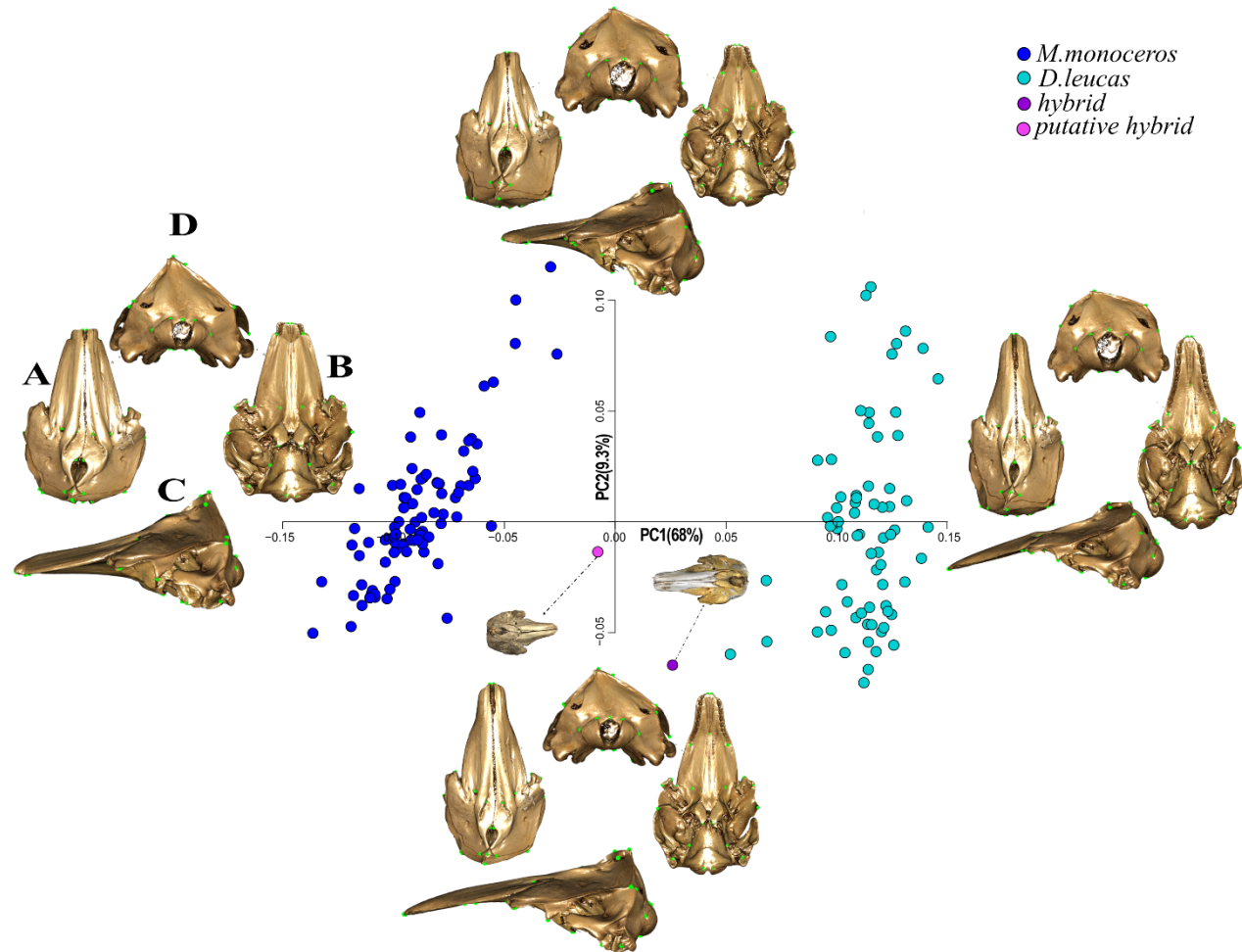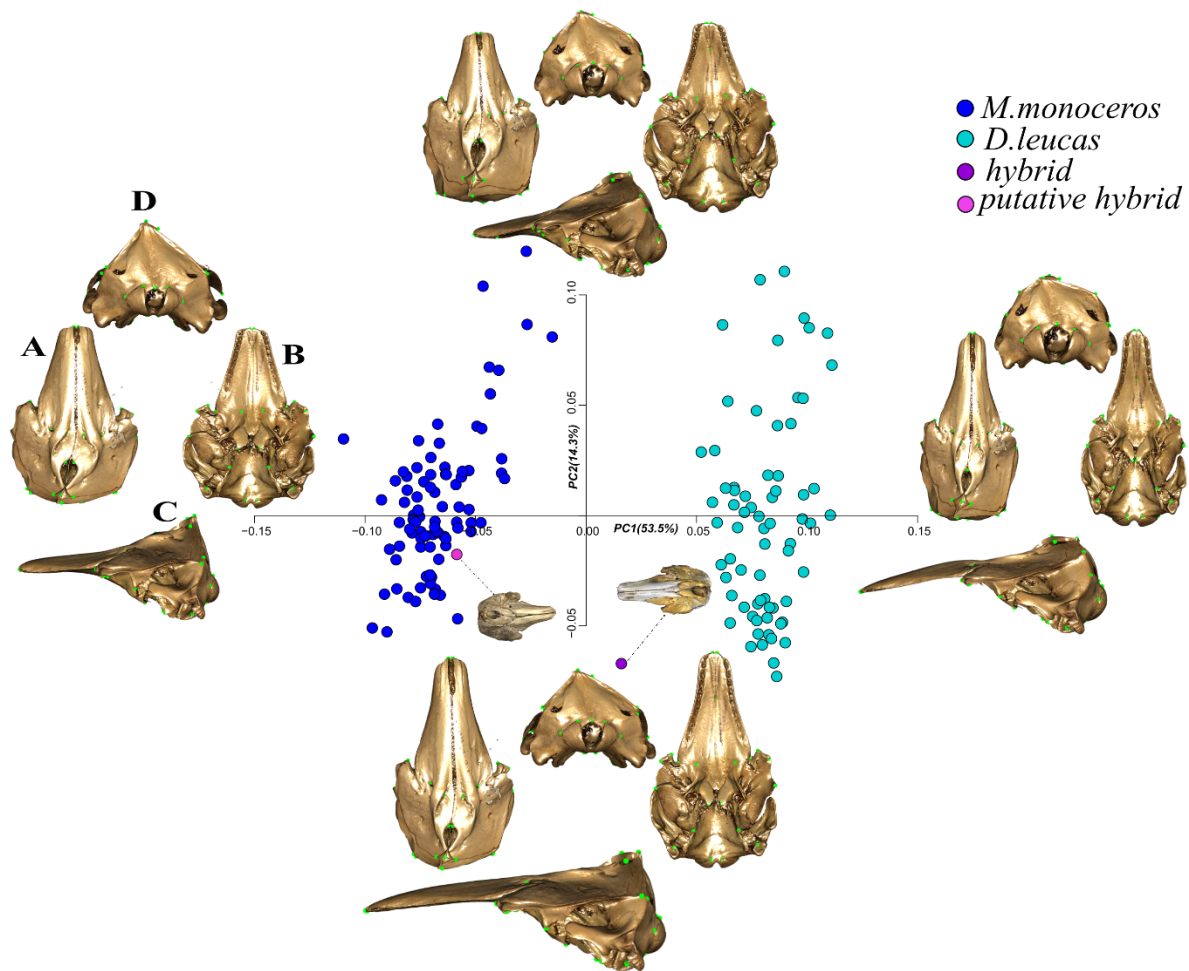
Figure 4.5 Scatterplot of the first two principal components obtained from PCA of 3D cranium shape configuration of 42 landmarks. Shape differences of positive and negative extremes of the principal component axes are shown in the 3D warping in A) dorsal, B) ventral, C) left lateral and D) posterior view.

Dataset 2: 40 landmarks

PC1 explained 53.5% of variation while PC2 explained 14.3% (**Figure 4.6**). These PCs were very similar to the previous PCs ran with 42 landmarks. The only difference is that the putative hybrid NHMD-1964.14.4 is now clearly clustering in the group of *Monodon monoceros*. Because this configuration is less affected by landmarks taken on the posterior most point of the alveolar groove, it was used for all the subsequent analyses.

Allometry - A significant impact of size on shape variation ($p < 0.001$) was found in this dataset with log CS explaining 26.42% of shape variance. The hybrid MCE-1356 is much larger than the putative hybrid specimen that falls clearly in the narwhals range (**Figure 4.7**). When the dataset was split by species (excluding hybrid and putative hybrid specimen), again a strong allometric component explained 34.27% in *Delphinapterus leucas* shape variation ($p < 0.0001$) and 23.13% in *Monodon monoceros* ($p < 0.001$). The angle computed between these two allometric trajectories was small (31.365°) and significantly different from 90 degrees ($p < 0.001$) supporting parallel slopes between the two species.

Figure 4.6 Scatterplot of the first two principal components obtained from PCA of 3D cranium shape configuration of 40 landmarks. Shape differences of positive and negative extremes of the principal component axes are shown in the 3D warping in A) dorsal, B) ventral, C) lateral and D) posterior view.
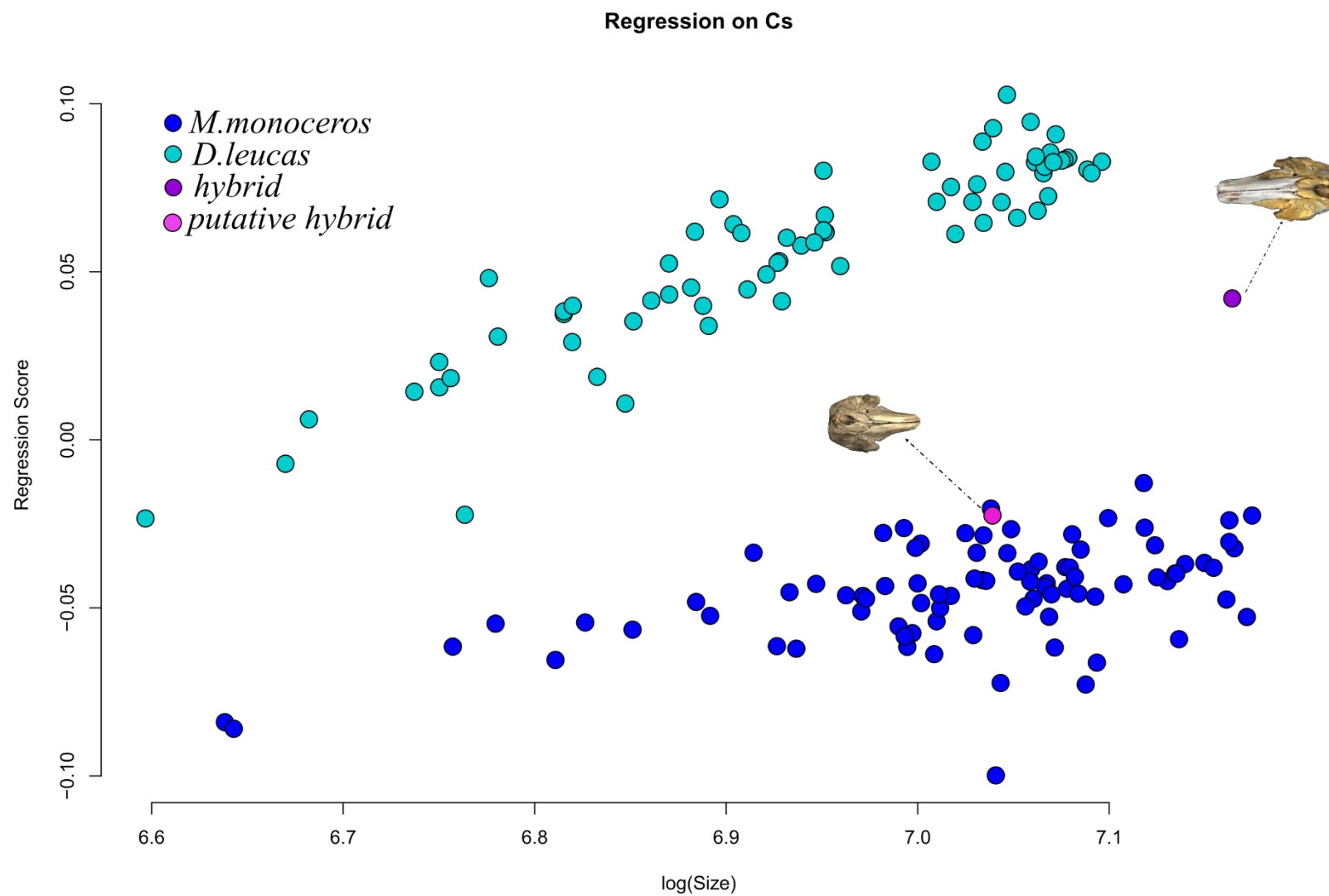
Figure 4.7 Scatter plot of the regression of the regression scores against the logCS for both species, to see the cranial shape changes in relation to size.

Sexual dimorphism

Procrustes ANOVA evidenced differences between sex allometric slopes within species for Centroid Size ($F_{2,73}$=1.842, *p=0.001*; **Table 4.3A).** When allometric trajectories were individually analysed for males and females within species, there was again a significant impact of size on shape that explained 41.25% of variance in *D. leucas* males (n =13; *p < 0.0001*), and 21.37% in *M. monoceros* males (n=24; *p < 0.0001*). Smaller and significant impact of size on shape was detected on females for both species explaining 15.93% of variance in *D. leucas* (n= 11, *p= 0.448*) and 32.40% in *M. monoceros* (n=25; *p < 0.0001*). The angle vector created between sexes for *D. leucas* was 61.94° (*p < 0.0001),* while it was 37.74° (*p < 0.0001)* for *M. monoceros*, meaning that the two vectors within each species are pointing in the same direction for both males and females. A boxplot showed greater values for CS in male specimens for both species (**Figure 4.8**). No significant shape differences were found between sexes within each species (*p = 0.354*; **Table 4.3B**), but differences were size related only (*p =0.001;* **Table 4.3B**).

Table 4.3 Procrustes ANOVA to test for A) slopes allometry and B) shape differences of sexes within species on crania shape of 73 monodontid specimens. Significance is highlighted in bold.

A) Shape~	Df	SS	MS	Rsq	F	Z	p
Cs	1	0.30081	0.30081	0.29663	87.3717	5.89845	**0.001**
Sex:Species	3	0.47046	0.15682	0.46392	45.548	7.57471	**0.001**
Cs:Sex:Species	3	0.01902	0.00634	0.01876	1.84195	3.79126	**0.001**
Residuals	65	0.22379	0.00344	0.22068			
Total	72	1.01410					
B) Shape~	Df	SS	MS	Rsq	F	Z	p
Sex	1	0.01246	0.01246	0.01229	2.7289	1.6559	0.071
Species	1	0.68183	0.68183	0.67234	149.3475	6.26	**0.001**
Sex:Species	1	0.00481	0.00481	0.00475	1.0541	0.3319	0.354
Residuals	69	0.31501	0.00457	0.31063			
Total	72	1.01411					
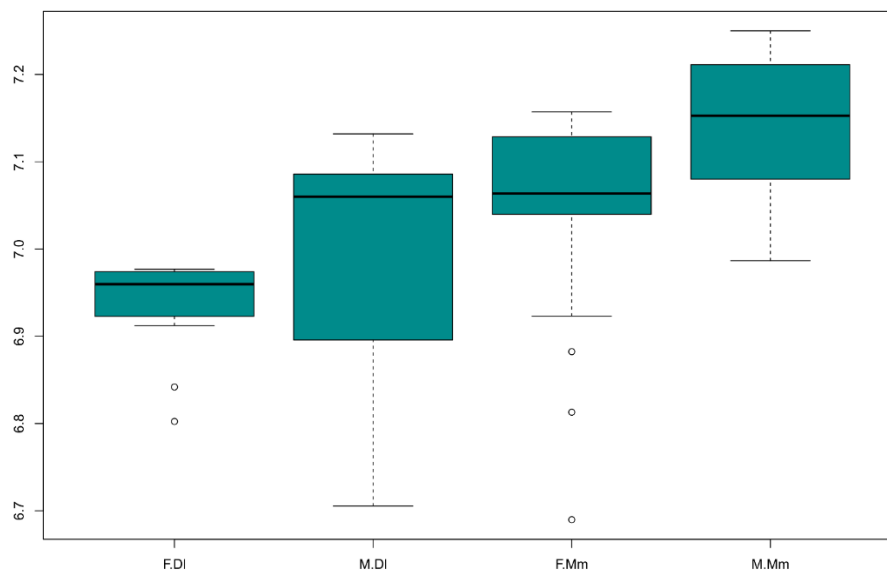
Figure 4.8 Boxplot showing logCS in Males (M) and Females (F) in *Delphinapterus leucas* (Dl) and *Monodon monoceros* (Mm).

Hybrid classification based on the cranium

The UPGMA phenogram (**Figure 4.9**) showed members of each species clustering together, while the putative hybride appeared to fall into the narwhal group, and the hybrid MCE-1356 was outside these two clusters. Cophenetic correlation for this UPGMA tree was quite high (r =0.9652), showing that it reflects well the similarity structure within the data.

DFA- After stepwise procedure, only 10 out of 113 shape PC vectors and log CS were selected by the DFA. A significant discriminant function vector was extracted to differentiate morphological groups (Wilk's lambda = 0.155, χ2 = 283.541, df= 2, *p < 0.0001*).

Cross-validation classification rates were pretty high for *D. leucas* specimens (95.7%) and allowed perfect assignation to *M. monoceros* specimens (100%). The DF function predicted the hybrid MCE-1356 as a *Delphinapterus leucas* and the putative hybrid NHMD-1964.14.4 as a *Monodon monoceros*.

This prediction was equally confirmed by the k-mean clustering algorithm (**Table 4.4)**
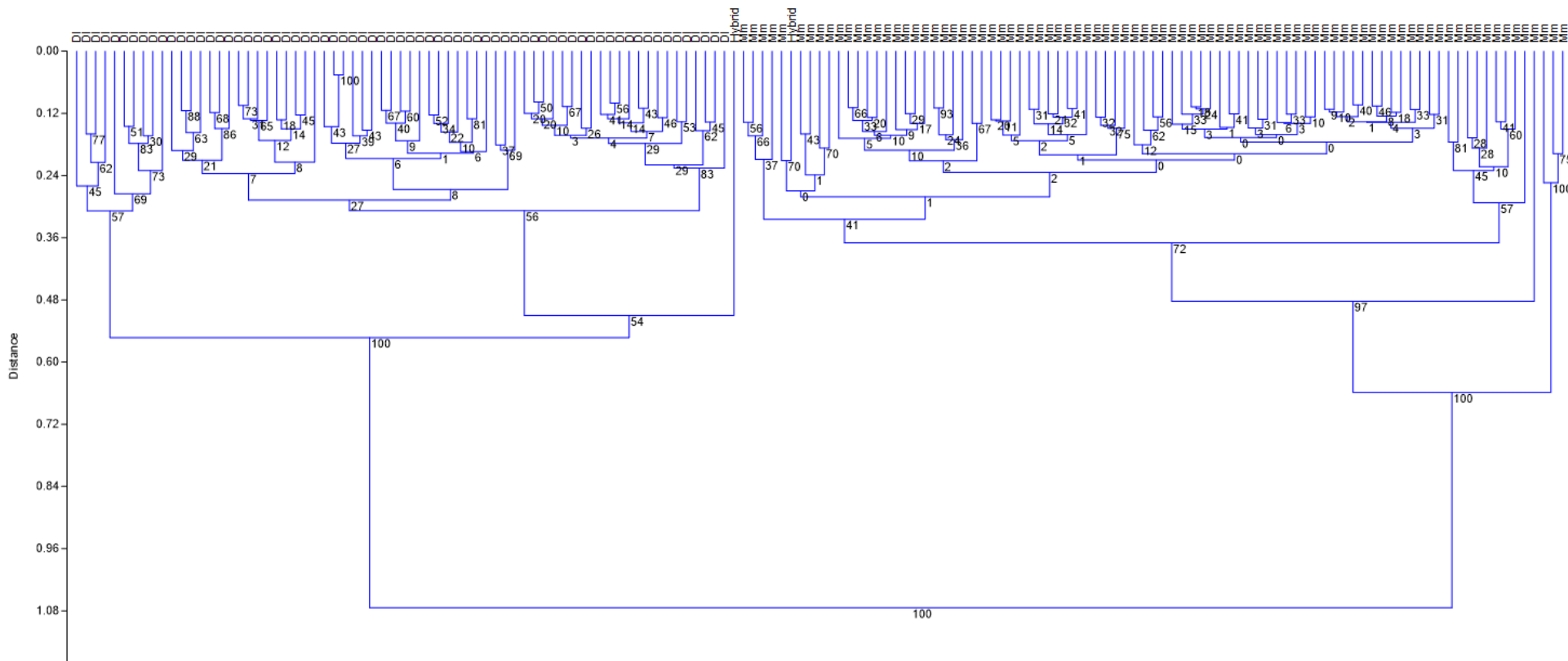
Figure 4.9 UPGMA computed on the matrix of the Procrustes distances among the crania shape of the Monodontidae family. Boot numbers tells us the reliability of groups. In this case 100% for Dl and 100% for Mm.

Table 4.4 Specimens classification in cluster after k-mean clustering

| Item	Cluster	Item	Cluster	Item	Cluster	Item	Cluster
Mm NHMD 12x	2	Mm NHMD 1428	2	Mm NHMD 1580	2	Mm MNHN 1903.103	2
Mm NHMD 1358.493	2	Mm NHMD 1432.2612	2	Mm NHMD 1583.4106	2	Mm NMS 1895.30.3	2
Mm NHMD 1361.537	2	Mm NHMD 1433.2619	2	Mm NHMD 1584-4107	2	Dl NHMD 085129	1
Mm NHMD 1364.655	2	Mm NHMD 1434.2614	2	Mm NHMD 1592M	2	Dl NHMD 085130	1
Mm NHMD 1365.656	2	Mm NHMD 1435.2619	2	Mm NHMD 1593.4115	2	Dl NHMD 1.17	1
Mm NHMD 1366.654	2	Mm NHMD 1437.2621	2	Mm NHMD 15x	2	Dl NHMD 1.4.1963	1
Mm NHMD 1370.3	2	Mm NHMD 1438.2623	2	Mm NHMD 17x	2	Dl NHMD 1.4.1963	1
Mm NHMD 1371.843	2	Mm NHMD 1439.2624	2	Mm NHMD 20	2	Dl NHMD 10	1
Mm NHMD 1372.5	2	Mm NHMD 1440.2626	2	Mm NHMD 2629.1443	2	Dl NHMD 11	1
Mm NHMD 1373.6	2	Mm NHMD 1441.2627	2	Mm NHMD 2751.1446	2	Dl NHMD 12	1
Mm NHMD 1378.850	2	Mm NHMD 1442.2628	2	Mm NHMD 2757	2	Dl NHMD 1306	1
Mm NHMD 1380	2	Mm NHMD 1445.2750	2	Mm NHMD 43	2		
Mm NHMD 1385.18	2	Mm NHMD 1451.2756	2	Mm NHMD 47	2		
Mm NHMD 1386.853	2	Mm NHMD 1452.2757	2	Mm NHMD 56x	2		
Mm NHMD 1387. 20	2	Mm NHMD 1454	2	Mm NHMD 5x	2		
Mm NHMD 1388.21	2	Mm NHMD 1455	2	Mm NHMD 84	2		
Mm NHMD 1389.22	2	Mm NHMD 1457.2768	2	Mm NHMD 847.1411	2		
Mm NHMD 1392. 25	2	Mm NHMD 1458.2769	2	Mm NHMD 85	2		
Mm NHMD 1393.26	2	Mm NHMD 1459.2770	2	Mm NHMD 888	2		
Mm NHMD 13x	2	Mm NHMD 1460.2771	2	Mm NHMD 950	2		
Mm NHMD 1406	2	Mm NHMD 1461	2	Mm NHMD 951	2		
Mm NHMD 1408	2	Mm NHMD 1462.2774	2	Mm NHMD 952	2		
Mm NHMD 1409.845	2	Mm NHMD 1463.2773	2	Mm NHMD 953	2		
Mm NHMD 1410	2	Mm NHMD 1464.2775	2	Mm NHMD 956	2		
Mm NHMD 1416	2	Mm NHMD 14x	2	Mm NHMD 974	2		
Mm NHMD 1422	2	Mm NHMD 1574	2	Mm NHMD 9x	2		
Mm NHMD 1423	2	Mm NHMD 1578	2	Mm NHMD 1456.2767	2		
Mm NHMD 1427	2	Mm NHMD 1579.2	2	Mm MNHN 1869.759	2		

Mandibles

The Procrustes ANOVA (**Table 4.5**) showed significant effect of individuals on shape ($p<0.0001$) and very little variance explained by error ($<5\%$). Also, the repeatability (R) score value was high (0.97).

Table 4.5 Procrustes ANOVA on replicas of mandibles 2D

Shape ANOVA							
Effect	SS	MS	df	F	P	Rsq	R
Species	0.06835	0.00683	10	39.72	<0.0001	0.30852	0.00667
Ind	0.14629	0.00017	850	21.65	<0.0001	0.66025	0.00684
Err-Rep	0.00691	7.9E-06	870			0.03122	**0.97**
Tot1	0.22156						
Tot2	0.15320						

The first two principal components on shape variables for the medial view of the mandible accounted for 37.8% and 26.4% of the shape variation (**Figure 4.10**) respectively, and showed a separation of the two species, while the hybrid occupied an intermediate position. Thin plate spline deformation grids showed that for positive PC1 scores mandibles are characterised by an enlargement of the mandibular foramen and a dorsoventrally lower mandible towards the tip. PC1 negative scores associate with a frontal posterior compression of the mandibular foramen, a dorsoventrally higher mandible along the dental groove, a slight change on the posterior ventral tip of the angular process (L7), and on the dorsal tip of the coronoid process (L3). PC3 and PC4 explain 9.7% and 5.8% of the variation respectively and did not show a partitioning between species.

Regression of shape against CS (**Figure 4.11**) for both species and the hybrid was significant ($p<0.001$) with size explaining 32.4% of the mandibular shape changes. No additional tests could be performed due to the low sample size per species and per sex, however a plot of size vs PC1 shape vector (**Figure 4.11**) shows the hydrid to cluster with *M. monoceros*.
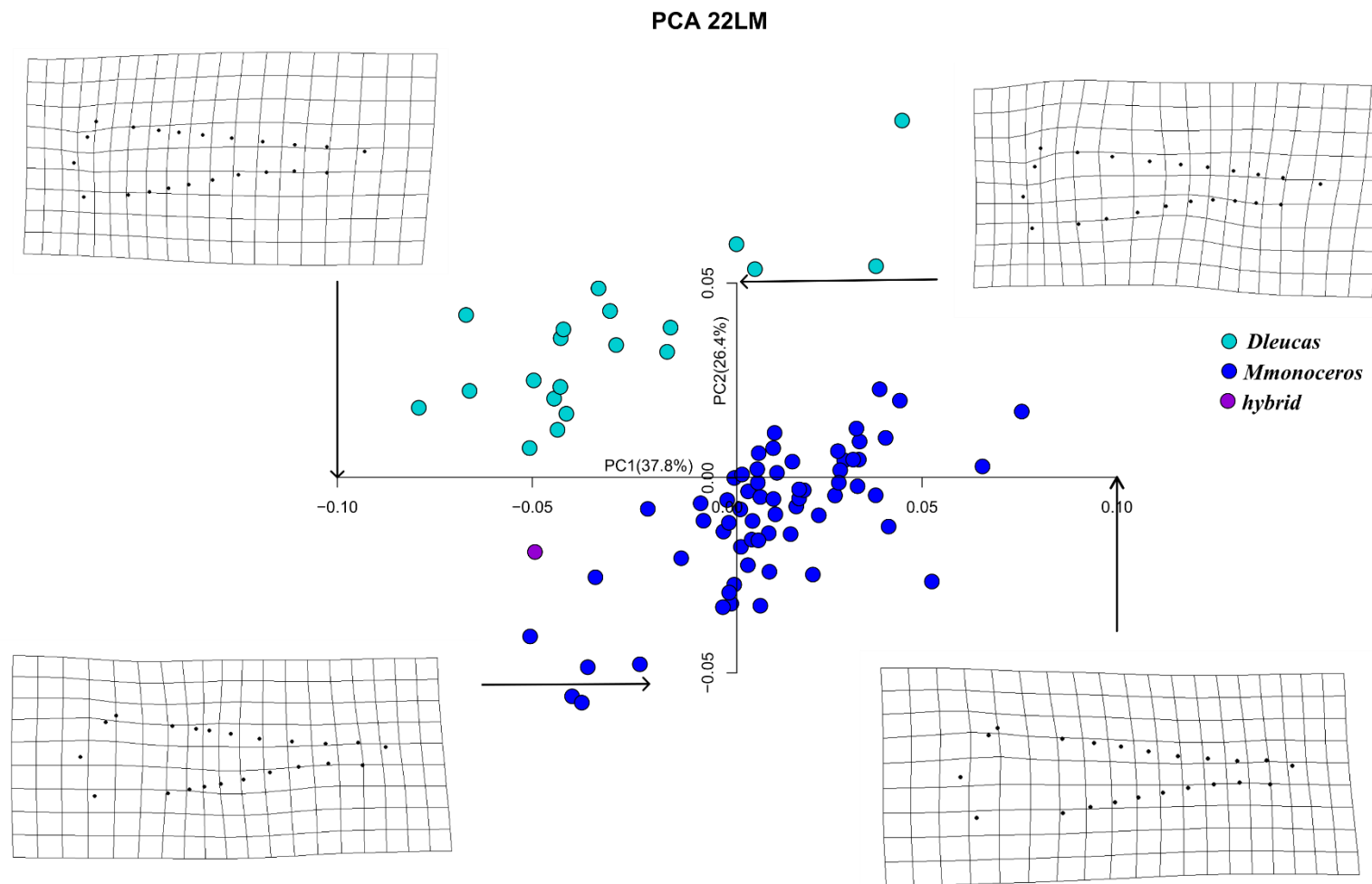
Figure 4.10 Scatterplot of the first two principal components obtained from PCA of 2D mandible shape configuration of 22 landmarks. Thin plate spline deformation grids show the shape differences of positive and negative extremes of the first and second principal component axis. See the text for details.
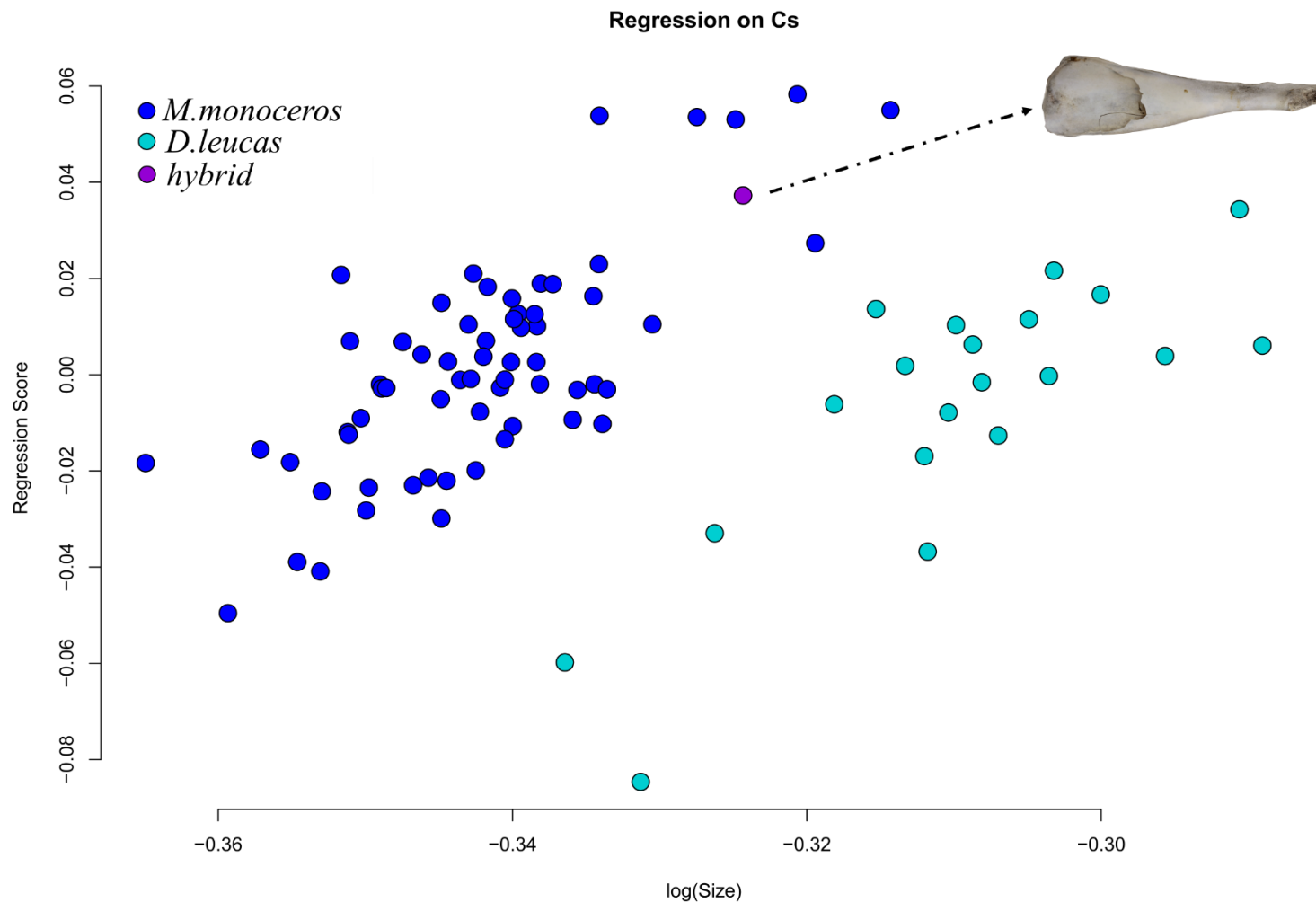
Figure 4.11 Scatter plot of the regression of the regression scores against the logCS for both species, to see the mandible shape changes in relation to size.

Hybrid classification based on the mandible

The UPGMA (**Figure 4.12**) cluster analysis identified a slight overlap between the species and the hybrid occupied an intermediate position, nearly outside *M. monoceros* and close to this overlap area, sharing similarities with both species. Cophenetic correlation for this cluster with Procrustes distances was r =0.7808.

k-mean clustering- This analysis supported MCE-1356 to belong to *D. leucas* group.

Figure 4.12 UPGMA computed on the matrix of the Procrustes distances among the mandible shape of the Monodontidae family. Light blue specimens correspond to *Delphinapterus leucas* specimens, dark blue to *Monodon monoceros* speciemens and violet to the hybrid specimen.

Cranial and Mandibular Integration

The 2B-PLS analysis is shown in **Figure 4.13.** The first pair of SAs accounted for 98.62% of the total squared covariance between cranium and mandible shape. The association between PLS1 scores of cranium and mandible was strong (r = 0.902) and significant (*p<0.0001*). Comparing the cranium axis of narwhals and belugas (excluding the hybrid), the PLS1 showed an angle of 89.764° and PLS2 an angle of 67.568°, and they were respectively not significant and significant (*p = 0.97469*; *p = 0.00221*; **Table 4.6**). The same results were obtained for the mandible, and the PLS1 showing an angle of 86.543°, and the PLS2 and angle of 59.343° (*p=0.64721*; *p= 0.00003;* **Table 4.6**).
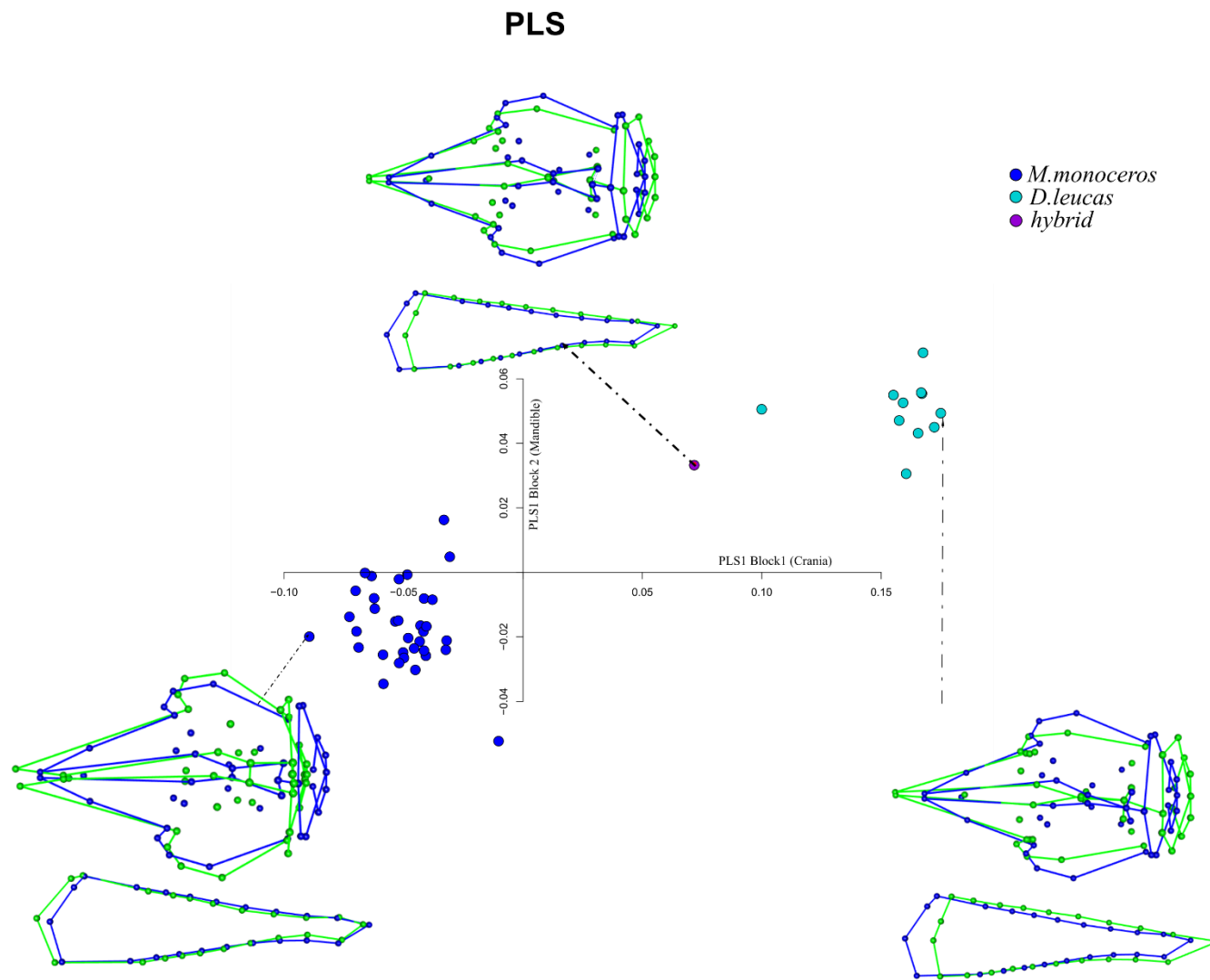
Figure 4.13 Plot of the firsts 2B-PLS dimension for the Monodontidae data. Ordinate, mandible; abscissa, cranium. Correlation is 0.902. Dotted line shows the hybrid wireframe.

Table 4.6 Angular comparison of PLS of block 1 (Crania) and 2 (Mandibles) axes between species. p-values of the above block1 and 2 PLS are highlighted in bold.

Block1	PLS1	PLS2	PLS3	PLS4
PLS1	**89.764** **0.97469**	43.514 <0.00001	87.438 0.73012	83.897 0.41085
PLS2	83.492 0.38042	**67.568** **0.00221**	87.103 0.69648	84.235 0.43725
Block2	**PLS1**	**PLS2**	**PLS3**	**PLS4**
PLS1	**86.543** **0.64721**	81.309 0.24914	71.096 0.01156	76.423 0.07101
PLS2	71.810 0.01517	**59.343** **0.00003**	63.579 0.00037	60.666 0.00007

4.2.2   Discussion

This study confirm that the "narluga" specimen numbered MCE-1356 is a narwhal-beluga hybrid, as previously demonstrated (Skovrind et al., 2019), but also that it displays cranial and mandibular characters that are closer to one parent species, the beluga.

The cranium in the two species is clearly distinct. Both have an elongated splanchnocranium with the *M. monoceros* group having a less pointed and more robust rostrum with asymmetric premaxilla. Maxilla provides insertion of the upper row of teeth in *D. leucas* while, unsurprisingly, part of the cranial differences in *M. monoceros* are explained by the development of the maxillary tusks. If all the shape characters are analysed, the hybrid MCE 1356 has an intermediate shape along the PC1 axis of variation. Contrary to the MCE 1356 hybrid, the putative hybrid NHMD 1963.44.1.4 is recovered in the *M. monoceros* morphospace in the dataset without landmarks on the posteriormost point of the alveolar groove (**Figure 4.6**). In fact, the DFA categorises the specimen NHMD 1963.44.1. 4 as a narwhal, suggesting that it is a narwhal with erupted teeth. DNA analyses have been performed by NHMD, confirming this result (data not yet published). In the recently published study by Skovrind et al. (2019) a genomic analysis confirmed the hybridisation between a female narwhal and a male beluga whale for the male specimen MCE 1356. Due to his particular dental formula, and higher δ^{13} C value, compared to its parental species, the hybrid has been identified as having a benthonic diet (Skovrind et al., 2019). In fact, the narluga tooth count was the strongest feature for its identification and teeth are apically worn testifying that the teeth were erupted during life and that the animal used them to catch its prey. This contrasts with the condition in NHMD-14.4.1964, here identified as a narwhal, which probably had unerupted teeth. It is notable that narwhals have 6 pairs of dental papillae in the maxillae (Heide--Jørgensen & Reeves, 1993). This is the first mention of a narwhal with a set of partly developed teeth other than the tusks. In the case of the specimen studied here, dental papillae may have developed in teeth, but without eruption out of the gum, a feature that is regularly observed in odontocetes with a reduced dentition (e.g., the sperm whale *Physeter macrocephalus*, one specimen is collected in the NHMD and several beaked whales; Boschma, 1938, 1951).

Sexual size dimorphism (SSD)- Sexual size dimorphism with males larger than females has already been observed in *Monodon monoceros* (Garde et al., 2007), and in 5 stocks of *Delphinapterus leucas* (Heide-Jørgensen & Teilmann, 1994; Ralls & Mesnick, 2009) in the Canadian Artic. Data on cranial SSD are in line with these previous observations, with both species having males bigger than females (**Figure 4.8**). Larger narwhal males show larger

tusks, which correlate with testes mass (Kelley et al., 2015) highlighting the males quality and fertility (Plön & Bernard, 2016). This would indicate the importance of the tusk for the narwhal mating system (Best, 1981), being a secondary sexual character that attracts females, and for sperm (female competition) competition (Kelley et al., 2015). SSD can also be explained by the age of attainment of maturity. In fact, narwhal males reach their physical maturity at a length of 457 cm at the age of 9 years while in females, this was found to be 396 cm in females at the age of 6-7 years (Garde, Heide-Jørgensen, Hansen, Nachman, & Forchhammer, 2007). Similar numbers can be found for belugas (Heide--Jørgensen & Teilmann, 1994).

Allometry- Allometry explains quite a significant portion of shape variation in the analysed sample with impact of size generally stronger on the skull shape of *D. leucas* rather than the narwhal. Clearly the narwhal sample extend its skull size beyond *D. leucas* but due to its lower impact on shape, it suggests that differences in adult growth and food partitioning might exists. This interpretation finds support when allometry is analysed by sex: the *M. monoceros* [whose males develop larger and with tusk] shows stronger impact of size vs shape in females rather than males, while in the beluga it is possible to observe the opposite. Such a difference in the sexes analysed is not due to different allometric trajectories perhaps it is the result of different variances (that is: in *M. monoceros* females adult vary much more in size than males whose selection towards large body homogenise their variation while in beluga it is the opposite).

PLS – Strong correlation between cranium and mandible was found. Dissimilarities in the morphological integration between cranium and mandible across the two parental species were detected as angular difference was near 90° between the PLS1 vectors for both blocks of landmarks. However, there were some significant similarities between some PLS axes, this can be related to the fact that some covariation pattern could be relatively similar. Plot displayed a clear separation of two species and their hybrid, having *D. leucas* with higher PLS1 scores, which follow the general pattern found in PCA. Most of the covariation in the first dimension of PLS describes differences in the length of the rostrum and mandible, and in the height of the braincase, placing the hybrid close to the belugas group. These differences were associated with a lengthening and strengthening of the tip of the mandible and a reduction of the mandibular foramen.

4.2.3 Conclusions

GM is a useful tool to determine and identify hybrids and mislabelled specimens in museum collections, genomic analyses can help to confirm if the hybridisation process occurred. This sample testifies that a hybridisation event occurred between the two species, and it expresses a phenotype closer to one of the parental species: the beluga.

References

Adams, D. C. *et al.* (2016) 'Geomorph: Software for geometric morphometric analyses'. Comprehensive R Archive Network.

Adams, D. C. and Otárola-Castillo, E. (2013) 'geomorph: an R package for the collection and analysis of geometric morphometric shape data', *Methods in Ecology and Evolution*. Wiley Online Library, 4(4), pp. 393–399.

Amaral, A. R. *et al.* (2009) 'Cranial shape differentiation in three closely related delphinid cetacean species: Insights into evolutionary history', *Zoology*. Elsevier, 112(1), pp. 38–47.

Arnason, U. (1990) 'Phylogeny of marine mammals-evidence from chromosomes and DNA', *Chromosomes today*, 10, pp. 267–278.

Árnason, Ú. *et al.* (1978) 'Banded karyotypes of three whales: Mesoplodon europaeus, M. carlhubbsi and Balaenoptera acutorostrata', *Hereditas*. Wiley Online Library, 87(2), pp. 189–200.

Árnason, Ú. *et al.* (2018) 'Whole-genome sequencing of the blue whale and other rorquals finds signatures for introgressive gene flow', *Science advances*. American Association for the Advancement of Science, 4(4), p. eaap9873.

Árnason, Ú. and Benirschke, K. (1973) 'Karyotypes and idiograms of sperm and pygmy sperm whales', *Hereditas*. Wiley Online Library, 75(1), pp. 67–74.

Baird, R. W. *et al.* (1998) 'An intergeneric hybrid in the family Phocoenidae', *Canadian Journal of Zoology*. NRC Research Press, 76(1), pp. 198–204.

Beauchamp, K. C. *et al.* (2020) 'Detection of hybrid Pyganodon grandis and P. lacustris (Bivalvia: Unionidae) using F-and M-type mitochondrial DNA sequences and geometric

morphometrics', *Journal of Molluscan Studies*.

Benirschke, K. and Kumamoto, A. (1978) 'The chromosomes of Cuvier's beaked whale, Ziphius cavirostris', *Mammal Chrom Newsl*, 19, pp. 70–72.

Bérubé, M. (2009) 'Hybridism', in *Encyclopedia of marine mammals*. Elsevier, pp. 588–592.

Bérubé, M. and Aguilar, A. (1998) 'A new hybrid between a blue whale, Balaenoptera musculus, and a fin whale, B. physalus: frequency and implications of hybridization', *Marine Mammal Science*. Wiley Online Library, 14(1), pp. 82–98.

Bianucci, G. *et al.* (2019) 'A new Monodontidae (Cetacea, Delphinoidea) from the lower Pliocene of Italy supports a warm-water origin for narwhals and white whales', *Journal of Vertebrate Paleontology*. Taylor & Francis, 39(3), p. e1645148.

Bookstein, F. (1991) '199 1. Morphometric Tools for Landmark Data: Geometry and Biology'. Cambridge Univ. Press, New York.

Bookstein, F. L. (1997) *Morphometric tools for landmark data: geometry and biology*. Cambridge University Press.

Boschma, H. (1938) *On the teeth and some other particulars of the sperm whale (Physeter macrocephalus L.)*. Temminckia.

Boschma, H. (1951) 'Rows of small teeth in ziphioid whales', *Zoologische Mededelingen*, 31(14), pp. 139–148.

Brunner, S. (2002) 'A probable hybrid sea lion—Zalophus californianus× Otaria byronia', *Journal of mammalogy*. American Society of Mammalogists 810 East 10th Street, PO Box 1897, Lawrence …, 83(1), pp. 135–144.

Cardini, A. (2014) 'Missing the third dimension in geometric morphometrics: how to assess if 2D images really are a good proxy for 3D structures?', *Hystrix, the Italian Journal of Mammalogy*, 25(2), pp. 73–81.

Costa, C. *et al.* (2006) 'Morphometric comparison of the cephalic region of cultured Acipenser baerii (Brandt, 1869), Acipenser naccarii (Bonaparte, 1836) and their hybrid', *Journal of Applied Ichthyology*. Wiley Online Library, 22(1), pp. 8–14.

Cozzi, B., Huggenberger, S. and Oelschläger, H. A. (2016) *Anatomy of dolphins: insights into body structure and function*. Academic Press.

Doupe, J. P. *et al.* (2007) 'Most northerly observation of a grizzly bear (Ursus arctos) in Canada: photographic and DNA evidence from Melville Island, Northwest Territories', *Arctic*. JSTOR, pp. 271–276.

Garde, E. *et al.* (2007) 'Age-specific growth and remarkable longevity in narwhals (Monodon monoceros) from West Greenland as estimated by aspartic acid racemization', *Journal of Mammalogy*. American Society of Mammalogists 810 East 10th Street, PO Box 1897, Lawrence …, 88(1), pp. 49–58.

Gaubert, P. *et al.* (2005) 'Patterns of cryptic hybridization revealed using an integrative approach: a case study on genets (Carnivora, Viverridae, Genetta spp.) from the southern African subregion', *Biological Journal of the Linnean Society*. Oxford University Press, 86(1), pp. 11–33.

Geiger, M. F. *et al.* (2016) 'Combining geometric morphometrics with molecular genetics to investigate a putative hybrid complex: a case study with barbels Barbus spp.(Teleostei: Cyprinidae)', *Journal of Fish Biology*. Wiley Online Library, 88(3), pp. 1038–1055.

Gligor, M. *et al.* (2009) 'Hybridization between mouse lemurs in an ecological transition zone in southern Madagascar', *Molecular Ecology*. Wiley Online Library, 18(3), pp. 520–533.

Grant, B. R. and Grant, P. R. (1996) 'High survival of Darwin's finch hybrids: effects of beak morphology and diets', *Ecology*. Wiley Online Library, 77(2), pp. 500–509.

Guidarelli, G. *et al.* (2014) 'Morphological variation and modularity in the mandible of three Mediterranean dolphin species', *Italian Journal of Zoology*. Taylor & Francis, 81(3), pp. 354–367.

Hammer, Ø., Harper, D. A. and Ryan, D. D. (2001) 'PAST: PALEONTOLOGICAL STATISTICS SOFTWARE PACKAGE FOR EDUCATION AND DATA ANALYSIS', *Palaeontologia Electronica 178kb. T. Harper. Geological Museum*. doi: 10.1016/j.bcp.2008.05.025.

Heide-Jørgensen, M. P. *et al.* (2010) 'The effect of sea-ice loss on beluga whales (Delphinapterus leucas) in West Greenland', *Polar Research*. Taylor & Francis, 29(2), pp. 198–208.

Heide-Jørgensen, M. P. and Reeves, R. R. (1993) 'Description of an anomalous monodontid skull from west Greenland: a possible hybrid?', *Marine Mammal Science*. Wiley Online

Library, 9(3), pp. 258–268.

Heide-Jørgensen, M. P. and Teilmann, J. (1994) 'Growth, reproduction. age structure and feeding habits of white whales (Delphinapterus leucas) in West', *Studies of White Whales (Delphinapterus leucas) and Narwhals (Monodon monoceros) in Greenland and Adjacent Waters*. Commission for Scientific Research in Greenland, p. 195.

IBM Corp.Released (2017) 'IBM SPSS Statistics for Windows, Version 25.0. Armonk, NY: IBM Corp'. NY: IBM Corp.

Jarrell, G. H. (1979) 'Karyotype of the bowhead whale (Balaena mysticetus)', *Journal of Mammalogy*. JSTOR, 60(3), pp. 607–610.

Kelley, T. C. *et al.* (2015) 'Mating ecology of beluga (Delphinapterus leucas) and narwhal (Monodon monoceros) as estimated by reproductive tract metrics', *Marine Mammal Science*. Wiley Online Library, 31(2), pp. 479–500.

Kelly, B. P., Whiteley, A. and Tallmon, D. (2010) 'The Arctic melting pot', *Nature*. Nature Publishing Group, 468(7326), p. 891.

Klingenberg, C. P. (2009) 'Morphometric integration and modularity in configurations of landmarks: tools for evaluating a priori hypotheses', *Evolution & development*. Wiley Online Library, 11(4), pp. 405–421.

Klingenberg, C. P. (2011) 'MorphoJ: An integrated software package for geometric morphometrics', *Molecular Ecology Resources*. doi: 10.1111/j.1755-0998.2010.02924.x.

Klingenberg, C. P. and Marugán-Lobón, J. (2013) 'Evolutionary covariation in geometric morphometric data: analyzing integration, modularity, and allometry in a phylogenetic context', *Systematic biology*. Oxford University Press, 62(4), pp. 591–610.

Kovacs, K. M. *et al.* (1997) 'A harp seal× hooded seal hybrid', *Marine Mammal Science*. Wiley Online Library, 13(3), pp. 460–468.

Kovarovic, K., Aiello, L.C., Cardini, A. and Lockwood, C.A., 2011. Discriminant function analyses in archaeology: are classification rates too good to be true? *Journal of Archaeological Science*, *38*(11), pp.3006-3018.

Kurihara, N. *et al.* (2017) 'Description of the karyotypes of Stejneger's beaked whale (Mesoplodon stejnegeri) and Hubbs' beaked whale (M. carlhubbsi)', *Genetics and molecular*

biology. SciELO Brasil, 40(4), pp. 803–807.

Lancaster, M. L. *et al.* (2006) 'Ménage à trois on Macquarie Island: hybridization among three species of fur seal (Arctocephalus spp.) following historical population extinction', *Molecular Ecology*. Wiley Online Library, 15(12), pp. 3681–3692.

Lancaster, M. L. *et al.* (2007) 'Lower reproductive success in hybrid fur seal males indicates fitness costs to hybridization', *Molecular Ecology*. Wiley Online Library, 16(15), pp. 3187–3197.

Lancaster, M. L., Goldsworthy, S. D. and Sunnucks, P. (2010) 'Two behavioural traits promote fine-scale species segregation and moderate hybridisation in a recovering sympatric fur seal population', *BMC evolutionary biology*. Springer, 10(1), p. 143.

MacQueen, J. (1967) 'Some methods for classification and analysis of multivariate observations', in *Proceedings of the fifth Berkeley symposium on mathematical statistics and probability*. Oakland, CA, USA, pp. 281–297.

Mallet, J. (2005) 'Hybridization as an invasion of the genome', *Trends in ecology & evolution*. Elsevier, 20(5), pp. 229–237.

McGowen, M. R., Spaulding, M. and Gatesy, J. (2009) 'Divergence date estimation and a comprehensive molecular tree of extant cetaceans', *Molecular Phylogenetics and Evolution*. Elsevier Inc., 53(3), pp. 891–906. doi: 10.1016/j.ympev.2009.08.018.

Meloro, C. (2011) 'Feeding habits of Plio-Pleistocene large carnivores as revealed by the mandibular geometry', *Journal of Vertebrate Paleontology*. Taylor & Francis, 31(2), pp. 428–446.

Meloro, C., Hudson, A. and Rook, L. (2015) 'Feeding habits of extant and fossil canids as determined by their skull geometry', *Journal of Zoology*. Wiley Online Library, 295(3), pp. 178–188.

Miller, E. H., Stewart, A. R. J. and Stenson, G. B. (1998) 'Bacular and testicular growth, allometry, and variation in the harp seal (Pagophilus groenlandicus)', *Journal of Mammalogy*. American Society of Mammalogists 810 East 10th Street, PO Box 1897, Lawrence …, 79(2), pp. 502–513.

Miralles, L. *et al.* (2016) 'Interspecific hybridization in pilot whales and asymmetric genetic introgression in northern Globicephala melas under the scenario of global warming', *PloS one*.

Public Library of Science San Francisco, CA USA, 11(8), p. e0160080.

do Nascimento Schaurich, M., Lopes, F. R. V. and de Oliveira, L. R. (2012) 'Hybridization phenomenon in cetacean and pinniped species', *Neotropical Biology and Conservation*, 7(3), pp. 199–209.

Patton, J. L. (1993) 'Hybridization and hybrid zones in pocket gophers (Rodentia, Geomyidae)', *Hybrid zones and the evolutionary process (RG Harrison, ed.). Oxford University Press, New York*, pp. 290–308.

Pause, K. C. *et al.* (2006) 'G-banded karyotype and ideogram for the North Atlantic right whale (Eubalaena glacialis)', *Journal of Heredity*. Oxford University Press, 97(3), pp. 303–306.

Plön, S. and Bernard, R. (2016) 'Testis, spermatogenesis, and testicular cycles', in *Reproductive Biology and Phylogeny of Cetacea: Whales, Porpoises and Dolphins*. CRC Press, pp. 227–256.

Pongracz, J. D. *et al.* (2017) 'Recent hybridization between a polar bear and grizzly bears in the Canadian Arctic', *Arctic*. JSTOR, pp. 151–160.

Preuß, A. *et al.* (2009) 'Bear-hybrids: behaviour and phenotype', *Der Zoologische Garten*. Elsevier, 78(4), pp. 204–220.

Ralls, K. and Mesnick, S. (2009) 'Sexual dimorphism', in *Encyclopedia of marine mammals*. Elsevier, pp. 1005–1011.

Reyes, J. C. (1996) 'A possible case of hybridism in wild dolphins', *Marine Mammal Science*. Wiley Online Library, 12(2), pp. 301–307.

Rohlf, F. J. (2015) 'The tps series of software.', *Hystrix*, 26(1).

Rohlf, F. J. and Marcus, L. F. (1993) 'A revolution morphometrics', *Trends in ecology & evolution*. Elsevier, 8(4), pp. 129–132.

Ross, A. H. and Williams, S. (2008) 'Testing repeatability and error of coordinate landmark data acquired from crania', *Journal of Forensic Sciences*. Wiley Online Library, 53(4), pp. 782–785.

Runck, A. M., Matocq, M. D. and Cook, J. A. (2009) 'Historic hybridization and persistence of a novel mito-nuclear combination in red-backed voles (genus Myodes)', *BMC Evolutionary Biology*. Springer, 9(1), p. 114.

Savriama, Y. *et al.* (2018) 'Bracketing phenogenotypic limits of mammalian hybridization', *Royal Society open science*. The Royal Society, 5(11), p. 180903.

Senn, H. V *et al.* (2010) 'Phenotypic correlates of hybridisation between red and sika deer (genus Cervus)', *Journal of Animal Ecology*. JSTOR, pp. 414–425.

Senn, H. V and Pemberton, J. M. (2009) 'Variable extent of hybridization between invasive sika (Cervus nippon) and native red deer (C. elaphus) in a small geographical area', *Molecular ecology*. Wiley Online Library, 18(5), pp. 862–876.

Sherratt, E. (2014) 'Quick guide to Geomorph v. 2.0', *Quick Guide to Geomorph.[Online][Accessed 5 July 2016] Available from: http://www. public. iastate. edu*.

Sherratt, E. (2015) *Tips & Tricks 8: Examining Replicate Error | R-bloggers*. Available at: https://www.r-bloggers.com/tips-tricks-8-examining-replicate-error/ (Accessed: 19 February 2019).

Shurtliff, Q. R. (2013) 'Mammalian hybrid zones: a review', *Mammal Review*. Wiley Online Library, 43(1), pp. 1–21.

Skovrind, M. *et al.* (2019) 'Hybridization between two high Arctic cetaceans confirmed by genomic analysis', *Scientific Reports*. Nature Publishing Group, 9(1), p. 7729.

Spiridonova, L. N. *et al.* (2006) 'Genetic evidence of extensive introgression of short-tailed ground squirrel genes in a hybridization zone of Spermophilus major and S. erythrogenys, inferred from sequencing of the mtDNA cytochrome b gene', *Russian Journal of Genetics*. Springer, 42(7), pp. 802–809.

Stirling, I. (2009) 'Polar Bear: Ursus maritimus', in *Encyclopedia of Marine Mammals*. Elsevier, pp. 888–890.

Sylvestre, J. P. and Tasaka, S. (1985) 'On the intergeneric hybrids in cetaceans', *Aquatic Mammals*, 11(3), pp. 101–108.

Team, R. D. C. and R Development Core Team, R. (2016) 'R: A Language and Environment for Statistical Computing', *R Foundation for Statistical Computing*. doi: 10.1007/978-3-540-74686-7.

Team, Rs. (2015) 'RStudio: Integrated Development for R', *[Online] RStudio, Inc., Boston, MA URL http://www. rstudio. com*. doi: https://www.nrel.gov/docs/fy16osti/65298.pdf.

Thulin, C.-G. *et al.* (2006) 'Species assignment and hybrid identification among Scandinavian hares Lepus europaeus and L. timidus', *Wildlife Biology*. BioOne, 12(1), pp. 29–38.

Valentin, A., Sévigny, J. and Chanut, J. (2002) 'Geometric morphometrics reveals body shape differences between sympatric redfish Sebastes mentella, Sebastes fasdatus and their hybrids in the Gulf of St Lawrence', *Journal of fish biology*. Wiley Online Library, 60(4), pp. 857–875.

Wiig, Ø. *et al.* (2012) 'Geographic variation in cranial morphology of narwhals (Monodon monoceros) from Greenland and the eastern Canadian Arctic', *Polar biology*. Springer, 35(1), pp. 63–71.

Willis, P. M. *et al.* (2004) 'Natural hybridization between Dall's porpoises (Phocoenoides dalli) and harbour porpoises (Phocoena phocoena)', *Canadian Journal of Zoology*. NRC Research Press, 82(5), pp. 828–834.

Yadzi, P. (2002) 'A possible hybrid between the dusky dolphin (Lagenorhynchus obscurus) and the southern right whale dolphin (Lissodelphis peronii)', *Aquatic Mammals*. EUROPEAN ASSOCIATION FOR AQUATIC MAMMALS, 28(2), pp. 211–217.

Yurkowski, D. J., Chambellant, M. and Ferguson, S. H. (2011) 'Bacular and testicular growth and allometry in the ringed seal (Pusa hispida): evidence of polygyny?', *Journal of Mammalogy*. American Society of Mammalogists 810 East 10th Street, PO Box 1897, Lawrence …, 92(4), pp. 803–810.

Zelditch, M. L., Swiderski, D. L. and Sheets, H. D. (2012) *Geometric morphometrics for biologists: a primer*. Academic Press.

Zelditch, M. L., Swiderski, D. L. and Sheets, H. D. (2013) 'A Practical Companion to Geometric Morphometrics for Biologists: Running analyses in freely-available software', *Free download from https://booksite. elsevier. com/9780123869036/(18 June 2013)*.

Zornetzer, H. R. and Duffield, D. A. (2003) 'Captive-born bottlenose dolphin× common dolphin (Tursiops truncatus× Delphinus capensis) intergeneric hybrids', *Canadian Journal of Zoology*. NRC Research Press, 81(10), pp. 1755–1762.

Appendix 4.1-List of monodonts crania specimens

Species	Museum	ID
M. monoceros	NHMD	12x
M. monoceros	NHMD	1358.493
M. monoceros	NHMD	1361.537
M. monoceros	NHMD	1364.655
M. monoceros	NHMD	1365.656
M. monoceros	NHMD	1366.654
M. monoceros	NHMD	1370.3
M. monoceros	NHMD	1371.843
M. monoceros	NHMD	1372.5
M. monoceros	NHMD	1373.6
M. monoceros	NHMD	1378.85
M. monoceros	NHMD	1380
M. monoceros	NHMD	1385.18
M. monoceros	NHMD	1386.853
M. monoceros	NHMD	1387.859.20
M. monoceros	NHMD	1388.21
M. monoceros	NHMD	1389.22
M. monoceros	NHMD	1392.864.25
M. monoceros	NHMD	1393.26
M. monoceros	NHMD	13x
M. monoceros	NHMD	1406
M. monoceros	NHMD	1408
M. monoceros	NHMD	1409.845
M. monoceros	NHMD	1410
M. monoceros	NHMD	1416
M. monoceros	NHMD	1422
M. monoceros	NHMD	1423
M. monoceros	NHMD	1427

Species	Museum	ID
M. monoceros	NHMD	1428
M. monoceros	NHMD	1432.261
M. monoceros	NHMD	1433.262
M. monoceros	NHMD	1434.261
M. monoceros	NHMD	1435.262
M. monoceros	NHMD	1437.262
M. monoceros	NHMD	1438.262
M. monoceros	NHMD	1439.262
M. monoceros	NHMD	1440.263
M. monoceros	NHMD	1441.263
M. monoceros	NHMD	1442.263
M. monoceros	NHMD	1445.275
M. monoceros	NHMD	1451.276
M. monoceros	NHMD	1452.276
M. monoceros	NHMD	1454
M. monoceros	NHMD	1455
M. monoceros	NHMD	1457.277
M. monoceros	NHMD	1458.277
M. monoceros	NHMD	1459.277
M. monoceros	NHMD	1460.277
M. monoceros	NHMD	1461
M. monoceros	NHMD	1462.277
M. monoceros	NHMD	1463.277
M. monoceros	NHMD	1464.278
M. monoceros	NHMD	14x
M. monoceros	NHMD	1574
M. monoceros	NHMD	1578
M. monoceros	NHMD	1579.2
M. monoceros	NHMD	1580
M. monoceros	NHMD	1583.411

Species	Museum	ID
M. monoceros	NHMD	1584-4107
M. monoceros	NHMD	1592M
M. monoceros	NHMD	1593.412
M. monoceros	NHMD	15x
M. monoceros	NHMD	17x
M. monoceros	NHMD	20
M. monoceros	NHMD	2629.144
M. monoceros	NHMD	2751.145
M. monoceros	NHMD	2757
M. monoceros	NHMD	43
M. monoceros	NHMD	47
M. monoceros	NHMD	56x
M. monoceros	NHMD	5x
M. monoceros	NHMD	84
M. monoceros	NHMD	847.1411
M. monoceros	NHMD	85
M. monoceros	NHMD	888
M. monoceros	NHMD	950
M. monoceros	NHMD	951
M. monoceros	NHMD	952
M. monoceros	NHMD	953
M. monoceros	NHMD	956
M. monoceros	NHMD	974
M. monoceros	NHMD	9x
M. monoceros	NHMD	1456.277
M. monoceros	MNHN	1869.759
M. monoceros	MNHN	1903.103
M. monoceros	NMS	1895.30.3
D. leucas	NHMD	85129
D. leucas	NHMD	85130

Species	Museum	ID
D. leucas	NHMD	1.17
D. leucas	NHMD	1.4.1963.37.1854
D. leucas	NHMD	1.4.1963.42.1854
D. leucas	NHMD	10
D. leucas	NHMD	11
D. leucas	NHMD	12
D. leucas	NHMD	1306
D. leucas	NHMD	1311
D. leucas	NHMD	1312
D. leucas	NHMD	1313
D. leucas	NHMD	1318
D. leucas	NHMD	1319
D. leucas	NHMD	1320
D. leucas	NHMD	1321
D. leucas	NHMD	1322
D. leucas	NHMD	1323
D. leucas	NHMD	1329
D. leucas	NHMD	1334
D. leucas	NHMD	1335
D. leucas	NHMD	1338
D. leucas	NHMD	1343
D. leucas	NHMD	1344
D. leucas	NHMD	1346
D. leucas	NHMD	1346
D. leucas	NHMD	1347
D. leucas	NHMD	1350
D. leucas	NHMD	1351
D. leucas	NHMD	1352
D. leucas	NHMD	1353
D. leucas	NHMD	1355

Species	Museum	ID
Hybrid	NHMD	1356
D. leucas	NHMD	279
D. leucas	NHMD	3.968
D. leucas	NHMD	34.15.3.1878
D. leucas	NHMD	350
D. leucas	NHMD	38.1854/1.4.1963
D. leucas	NHMD	39.1.4.1965.1854
D. leucas	NHMD	4.3.1870
D. leucas	NHMD	40.1.4.1963.1854
D. leucas	NHMD	41.1.4.1963.1854
D. leucas	NHMD	43.1.4.63.1854
D. leucas	NHMD	43.14.12.1893
D. leucas	NHMD	44.7.8.1905
M. monoceros	NHMD	44.1.4.1963
D. leucas	NHMD	45
D. leucas	NHMD	47
D. leucas	NHMD	50
D. leucas	NHMD	51
D. leucas	NHMD	52
D. leucas	NHMD	54
D. leucas	NHMD	55
D. leucas	NHMD	56
D. leucas	NHMD	57
D. leucas	NHMD	58
D. leucas	NHMD	59
D. leucas	NHMD	60
D. leucas	NHMD	61
D. leucas	NHMD	63
D. leucas	NHMD	9
D. leucas	MNHN	1894.328

Species	Museum	ID
D. leucas	MNHN	1928.196
D. leucas	MNHN	1928.197
D. leucas	MNHN	1971.156
D. leucas	MNHN	1885.606
D. leucas	MNHN	1894.325
D. leucas	MNHN	1901.48
D. leucas	NMS	1876.12.1
D. leucas	NMS	2014.9
D. leucas	LaS	868

5 Chapter 5: Skull morphological variation in a British stranded population of false killer whale, (*Pseudorca crassidens, Owen 1846*): a 3D geometric morphometric approach

Abstract

The false killer whale *Pseudorca crassidens* (Owen, 1846) is a globally distributed delphinid, that shows geographical differentiation in its skull morphology. I explored cranial morphological variation in a sample of 85 skulls belonging to a mixed sex population stranded in the Moray Firth, Scotland in 1927. By using microscribe 3D 2GX, 37 anatomical landmarks were placed on the cranium and 25 placed on the mandible and subsequently analysed with geometric morphometrics techniques to extrapolate size and shape variation and to explore sexual dimorphism. Males showed greater overall skull size than females whilst no sexual dimorphism could be identified in cranial and mandibular shape. Allometric skull changes occurred in parallel for both males and females supporting the lack of sexual shape dimorphism in this particular sample. Also, fluctuating asymmetry did not differ between crania of males and females. This study confirms the absence of sexual shape dimorphism, and the presence of a sexual size dimorphism in this false killer whale population.

5.1   Introduction

The false killer whale, *Pseudorca crassidens* (Owen, 1846) is a large cetacean with a cosmopolitan distribution that ranges between 50°N and 50°S in latitude (Baird, 2009b). Adults can reach total body lengths (TBL) of 5m (females) to 6m (males) making this species one of the largest members of the Delphinidae family (Baird, 2009b).Together with the true killer whale (*Orcinus orca*) , *P.crassidens* shows an occasional tendency to eat marine mammals such as small and large cetaceans (Alonso et al., 1999; Baird, 2009b; Odell & McClune, 1999) although their main prey is squid and fish (Alonso et al., 1999; Baird, 2009b).

Morphological variation in the false killer whale is poorly understood and there have been few studies on the skull morphology of this large cetacean. The cranium has conical and large teeth, and the tooth count is 7-11 for the upper jaws and 8-12 for the lower jaws (Baird, 2009b; Yamada, 1956). Stranded cetacean populations provide a rich source of morphological data. A previous analysis from a stranding described a degree of sexual dimorphism in body size with males generally larger in overall body length and weight (Baird, 2009b). Mead (1975) and Baird (2009) also reported differences in the shape of the head due to the melon that is generally more pronounced in males than in females. Since the melon is an organ of sound production and transmission it might be likely that this is associated with sexual difference in false killer whale echolocation.

Skull morphologies can be good proxies for understanding factors which influence variation (sexual or ecogeographical) in the false killer whale. To date, only one study has identified skull sexual dimorphism and population differences in *P. crassidens* from South Africa and Scotland (Kitchener, Ross, & Caputi, 1990). They detected significant sexual differences in the rostrum, the ventral cranium and the temporal fossa. Another study of Japanese and South African false killer whales identified that both sexes of South African whales were smaller than Scottish individuals (Inês M Ferreira, Kasuya, Marsh, & Best, 2014). However, no other studies have described skull size and shape variation in this species.

Geometric morphometrics (Rohlf & Marcus, 1993) can be a useful tool for studying skull morphological variation (Marcus, Hingst-Zaher, & Zaher, 2000). This method quantifies size and shape variation via the digitisation of a set of anatomically and/or geometrically defined homologous landmarks (2D/3D) on specimens (Adams & Otárola-Castillo, 2013; Adams, Rohlf, & Slice, 2004). Previous geometric morphometric approaches on cetaceans have successfully separated geographic populations, ontogenetic sequences, sexes and species in

many odontocetes (del Castillo et al., 2014; Loy, Tamburelli, Carlini, & Slice, 2011; Monteiro-Filho, Monteiro, & dos Reis, 2002; Nicolosi & Loy, 2010; Westgate, 2007; Wiig et al., 2012) and so it stands to reason that these methods can successfully identify size and/or shape affinities/disparities between male and female false killer whales.

By using geometric morphometrics this study aims to address the following research questions pertinent to *P. crassidens*: To what extent does a single population display a degree of intraspecific morphological variability in the skull? Is skull size and shape sexually dimorphic? Do males and females show differences in the degree of cranial asymmetry and skull integration (Klingenberg, 2009)? It is predictable that skulls of false killer whales should exhibit a significant degree of size differentiation between sexes (Kitchener et al., 1990), whilst shape differences might be subtle and difficult to identify (Loy et al., 2011). It is predictable that integration/modularity between crania and mandibles should occur in both sexes. Previous morphological studies on mammals showed a significant degree of association between cranial and mandibular morphology at both intra and interspecific scale (Figueirido, Tseng, & Martín-Serra, 2013). However, not many studies have yet explored such pattern of integration in cetaceans (Churchill et al., 2019). Since these marine mammals do not chew their food extensively and their mandible is also involved in sound reception (Cranford & Krysl, 2018; Cranford, Amundin, & Krysl, 2015; Cranford et al., 2008), it is expected to find a relatively low level of integration compared to other groups. Additionally, if diet and sound reception differ between sexes it might be possible that the level of integration also shows some degree of differentiation between males and females.

5.2 Materials and Methods

Samples- I examined 85 crania and 29 mandibles of *Pseudorca crassidens* housed at the Natural History Museum, London, UK (**Appendix 5.1**). Though these specimens have two different groups of catalogue numbers – 1961 and 1992, all are considered related to a mass-stranding event which took place in October 1927 at the Dornoch Firth, Scotland. Specimens labelled 1992 were collected from Ardgay Bay and along the Kyle (a narrow sea channel) beyond Bonar Bridge to Invershin. Donorch Firth is part of the larger Moray Firth embayment located on the east coast of the Highlands in the north of Scotland. Ardgay and Bonar Bridge are respectively on the south and north shore of Donorch Firth about 1.6 km apart. Donorch Firth is part of the larger Moray Firth embayment located on the east coast of the Highlands in the north of Scotland. Ardgay and Bonar Bridge are respectively in the south and north shore of Donorch Firth about 1.6 km apart. Information regarding the gender of the specimens with the catalogue number 1992 is missing. Two subadults specimens were identified as the maxillary bones did not reach the nuchal crest caudally, and part of the frontal bone was visible in dorsal view (Cozzi et al., 2016).

Sampling- Three dimensional (3D) coordinates of 37 anatomically-defined homologous landmarks were placed on 85 crania (♂=37; ♀=39; ND = 9; **Figure 5.1; Table 5.1**), and twenty-five landmarks were placed on 29 mandibles (♂=12; ♀=17; **Figure 5.1**; **Table 5.2**) using Microscribe G2X at an accuracy of 0.23 mm (Immersion Corp, 2013). Due to the large size of the specimens two landmarking sessions for each specimen were recorded by the same researcher (DV) on the skull in order to cover both dorsal and ventral part. These were then merged using DVLR software (Dorsal-Ventral-Left-Right fitting, http://www.nycep.org/nmg). Coordinates on mandibles were captured in a single landmarking session by the same researcher (DV). Landmarks were imported into Morpheus (Slice, 2014) and MorphoJ (Klingenberg, 2011) to ensure that all the landmarks were captured in an identical, sequential order.

Measurement error- To explore the degree of measurement error introduced by the 3D landmarking, linear measurements between selected anatomical landmarks were taken with a measuring tape on crania (accuracy of 0.1 mm), and successively compared with inter-landmark distances taken on the dorsal and ventral views and on the combined landmarks configurations with DVLR. To test the Microscribe degree of accuracy during the data collection, 18 landmarks on a 5 cm scalebar were taken right before the beginning of each

landmarking session on crania. To evaluate the reliability of the landmark configuration, a repeatability index was calculated on 85 skulls using the Procrustes ANOVA in MorphoJ. The operator (DV) digitized each skull twice and followed standard protocol procedures and analyses described in Fruciano (2016), and Cardini (2004).

Geometric Morphometrics (GMM)- Landmarks were superimposed using a Generalised Procrustes Analysis (GPA) which removes the effects of differences in size, position, and orientation from the 3D spatial coordinates (Rohlf & Marcus, 1993). This is an iterative procedure where variation in size is first removed by scaling each configuration so that it has a centroid size (CS = the square root of the sum of squared distances between each landmark and the centroid) equal to 1.0; rotation and translation are taken into account by centring and rotating the landmark configuration in order to obtain an optimal solution that minimizes the quadratic distances between homologous points (Bookstein, 1997). After GPA, a new set of coordinates (named Procrustes) are created and then used as a proxy for shape variables to explore the potential for differences in cranial and mandibular morphology between sexes.
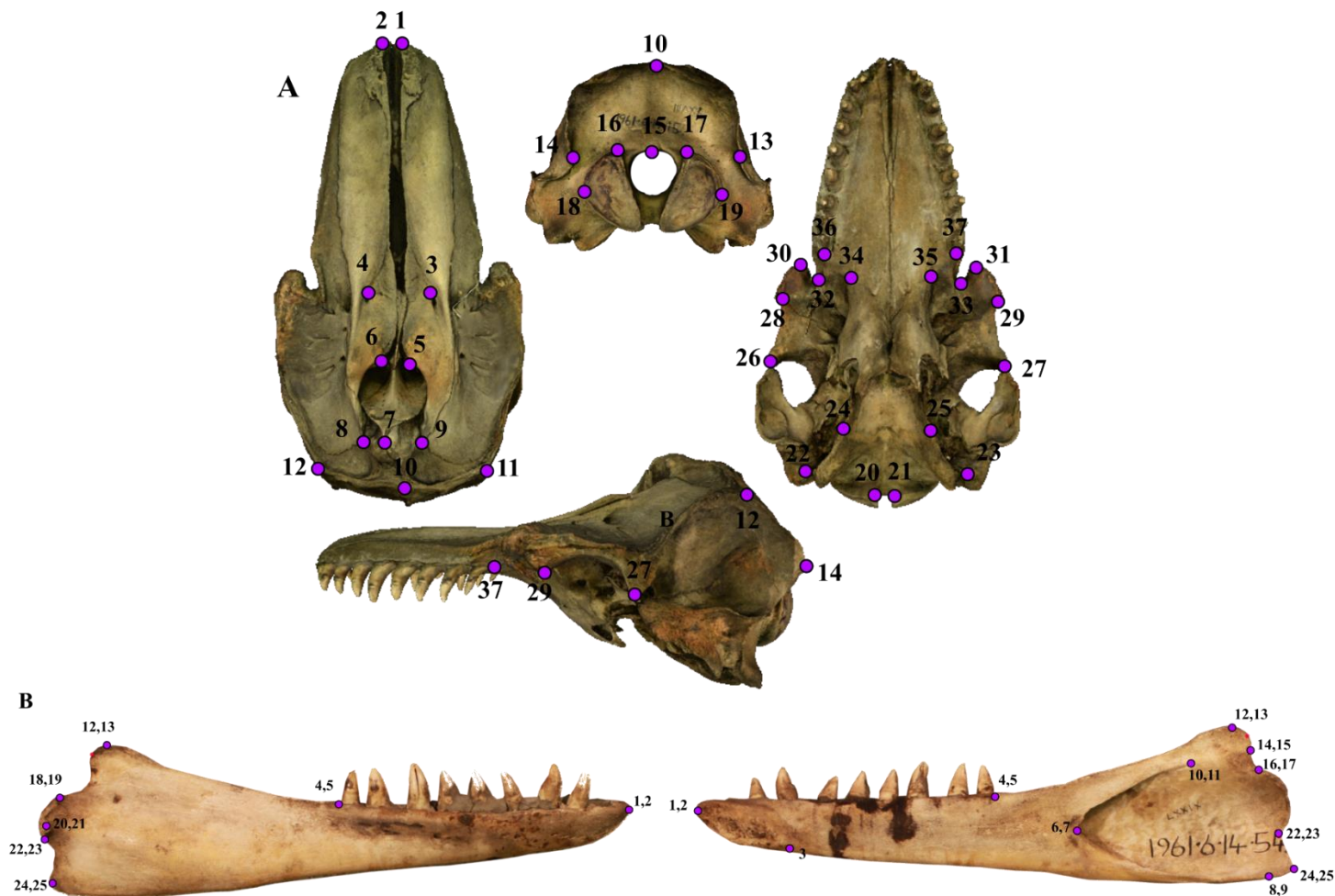
Figure 5.1 Landmark configuration on the A) cranium photogrammetric-based 3D model of the specimen (*Pseudorca crassidens* 1961.6.14.15 NHM, London) in Dorsal, Ventral, left lateral, and Occipital view and B) right hemi-mandible of the specimen *Pseudorca crassidens* 1961.6.14.54 NHM, London, in labial and lingual view. See **Table 5.1** and **Table 5.2** for description.

Table 5.1 Description of 37 landmarks taken on Pseudorca crassidens skull used in the GMM analysis

	Landmarks homologous on the skull
1-2	Tip of the rostrum
3-4	Anteriormost point of the premaxillary foramen
5-6	Posteriormedial point of the premaxilla
7	Anteriormost point of the medial suture between the nasal bones
8-9	Sutural triple-junction between nasal, frontal and maxilla
10	External occipital protuberance or lambdoid crest
11-12	Sutural triple-junction between supraoccipital, frontal and parietal
13-14	Posteriormost point on the temporal crest
15	*Opisthion*; middle point of the dorsal border of the *foramen magnum* on the intercondyloid notch
16-17	Dorsal tip of the occipital condyle
18-19	Lateral tip of the occipital condyle
20-21	Ventral tip of the occipital condyle
22-23	Medial tip of the paraoccipital process; ventralmost point of the paraoccipital process
24-25	Suture of pterygoid and basioccipital at the junction between pharyngeal crest and basioccipital crest
26-27	Posteroventral point of the postorbital process
28-29	Anteroventral point of the preorbital process
30-31	Anterior tip of lacrimal bone
32-33	Posteriormost point of the antorbital notch
34-35	Anteriormost point of the palatine
36-37	Posteriormost point of the upper alveolar groove

Table 5.2 Description of 25 landmarks taken on false killer whale 3D mandibles used in GM analysis.

Landmarks homologous on mandible	
1-2	*Pogonion*; Tip of the mandible
3	*Gnathion*, the lowest point along the midline of the mandibular symphysis
4-5	Posterior end of the alveolar groove
6-7	Anteriormost point of the mandibular foramen
8-9	Posteroventral point of the mandibular foramen
10-11	Posterodorsal point of the mandibular foramen
12-13	Dorsal tip of the coronoid process
14-15	Most anterior point of the mandibular notch
16-17	Innermost point of the condyle
18-19	Outer point of the condyle
20-21	Medialmost point of the condyle
22-23	Ventralmost extreme point of the condylar process
24-25	Posteroventral tip of the angular process

Data analyses on 3D crania and mandibles- GMM permits partitioning of the asymmetric and symmetric components of shape variation (Klingenberg et al., 2002). As many species of odontocetes show a high degree of asymmetry in their crania (Churchill et al., 2019; Fahlke et al., 2011; Fahlke & Hampe, 2015; Huggenberger et al., 2017; MacLeod, 2002), and the asymmetric component is relevant for the aim of the study, these variables were partitioned following the guidelines of Klingenberg et al. (2002).

A Procrustes analysis of variance (ANOVA) was performed on crania replicates to investigate the presence of Directional (DA) and Fluctuating Asymmetry (FA) between individual and side (Ind*Side) in MorphoJ (Klingenberg, 2011). The DA is a deviation from symmetry showed in most of the individuals belonging to the same species (MacLeod et al., 2007). The FA can be described as the difference in mean absolute value of left and right sides in the same individual (Klingenberg et al., 2002). When the mean value is close to zero, it means that the structure shows an almost perfect symmetry (Tomkins & Kotiaho, 2001). A two-sample-t-test (or independent sample-t-test) was performed to assess possible sexual differences in FA scores.

Because odontocete mandibles are generally considered symmetrical (Barroso et al., 2012) the full shape of the mandible was captured. To explore the degree of intraspecific symmetric shape variation in the cranium and mandible a Principal Component Analysis (PCA) was performed using the geomorph package (Adams et al., 2016) within R (R Team, 2015).

ANOVA and Procrustes ANOVA (using the function procD.lm of "geomorph") were performed to test for sexual dimorphism in skull size and shape respectively, while the same function was equally employed to test for allometry (with log transformed CS as X and symmetric shape component as Y) and slope differences between sexes (after the exclusion of 2 subadults specimens).

Patterns of covariation between cranium and mandibular shape were explored using two- block Partial Least Squares (2B-PLS) analysis (Zelditch et al., 2012, 2013) in a dataset of 29 complete skulls (the combined cranium and mandible). PLS is a useful method for studies investigating integration/modularity between two different blocks of variables (Klingenberg, 2009; Klingenberg & Marugán-Lobón, 2013; Zelditch et al., 2012), such as the mandible and cranium shape in this instance. Unlike the PCA, the PLS method uses singular value decomposition (SDV) to identify vectors called singular axes (SAs; Zelditch et al. 2012), which explains covariance in the same way that PCA explains variance. Unlike the PCs, SAs comes in pairs,

and each SA score accounts for the covariance between blocks (Klingenberg, 2009; Zelditch et al., 2012). Differences in covariation trajectories between sexes were tested using angular comparison of the PLS vectors in MorphoJ (Klingenberg, 2011; Klingenberg & Marugán-Lobón, 2013). Like the PCs, SAs can be described by deformation along axes, helping with the interpretation of the results (Zelditch, Swiderski and Sheets, 2012). Statistical significance was tested with a 1000 permutation test against the null hypothesis of no covariation between cranium and mandible (Zelditch, Swiderski and Sheets, 2012).

5.3   Results

<u>Cranial dataset</u>

Measurement error- The Procrustes ANOVA (**Table 5.3**) showed significant effects of individuals on shape as well as side representing the Directional Asymmetry (DA), and interaction between individual and side, representing Fluctuating Asymmetry (FA). Sum of squares (SS) was greater in DA and smaller in landmarking error. The Repeatability (R) score for shape was 0.95.

Table 5.3 Procrustes ANOVA on whole sample of 85 cranial specimens replicas to evaluate Repeatability index (R) as well as Fluctuating (FA) and Directional Asymmetry (DA).

Effect	SS	MS	df	F	p	R
Individual	0.26783	6.65E-05	4028	5.36	<0.0001	**0.95**
Side (DA)	0.12401	0.00243	51	195.88	<0.0001	
Ind*Side(FA)	0.04811	1.24E-05	3876	2.1	<0.0001	
Err (Rep)	0.04729	5.91E-06	8008			

Symmetric component- PC1 and PC2 (**Figure 5.2A**) on symmetric component of the shape summarized 32.08% of the total variance (**Appendix 5.2**). PC1 positive scores correspond to a more laterally compressed facial region, an area bounded posteriorly by the dorsal apex of the nuchal crest defined by landmark 10. PC1 negative scores represent a shorter rostrum and a transverse widening of the neurocranium, resulting in a more tapered skull shape. For the area of the occipital condyles described by 7 landmarks (LM 15, 16, 17, 18, 19, 20, 21), negative PC scores represent a wider shape together with an enlargement of the medial wall of the temporal fossa formed by a small portion of the squamosal (squamosal plate) and by the parietal described by 3 landmarks (LM 12, 14 27). The PC2 axis describes changes in the curvature of the rostrum profile and the position of the neurocranium relative to the rostrum. PC2 negatives scores reflect a high degree of curvature in the skull profile and a wider neurocranium with the displacement of landmarks 10, 11, 12. Landmarks 10 and 7 are farther apart compared to PC2 positive scores. The plot of PC1 against PC2 (**Figure 5.2A**) indicated considerable male-female overlap in the morphospace. Splitting the sample into males and females in MorphoJ also allowed for a comparison of angle vectors in PCs. PC1-3 vectors showed that the angles between males and females range from 35 to 54 degrees indicating similarities between males and females (all p values of highlighted angles are generally significant; **Table 5.4**). Although a difference was identified in PC4 (variance 7.3%, *p= 0.96*; **Table 5.4**). Equally, Procrustes ANOVA highlighted no significant (*p= 0.08*) difference in skull shape between males and females.
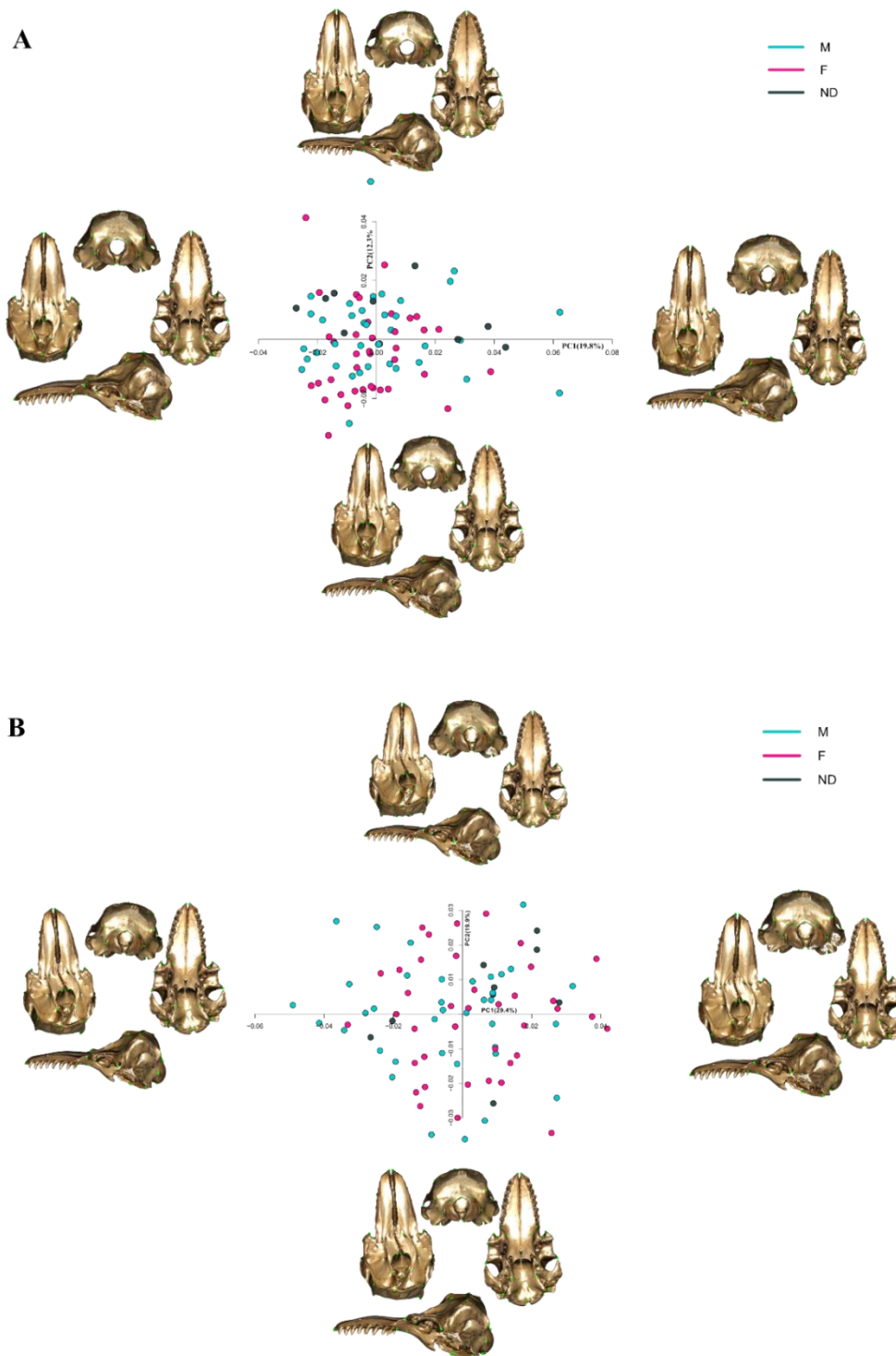
Figure 5.2 Principal component plot of the symmetric (A) and asymmetric (B) component of shape for 3D skull dataset. Colours indicate sex categories. Shape differences along the axis of the PC1 and PC2 are visualised with warping of the crania 3D models.

Table 5.4 Angular comparison of vector direction in the first 4 Pcs between females and males dataset. p-values of above highlighted angles are significant.

	PC1	PC2	PC3	PC4
PC1	**35.00**	85.3	66.96	87.14
	<0.00001	0.56	0.003	0.72
PC2	85.56	**43.41**	70.003	86.57
	0.57	**<0.00001**	0.01137	0.66
PC3	64.7	72.874	**53.26**	79.90
	0.00128	0.031	**<0.00001**	0.20
PC4	87.08	78.42	82.89	89.66
	0.71	0.14	0.37	0.96

Allometry-The regression of Procrustes coordinates versus CS revealed a significant (*p=0.001*) allometric component with size explaining 13% of variance (**Figure 5.3**). The warping showed a strengthening of the facial region and rostrum in larger individuals. Procrustes ANOVA evidenced no difference between sex allometric slopes for CS ($F_{2,74}$=1.1692, *p=0.259*; **Table 5.5**) or TBL ($F_{2,74}$=0.8252, *p= 0.661;* **Table 5.5**). When allometric trajectories were individually analysed for males and females it was possible to note again a significant impact of size on shape that explained 16.34% of variance in males (n = 37; *p < 0.001*), and 12.59% of variance in females (n= 39, *p < 0.001*). The angle vector is 26.13° with *p < 0.001*, meaning that the two vectors are pointing in the same direction, and they have similar allometric trajectories. A boxplot showed greater values for CS and TBL in male specimens confirmed by t-tests (CS: *p=0.007*; TBL: *p= 0.05*) (**Figure 5.4A-B**).

Asymmetric component- In the PCA of the asymmetric component of the shape, the PC1 summarized 29.4% of the variation (**Figure 5.2 B**). Along this axis, individuals that are located towards the negative region show an accentuation of the DA while those in the positive region of the axis have less asymmetrical crania. Males and females showed no differences in the average of the FA scores between the two sexes no matter if Mahalanobis (*p=0.2451*) or Procrustes FA scores (*p=0.9847*) were considered (**Figure 5.5**).
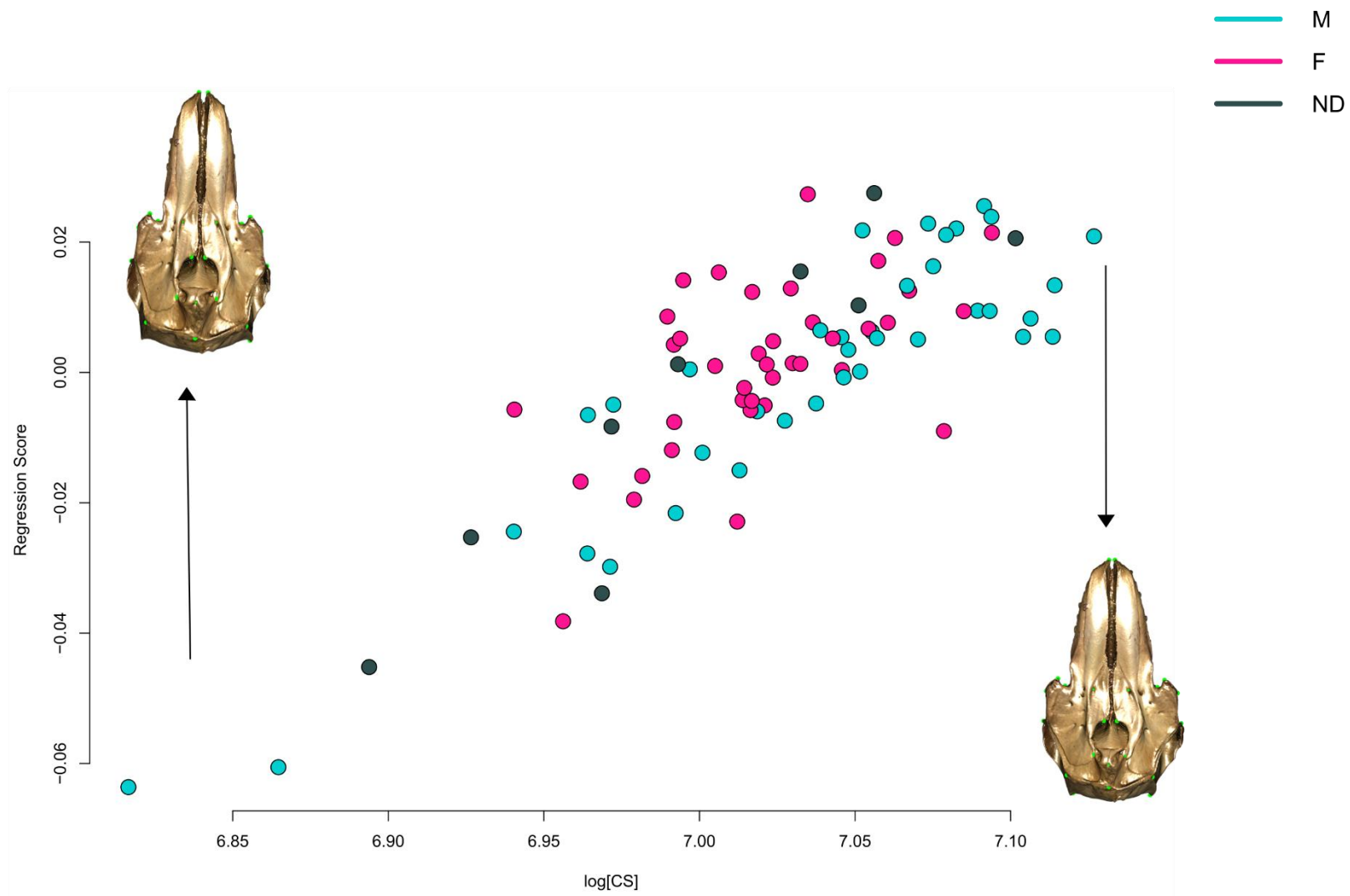
Figure 5.3 Shape variables against log[CS]. Shape change of biological forms from subadults (6.85) to adults (7.10) can be visualized through warping.

Table 5.5 Procrustes ANOVA to test for slopes allometry of sexes on skull CS and TBL and shape of 74 *Pseudorca crassidens* specimens. Significance is highlighted in bold.

| ~ Shape	df	SS	MS	R²	F	Z	p
CS	1	0.00517	0.00517	0.04132	3.1459	3.4733	**0.001**
Sex	1	0.00298	0.00298	0.02382	1.8135	1.8652	**0.028**
CS:Sex	1	0.00192	0.00192	0.01536	1.1692	0.6291	0.259
Residuals	70	0.11505	0.00164	0.9195			
Total	73	0.12512					
TBL	1	0.00749	0.00749	0.05988	4.6288	4.4575	**0.001**
Sex	1	0.00299	0.00299	0.02388	1.8459	1.932	**0.025**
TBL:Sex	1	0.00134	0.00134	0.01068	0.8252	-0.419	0.661
Residuals	70	0.1133	0.00162	0.90556			
Total	73	0.12512					
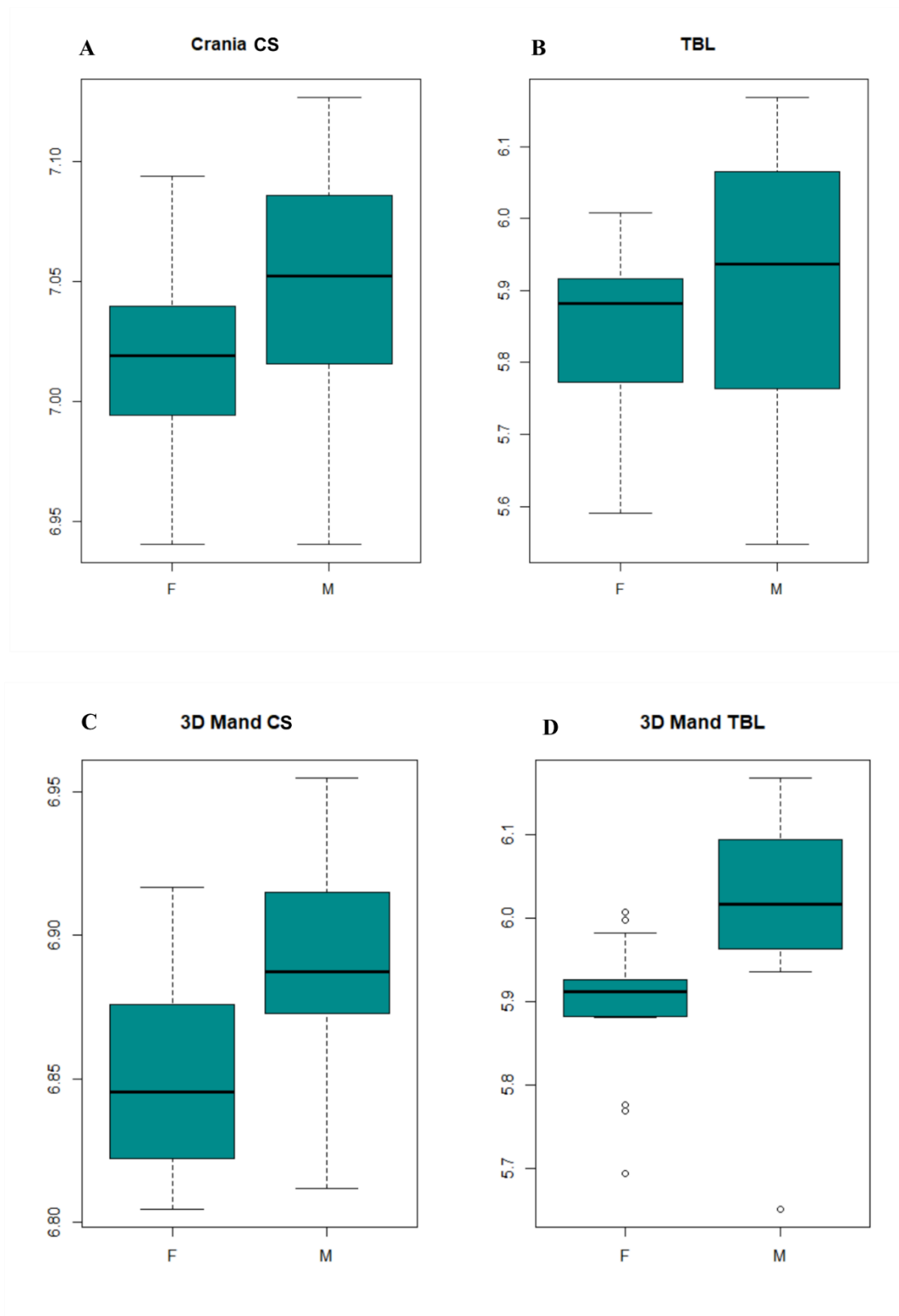
Figure 5.4 Box-whisker plots of crania dataset (n=74) log[CS] (A) and TBL (B) and mandibles dataset (n=29) log[CS] (C) and TBL (D) of false killer whales.
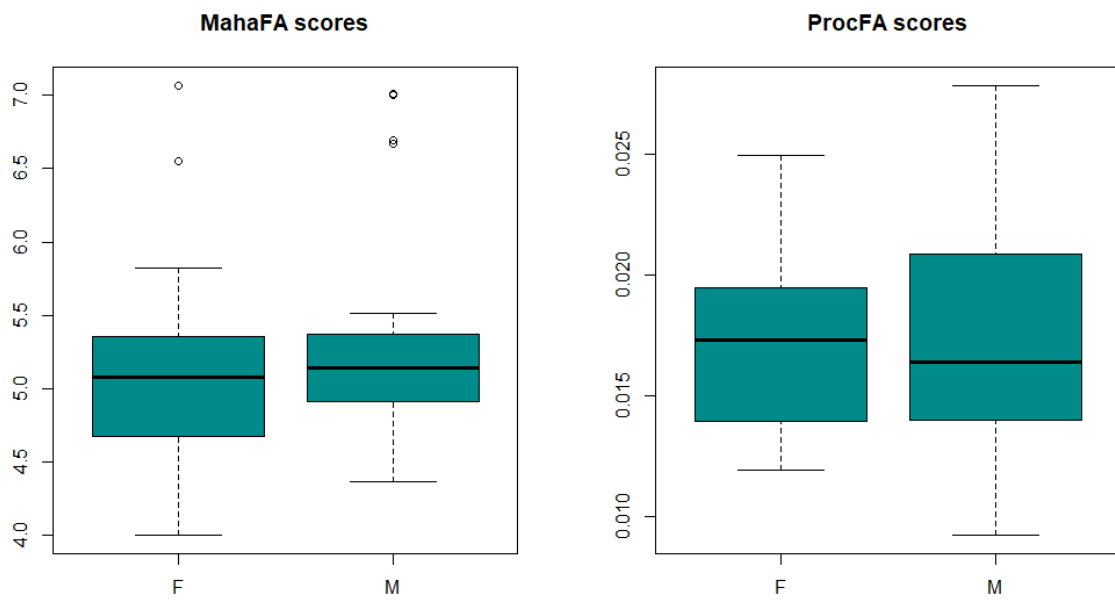
Figure 5.5 Boxplots of Mahalanobis and Procrustes FA scores among female and male specimens.

3D Mandibles dataset

Shape analyses- PC1 and PC2 accounted for 42.8% of the total variance (**Figure 5.6; Appendix 5.3**) and showed mixed scores belonging to male and female specimens. Positive scores on PC1 scores describe a lengthened mandible, a forward shift of the landmarks 6 and 7 that represent the most anterior point of the mandibular foramen on the medial side or the acoustic window on the lateral side (Mead & Fordyce, 2009). The right and left sides of the mandibular foramen show a different angle compared to PC1 negative values. Indeed, the hemi-mandibles create a more obtuse angle on PC1 positive values, and the mandible appears more elongated (**Figure 5.6,** wireframe in occipital, ventral and lateral view). Also, PC1 on the positive values represents a backward shift in the space of the landmarks 4 and 5 describing the posterior end of the dental groove on the alveolar border of the mandible while landmarks 12 and 13 (the coronoid process) shift upward. PC2 describes the curvature of the mandible, with negative values showing a more convex dorsal margin and larger mandibular body. A permutation test based on Procrustes distances highlighted no differences in mandible shape between males and females ($p = 0.9864$). Procrustes ANOVA on the total sample of 29 specimens showed that size explained 5.8% of total mandible shape variance (**Table 5.6**), although this was not significant and no significant effect was also detected for sex (**Table 5.6**). If TBL was considered as a factor against mandibular shape, rather than CS, this result was unaffected (**Table 5.6**). Both CS and TBL demonstrated that males were generally larger than females (**Figure 5.4C-D;** CS: *p=0.007*; TBL: *p=0.01*).
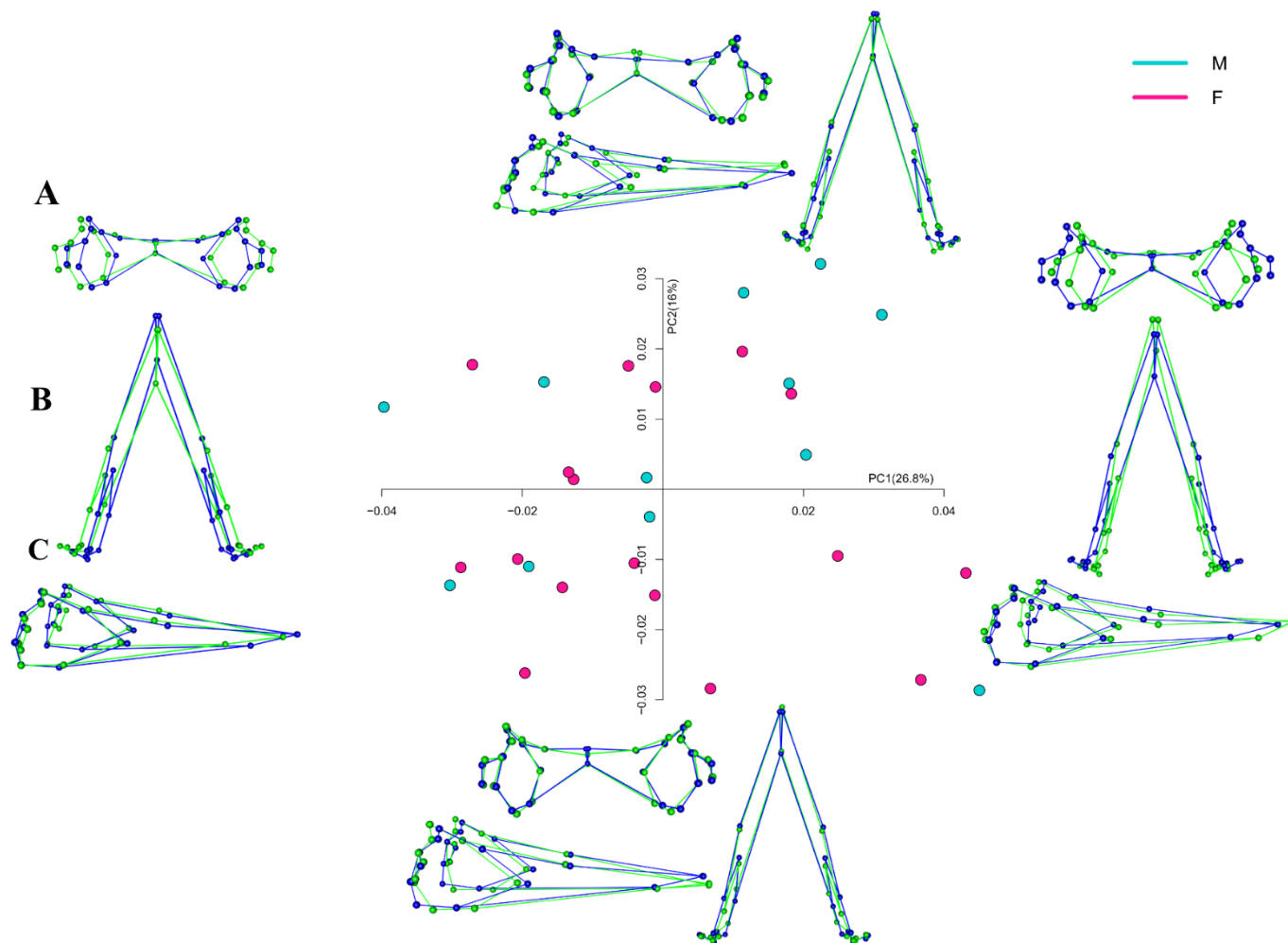
Figure 5.6 Principal component plot of the symmetric component of shape for 3D mandible dataset, in R. Colours indicate sex categories. Shape differences along the axis of the PC1 and PC2 can be viewed by wireframe in A) occipital, B) dental, and C) lateral view. The blue colour refers to the mean shape of the individuals while the green colour refers to the extreme individual on the negative and positive PC axes.

Table 5.6 Procrustes ANOVA to test for slopes allometry of sexes on mandibles CS and TBL and shape of 29 *Pseudorca crassidens* specimens.

~Shape	df	SS	MS	R^2	F	Z	p
CS	1	0.00322	0.00322	0.05842	1.7004	1.4716	0.071
Sex	1	0.00175	0.00175	0.03174	0.9238	0.01438	0.474
CS:Sex	1	0.0028	0.0028	0.05091	1.4817	1.0704	0.144
Residuals	25	0.0473	0.00189	0.85893			
Total	28	0.05507					
TBL	1	0.00281	0.00281	0.0511	1.4803	1.163	0.128
Sex	1	0.00242	0.00242	0.04399	1.2743	0.75185	0.201
TBL:Sex	1	0.00231	0.00231	0.04199	1.2166	0.63567	0.262
Residuals	25	0.04752	0.0019	0.86292			
Total	28	0.05507					

Cranial and Mandibular Integration

 The 2B-PLS analysis is shown in **Figure 5.7**. The first pair of SAs account for 62.52% of the total squared covariance between cranium and mandible. The strength of association between scores of cranium and mandible (r = 0.795) was not significant (*p= 0.081)*. Comparing the cranium axis of males and females, the PLS1 showed an angle of 56.937°, and PLS2 an angle of 57.603°, and both were significant (*p <0.00002; p = 0.00003;* **Table 5.7**). Similar results were obtained for the mandible, with the PLS1 showing an angle of 38.785°, and the PLS2 an angle of 60.013° (*p<0.00001*; *p=0.00223;* **Table 5.7**).
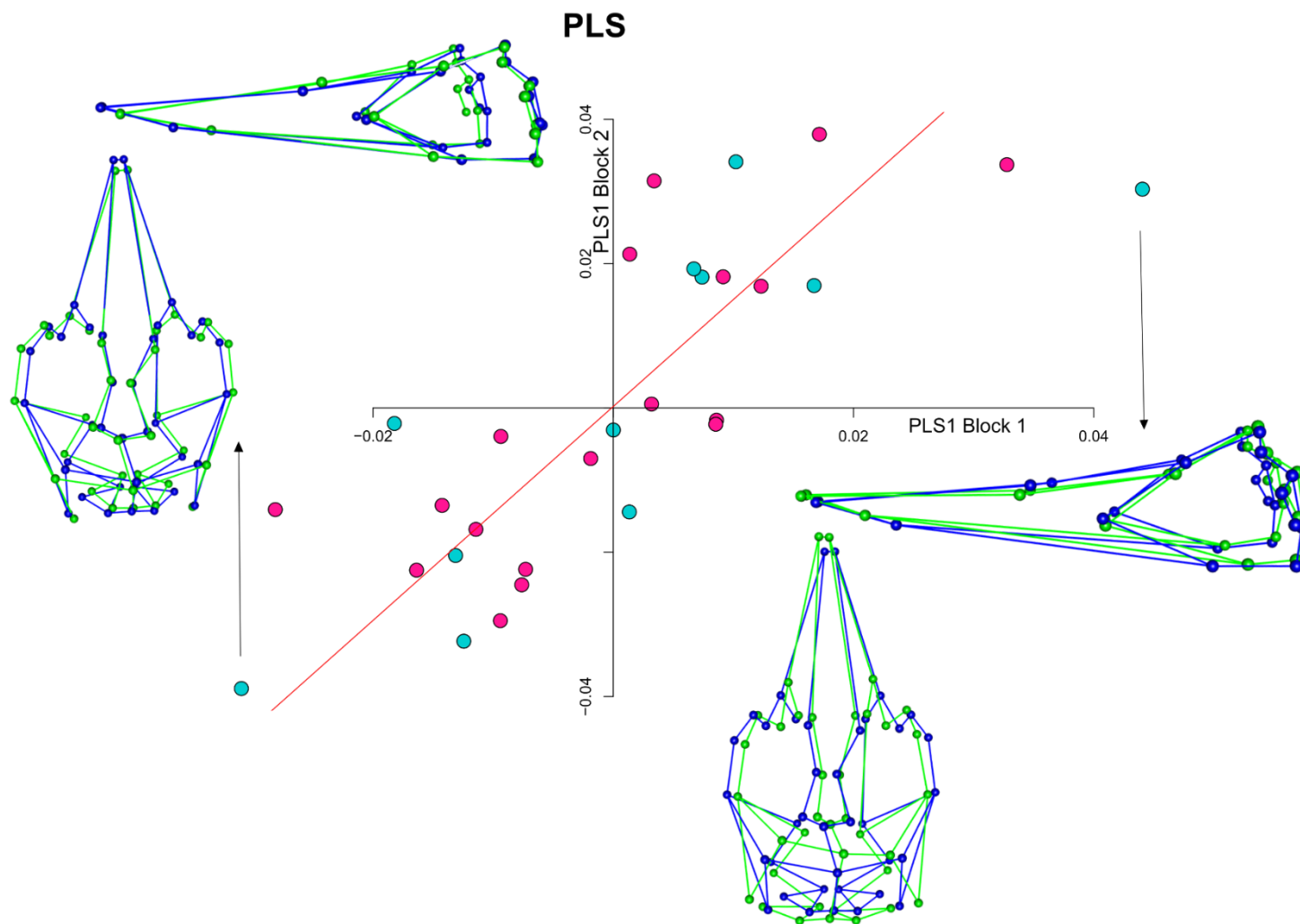
Figure 5.7 Scatter plot of the PLS1 of block1 (Cranium) and block2 (Mandible). Shape differences can be viewed by wireframe. The blue colour refers to the mean shape of the individuals while the green colour refers to extreme most individual on the PLS1 axes.

Table 5.7 Angular comparison of PLS of block 1 and 2 axes between sexes. p-values of the above block1 and 2 PLS are highlighted in bold.

Block1	PLS1	PLS2	PLS3	PLS4
PLS1	**56.937** **<0.00002**	81.210 0.26994	85.647 0.47022	84.240 0.05357
PLS2	85.928 0.60988	**57.603** **0.00003**	81.735 0.29971	83.487 0.41415
PLS3	89.520 0.95204	75.890 0.07566	84.475 0.48862	88.435 0.84457
PLS4	85.119 0.54074	85.692 0.58927	84.561 0.49541	77.145 0.10587
Block2	**PLS1**	**PLS2**	**PLS3**	**PLS4**
PLS1	**38.785** **<0.00001**	76.449 0.17549	86.124 0.69965	82.989 0.48487
PLS2	77.996 0.23058	**60.013** **0.00223**	88.798 0.90479	81.081 0.37383
PLS3	67.504 0.02330	79.592 0.29902	88.326 0.86768	89.520 0.96187
PLS4	86.546 0.73099	88.328 0.86788	62.253 0.00483	58.737 0.00140

5.4 Discussion

This study identified sexual size dimorphism (SSD) in skull size, but not sexual shape dimorphism for individuals of *Pseudorca crassidens*. In keeping with Kitchener et al. (1990), males are characterised by larger crania and mandibles, confirming previous results obtained from field work data (Stacey, Baird, & Leatherwood, 1994). Shape traits were generally overlapping between males and females, although sexual dimorphism has been described in the shape of the external head (Stacey et al., 1994).

The absence of skull shape sexual dimorphism seems to be common in cetacean species that live in monospecific groups (de Francesco & Loy, 2016). This might be partly related to the conservative social structure that both males and females maintain for niche partitioning during aquatic foraging or could instead be related to food sharing within the group (Baird, 2009b; Ralls & Mesnick, 2009). In fact, adult specimens show an enlargement of the area of the temporal fossa (formed by the alisphenoid, frontal, parietal and squamosal bones). Having a large temporal area allows for a larger attachment of the temporal muscle (Cozzi et al., 2016), which produces a stronger bite force. A reduction in the size of this area would cause the mouth to close faster (i.e. in subadults specimens) at the expense of the bite force, because force and velocity are inversely proportional with a well-established trade-off (Marshall, 2009). The temporal muscle is inserted along the dorsal ridge of the mandible, with a stronger and somewhat tendinous attachment over the coronoid process (landmarks 12 and 13) and a weaker attachment anteriorly along the dorsal margin of the mandibular foramen (Seagers, 1982). It can also be used to predict a different diet (Marshall, 2009). If this area had been greater in males it may have testified for a male-male aggression character, related to sexual dimorphism.

To date little is known about male and female *P. crassidens* social behaviour. In general males and females share the same diet and exhibit high fidelity to the natal group (Martien, Baird, Chivers, Oleson, & Taylor, 2011). They feed on a variety of squid, fish, and occasionally mammals such as the sperm whale (Baird, 2009b; Odell & McClune, 1999; Palacios & Mate, 1996; Stacey et al., 1994). They catch their food mostly during the day exceeding dive depths of 200m and at shallow depths during the night (Baird, 2009a; Minamikawa, Watanabe, & Iwasaki, 2013). Prey specialisation has also been suggested in different populations (Botta, Hohn, Macko, & Secchi, 2012; Ferreira, 2008). The absence of a sexual shape dimorphism or monomorphism in *P. crassidens* might be due to their ability to socialize and share food resources within the pod (Baird, 2009b; Odell & McClune, 1999; Stacey et al., 1994) and this

has been confirmed by stable isotope studies (Botta et al., 2012; Riccialdelli & Goodall, 2015). It is noteworthy that in the regression of symmetric skull component on centroid size (**Figure 5.3**) subadults specimens show a less robust cranium than adults, probably related to their different diet. Isotope studies revealed that nursing periods might be prolonged in calves up to two years old (Riccialdelli & Goodall, 2015). Similar to the results presented here, previous studies on other, smaller delphinids *Cephalorhynchus commersoni*, *Tursiops truncatus, Delphinus delphis, Stenella coeruleoalba* and *S.attenuata* (Amaral et al., 2009; Clark & Odell, 1999; del Castillo et al., 2016; Murphy & Rogan, 2006; Parés-Casanova & Fabre, 2013; Sanvicente-Añorve, López-Sánchez, Aguayo-Lobo, & Medrano-González, 2004; Wilson, Hammond, & Thompson, 1999) found no sexual dimorphism in skull shape, suggesting that males and females have a similar diet.

Asymmetry - In this study the percentage of variance explained by DA was greater than FA. As the odontocete skull shows asymmetry related to the production of echolocation high frequency sounds (Cozzi et al., 2016; T. W. Cranford et al., 1996; Fahlke & Hampe, 2015), these results agree with expectations based on previous studies (del Castillo et al., 2014, 2016, 2017). The DA accounted for 25% and the FA for 10% of total shape variation in *Pseudorca crassidens* (**Table 5.3**). Similar results for FA were found for *Lagenorhynchus australis* (8.5%), *Lagenorhynchus obscurus* (9.5%; del Castillo et al., 2017) and *Cephalorhynchus commersoni* (10%; del Castillo et al., 2016). Also, in these species the DA accounted for 43%, 25% and 34% respectively (del Castillo et al., 2017). Therefore, the DA can be argued to be functionally linked to echolocation (Fahlke & Hampe, 2015), and prey size (MacLeod et al., 2007; McCurry, Fitzgerald, et al., 2017). In fact, the two sympatric species *L.osburus* and *L.australis* showed a different degree of DA and different suction feeding abilities (del Castillo et al., 2017). Indeed, in Lissodelphininae there is variation in the magnitude of directional asymmetry between species related to ecological partitioning (del Castillo et al., 2017; Galatius & Goodall, 2016). The nasal area is the most affected area by the asymmetric component (**Figure 5.2B**) in both males and females. This contrasts with the pontoporiid *Pontoporia blainvillei* which showed DA differences in the bony nares region between sexes, probably due to a different vocalization (del Castillo et al., 2014). Different fluctuating asymmetry scores have not been detected in false killer whale females and males (**Figure 5.5**). For this reason, differences in the shape of the head between sexes are most likely related to the shape of soft tissues such as the melon, involved in emission beam production, although this cannot be tested with this dataset.

Sexual size dimorphism (SSD)- Sexual dimorphism can be described as the difference between features such as body size between males and females (Ralls & Mesnick, 2009). SSD can evolve for different reasons and can be explained by factors such as sexual maturity age, mating system, contest competition, female choice and sound production.

Female false killer whales in Scotland attain sexual maturity earlier than males (Purves & Pilleri, 1978). Whilst males reach maturity when their body length is 396-457 cm, roughly around the age of 11-18 (Kitchener et al., 1990; Stacey et al., 1994)(Gorter et al., 2002), females reach maturity between the ages of 8-11 (Ferreira et al., 2014) and 336 cm body length (Stacey et al., 1994). Their breeding age range is similar to *Orcinus orca* (Ottensmeyer and Whitehead, 2000), as males stop growing after 15 years of age (Duffield and Miller, 1988), females reach reproductive age earlier than males. Males might not provide parental care for calves and instead, invest that energy in growth (Nowak & Walker, 1999). In addition, having males with a larger body size can increase their ability to dive to greater depths (Baird, Hanson, & Dill, 2005; Beck, Bowen, McMillan, & Iverson, 2003; Goldbogen et al., 2019; Piscitelli et al., 2010; Riccialdelli & Goodall, 2015). Food intake in two females and one male of false killer whales in captivity indicates an increase in annual food consumption for the male from the fourth to the sixth years of age (Kastelein, Mosterd, Schooneman, & Wiepkema, 2000). This might confirm the hypothesis that males use the energy to grow and increase their body size, whilst females use the energy to take care of the offspring. Sexual size dimorphism with males larger than females has also been observed in *Lagenorhynchus* spp. (del Castillo et al., 2017; Galatius, 2010; Reeves, Smeenk, Brownell, & Kinze, 1999), *Lissodelphis borealis* (Mesnick & Ralls, 2018), *Tursiops truncatus* (Amaral et al., 2009; Parés-Casanova & Fabre, 2013; Tolley et al., 1995), *Orcinus orca*, *Globecephala* spp. (Mesnick & Ralls, 2018) among the other delphinids, in the monodontids *Delphinapterus leucas* (Mesnick & Ralls, 2018) and *Monodon monoceros* (Garde et al., 2007; Mesnick & Ralls, 2018), in the ziphiid *Mesoplodon densirostris,* in *Physeter macrocephalus* (Mesnick & Ralls, 2018), and in *Inia geoffrensis* (Mesnick & Ralls, 2018). Instead, a reversed sexual dimorphism, with females being bigger than males, has been observed in *Cephalorhynchus* spp. (del Castillo et al., 2016; Mesnick & Ralls, 2018) among the other delphinids, in the phocoenid *Phocoena phocoena, P.sinus* (Mesnick & Ralls, 2018), in the pontoporiid *Pontoporia blainvillei* (del Castillo et al., 2014; Mesnick & Ralls, 2018; Ramos et al., 2002), in the ziphiid *Berardius spp.* (Mesnick & Ralls, 2018), in the extinct *Lipotes vexillifer* (Mesnick & Ralls, 2018) and also in 13 species of mysticetes (Ralls & Mesnick, 2009). In *Phocoena phocoena* females are larger than males

allowing a higher reproducibility potential for annual reproduction (Galatius, 2010; Gol'din & Vishnyakova, 2016; Read & Gaskin, 1990). Females reach sexual maturity later than males (C Lockyer, Heide-Jørgensen, Jensen, & Walton, 2003; Christina Lockyer, 2003; Marino et al., 2004; Mclellan et al., 2002; Sørensen & Kinze, 1994), can better compete for resources, and their calves have a more adequate size to maintain body temperature (Ralls, 1976).

Body size changes can also be related to biosonar types (Jensen et al., 2018), and communication sounds, with sexual dimorphism being observed for calls (Ralls & Mesnick, 2009) such as in *Globicephala melas*, or on emission beam patterns (Au, Pawloski, Nachtigall, Blonz, & Gisner, 1995; Kloepper, Nachtigall, Donahue, & Breese, 2012). Most of the largest odontocete species were recognized as having the greatest degree of SSD: *Physeter macrocephalus*, *Orcinus orca, Hyperoodon* spp*., Monodon monoceros, Delphinapterus leucas, Globicephala* spp., *Berardius bairdii*, *Ziphius cavirostris*, and *Mesoplodon* spp. (Cranford, 1999; Goldbogen et al., 2019; MacLeod, 2010; MacLeod & MacLeod, 2009; Ralls & Mesnick, 2009). It is known that the larger the animal, the louder sound it will produce (Ralls & Mesnick, 2009). False killer whales are extremely vocal (Murray, Mercado, & Roitblat, 1998) and differences in vocalization were recorded between populations but not between sexes (Barkley, Oleson, Oswald, & Franklin, 2019; Oswald, Barlow, & Norris, 2003; Rendell, Matthews, Gill, Gordon, & Macdonald, 1999; Sanino & Fowle, 2006).

5.5   Conclusion

In conclusion, although false killer whales are sexually dimorphic in the external shape of the head (Stacey et al., 1994), this study showed no sexual skull shape dimorphism but Sexual Size Dimorphism (SSD) only. Combining the results and the interpretations above, it is likely that false killer whales are polygynandries (Nowak & Walker, 1999; Shirihai, 2006), with males larger than females, although both sexes are likely to share food resources (Botta et al., 2012; Riccialdelli & Goodall, 2015). This study provides new insights into cranial asymmetry in individuals belonging to the same populations by using size-free 3D variables. Further studies using stable isotopes and DNA extraction from these specimens might improve our understanding of the ecology and genetics of false killer whale populations.

References

Adams, D. C. *et al.* (2016) 'Geomorph: Software for geometric morphometric analyses'. Comprehensive R Archive Network.

Adams, D. C. and Otárola-Castillo, E. (2013) 'geomorph: an R package for the collection and analysis of geometric morphometric shape data', *Methods in Ecology and Evolution*. Wiley Online Library, 4(4), pp. 393–399.

Amaral, A. R. *et al.* (2009) 'Cranial shape differentiation in three closely related delphinid cetacean species: Insights into evolutionary history', *Zoology*. Elsevier, 112(1), pp. 38–47.

Arnason, U. (1990) 'Phylogeny of marine mammals-evidence from chromosomes and DNA', *Chromosomes today*, 10, pp. 267–278.

Árnason, Ú. *et al.* (1978) 'Banded karyotypes of three whales: Mesoplodon europaeus, M. carlhubbsi and Balaenoptera acutorostrata', *Hereditas*. Wiley Online Library, 87(2), pp. 189–200.

Árnason, Ú. *et al.* (2018) 'Whole-genome sequencing of the blue whale and other rorquals finds signatures for introgressive gene flow', *Science advances*. American Association for the Advancement of Science, 4(4), p. eaap9873.

Árnason, Ú. and Benirschke, K. (1973) 'Karyotypes and idiograms of sperm and pygmy sperm whales', *Hereditas*. Wiley Online Library, 75(1), pp. 67–74.

Baird, R. W. *et al.* (1998) 'An intergeneric hybrid in the family Phocoenidae', *Canadian Journal of Zoology*. NRC Research Press, 76(1), pp. 198–204.

Beauchamp, K. C. *et al.* (2020) 'Detection of hybrid Pyganodon grandis and P. lacustris (Bivalvia: Unionidae) using F-and M-type mitochondrial DNA sequences and geometric morphometrics', *Journal of Molluscan Studies*.

Benirschke, K. and Kumamoto, A. (1978) 'The chromosomes of Cuvier's beaked whale, Ziphius cavirostris', *Mammal Chrom Newsl*, 19, pp. 70–72.

Bérubé, M. (2009) 'Hybridism', in *Encyclopedia of marine mammals*. Elsevier, pp. 588–592.

Bérubé, M. and Aguilar, A. (1998) 'A new hybrid between a blue whale, Balaenoptera musculus, and a fin whale, B. physalus: frequency and implications of hybridization', *Marine Mammal Science*. Wiley Online Library, 14(1), pp. 82–98.

Bianucci, G. *et al.* (2019) 'A new Monodontidae (Cetacea, Delphinoidea) from the lower Pliocene of Italy supports a warm-water origin for narwhals and white whales', *Journal of Vertebrate Paleontology*. Taylor & Francis, 39(3), p. e1645148.

Bookstein, F. (1991) '199 1. Morphometric Tools for Landmark Data: Geometry and Biology'. Cambridge Univ. Press, New York.

Bookstein, F. L. (1997) *Morphometric tools for landmark data: geometry and biology*. Cambridge University Press.

Boschma, H. (1938) *On the teeth and some other particulars of the sperm whale (Physeter macrocephalus L.)*. Temminckia.

Boschma, H. (1951) 'Rows of small teeth in ziphioid whales', *Zoologische Mededelingen*, 31(14), pp. 139–148.

Brunner, S. (2002) 'A probable hybrid sea lion—Zalophus californianus× Otaria byronia', *Journal of mammalogy*. American Society of Mammalogists 810 East 10th Street, PO Box 1897, Lawrence …, 83(1), pp. 135–144.

Cardini, A. (2014) 'Missing the third dimension in geometric morphometrics: how to assess if 2D images really are a good proxy for 3D structures?', *Hystrix, the Italian Journal of Mammalogy*, 25(2), pp. 73–81.

Costa, C. *et al.* (2006) 'Morphometric comparison of the cephalic region of cultured Acipenser baerii (Brandt, 1869), Acipenser naccarii (Bonaparte, 1836) and their hybrid', *Journal of Applied Ichthyology*. Wiley Online Library, 22(1), pp. 8–14.

Cozzi, B., Huggenberger, S. and Oelschläger, H. A. (2016) *Anatomy of dolphins: insights into body structure and function*. Academic Press.

Doupe, J. P. *et al.* (2007) 'Most northerly observation of a grizzly bear (Ursus arctos) in Canada: photographic and DNA evidence from Melville Island, Northwest Territories', *Arctic*. JSTOR, pp. 271–276.

Garde, E. *et al.* (2007) 'Age-specific growth and remarkable longevity in narwhals (Monodon monoceros) from West Greenland as estimated by aspartic acid racemization', *Journal of Mammalogy*. American Society of Mammalogists 810 East 10th Street, PO Box 1897, Lawrence …, 88(1), pp. 49–58.

Gaubert, P. *et al.* (2005) 'Patterns of cryptic hybridization revealed using an integrative approach: a case study on genets (Carnivora, Viverridae, Genetta spp.) from the southern African subregion', *Biological Journal of the Linnean Society*. Oxford University Press, 86(1), pp. 11–33.

Geiger, M. F. *et al.* (2016) 'Combining geometric morphometrics with molecular genetics to investigate a putative hybrid complex: a case study with barbels Barbus spp.(Teleostei: Cyprinidae)', *Journal of Fish Biology*. Wiley Online Library, 88(3), pp. 1038–1055.

Gligor, M. *et al.* (2009) 'Hybridization between mouse lemurs in an ecological transition zone in southern Madagascar', *Molecular Ecology*. Wiley Online Library, 18(3), pp. 520–533.

Grant, B. R. and Grant, P. R. (1996) 'High survival of Darwin's finch hybrids: effects of beak morphology and diets', *Ecology*. Wiley Online Library, 77(2), pp. 500–509.

Guidarelli, G. *et al.* (2014) 'Morphological variation and modularity in the mandible of three Mediterranean dolphin species', *Italian Journal of Zoology*. Taylor & Francis, 81(3), pp. 354–367.

Hammer, Ø., Harper, D. A. and Ryan, D. D. (2001) 'PAST: PALEONTOLOGICAL STATISTICS SOFTWARE PACKAGE FOR EDUCATION AND DATA ANALYSIS', *Palaeontologia Electronica 178kb. T. Harper. Geological Museum*. doi: 10.1016/j.bcp.2008.05.025.

Heide-Jørgensen, M. P. *et al.* (2010) 'The effect of sea-ice loss on beluga whales (Delphinapterus leucas) in West Greenland', *Polar Research*. Taylor & Francis, 29(2), pp. 198–208.

Heide-Jørgensen, M. P. and Reeves, R. R. (1993) 'Description of an anomalous monodontid skull from west Greenland: a possible hybrid?', *Marine Mammal Science*. Wiley Online Library, 9(3), pp. 258–268.

Heide-Jørgensen, M. P. and Teilmann, J. (1994) 'Growth, reproduction. age structure and feeding habits of white whales (Delphinapterus leucas) in West', *Studies of White Whales (Delphinapterus leucas) and Narwhals (Monodon monoceros) in Greenland and Adjacent Waters*. Commission for Scientific Research in Greenland, p. 195.

IBM Corp.Released (2017) 'IBM SPSS Statistics for Windows, Version 25.0. Armonk, NY: IBM Corp'. NY: IBM Corp.

Jarrell, G. H. (1979) 'Karyotype of the bowhead whale (Balaena mysticetus)', *Journal of Mammalogy*. JSTOR, 60(3), pp. 607–610.

Kelley, T. C. *et al.* (2015) 'Mating ecology of beluga (Delphinapterus leucas) and narwhal (Monodon monoceros) as estimated by reproductive tract metrics', *Marine Mammal Science*. Wiley Online Library, 31(2), pp. 479–500.

Kelly, B. P., Whiteley, A. and Tallmon, D. (2010) 'The Arctic melting pot', *Nature*. Nature Publishing Group, 468(7326), p. 891.

Klingenberg, C. P. (2009) 'Morphometric integration and modularity in configurations of landmarks: tools for evaluating a priori hypotheses', *Evolution & development*. Wiley Online Library, 11(4), pp. 405–421.

Klingenberg, C. P. (2011) 'MorphoJ: An integrated software package for geometric morphometrics', *Molecular Ecology Resources*. doi: 10.1111/j.1755-0998.2010.02924.x.

Klingenberg, C. P. and Marugán-Lobón, J. (2013) 'Evolutionary covariation in geometric morphometric data: analyzing integration, modularity, and allometry in a phylogenetic context', *Systematic biology*. Oxford University Press, 62(4), pp. 591–610.

Kovacs, K. M. *et al.* (1997) 'A harp seal× hooded seal hybrid', *Marine Mammal Science*. Wiley Online Library, 13(3), pp. 460–468.

Kurihara, N. *et al.* (2017) 'Description of the karyotypes of Stejneger's beaked whale (Mesoplodon stejnegeri) and Hubbs' beaked whale (M. carlhubbsi)', *Genetics and molecular biology*. SciELO Brasil, 40(4), pp. 803–807.

Lancaster, M. L. *et al.* (2006) 'Ménage à trois on Macquarie Island: hybridization among three species of fur seal (Arctocephalus spp.) following historical population extinction', *Molecular Ecology*. Wiley Online Library, 15(12), pp. 3681–3692.

Lancaster, M. L. *et al.* (2007) 'Lower reproductive success in hybrid fur seal males indicates fitness costs to hybridization', *Molecular Ecology*. Wiley Online Library, 16(15), pp. 3187–3197.

Lancaster, M. L., Goldsworthy, S. D. and Sunnucks, P. (2010) 'Two behavioural traits promote fine-scale species segregation and moderate hybridisation in a recovering sympatric fur seal population', *BMC evolutionary biology*. Springer, 10(1), p. 143.

MacQueen, J. (1967) 'Some methods for classification and analysis of multivariate observations', in *Proceedings of the fifth Berkeley symposium on mathematical statistics and probability*. Oakland, CA, USA, pp. 281–297.

Mallet, J. (2005) 'Hybridization as an invasion of the genome', *Trends in ecology & evolution*. Elsevier, 20(5), pp. 229–237.

McGowen, M. R., Spaulding, M. and Gatesy, J. (2009) 'Divergence date estimation and a comprehensive molecular tree of extant cetaceans', *Molecular Phylogenetics and Evolution*. Elsevier Inc., 53(3), pp. 891–906. doi: 10.1016/j.ympev.2009.08.018.

Meloro, C. (2011) 'Feeding habits of Plio-Pleistocene large carnivores as revealed by the mandibular geometry', *Journal of Vertebrate Paleontology*. Taylor & Francis, 31(2), pp. 428–446.

Meloro, C., Hudson, A. and Rook, L. (2015) 'Feeding habits of extant and fossil canids as determined by their skull geometry', *Journal of Zoology*. Wiley Online Library, 295(3), pp. 178–188.

Miller, E. H., Stewart, A. R. J. and Stenson, G. B. (1998) 'Bacular and testicular growth, allometry, and variation in the harp seal (Pagophilus groenlandicus)', *Journal of Mammalogy*. American Society of Mammalogists 810 East 10th Street, PO Box 1897, Lawrence …, 79(2), pp. 502–513.

Miralles, L. *et al.* (2016) 'Interspecific hybridization in pilot whales and asymmetric genetic introgression in northern Globicephala melas under the scenario of global warming', *PloS one*. Public Library of Science San Francisco, CA USA, 11(8), p. e0160080.

do Nascimento Schaurich, M., Lopes, F. R. V. and de Oliveira, L. R. (2012) 'Hybridization phenomenon in cetacean and pinniped species', *Neotropical Biology and Conservation*, 7(3), pp. 199–209.

Patton, J. L. (1993) 'Hybridization and hybrid zones in pocket gophers (Rodentia, Geomyidae)', *Hybrid zones and the evolutionary process (RG Harrison, ed.). Oxford University Press, New York*, pp. 290–308.

Pause, K. C. *et al.* (2006) 'G-banded karyotype and ideogram for the North Atlantic right whale (Eubalaena glacialis)', *Journal of Heredity*. Oxford University Press, 97(3), pp. 303–306.

Plön, S. and Bernard, R. (2016) 'Testis, spermatogenesis, and testicular cycles', in

Reproductive Biology and Phylogeny of Cetacea: Whales, Porpoises and Dolphins. CRC Press, pp. 227–256.

Pongracz, J. D. *et al.* (2017) 'Recent hybridization between a polar bear and grizzly bears in the Canadian Arctic', *Arctic*. JSTOR, pp. 151–160.

Preuß, A. *et al.* (2009) 'Bear-hybrids: behaviour and phenotype', *Der Zoologische Garten*. Elsevier, 78(4), pp. 204–220.

Ralls, K. and Mesnick, S. (2009) 'Sexual dimorphism', in *Encyclopedia of marine mammals*. Elsevier, pp. 1005–1011.

Reyes, J. C. (1996) 'A possible case of hybridism in wild dolphins', *Marine Mammal Science*. Wiley Online Library, 12(2), pp. 301–307.

Rohlf, F. J. (2015) 'The tps series of software.', *Hystrix*, 26(1).

Rohlf, F. J. and Marcus, L. F. (1993) 'A revolution morphometrics', *Trends in ecology & evolution*. Elsevier, 8(4), pp. 129–132.

Ross, A. H. and Williams, S. (2008) 'Testing repeatability and error of coordinate landmark data acquired from crania', *Journal of Forensic Sciences*. Wiley Online Library, 53(4), pp. 782–785.

Runck, A. M., Matocq, M. D. and Cook, J. A. (2009) 'Historic hybridization and persistence of a novel mito-nuclear combination in red-backed voles (genus Myodes)', *BMC Evolutionary Biology*. Springer, 9(1), p. 114.

Savriama, Y. *et al.* (2018) 'Bracketing phenogenotypic limits of mammalian hybridization', *Royal Society open science*. The Royal Society, 5(11), p. 180903.

Senn, H. V *et al.* (2010) 'Phenotypic correlates of hybridisation between red and sika deer (genus Cervus)', *Journal of Animal Ecology*. JSTOR, pp. 414–425.

Senn, H. V and Pemberton, J. M. (2009) 'Variable extent of hybridization between invasive sika (Cervus nippon) and native red deer (C. elaphus) in a small geographical area', *Molecular ecology*. Wiley Online Library, 18(5), pp. 862–876.

Sherratt, E. (2014) 'Quick guide to Geomorph v. 2.0', *Quick Guide to Geomorph.[Online][Accessed 5 July 2016] Available from: http://www. public. iastate. edu*.

Sherratt, E. (2015) *Tips & Tricks 8: Examining Replicate Error | R-bloggers*. Available

at: https://www.r-bloggers.com/tips-tricks-8-examining-replicate-error/ (Accessed: 19 February 2019).

Shurtliff, Q. R. (2013) 'Mammalian hybrid zones: a review', *Mammal Review*. Wiley Online Library, 43(1), pp. 1–21.

Skovrind, M. *et al.* (2019) 'Hybridization between two high Arctic cetaceans confirmed by genomic analysis', *Scientific Reports*. Nature Publishing Group, 9(1), p. 7729.

Spiridonova, L. N. *et al.* (2006) 'Genetic evidence of extensive introgression of short-tailed ground squirrel genes in a hybridization zone of Spermophilus major and S. erythrogenys, inferred from sequencing of the mtDNA cytochrome b gene', *Russian Journal of Genetics*. Springer, 42(7), pp. 802–809.

Stirling, I. (2009) 'Polar Bear: Ursus maritimus', in *Encyclopedia of Marine Mammals*. Elsevier, pp. 888–890.

Sylvestre, J. P. and Tasaka, S. (1985) 'On the intergeneric hybrids in cetaceans', *Aquatic Mammals*, 11(3), pp. 101–108.

Team, R. D. C. and R Development Core Team, R. (2016) 'R: A Language and Environment for Statistical Computing', *R Foundation for Statistical Computing*. doi: 10.1007/978-3-540-74686-7.

Team, Rs. (2015) 'RStudio: Integrated Development for R', *[Online] RStudio, Inc., Boston, MA URL http://www. rstudio. com*. doi: https://www.nrel.gov/docs/fy16osti/65298.pdf.

Thulin, C.-G. *et al.* (2006) 'Species assignment and hybrid identification among Scandinavian hares Lepus europaeus and L. timidus', *Wildlife Biology*. BioOne, 12(1), pp. 29–38.

Valentin, A., Sévigny, J. and Chanut, J. (2002) 'Geometric morphometrics reveals body shape differences between sympatric redfish Sebastes mentella, Sebastes fasdatus and their hybrids in the Gulf of St Lawrence', *Journal of fish biology*. Wiley Online Library, 60(4), pp. 857–875.

Wiig, Ø. *et al.* (2012) 'Geographic variation in cranial morphology of narwhals (Monodon monoceros) from Greenland and the eastern Canadian Arctic', *Polar biology*. Springer, 35(1), pp. 63–71.

Willis, P. M. *et al.* (2004) 'Natural hybridization between Dall's porpoises (Phocoenoides dalli) and harbour porpoises (Phocoena phocoena)', *Canadian Journal of Zoology*. NRC Research

Press, 82(5), pp. 828–834.

Yadzi, P. (2002) 'A possible hybrid between the dusky dolphin (Lagenorhynchus obscurus) and the southern right whale dolphin (Lissodelphis peronii)', *Aquatic Mammals*. EUROPEAN ASSOCIATION FOR AQUATIC MAMMALS, 28(2), pp. 211–217.

Yurkowski, D. J., Chambellant, M. and Ferguson, S. H. (2011) 'Bacular and testicular growth and allometry in the ringed seal (Pusa hispida): evidence of polygyny?', *Journal of Mammalogy*. American Society of Mammalogists 810 East 10th Street, PO Box 1897, Lawrence …, 92(4), pp. 803–810.

Zelditch, M. L., Swiderski, D. L. and Sheets, H. D. (2012) *Geometric morphometrics for biologists: a primer*. Academic Press.

Zelditch, M. L., Swiderski, D. L. and Sheets, H. D. (2013) 'A Practical Companion to Geometric Morphometrics for Biologists: Running analyses in freely-available software', *Free download from https://booksite. elsevier. com/9780123869036/(18 June 2013)*.

Zornetzer, H. R. and Duffield, D. A. (2003) 'Captive-born bottlenose dolphin× common dolphin (Tursiops truncatus× Delphinus capensis) intergeneric hybrids', *Canadian Journal of Zoology*. NRC Research Press, 81(10), pp. 1755–1762.

Appendix 5.1 LIST OF ANALYZED FALSE KILLER WHALES SPECIMENS

Species	Catalogue No	Sex	Mandibles 3D
Pseudorca crassidens	1961.6.14.1	F	
Pseudorca crassidens	1961.6.14.10	F	✓
Pseudorca crassidens	1961.6.14.11	N/A	
Pseudorca crassidens	1961.6.14.12	M	✓
Pseudorca crassidens	1961.6.14.13	M	
Pseudorca crassidens	1961.6.14.14	M	
Pseudorca crassidens	1961.6.14.15	F	✓
Pseudorca crassidens	1961.6.14.16	F	✓
Pseudorca crassidens	1961.6.14.17	M	
Pseudorca crassidens	1961.6.14.18	F	✓
Pseudorca crassidens	1961.6.14.19	M	✓
Pseudorca crassidens	1961.6.14.2	F	✓
Pseudorca crassidens	1961.6.14.20	F	
Pseudorca crassidens	1961.6.14.21	M	✓
Pseudorca crassidens	1961.6.14.22	F	✓
Pseudorca crassidens	1961.6.14.24	M	
Pseudorca crassidens	1961.6.14.25	M	
Pseudorca crassidens	1961.6.14.26	M	
Pseudorca crassidens	1961.6.14.27	F	✓
Pseudorca crassidens	1961.6.14.28	F	✓
Pseudorca crassidens	1961.6.14.29	M	✓
Pseudorca crassidens	1961.6.14.3	M	✓
Pseudorca crassidens	1961.6.14.30	M	✓
Pseudorca crassidens	1961.6.14.31	M	
Pseudorca crassidens	1961.6.14.32	M	
Pseudorca crassidens	1961.6.14.33	F	

Pseudorca crassidens	1961.6.14.34	F	✓
Pseudorca crassidens	1961.6.14.35	F	✓
Pseudorca crassidens	1961.6.14.36	F	
Pseudorca crassidens	1961.6.14.37	F	
Pseudorca crassidens	1961.6.14.38	M	
Pseudorca crassidens	1961.6.14.4	M	✓
Pseudorca crassidens	1961.6.14.40	F	
Pseudorca crassidens	1961.6.14.41	F	
Pseudorca crassidens	1961.6.14.42	M	
Pseudorca crassidens	1961.6.14.43	M	
Pseudorca crassidens	1961.6.14.44	M	✓
Pseudorca crassidens	1961.6.14.45	F	✓
Pseudorca crassidens	1961.6.14.47	M	
Pseudorca crassidens	1961.6.14.48	M	
Pseudorca crassidens	1961.6.14.49	M	
Pseudorca crassidens	1961.6.14.5	F	✓
Pseudorca crassidens	1961.6.14.50	M	
Pseudorca crassidens	1961.6.14.51	F	
Pseudorca crassidens	1961.6.14.52	F	
Pseudorca crassidens	1961.6.14.54	F	
Pseudorca crassidens	1961.6.14.55	F	✓
Pseudorca crassidens	1961.6.14.56	F	
Pseudorca crassidens	1961.6.14.57	F	
Pseudorca crassidens	1961.6.14.58	F	
Pseudorca crassidens	1961.6.14.59	M	
Pseudorca crassidens	1961.6.14.6	M	
Pseudorca crassidens	1961.6.14.60	M	
Pseudorca crassidens	1961.6.14.61	M	
Pseudorca crassidens	1961.6.14.62	F	
Pseudorca crassidens	1961.6.14.63	M	✓

Pseudorca crassidens	1961.6.14.64	M	
Pseudorca crassidens	1961.6.14.65	F	
Pseudorca crassidens	1961.6.14.66	F	✓
Pseudorca crassidens	1961.6.14.67	F	✓
Pseudorca crassidens	1961.6.14.68	M	
Pseudorca crassidens	1961.6.14.69	F	✓
Pseudorca crassidens	1961.6.14.7	M	
Pseudorca crassidens	1961.6.14.70	F	
Pseudorca crassidens	1961.6.14.72	F	
Pseudorca crassidens	1961.6.14.73	M	
Pseudorca crassidens	1961.6.14.74	F	
Pseudorca crassidens	1961.6.14.75	F	
Pseudorca crassidens	1961.6.14.78	N/A	
Pseudorca crassidens	1961.6.14.8	F	✓
Pseudorca crassidens	1961.6.14.81	M	✓
Pseudorca crassidens	1961.6.14.83	M	
Pseudorca crassidens	1961.6.14.84	F	
Pseudorca crassidens	1961.6.14.86	M	✓
Pseudorca crassidens	1961.6.14.87	F	
Pseudorca crassidens	1961.6.14.89	M	✓
Pseudorca crassidens	1961.6.14.9	F	
Pseudorca crassidens	1961.6.14.90	N/A	
Pseudorca crassidens	1961.6.14.91	N/A	
Pseudorca crassidens	1992.234	N/A	
Pseudorca crassidens	1992.235	N/A	
Pseudorca crassidens	1992.236	N/A	
Pseudorca crassidens	1992.238	N/A	
Pseudorca crassidens	1992.240	M	
Pseudorca crassidens	1992.244	N/A	

N/A, data not available

Appendix 5.2 PCS OF SKULL SYMMETRIC COMPONENT OF *Pseudorca crassidens* (n=85)

	% Variance	% Cumulative
PC1	0.19764	0.19764
PC2	0.1232	0.32084
PC3	0.10007	0.42091
PC4	0.07268	0.49359
PC5	0.05837	0.55196
PC6	0.05187	0.60383
PC7	0.03392	0.63776
PC8	0.03063	0.66839
PC9	0.02945	0.69784
PC10	0.02775	0.72558

Appendix 5.3 PCS OF 3D MANDIBLES OF *Pseudorca crassidens* (n=29)

	% Variance	% Cumulative
PC1	0.26849	0.26849
PC2	0.16042	0.42891
PC3	0.09319	0.5221
PC4	0.07364	0.59574
PC5	0.06326	0.659
PC6	0.05147	0.71047
PC7	0.04353	0.754
PC8	0.04034	0.79434
PC9	0.03364	0.82798

6   Final remarks

Toothed whale cranium shape can be driven by a variety of ecological factors. One of the scopes of this thesis was to understand which of these might have determined its cranial shape within Odontocetes.

First, I created and tested the reliability and validity of toothed whales database by using three different digitising methods (M, Ph, Br; *Chapter two*). Then, I focused on multiples ecological aspects of toothed whales ecomorphology as previous studies focused on single aspects only, and a whole survey was still lacking (*Chapter three*).

In *Chapter three* I was able to highlight the cranial ecomorphology complexity of the toothed whales, and to identify selective pressures that might have driven cranial size and shape and its function. One of the most interesting findings that emerge from the data in this chapter is that cranial size is a good predictor of biosonar mode (Jensen *et al.*, 2018). So far, only association between mandible size and biosonar parameters was tested and validated due to the role of mandibles in sound reception (Barroso et al., 2012). Furthermore, cranial shape is a good predictor for prey size (McCurry et al., 2017). This provides additional support for the theory of predation as a main driving force in the odontocetes macroevolution (Galatius et al., 2018). Both results can also be used on fossils specimens to better understand their paleoecology. It would be interesting to confront different allometric slopes within each species of toothed whale to understand how micro evolutionary phenotypic changes can be transferred at a macroevolutionary scale producing macro-evolutionary patterns in toothed whales. That could be done analysing the allometric intraspecific patterns within each species to see if they are shared across different families (Fruciano et al., 2019).

Going from a macroevolutionary to a microevolutionary scenario in *Chapter four*, GM appeared to provide useful data in skull morphology studies to recognize hybrid phenotypes. This study provides a base for future works aiming at recognizing hybrid specimen as well as being the first to describe morphologically through 3D GM analyses the skull of a narluga hybrid toothed whale specimen. Results are in line with genetic investigations (Skovrind et al., 2019), and previous skull description (Heide-Jørgensen and Reeves, 1993). The hybrid expressed the dominant phenotype of its father: the beluga, which confirms that hybrid always express the phenotype of one of their parental species. With regards to the mislabelled specimen, here tested as a putative hybrid, genetic analyses performed by the Natural History

Museum of Denmark (NHMD) will be added to the morphological analyses before submitting this work to a peer reviewed journal.

Chapter five provides additional evidence of sexual size dimorphism with males bigger than females in a British stranded population of false killer whales. This is in line with previous traditional morphometric studies on the same subject (Kitchener, Ross and Caputi, 1990). While a difference in skull shape and degree of asymmetry between sexes has not been detected. As this study focuses in samples belonging to the same population, future researches should consider to extract the DNA and see how the shape can be correlated with the genetic to build the family tree of this population. Although, mass stranding is a quite catastrophic episode, it can also give information regarding cetacean life style and reproduction that cannot be detected during a single whale monitoring session. It is also important to work on the asymmetric and symmetric component of shape and cranial and mandibular integration in toothed whales as well and FA scores to assess if the degree of asymmetry is related to sexual and/or to geographical differences can be detected. At the moment three papers are known to focus on skull modularity in the Cetacea skull (Guidarelli *et al.*, 2014; del Castillo *et al.*, 2016; Churchill *et al.*, 2019). *Chapter five* is the first paper to analyse covariation between cranium and mandible in false killer whales.

With this thesis, I also invite to generate a stronger link between two very disparate branches of science: functional morphology and field ecology. This link is essential for broadening our research perspective to understand how data collected in the field can be used to test more functional hypotheses on the toothed whale skull ecomorphology.

References

del Castillo, D. L. *et al.* (2016) 'Cranial development and directional asymmetry in Commerson's dolphin, Cephalorhynchus commersonii commersonii: 3D geometric morphometric approach', *Journal of Mammalogy*. Oxford University Press US, 97(5), pp. 1345–1354.

Churchill, M. *et al.* (2019) 'Asymmetry drives modularity of the skull in the common dolphin (Delphinus delphis)', *Biological Journal of the Linnean Society*. Oxford University Press UK, 126(2), pp. 225–239.

Fruciano, C. *et al.* (2019) 'Dissecting Phenotypic Integration and Connecting Micro-and Macro-Evolutionary Time Scales', in *JOURNAL OF MORPHOLOGY*. WILEY 111 RIVER ST, HOBOKEN 07030-5774, NJ USA, pp. S14–S14.

Galatius, A. *et al.* (2018) 'Raising your voice : evolution of narrow-band high- frequency signals in toothed whales (Odontoceti)', *Biological Journal of the Linnean Society*, pp. 1–12.

Guidarelli, G. *et al.* (2014) 'Morphological variation and modularity in the mandible of three Mediterranean dolphin species', *Italian Journal of Zoology*. Taylor & Francis, 81(3), pp. 354–367.

Heide-Jørgensen, M. P. and Reeves, R. R. (1993) 'Description of an anomalous monodontid skull from west Greenland: a possible hybrid?', *Marine Mammal Science*. Wiley Online Library, 9(3), pp. 258–268.

Jensen, F. H. *et al.* (2018) 'Narrow Acoustic Field of View Drives Frequency Scaling in Toothed Whale Biosonar', *Current Biology*. Elsevier, 28(23), pp. 3878–3885.

Kitchener, D. J., Ross, G. J. B. and Caputi, N. (1990) 'Variation in skull and external morphology in the false killer whale, Pseudorca crassidens, from Australia, Scotland and South Africa', *Mammalia*. Walter de Gruyter, Berlin/New York, 54(1), pp. 119–136.

McCurry, M. R. *et al.* (2017) 'The remarkable convergence of skull shape in crocodilians and toothed whales', *Proceedings of the Royal Society B: Biological Sciences*. The Royal Society, 284(1850), p. 20162348.

Skovrind, M. *et al.* (2019) 'Hybridization between two high Arctic cetaceans confirmed by genomic analysis', *Scientific Reports*. Nature Publishing Group, 9(1), p. 7729.